High Strength Fibre Reinforced Concrete

Static and fatigue behaviour in bending

PROEFSCHRIFT

ter verkrijging van de graad van doctor
aan de Technische Universiteit Delft,
op gezag van de Rector Magnificus prof.dr.ir. J.T. Fokkema
voorzitter van het College voor Promoties,
in het openbaar te verdedigen
op donderdag 28 juni 2007 om 10:00 uur

door

Eleni Sofia LAPPA

Diplom-Ingenieurin, Technische Universiteit Darmstadt
geboren te Darmstadt (Duitsland)

Dit proefschrift is goedgekeurd door de promotor:

Prof.dr.ir. J.C. Walraven

Samenstelling Promotiecommissie

Rector Magnificus,	voorzitter.
Prof.dr.ir. J.C. Walraven,	Technische Universiteit Delft, promotor.
Prof.Dr.-Ing. J.D. Wörner,	Deutsches Zentrum für Luft- und Raumfahrt, Duitsland.
Prof.dr.ir. L.Taerwe,	Universiteit Gent, België.
Prof.Dr.-Ing. H.S. Müller,	Universität Karslruhe, Duitsland.
Prof.ir. A.C.W.M. Vrouwenvelder,	Technische Universiteit Delft.
Dr.ir. C. van der Veen,	Technische Universiteit Delft.
Dr.ir. A.J. Bigaj-van Vliet,	TNO Bouw en Ondergrond, Delft.
Prof.ir. A.Q.C. van der Horst	Technische Universiteit Delft, reservelid.

ISBN 978-90-9021935-6

Keywords: high strength concrete, ultra high strength concrete, UHPC, steel fibres, fatigue.

This research was supported by the Technology Foundation STW, applied science division of NOW and the technology programme of the Ministry of Economic Affairs.

Printed in the Netherlands by Gildeprint, Enschede.

As you set out for Ithaka,
hope your road is a long one,
full of adventure, full of discovery.
Ithaka, C.P. Cavafy, 1911.

Σα βγεις στον πηγαιμό για την Ιθάκη,
να εύχεσαι νάναι μακρύς ο δρόμος,
γεμάτος περιπέτειες, γεμάτος γνώσεις.
Ιθάκη, Κ.Π. Καβάφης, 1911.

To my grandparents and Johnny Cash

Damaged building by the Athens 1999 Earthquake, picture by P. Yannopoulos

SUMMARY

High strength fibre reinforced concrete – static and fatigue behaviour in bending

Recently, a number of high strength and ultra high strength steel fibre concretes have been developed. The number of practical applications with such materials is continuously increasing, consequently also the demand for suitable material models and design regulations. Since these materials seem very suitable for structures that might be prone to fatigue failure, such as bridge decks, the understanding of the static and fatigue bending behaviour is vital.

In order to evaluate the bending behaviour of high and ultra high strength concretes, an experimental and analytical approach was followed. First, suitable mixtures were chosen, that included a variation in the compressive strength, the tensile and flexural tensile response, the fibre geometry and content, and the maximum aggregate size. Four mixtures were chosen, two ultra high strength concretes, with a compressive strength of more than 200 MPa, and two high strength concretes, with a compressive strength of 120 MPa. The two ultra high strength concretes can be classified as coarse mixtures, with maximum aggregate sizes of 7 and 8 mm, and have a fibre content of 2.5% in volume. One of them, named 'BSI/CERACEM', is a commercially available industrial mixture, which has already found a number of structural applications. The other one, denoted as 'UHPC', was developed by the University of Karlsruhe, Germany, where a collaboration existed within this project in the scope of a joint research programme on durability and fatigue. The two high strength mixtures do not have the addition of coarse aggregates, so the maximum aggregates size is 0.5 and 2 mm, and the total fibre content is lower than in the ultra high strength mixtures, at 1.5% and 1.6% in volume. One of these two mixtures is additionally a 'hybrid' mixture, referred to as 'hybrid HSFRC'. The term 'hybrid' implies a combination of two different fibre geometries: it contains 0.5% of 13 mm short straight-end steel fibres, and 1% of 60 mm long hooked-end steel fibres. This combination allows an increase of the tensile strength, due to the shorter fibres that bridge microcracks, and a ductile and improved postpeak load bearing capacity, due to the bridging ability of the macrocracks by the longer fibres. The other high strength mixture, the HSFRC, contains only 13 mm long fibres, but was the mixture with the best workability in this study.

After having chosen the mixtures needed for the evaluation of the hardened state properties in bending, an experimental programme was performed for the determination of the bending behaviour under static and fatigue loads. The main testing method was the four point bending test on un-notched beam specimens of dimension 125/125/1000 mm. The beams were tested at a span of 750 mm, loaded

in their third points. With the BSI/CERACEM, HSRFRC and hybrid HSFRC mixtures, first a series of static bending tests were performed, followed by a number of fatigue bending tests under different values of the upper load level. The fatigue tests were necessary in order to evaluate the fatigue bending behaviour and to provide S-N lines, which are commonly used in fatigue design verifications of structures. A point of further attention was the fibre alignment and dispersion: this was examined with image analysis on photographs of beam cross-sections taken at the fracture surface. With the UHPC mixture, the static and fatigue tests were performed in the scope of a combined fatigue-durability testing programme. Moreover, additional tests were performed with the HSFRC mixture: four and three point bending tests on notched beams, as well as uniaxial tensile tests. With these tests, a thorough evaluation of the material behaviour of this particular mixture was possible.

The tests showed that first of all, except for the UHPC mixture, all other mixtures were deflection hardening materials and also strain hardening materials in tension, an important characteristic of the mixtures. The HSFRC mixture, which was the mixture with the best workability, had the lowest scatter in the static and fatigue behaviour, and this highlights the effect of the fresh state properties on the material behaviour in the hardened state. Moreover, it shows that it is not by definition the material with the highest material strength in static loading, which in this study was the BSI/CERACEM that will also have the best resistance in fatigue loading, which in this case was the HSFRC. The fibre count showed that even though a direct relation was found between the number of fibres in the critical cross-section and the flexural strength of the beam in static loading, such a clear relation was not found in fatigue loading. More parameters than the fibres alone are responsible for fatigue failure. Also, while in plain concrete the static load-displacement curve has been reported to function as an envelope curve for fatigue displacements, this was not valid for the flexural tests of this study. Only the HSFRC mixture showed an improved fatigue resistance in comparison with plain concrete, while the other two mixtures had a comparable fatigue performance with plain concrete. This shows that a good workability, which in self-compacting fibre concretes improves the homogeneity in the fibre alignment, can significantly reduce the scatter in fatigue results. Due to the better fibre alignment, the fatigue resistance is improved. A general conclusion derived from the fatigue tests of the mixtures in this study, is that the fatigue regulations, as used for normal strength concrete, remain suitable for a safe fatigue design with high and ultra high strength concretes.

The experimental results were confirmed with an analytical model, the multi-layer model that can be used for calculating the material response in bending of the beams in this study. The tensile material input parameters were obtained from uniaxial tensile tests. For the BSI/CERACEM and the hybrid HSFRC, results of tensile tests from other researchers were available for that purpose. For the HSFRC, tensile tests were performed in this study, and it was shown that the uniaxial tensile response, measured on a length of 35 mm, was suitable for a good reproduction of

the experimental results with the model. The model is better suitable for the response of notched beam specimens. Its use for un-notched specimens has been justified in this study by the fact that at postpeak, crack localisation always took place in a single crack. The model predicts the crack openings from the modelled tensile strain at the bottom of the beam. The deflections are modelled from a linear elastic part, derived from equilibrium considerations on a simply supported beam, and an inelastic part. The inelastic deflections can be determined from rigid body kinematics and depend on a variable rotation depth that is proportional to the crack length. In case of un-notched specimens, a constant rotation depth has to be assumed during the deflection hardening, as was verified by the experimental results. An alternative approach was also proposed, as of a combination of the material input relations for ideal single crack and ideal multiple cracking materials.

Further, the same multi layer model was adapted and used for the fatigue behaviour. A suitable material input relation is proposed, that contains a gradual stiffness and strength decrease with increasing number of load repetitions. With this approach, all three stages of the deformation evolution of a fatigue experiment can be modelled. The fatigue calculations were only evaluated for the HSFRC mixture, but the results can be applied to the other mixtures of this study, since the upper load level in the model was set in accordance with the peak load, as predicted in the calculations of the static response with the same multi-layer model. With this proposed material input, the predicted fatigue life for each load level was in good agreement with the experimental results of the un-notched HSFRC beams. The modelled and calculated strain distributions during a fatigue experiment were in good agreement. The proposed model can be easily implemented into existing finite element codes, and can therefore be used for fatigue verifications of larger structural elements of various shapes.

Eleni Sofia Lappa

SAMENVATTING

Hoge sterkte staalvezelbeton – materiaalgedrag (buiging) onder statische belasting en vermoeiing

Gedurende de afgelopen jaren zijn een groot aantal vezelbetonsoorten met hoge en zeer hoge sterkte ontwikkeld. De hoeveelheid praktische toepassingen van dergelijke materialen stijgt continu, en daarmee ook de vraag naar geschikte materiaalmodellen en richtlijnen. Gezien het feit dat deze materialen op het eerste gezicht zeer geschikt zijn voor toepassing in constructies die aan vermoeiingsbelasting zijn blootgesteld, zoals brugdekken, is inzicht in het materiaalgedrag op buiging, zowel onder statische als onder dynamische belasting, van belang.

Om het materiaalgedrag van hoge en zeer hoge sterkte beton op buiging te evalueren, is experimenteel en analytisch onderzoek uitgevoerd. Hiertoe werden mengsels gekozen, die garant stonden voor een breed spectrum aan materiaaleigenschappen. Dit betrof de mengselsamenstelling, de karakteristieken van de staalvezels en de druk-, trek- en buigtreksterkte. Uitgegaan werd van vier mengsels: twee vezelbetonmengsels met een druksterkte van 200 MPa, en twee vezelbetonmengsels met een druksterkte van 120 MPa. De twee mengsels met de hoogste sterkte bevatten een "grove" toeslag, met een maximale korrelafmeting van 7, respectievelijk 8 mm, en waren voorzien van 2,5 vol.% vezels. Een daarvan, genaamd BSI/CERACEM, is een product uit de industrie, dat reeds voor diverse praktische toepassingen is gebruikt. De andere, aangeduid met de afkorting "UHPC" is ontwikkeld door de Universiteit Karlsruhe, Duitsland. Met deze universiteit bestond een samenwerkingsverband in de vorm van een gezamenlijk onderzoek naar het vermoeiingsgedrag en de duurzaamheid. De twee andere betonmengsels bevatten geen "grof" toeslagmateriaal: de maximale korreldiameter was 0,5, respectievelijk 2 mm. De vezelpercentages waren 1,5 en 1,6 vol.%. Een van deze mengsels, genaamd "hybrid HSFRC" bevatte twee soorten vezels: 0,5% 13 mm lange gladde vezels en 1% 60 mm lange vezels met eindverankering in de vorm van haakjes. De korte vezels remmen de uitbreiding van microscheuren, waardoor de treksterkte toeneemt, en de lange vezels werken de opening van de macroscheuren tegen, waardoor de vervormbaarheid toeneemt. Het andere mengsel, de HSFRC, bevatte slechts vezels met een lengte van 13 mm: dit mengsel was het best verwerkbaar.

Voor de beschreven mengsels werd een serie experimenten opgezet, waarin het gedrag op buiging werd onderzocht, zowel onder statische als onder vermoeiingsbelasting. De meest gebruikte testmethode was een vierpuntsbuigproef op 125/125/1000 mm balkjes zonder kerf. De overspanning van de balkjes was 750 mm. De afstand tussen de lasten was steeds 250 mm. Voor de mengsels BSI/CERACEM, HSFRC en hybrid HSFRC werd eerst een serie proeven onder statische belasting uitgevoerd, gevolgd door proeven onder wisselende belasting met

verschillende belastingniveaus. Uit deze vermoeiingsproeven werden Wöhlerlijnen (S-N lijnen) afgeleid, gangbaar in voorschriften. Een belangrijk aspect van het onderzoek was de vezeloriëntatie. Hierbij werd gebruik gemaakt van digitale beeldanalyses van foto's van een balkdoorsnede direct naast het scheurvlak.

De proeven op het UHPC mengsel, onder statische en vermoeiingsbelasting, werden alleen uitgevoerd in het kader van het gezamenlijke onderzoek met de TU Karlsruhe naar de combinatie duurzaamheid en vermoeiing. Verder werden nog extra proeven uitgevoerd op balkjes gemaakt met het HSFRC mengsel. Dit betrof drie- en vierpunts buigproeven op gekerfde balkjes en trekproeven. Met deze proeven was een complete evaluatie van het materiaalgedrag van het HSFRC mengsel mogelijk.
Alle betonsoorten, afgezien van het UHPC mengsels, vertoonden een zeer ductiel gedrag, zowel op buiging als op zuivere trek, wat een zeer belangrijk kenmerk is van dit soort materialen. Het HSFRC mengsel, dat het best verwerkbaar was, had de laagste spreiding in materiaalgedrag, zowel onder statische als onder vermoeiingsbelasting. Dit geeft aan dat er een relatie is tussen het gedrag in de vloeibare fase en het gedrag in de verharde toestand. Verder bleek dat een toename van de sterkte niet hoeft te leiden tot een verbetering van het vermoeiingsgedrag (BSI/CERACEM versus HSFRC). Uit de bepaling van de vezelorientatie bleek dat er een directe relatie is tussen het aantal vezels in de kritische doorsnede en de buigtreksterkte. Dit gold echter niet voor de vermoeiingssterkte. Dit toont aan dat meer parameters voor het vermoeiingsgedrag verantwoordelijk zijn dan de vezelorientatie alleen. In ongewapend conventioneel beton is de kracht-verplaatsingsrelatie onder statische belasting de omhullende voor de verplaatsingen onder vermoeiingsbelasting. Dit werd niet bevestigd door de proeven op hoge sterkte vezelbeton in dit onderzoek. Verder bleek dat alleen het HSFRC mengsel een beter vermoeiingsgedrag toonde dan traditioneel beton. De andere twee mengsels toonden een gedrag dat vergelijkbaar is met dat van gewoon beton. Duidelijk werd dat een goede verwerkbaarheid de spreiding in vermoeiingsresultaten vermindert. Door een betere vezeloriëntatie wordt het vermoeiingsgedrag beter. Tenslotte is een algemene conclusie van dit onderzoek dat een ontwerp tegen vermoeiing in overeensteming met de gangbare voorschriften voor conventioneel beton ook geschikt is voor vezelbeton met hoge en zeer hoge sterkte.

De uit de experimenten gevonden resultaten werden met een analytisch rekenmodel bevestigd. Hierbij werd uitgegaan van een laagjesmodel (multi-layermodel), dat geschikt is voor het narekenen van het buiggedrag van de balkjes in dit onderzoek. De inputparameters waren gebaseerd op éénassige trekproeven. Voor de mengsels BSI/CERACEM en hybrid HSFRC waren resultaten van trekproeven van andere onderzoekers beschikbaar. De trekproeven op het HSFC mengsel werden in dit onderzoek uitgevoerd. De resultaten van de trekproeven, met meetlengten van 35mm, lieten een goede overeenkomst tussen het experimentele en het berekende buiggedrag zien. Het model geeft de beste resultaten voor balkjes met kerf. Niettemin kan het model ook voor balkjes zonder kerf gebruikt worden, omdat de

vervorming zich na het bereiken van de maximale belasting in een enkele scheur lokaliseert. Het model voorspelt de ontwikkeling van de scheurwijdte met behulp van de berekende rek aan de onderzijde van de balk. De doorbuiging bestond uit een lineair en een niet-lineair elastisch gedeelte. Het lineaire deel wordt direct op grond van een evenwichtsbeschouwing afgeleid. Het niet-lineaire deel volgt uit een beschouwing van het kinematische gedrag. De vervorming is hierbij afhankelijk van een variabele rotatiehoogte, die proportioneel is met de scheurlengte. In het geval van balkjes zonder kerf moet in overeenstemming met de proefresultaten een constante rotatiehoogte tijdens het verstevigingsgedrag vastgelegd worden.
Tenslotte werd het laagjesmodel aangepast om ook het gedrag onder vermoeiing te beschrijven. Hiertoe werd een geschikte inputrelatie voorgesteld, waarbij stijfheid en sterkte afnemen met toenemend aantal lastwisselingen. Met deze benadering zijn alle drie stadia van de vermoeiingsvervormingen in het model zichtbaar. Het vermoeiingsmodel werd alleen getoetst op het HSFRC mengsel, maar de resultaten zijn ook toepasbaar op de andere mengsels, omdat het niveau van de vermoeiingsbelasting in relatie tot de met het laagjesmodel berekende statische belasting hetzelfde was. Met deze input werd het vermoeiingsgedrag van de balkjes met kerf beter beschreven dan die zonder kerf. De berekende en gemeten rekverdelingen komen goed met elkaar overeen. Het ontwikkelde model kan eenvoudig worden geïmplementeerd in bestaande elementenprogramma's. Op deze manier kan ook het vermoeiingsgedrag van constructies worden geanalyseerd.

Elena Sofia Lappa

Contents

1.

High strength fibre reinforced concrete under static and fatigue loading

In this chapter, the main aspects of this study will be highlighted. These are: the development of self-compacting, high strength materials, their behaviour under both static and fatigue loading conditions, and suitable material models to describe this behaviour. The objectives of this thesis will be shown, and the research strategy that was followed in order to solve them. Additionally, a brief outline of the thesis is given.

1.1 Scope of the research

This thesis shows the behaviour of high and ultra high strength fibre reinforced concrete under static and fatigue bending loads. As an introduction, first some words on the materials, their static structural behaviour and on fatigue have to be written.

1.1.1 Self-compacting high and ultra high strength concretes

Concrete as a building material has established itself in the building industry, and it has by now evolved into a material that can be 'tailored' to fit individual needs of the desired application, the expected lifetime of a structure, and the expected loads a structure will encounter during its service life. The materials of this study take advantage of two recent innovations of the concrete production industry, namely the development of self-compacting concretes and the development of high strength, and recently also ultra high strength, concretes.

Self-compacting concrete was developed recently, and it has been widely used in the Netherlands in the last decade, especially in the pre-cast concrete industry. As the name already implies, these concretes do not need any external vibration for compaction in order to fill the moulds or to release the air that is entrapped inside the fresh material during the mixing process. Removing the need for external vibration, that used to be an essential requirement for concrete applications, has

brought numerous advantages. To name a few, since self-compacting concrete is very flowable, and can be used for structural elements of complex shapes, that could not be build before if not all parts in the mould could be reached and vibrated. Less working personnel is required, since in the casting process, the vibration works are not necessary. And, especially at pre-cast concrete plants, the abandoned vibration has significantly reduced the noise and therefore improved the working conditions. In this thesis, all materials cast in the scope of this research project were self-compacting, therefore utilising all the above advantages of this feature.

High and even ultra high strength concretes were developed in recent years, with new mixture optimisation techniques and utilisation of fine filler materials and new additives and admixtures such as superplasticisers. Even the notion of 'high strength' has changed with the years; in the 80s, a compressive strength of 60 MPa would have been considered high strength, opposed to the conventional concrete strengths of 25-40 MPa. Nowadays, with the term 'high strength' strengths of 80-110 MPa are associated. Recently, 'ultra' high strength concretes have been developed, which exhibit compressive strengths of 150-200 MPa and sometimes even above 200 MPa. Of the materials used in this study, two can be classified as high strength concretes, with compressive strengths of 100-120 MPa, and two as ultra high strength concretes with a compressive strength in the range of 200 MPa.

1.1.2 Static material behaviour - strain hardening materials

The development of a new material has as a consequence that its material properties, and especially its strengths under certain loading directions and conditions, have to be determined before this material can be used for structural applications. The strength properties need to be determined experimentally, and suitable model and material input values have to be established in order to enable a safe design. The final goal is to establish national or even international design regulations and guidelines for these materials, which would further promote the materials and enable more interesting and challenging applications.

Concrete is a material with a rather poor tensile load bearing capacity, at least compared to its load bearing capacity in compression. Moreover, unreinforced concrete can be classified as a brittle material, compared to rock materials, and cannot provide the deformation ability and ductility of metals. Increasing the concrete strength, from normal strength to high or ultra high strength concrete, has as a consequence that the brittleness increases even more. This 'defect' can be overcome by adding fibres. Fibres increase the deformation ability and the tensile load bearing capacity of brittle materials. The principle of adding fibres to a brittle material is well-known from early human building history: in ancient Egypt for example, straw fibres were added to clay bricks as a reinforcement. Without fibres, high and ultra high strength concretes can show a very sudden, almost explosive type of failure under certain loading conditions. Such a behaviour is unwanted for a building material out of safety considerations, where an early announced and

controlled failure is desired. Therefore, for these materials the fibre addition is a necessity for most types of applications. In this study, all used materials contain steel fibres, and these fibres play a substantial role in the static material behaviour, especially when subjected to tension and flexural tension.

The role of fibres is significant for the static material behaviour: in most cases, the fibres will not increase the compressive strength, but will increase the deformation ability. In tension, depending on the chosen fibre type and content, not only the deformation ability, but also the material strength can be increased. When the tensile strength is increased, then such materials are often called 'strain hardening' materials. The strain hardening phase is accompanied by the opening of very fine multiple cracks. This characteristic was present in most of the materials used in this thesis, therefore this characteristic, and the role of fibres in order to achieve it, will be highlighted further in the appropriate chapters in this study.

1.1.3 Fatigue

Fatigue can be a possible failure mechanism of a material when it is subjected to repeated loading. It was first observed in metals in the 19th century, when wheel axes of trains failed even at loads that were significantly below the strength limit of the material. In metals, fatigue cracks show a distinctive crack pattern and therefore can be recognised at inspections and repaired. Also, appropriate verifications for structures subjected to repeated loading have been integrated in the codes so that fatigue failure is prevented for the expected loads and service life of structures. In concrete however, fatigue cracks cannot be distinguished from other types of concrete cracks. Therefore, fatigue of concrete was not recognised as a possible failure mode until the 70s, when damage was observed at a number of prestressed concrete bridges that was eventually attributed to fatigue. Since then, fatigue of concrete has been a research topic and fatigue models and design verifications have been proposed and implemented into concrete codes.

Knowledge of the fatigue behaviour and the existence of appropriate fatigue verifications is essential in structures that are expected to be subjected to a high number of load repetitions, such as traffic loads in case of bridges, or wind and wave loads in offshore structures. High and ultra high strength fibre concretes seem very suitable to find application in such kind of structures. However, up to now very limited research has been reported on the fatigue behaviour of these materials. This need resulted into the present study, which gives insight into the fatigue performance and failure mechanisms of these materials, in order to promote the materials' applications in structures prone to fatigue failure. A good knowledge and understanding of the static material behaviour is needed in order to have a sound fatigue evaluation. Therefore, this thesis focuses on the static and fatigue behaviour of these new materials in equal parts.

1.2 Research objectives and strategy

The main objective of the thesis is to specify the failure mechanisms of high strength fibre reinforced concretes under static and fatigue (flexural) loading conditions. In doing so, it will:

- Determine the novelties and special characteristics of the materials involved, compare them to plain concrete and point out the differences in the material (bending) behaviour and failure modes. It will show how the fresh state properties (workability, flow ability) influence the material behaviour, especially the fibre alignment and distribution.
- Show the material characteristics, structural behaviour, and failure modes under both static and fatigue loading conditions.
- Point out the differences in the failure modes under static and fatigue loading conditions.
- Highlight the role of the steel fibres with regard to the static and fatigue performance.
- Provide suitable material models for static and fatigue loading conditions, and compare the calculated results with these models to the experimental findings.

The following research strategy was followed in order to meet the listed objectives: First, appropriate concrete mixtures were chosen that were suitable for the research, a total of four mixtures were used in this study. Second, an experimental programme was initiated, that consisted of static three point bending tests, static four point bending tests, static uniaxial tensile tests and fatigue four point bending tests, apart from standard compressive and splitting tensile strength tests that were always performed in the scope of quality control of the mixtures. Of these, the main testing method were the static and fatigue four point bending tests on un-notched beams. This programme was found suitable to provide answers on the objectives listed above. Third, and last, an analytical equilibrium based model was used in order to evaluate and reproduce the experimental results. The material input parameters were in accordance with results obtained from the standard compressive strength tests and uniaxial tensile tests.

1.3 Outline of this thesis

This thesis can be subdivided into four main parts, each part consisting of at least one chapter. An overview of the outline and structure is given in Figure 1.1. First, a general introduction is given on the main aspects and objectives of the research. Second, the experimental results are presented. Third, the results of the proposed material model are shown, while fourth, conclusions are drawn and

recommendations for further research are given. Except for the Chapters 1 and 8, each chapter contains also a brief literature review on existing research on the topic.

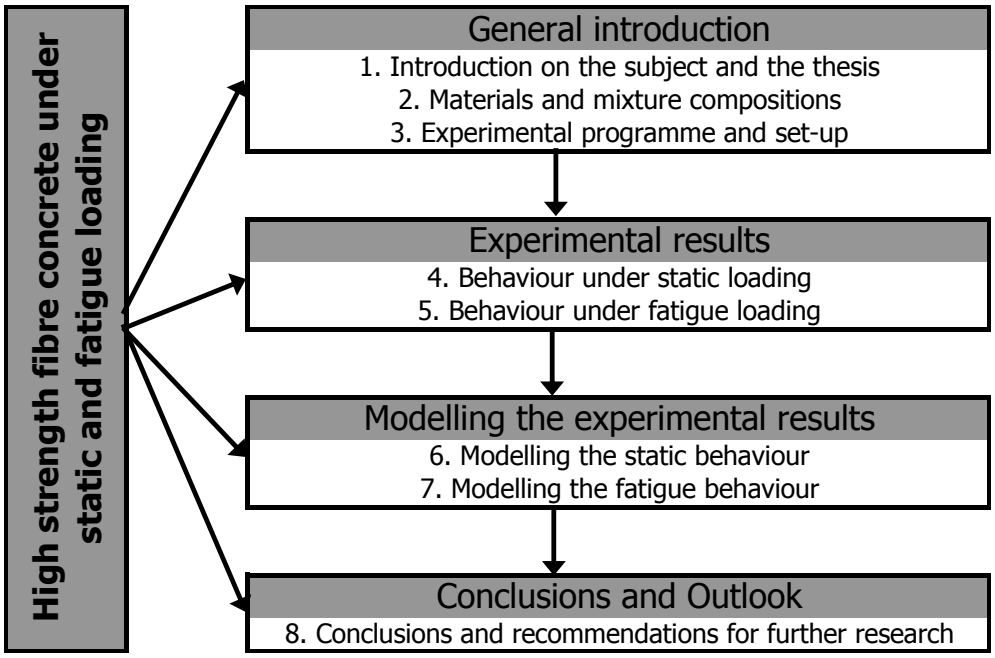

Figure 1.1: Outline of this thesis.

The general introduction consist of the first three chapters and, after mentioning the scope and objectives of the thesis, introduces the materials and the experimental approach followed in the research. Chapter 1 gives a general introduction on the research and this thesis. Chapter 2 focuses on the materials used in this thesis, and presents the material properties in the fresh state. Chapter 3 gives an overview of the complete experimental programme and the experimental setup that was needed in order to meet the research objectives.

The following two chapters, 4 and 5, form the biggest part in this study, the part on the experimental results. These chapters give valuable insight on the static and fatigue material behaviour of the used high strength mixtures. Chapter 4 shows the results of all static tests performed in this study, this includes four point bending tests on un-notched beams with all concrete mixtures used in this study, and additional three and four point bending tests on notched beams as well as uniaxial tensile test for the one particular mixture. An important part in this chapter are the definitions of multiple cracking and the fibre dispersion and orientation. Chapter 5 shows the results of the fatigue bending tests, which were mainly fatigue bending tests on un-notched beams for all mixtures, and a limited number of notched fatigue tests for one particular mixture. This chapter also shows the results of a brief microscopical study, and it contains the results of a joint durability and fatigue study performed together with the University of Karlsruhe.

Chapters 6 and 7 present a model that is suitable to predict the experimental results and model the material behaviour of the mixtures in this study under static and fatigue bending loads. Chapter 6 shows the methodology of the used model, and the chosen input parameters for each of the three mixtures, and compares the modelled results to the experimental ones. A brief parameter study shows the influence of certain input parameters on the outcome of the model and shows the limitations of applicability of the model. Chapter 7 is based on the same analytical model used in Chapter 6, but after implementation of a suitable material input, which depends on the number of load repetitions, and can in that way show the effects of fatigue loading. A material input model is proposed that is capable of showing the basic mechanisms of the evolution of displacements and eventually predict failure due to fatigue.

Finally, in the last part which consists of Chapter 8, the final conclusions of this study are given, and an outlook on the future is made in the form of recommendations for future research that evolved from the performed experiments and calculations.

2.

Mixture compositions for (ultra) high strength concretes: theoretical considerations and development of mixtures for testing

This chapter gives an overview of the materials used in order to determine the static and fatigue failure mechanisms of high strength fibre reinforced concretes. After a literature review, that shows theoretical considerations needed in order to develop ultra high strength concretes, the chosen mixtures for this study and their characteristics are given.

Four different concrete mixtures were examined in this study, which were chosen in order to represent a broad range of mixtures with similar characteristics. Two of these mixtures were actually developed at Delft University, one is a commercially available mixture from the industry, and the fourth one is developed at the concrete technology department of Karlsruhe University, which collaborated in the research project. These mixtures can be classified, in the order they are mentioned above: a high strength concrete reinforced only with short straight fibres, a high strength concrete that innovatively uses two different fibre geometries in order to combine their properties into an improved total material mechanical behaviour, an industrial ultra high strength fibre reinforced concrete, and one ultra high strength fibre reinforced concrete. Even though this chapter is mainly dealing with the mixture composition, some results concerning the fresh-state properties of the material will be included. This is due to the fact that the fresh-state properties can be considered as a unique characteristic of each mixture. Moreover, since this thesis focuses on the properties in the hardened state, it seemed more appropriate to include this results in this chapter.

2.1 High Strength Fibre Concretes – Theory

This section will show the basic principles of concrete technology needed in order to design and produce high and ultra high strength fibre reinforced concretes. It is also a literature review on existing compositions and ready made industrial premixes and final concretes that are comparable to the materials used in this study.

In order to design a high or ultra high strength concrete, the materials have to be carefully selected in such a way, that a very dense and compact cement matrix is created. Therefore, the water cement ratio w/c is reduced to a minimum and fine fillers, such as silica fume or fly ash, are added that fill the voids between the cement particles. Often only sand is used as the aggregate component: therefore the first ultra high strength concretes were often called reactive powder concretes (RPC), with the notion that they contained only fine particles, or powders. However, referring to the fact that also concretes with coarse aggregates (maximum size up to 8 mm) and a very high compressive strength have been developed on the basis of appropriate component selection and optimised packing models, the name ultra high performance concrete (UHPC) is used more widely. Richard and Cheyrezy (1995) list materials, compositions and production methods for reactive powder concretes, while, among others, Fehling et al. (2005) list the equivalent information for fine but also coarse ultra high strength mixes (UHPC), with maximum aggregate sizes up to 8 mm.

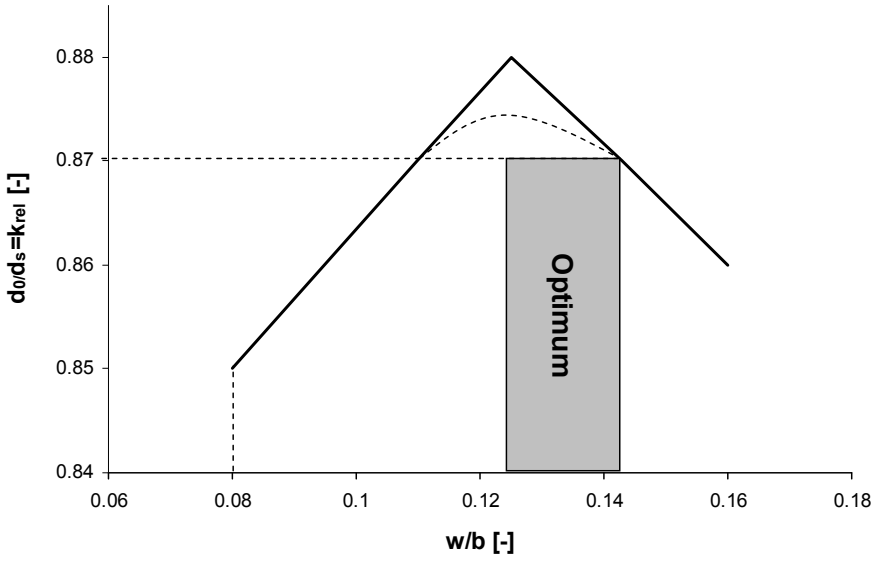

Figure 2.1: Relative density in relation to the water-to-binder ratio and determination of the optimium packing density after Richard and Cheyrezy (1995).

The packing of cement, filler and aggregates is of great importance for the development of (ultra) high strength concretes and different models for the

optimisation of the granular skeleton have been developed in order to optimise the mixture composition. These models can be experimental or numerical. For ultra high strength concrete, the experimental model developed by Richard and Cheyrezy (1995) has proven to be an efficient tool. In this model, the variation of the relative density with the water content is shown. The relative density k_{rel} is expressed by the ratio d_0/d_s, with d_0 being the density of the concrete at demoulding and d_s the solid density of the granular mixture. The water content is expressed by the water-to-binder ratio w/b. According to the model, a maximum density level is reached corresponding to a theoretical water content ($w/b \approx 0.13$), when the mixture does not contain any entrapped air. Such a low w/b content is not feasible due to mixing and workability constraints, so that an optimised packing density, close to the maximum value, is obtained instead. This density can be realised for two different water contents, as indicated in Figure 2.1. The preferable value of the two is the one with the higher w/b since the extra water provides a better hydration and therefore better mechanical properties, and also the rheological properties are better. According to the model, the optimum water-to-binder ratio lies between the theoretical maximum at 0.13 and approximately 0.15. In more recent developments, also ultra high strength concretes with w/b ratios above 0.15 have been developed that can reach compressive strengths above 180 MPa, and the packing of these mixtures has often been optimised by numerical methods. Of the numerical methods, the method after De Larrard and Sedran (1994) is well-known, which distinguishes between a virtual and an actual packing density and takes into effect the interaction between particles and the rate of compaction. Apart from that, it is possible to use micro-computertomography for a numerical description of very fine particles starting from 2µm, and this method has been used by Geisenhanslüke and Schmidt (2004) for a numerical packing model that can result in grading curves for the filler and aggregate materials for mixtures with a minimised pore distribution.

The dense and high strength matrix results into a brittle material, with a higher brittleness than normal strength concrete. In order to overcome this defect and increase the deformation ability, fibres can be added. In most cases these are short straight steel fibres; since the maximum aggregate size is not greater than 8 mm, long steel fibres would decrease the homogeneity and density of the matrix. With the term 'long' steel fibres, fibre lengths greater than 20 mm are implied. Instead of steel fibres, organic or synthetic fibres can be used as well. For ultra high strength concretes, most common fibres are steel fibres with diameters between 0.1 and 0.2 mm and with a fibre length ranging between 3 and 20 mm.

In addition to the careful selection of the material components and their packing density, attention has to be given to the mixing procedure, preparation and curing of the concrete specimens in order to obtain a workable mixture with the desired strength properties in the hardened state. Without superplasticisers, these high strength mixtures cannot be produced with such a low w/c ratio and such a high volume of fine material. Most suitable are plasticisers on the basis of polyacrylates or

polycarboxylic ethers (Gay et al., 2003, Holschemacher and Dehn, 2003, Fehling et al., 2005, Richard and Cheyrezy, 1995); in this project, polycarboxylic ether based superplasticisers were exclusively used.

The very high volume of fines also counteracts the homogenisation during the mixing process. For this reason it is essential to use a concrete mixer with a high mixing intensity (Dehn, 2003, Orgass and Ma, 2004, Schachinger, 2000). It can be difficult for the entrapped air to escape in such a dense an compact matrix: in that case the use of vacuum mixers can be beneficial. The mixing time necessary for such mixtures is between 5 minutes and 15 minutes. A mixing time of more than 10 minutes can have as a consequence a high fresh state temperature and an accelerated stiffening of the mix, which reduces the time that the mixture stays workable. Different mixing procedures have been developed, but most researchers recommend to add the fibres after the superplasticiser has enabled a flowable and workable mixture. Often vibration is needed for compaction, and even if vibration is not needed, it is common that these mixtures have a reduced workability compared to normal strength self-compacting concrete. Recently also self-compacting ultra high strength mixtures with high flowability have been developed (Dietz and Ma, 2003). Heat treatment or confining pressure might be needed for the concrete to reach the desired compressive strength, especially when values of 200 MPa and more are targeted.

In the past decade, a number of mixtures have been developed both in university or state-owned laboratories, and in private laboratories of cement production or construction companies. The mixtures from the private sector have mostly been patented. The BSI/CERACEM, which is one of the mixtures used in this project, is such an industrial mixture. In the following, a brief list of available mixtures, mostly developed in the private sector, is given.

As already mentioned, there is the BSI/CERACEM (Maeder et al., 2004) which has been developed initially by the construction companies Quillery and Eiffage and developed further under the collaboration with the construction chemicals manufacturer Sika. It is a self-compacting, high strength mixture with steel or synthetic fibres up to 3.5 Vol.% with an average compressive strength of 200 MPa. It was already applied in beams for a nuclear power plant (Birelli et al., 1998), in prefab beam elements for road bridges (Hajar et al., 2004) and for the roof of the Millau toll gate (Thibaux et al., 2004). Lafarge, Bouygues and Rhodia introduced DUCTAL (Acker and Behloul, 2004). It contains either organic or steel fibres, reaches characteristic values of the compressive strengths of 150-180 MPa, and as its name implies, it shows a high deformation ability (for a cement-bound material). It is self-compacting in most cases, though vibration might be necessary occasionally. At the Laboratoire Central des Ponts et Chausées (LCPC), the CEMTEC$_{multiscale}$ (Rossi et al., 2005) has been developed which contains steel fibres in three different lengths at a total quantity of 11 % by volume, and reaches an average compressive strength of 220 MPa. At Cardiff University, mixtures with compressive strength 180-200 MPa

have been developed, reinforced with a combination of 6 and 13 mm long steel fibres, known as CARDIFRC (Benson and Karihaloo, 2006). This count is by no means a complete overview of all mixtures, as more mixtures are being developed and entering the market from different laboratories and universities.

All the above described mixtures were designed with the main aim to reach a high compressive strength, while the improvement of the tensile and flexural tensile strength was of secondary interest. Another, different group of fibre reinforced concretes has also been developed where instead of the compressive strength, the focus was set on improving the tensile load bearing capacity, and especially the tensile deformation capacity. These 'ductile' concretes are often called 'high performance fibre reinforced cementitious composites' (HPFRCC) (Li, 2004), with a specialised version of them being the so-called 'engineered cementitious composites' (ECC). Even though the mixtures used in this study were not designed with ECC criteria, but were aiming a high compressive strength, they do have a high deformation ability in tension and their properties show similarities to this group of high performance materials.

2.2 Materials used in this thesis

Four different cementitious composites have been used in this study. From now on, they will be referred to by the names as defined in the headings of the following four subsections, namely BSI/CERACEM, HSFRC, hybrid HSFRC and UHPC. Here, first a brief description of the raw materials used to compose them will be given, followed by a brief description of the mixing procedure. Since the main aim of the thesis is to examine the flexural behaviour in the hardened state under static and fatigue loading, and due to the fact that an experimental fatigue programme is very extensive in its duration, it was decided not to perform an extensive mix design and develop own mixtures, but to use existing ones if possible. Therefore, the HSFRC is the only mixture which was developed in this study (Lappa et al., 2003a), and even this mixture was mainly an adaptation of an existing mixture (Grünewald et al., 2000, Sato et al., 2000). All other mixtures have been developed by other researchers and have been used in this study without altering their material components or mixing procedure. This chapter intends to give an overview of the mixtures and their mixing procedure, and some results of their fresh state properties. However, indicatively the measured values of the compressive strength will also be mentioned, even though the hardened state results will be provided in Chapters 4 and 5, since the compressive strength values can be used for classification of the used materials. In this thesis, all mixtures will also be denoted as concretes, even though the HSFRC and hybrid HSFRC can also be classified as mortars, since they have a maximum aggregate size of not more than 2 mm. The term concrete is used

for these two mixtures since it is more appropriate for the intended applications of the materials in structures.

2.2.1 BSI/CERACEM

The BSI/CERACEM is a commercially available mixture, composed out of the patented premix CERACEM B1M2.5U1D7, developed by the companies Sika and Eiffage. The premix is made out of a white Portland cement, microsilica and aggregates with a maximum diameter of 7 mm. Indicatively, the percentages of cement, microsilica and aggregates contained in the premix are 47%, 7% and 45% respectively. 195 kg/m^3 of steel fibres (2.5% by volume), 195 kg/m^3 of water and 44.6 kg/m^3 of a polycarboxylic ether based superplasticiser are added to 2355 kg/m^3 of the premix to result in a self-compacting concrete mixture. The steel fibres are straight with a round cross-section of 0.3 mm in diameter, and have a total length of 20 mm. They are normal strength steel fibres, this implies a tensile strength of at least 1250 MPa. All ingredients were kindly delivered to Delft University by SIKA.

This mixture is one of the commercially available 'special industrial concretes', BSI (Beton Spécial Industriel) and this special mixture has already found some industrial applications. The most well-known application so far is the roof of the toll building of the Millau viaduct in the south of France (Thibaux et al., 2004). For this roof, precast elements of this material were constructed to form a thin, helically shaped roof. The elements contained only prestressing strands and steel fibres as reinforcement, and no additional rebars. In that way, a slender and elegant structure could be created.

Regarding the strength, this mixture is the only one of the mixtures cast in the Stevin Laboratory in Delft for this project that can be classified as ultra high strength concrete, with a compressive strength greater than 200 MPa. Regarding the material performance in the hardened state, and therefore also individual strength values, more detailed information will be given in Chapter 4.

Figure 2.2 shows an image of a sawn part of the mixture in order to provide an impression of its appearance in the hardened state; the cement matrix, the coarse aggregates and the steel fibres are visible.

2.2.2 HSFRC

The high strength steel fibre reinforced concrete (HSFRC) is composed of 358 kg/m^3 Portland cement CEM I 52.5R, 555 kg/m^3 blast furnace slag cement CEM III/A 52.5, 61 kg/m^3 microsilica, 1067 kg/m^3 sand with a maximum aggregate size of 2 mm, 17.9 kg/m^3 polycarboxylic-ether based superplasticiser, 207 kg/m^3 water and 125 kg/m^3 (1.6% by volume) steel fibres. The fibres are 13 mm long, straight with a round cross-section of 0.16 mm in diameter. They are high strength fibres, which have a tensile strength of at least 2000 MPa.

This mixture can be classified as a high strength (and not ultra high strength) fibre reinforced concrete with respect to its compressive strength, which shows a

characteristic value of 100-110 MPa and an average value of 145 MPa tested with cubes of 100 mm length. The mixture is the main mixture of the research, and has been studied in detail. As will be shown later, numerous tests on beams of different dimensions, notched and un-notched, and also uniaxial tensile tests have been performed, that give a good overview of the structural material behaviour. Regarding the development of the mixture and its composition, more detailed information can be found in Lappa et al. (2003b).

Figure 2.3 shows the mixture's appearance in the hardened state: the cement matrix and fibres are visible.

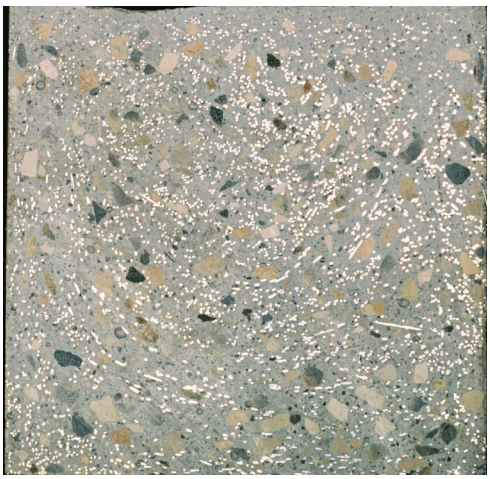

Figure 2.2: BSI/CERACEM in the hardened state, beam cross section of 125x125 mm.

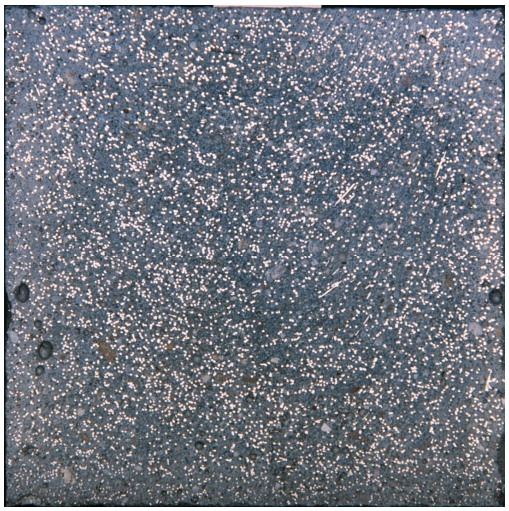

Figure 2.3: HSFRC in the hardened state, beam cross section of 125x125 mm.

2.2.3 Hybrid HSFRC

The hybrid high strength steel fibre concrete (hybrid HSFRC) is composed of 996 kg/m^3 blast furnace slag cement CEM III/A 52.5N, 32 kg/m^3 microsilica, 12 kg/m^3 polycarboxylic-ether based superplasticiser, 1040 kg/m^3 sand with a maximum aggregate size of 0.5 mm and 198 kg/m^3 water. The mixture is called 'hybrid' since it contains two different types of steel fibres: 39 kg/m^3 (0.5% by volume) of straight, 13 mm long steel fibres with a diameter of 0.2 mm and 79 kg/m^3 (1% by volume) of 60 mm long, hooked-end steel fibres with a round cross-section of 0.75 mm in diameter. Both fibre types are high strength fibres with a tensile strength of at least 2000 MPa. The fibres of this mixture and the HSFRC were kindly provided by the company Bekaert.

This mixture was developed by Markovic (2006) and it forms part of a number of hybrid fibre concretes that were developed in his PhD research. As will be shown in the following chapters, the combination of short and long fibres provides an excellent combination of strength increase and strain hardening in the pre-peak part of the stress-strain material curve, due to the microcrack bridging action of short fibres, and an improved load-bearing capacity in the post-peak part due to the macrocrack bridging action as provided by the longer fibres. A more detailed analysis of the combined fibre action of the two fibre types can be found in the PhD thesis (Markovic, 2006).

Also this mixture can be classified as a high strength concrete, with a characteristic compressive strength value of approximately 110 MPa, and an average value of 130 MPa as tested with cubes with a length of 100 mm. As a final remark, the term 'hybrid' might be more appropriate as used by other researchers in order to classify concretes that have a combination of two different fibre materials, for example a combination of polyvinyl alcohol fibres and steel fibres. Since this mixture was developed by Markovic and he consistently used the term 'hybrid' to classify it, this terminology will be applied in this study as well.

Figure 2.4 shows the mixture in the hardened state: the cement matrix, and both types of steel fibres. The short ones are visible as small dots. The long ones, which are thicker, are visible as larger areas on the image.

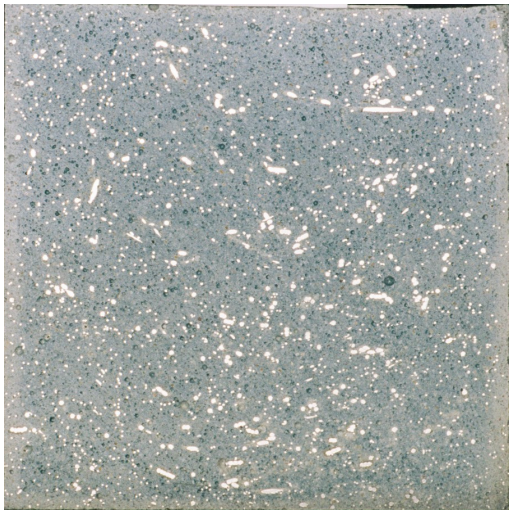

Figure 2.4: Hybrid HSFRC in the hardened state, beam cross section of 125x125 mm.

These three mixtures are the main mixtures used in this thesis and their composition is summarised in Table 2.1.

Table 2.1: Compositions of the three main mixtures in this study

Components	BSI/CERACEM [kg/m^3]	HSFRC [kg/m^3]	hybrid HSFRC [kg/m^3]
Premix B1M2.5U1D7	2355		
CEM I 52.5R		358	
CEM III/A 52.5		555	996
Microsilica		61	32
Sand 0-0.5mm			1040
Sand 0-2mm		1067	
Steel fibres 20/0.3	195		
Steel fibres 13/0.16		125	
Steel fibres 13/0.2			39
Steel fibres 60/0.75			79
Superplasticiser	44.6	17.9	12
Water	195	207	198

2.2.4 UHPC

Another ultra high performance concrete has been tested within this project, with a limited number of tests. This is a mixture developed and produced by the concrete technology laboratory of the University of Karlsruhe in Germany by Scheydt (2004). The use of this concrete is within the scope of a collaboration between Delft and Karlsruhe on the durability and fatigue of such concrete mixtures, and in that aspect beams were cast at both laboratories to be tested under a combined freeze-thaw or chloride attack and fatigue loading. Since this mixture was always cast at Karlsruhe

University and only the hardened state material properties were tested in Delft, no information on the fresh state properties is given here. Worth mentioning however is the fact that this mixture, unlike the previous three, was not an entirely self-compacting mixture and therefore external vibration has been used to compact the concrete of the test specimens.

The concrete considered is a rather coarse ultra high performance concrete with basalt aggregates with a maximum aggregate size of 8 mm. It is composed of 583 kg/m^3 of a Portland cement CEM I 52.5R HS/NA, 178 kg/m^3 microsilica, 715 kg/m^3 coarse basalt aggregate 2-8 mm, 356 kg/m^3 quartz sand and 459 kg/m^3 fine and ultra fine quartz powder filler, together with 196 kg/m^3 of (normal strength) straight steel fibres with a length of 8 mm and a diameter of 0.175 mm, 32 kg/m^3 superplasticiser and 136 kg/m^3 added water. The fibre volume equals 2.5%.

The compressive strength reaches values above 200 MPa after a 7-day heat treatment or 190 MPa (average value of 150 mm cubes) after a 28-day storage under water. In Chapter 4 detailed information on the strength values of these mixtures are given.

2.3 Mixing procedure and fresh state characteristics

2.3.1 Mixing procedure

Before mentioning the mixing procedure of the three mixtures cast in the Stevin laboratory, it has to be mentioned that two different concrete mixers were used during the project, since a newer mixer was obtained while the experimental testing programme was in progress. Initially, a forced pan type mixer (Zyklos) was used, with a maximum capacity of 120 litres. Later on, an intensive pan laboratory mixer (Eirich) was used with a maximum capacity of 150 litres. With both mixer types, the volume of a batch needed to prepare the tests specimens was usually between 60 and 70 litres.

The mixing procedure of the BSI/CERACEM was as follows (Figure 2.5): First, the premix was briefly mixed. Then the water was added, followed by the superplasticiser and at last the steel fibres. After 12 minutes of mixing, the fresh state properties were tested: the temperature of the fresh mix, the air content and the slump spread, determined with a cone of 200 mm height, 130 mm top diameter and 200 mm bottom diameter, were measured. The slump spread should be around 600 mm two minutes after the removal of the cone, and the air content below 3%. All BSI/CERACEM beams for the initial static and fatigue testing series were cast with the forced pan type mixer. Only the beams cast for the joint durability/fatigue experiments were produced with the intensive pan mixer. The mixing procedure was not altered between the two mixer types and no significant differences were noted in

the fresh state material properties that were depending on which mixer type was used.

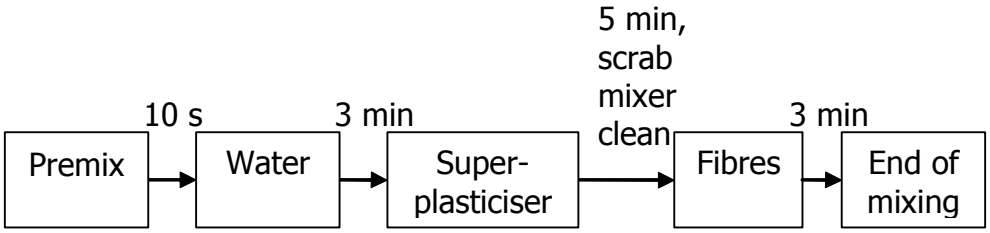

Figure 2.5: Mixing procedure of the BSI/CERACEM

Only the specimens for the notched three point bending tests of the HSFRC were cast with the forced pan type mixer. All other test specimens were cast with the intensive pan mixer. The latter was used to cast all hybrid HSFRC specimens tested in this study. Markovic (2006), however, cast specimens for notched three point bending tests and uniaxial tensile tests with the forced pan type mixer, also the hybrid HSFRC mixture of this study. Once again, no significant difference was found between the two mixers for the same mixing procedure. The mixing procedure was similar for the two HSFRC mixtures: The dry materials were briefly mixed first, then the water and superplasticiser were added, followed by the microsilica slurry suspension and at last the steel fibres. The total mixing time was shorter than for the BSI/CERACEM, namely 5-7 minutes (Figure 2.6). It has to be noted that for the hybrid HSFRC, a batch of 70 litres provided some difficulty in the intensive pan mixer due to the high content of fine solid materials. Therefore, only half of the sand was added initially and the remaining sand was added just before the steel fibres, when the mixture in the mixer had become flowable. In the fresh state, for both mixtures the slump spread was tested, just like for the BSI/CERACEM but with a cone of different dimensions, namely a height of 300 mm, a top diameter of 100 mm and a bottom diameter of 200 mm. The slump spread should be around 700 mm, and the air content around 3% for both mixtures.

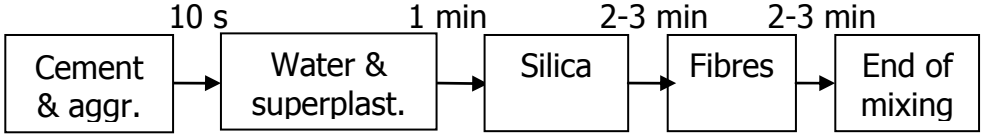

Figure 2.6: Mixing procedure of the two HSFRCs

2.3.2 Fresh state properties

Even though this thesis focuses on the hardened state and not the fresh state properties of high strength fibre concretes, the fresh state properties are important and can influence the fibre orientation and fibre distribution and therefore influence

significantly the material behaviour in the hardened state. The exact influence of the fresh state properties on the hardened material behaviour will be discussed in Chapters 4 and 5 together with the results in the hardened state. Compared to research on self-compacting concrete, where numerous tests are performed to test a lot of different parameters in the fresh state, in this study only a limited number of parameters has been determined, for quality control of the mixtures, with the main one being the slump spread.

Figure 2.7 shows the slump spreads of the three mixtures. It can be seen that the appearance of the BSI/CERACEM differs significantly from the other two HSFRCs. While a rather uniform slump spread was observed for the HSFRC with a uniform fibre distribution, this is not the case for the BSI/CERACEM, where a high fibre concentration was observed in the middle part just below the position of the original cone before it was lifted, and almost no fibres were found at the edges. This indicates that the mixture in the fresh state is less stable (regarding the embedment of fibres and aggregates) and more prone to segregation. Also, during the casting process the BSI/CERACEM is more viscous and less flowable than the other two mixtures. However, this is the mixture with the highest fibre content, and it is expected that such a fibre content would also reduce the workability and flowability of the other two mixtures as well, although possibly to a lesser extent. As far as the two HSFRCs are concerned, which have similar fresh state properties, the HSFRC is slightly better flowable than the hybrid HSFRC. The hybrid HSFRC is very workable just after casting but a short period of time after mixing it forms a 'skin' at the top surface which reduces the flowability. On average, the slump spread of the BSI/CERACEM was around 600-650 mm, and that of the two HSFRCs was 700-750 mm. However, as mentioned before, these values were determined by cones of different dimensions.

BSI/CERACEM HSFRC Hybrid HSFRC

Figure 2.7: Appearance of the slump spread of the three mixtures.

The mixtures cast in the Stevin Laboratory were all self-compacting, and for self-compacting concrete a variety of test methods have been developed in order to test different properties in the fresh state, such as the flowability, the ability to flow along obstacles (reinforcing bars) and the stability with respect to segregation (Bartos,

2005). Since in the scope of this research the focus was set on the hardened state properties, mainly the slump spread and the flow time T_{50}, that is the time needed in order to reach a slump spread of 50 cm, were measured during casting. In a smaller preliminary mixture optimisation test series, more tests have been performed for the determination of the fresh state properties, such as the V-funnel flow time test and the U-box for the flow between obstacles. Results of this study can be found elsewhere (Lappa et al., 2003b).

References

ACKER, P. & BEHLOUL, M. (2004) DUCTAL Technology: a large spectrum of properties, a wide range of applications. IN SCHMIDT, M., FEHLING, E. & GEISENHANSLÜKE, C. (Eds.) *International Symposium on Ultra High Performance Concrete.* No. 3 ed. Kassel, Kassel University Press GmbH.

BARTOS, P. J. M. (2005) Testing-SCC: Towards new European Standards for fresh SCC. IN YU, Z., SHI, C., KHAYAT, K. H. & XIE, Y. (Eds.) *SCC'2005-China: 1st International Symposium on Design, Performance and Use of Self-Consolidating Concrete.* Changsha, Hunan, China, RILEM publications S.A.R.L.

BENSON, S. D. P. & KARIHALOO, B. L. (2006) CARDIFRC - Development and mechanical properties. Part I: Development and workability. *Magazine of Concrete Research,* 57**,** 347-352.

BIRELLI, G., CADORET, G., DUTALLOIR, F. & THIBAUX, T. (1998) A new, very high performance concrete. *High Performance and Reactive Powder Concrete.* Sherbrooke, Canada.

DE LARRARD, F. & SEDRAN, T. (1994) Optimization of Reactive Powder Cocretes. *Cement and Concrete Research,* 25**,** 997-1009.

DEHN, F. (2003) Herstellung, Verarbeitung und Qualitätssicherung von UHPC. *Ultrahochfester Beton. Planung und Bau der ersten Brücke mit UHPC in Europa. Tagungsbeiträge zu den 3. Kasseler Baustoff-und Massivbautagungen.* Kassel.

DIETZ, J. & MA, J. (2003) Selbstverdichtender Ultrahochleistungsbeton. IN KÖNIG, G., HOLSCHEMACHER, K. & DEHN, F. (Eds.) *Ultrahochfester Beton.* Leipzig, Bauwerk Verlag GmbH.

FEHLING, E., SCHMIDT, M., TEICHMANN, T., BUNJE, K., BORNEMANN, R. & MIDDENDORF, B. (2005) *Entwicklung, Dauerhaftigkeit und Berechnung Ultrahochfester Betone (UHPC). Forschungsbericht DFG FE 497/1-1*, Kassel University Press GmbH, Kassel.

GAY, M., KLEEN, E. & NIEPMANN, D. (2003) Zusatzmittel für Ultrahochleistungsbeton. IN KÖNIG, G., HOLSCHEMACHER, K. & DEHN, F. (Eds.) *Ultrahochfester Beton.* Leipzig, Bauwerk Verlag GmbH.

GEISENHANSLUEKE, C. & SCHMIDT, M. (2004) Methods for Modelling and Calculation of High Density Packing for Cement and Fillers in UHPC. IN SCHMIDT, M., FEHLING, E. & GEISENHANSLUEKE, C. (Eds.) *International Symposium on Ultra High Performance Concrete.* No. 3 ed. Kassel, Germany, Kassel University Press GmbH.

GRÜNEWALD, S., BOLO, T., VAN DER VEEN, C. & WALRAVEN, J. C. (2000) Performance-based design of a high strength self-compacting fibre reinforced mortar. *Stevin-report no 25.5-01-30.* Delft University of Technology.

HAJAR, Z., LECOINTRE, D., SIMON, A. & PETITJEAN, J. (2004) Design and construction of the world first ultra-high performance concrete road bridges. IN SCHMIDT, M., FEHLING, E. & GEISENHANSLÜKE, C. (Eds.) *International Symposium on Ultra High Performance Concrete.* No. 3 ed. Kassel, Germany, Kassel University Press GmbH.

HOLSCHEMACHER, K. & DEHN, F. (2003) Ultrahochfester Beton - Stand der Technik und Entwicklungsmöglichkeiten. IN KÖNIG, G., HOLSCHEMACHER, K. & DEHN, F. (Eds.) *Ultrahochfester Beton.* Leipzig, Bauwerk Verlag GmbH.

LAPPA, E. S., VAN DER VEEN, C. & WALRAVEN, J. C. (2003a) Self-compacting, high strength steel fibre reinforced mortar for pre-cast sheet piles. IN WALLEVIK, O. & NIELSSON, I. (Eds.) *3rd International Symposium on Self-Compacting Concrete.* Reykjavik, Iceland, RILEM Publications S.A.R.L.

LAPPA, E. S., VAN DER VEEN, C. & WALRAVEN, J. C. (2003b) High strength, self-compacting steel fibre reinforced mortar for precast sheet piles. Delft University of Technology.

LI, V. (2004) Strategies for High Performance Fiber Reinforced Cementitious Composites Development. IN AHMAD, S., DI PRISCO, M., MEYER, C., PLIZZARI, G. A. & SHAH, S. (Eds.) *Fiber reinforced concrete from theory to practice.* Bergamo, Italy, Starrylink Editrice Brescia.

MAEDER, U., LALLEMANT-GAMBOA, I., CHAIGNON, J. & LOMBARD, J. P. (2004) Ceracem, a new high performance concrete: characterisations and applications. IN SCHMIDT, M., FEHLING, E. & GEISENHANSLÜKE, C. (Eds.) *International Symposium on Ultra High Performance Concrete.* No. 3 ed. Kassel, Germany, Kassel University Press GmbH.

MARKOVIC, I. (2006) High-Performance Hybrid-Fibre Concrete - Development and Utilisation. *PhD Thesis.* Delft University of Technology.

ORGASS, M. & MA, J. (2004) Ultrahochfester Beton (UHFB) -Entwicklungs- und Forschungsarbeiten. *Beitrag zur VDB Regionaltagung.* Hardheim.

RICHARD, P. & CHEYREZY, M. (1995) Composition of reactive powder concretes. *Cement and Concrete Research,* 25**,** 1501-1511.

ROSSI, P., ARCA, A., PARANT, E. & FAKHRI, P. (2005) Bending and compressive behaviours of a new cement composite. *Cement and Concrete Research,* 35**,** 27-33.

SATO, Y., VAN MIER, J. G. M. & WALRAVEN, J. C. (2000) Mechanical characteristics of multimodal fibre reinforced cement based composites. IN ROSSI, P. & CHANVILLARD, G. (Eds.) *International RILEM symposium on Fibre Reinforced Composites (BEFIB 2000).* Lyon.

SCHACHINGER, I. (2000) Untersuchungen an Hochleistungs-Feinkorn-Beton. *Beiträge zum 38. Forschungskolloquium des DAfStB.* München.

SCHEYDT, J. (2004) Dauerhaftigkeit von ultrahochfestem Beton. *Institut für Massivbau und Baustofftechnologie.* Karlsruhe University.

THIBAUX, T., HAJAR, Z., SIMON, A. & CHANUT, S. (2004) Construction of an ultra-high-performance fibre-reinforced concrete thin-shell structure over the Millau viaduct toll gates. IN M. DI PRISCO, R. F., G.A. PLIZZARI (Ed.) *6th International RILEM Symposium on Fibre Reinforced Concrete (FRC), BEFIB 2004.* Varenna, Lake Como, RILEM Publications S.A.R.L.

3.

Development of an experimental programme for static and fatigue loading

After introducing the materials used in this work, the experimental programme will be given in detail. The experiments form a major part of this work. The conducted experiments give insight in the tensile and especially flexural tensile behaviour of high strength fibre reinforced composites, the influence of a notch on the test results and the relation between bending tests of different dimension and uniaxial tension tests. The main experimental programme consisted of static and fatigue four point bending tests with all three mixtures on un-notched beams. For the HSFRC mixture, also three point bending tests on notched beams, four point bending tests on notched beams under static and fatigue loading conditions, and uniaxial tensile tests were performed. The setup of all tests is explained here, while the test results will be given in the following two chapters.

3.1 Experimental programme

In order to test the structural behaviour of high strength mixtures, an experimental programme of static and fatigue bending tests on the three mixtures was conducted, with the main testing method being the four-point bending test (for static and fatigue loading) on un-notched beam specimens. This method was applied to all three mixtures. The HSFRC mixture with 1.6% by volume of 13 mm long steel fibres is the main mixture of this thesis and has been tested at a greater extent; for this mixture, also three point bending tests on notched beams, uniaxial tensile tests, and four point bending tests on notched beams have been carried out. An overview of the complete experimental programme is included in Table 3.1, and in the following sections the preparation of the test specimens and detailed descriptions of all the test set-ups will be presented.

Table 3.1: Overview of the complete experimental programme.

	Method	Dimensions	Mixtures	Aim
Compression	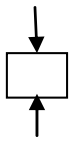	100 mm cubes	All mixtures	Compressive strength 28d; quality control of concrete
	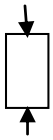	Prisms 100 /100 /400mm	HSFRC only	E-Modulus; Compressive strength; σ-ε diagram in compression
Tension	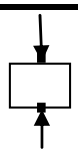	100 mm cubes	All mixtures	Splitting tensile strength; quality control of concrete
	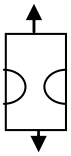	dogbone specimens 140/100/70	HSFRC only	Uniaxial tensile strength; σ-ε diagram in tension
Bending	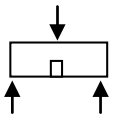	150/150/600mm; 25mm notch	HSFRC only	Static flexural tensile strength (preliminary testing series)
	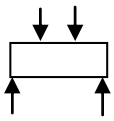	125 /125 /1000mm	All mixtures	Static and fatigue tests.Load-deflection diagram; multiple cracking evaluation; fatigue behaviour (S-N curve)
	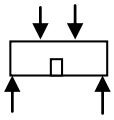	125 /125 /1000mm; 20mm notch	HSFRC only	Static and fatigue tests. Load-crack opening relation; strains compressive zone.
	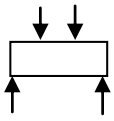	joint research Delft-Karlsruhe	BSI/CERACEM and UHPC	Combined durability / fatigue experiments

Preparation of the test specimens

If not stated otherwise, the following procedure was applied for the preparation of test specimens. The specimens were cast into steel moulds of the desired dimensions (see Figure 3.1, moulds for the four point bending tests). Almost all test specimens were cast from one end of the mould, therefore allowing the concrete to flow ('flow method'). All mixtures were self-compacting: no vibration was necessary for compaction in the moulds. Only for a number of beams of the BSI/CERACEM mixture, a different casting method, which reduced the concrete flow, was examined additionally. With this method, the concrete was poured from the bucket in small patches into the mould, while the bucket was moved along the mould, so that the fresh concrete entered the mould at different places and the flow of the concrete from one end to the other was significantly reduced. Beams cast with this method were only tested under static loading. After evaluating the results of the static tests of the specimens cast with these two methods, it was decided to cast all fatigue specimens with the first method, the 'flow' method, for the main reason that this method had shown a lower material scatter in the static tests. Since fatigue experiments by nature exhibit a significant scatter, it was anticipated that when keeping the scatter of the static material strength as low as possible this would have beneficial effect regarding the scatter in fatigue experiments.

Figure 3.1: Moulds for the four point bending tests filled with BSI/CERACEM.

After the concrete was placed into the moulds and its surface was leveled off, a thin plastic sheet was placed on its top in order to prevent drying of the outer concrete surface. The specimens were removed from their moulds one day after casting and placed into a fog room at 95-100% relative humidity (RH) and ±20°C until an age of 23-25 days when they were placed in the laboratory at room

temperature conditions, 60 RH and 20°C. In the lab, they were prepared for testing and were tested at an age of 28±1 days in case of static testing. Specimens intended for fatigue loading were cast at a minimum age of 28 days, but the actual day of testing varied and could be up to 90 days. This is due to the fact that the duration of one fatigue test could be up to 10 days. Specimens of the same age were all removed from the fog room at an age of approximately 25 days and were kept in the laboratory until they were tested. The first two beams of this series were tested at an age of 28 days. The remaining beams were placed into the setup and were tested as soon as soon as the testing of the previous beams was finished. Depending on the amount of load repetition a beam could survive, the next beam could be placed into the setup the earliest one day after the previous beam and the latest 10 days after. The age of the beam (within this timeframe), however, was considered to have a negligible influence on the static strength. The strength development of a beam in the timeframe of 28-90 days will be discussed further in Chapter 4.

It should be noted that the beams were cast in batches of 65 litres, which is a reasonable quantity for the available laboratory mixer. With the chosen beam dimensions only three beams could be cast from one batch; therefore, it was impossible to have fatigue tests and static tests out of the same batch and the fatigue upper load level had to be in accordance of the average static strength of a different batch. In order to evaluate the reproducibility and the scatter in the static strength, always more than three beams were tested statically, implying that at least two batches of the same mixture were tested and the average of two batches was used to set the upper fatigue load level. The variation in strength between individual batches was found to be not too high in terms of scatter.

Only for the uniaxial tensile tests with the HSFRC mixture, timber moulds instead of steel moulds were used, as can be seen in Figure 3.2. These moulds were available in the lab from the research of Markovic (2006). Curing conditions for these specimens were identical to those of the beams; more information on the preparation of these tensile test specimens is given in Section 3.4.

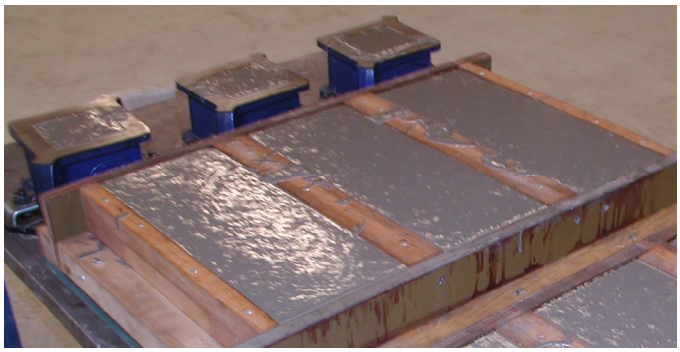

Figure 3.2: Timber moulds for the dogbone tensile HSFRC specimens.

3.2 Four point bending tests

The four point bending test is the main test method used in the scope of this thesis, mainly on un-notched beams. Initially, one testing frame was erected in the Stevin laboratory, and eventually two parallel frames were erected for fatigue testing which proved to be very efficient since fatigue tests need a significant testing time. The test setup can be seen in Figure 3.3.

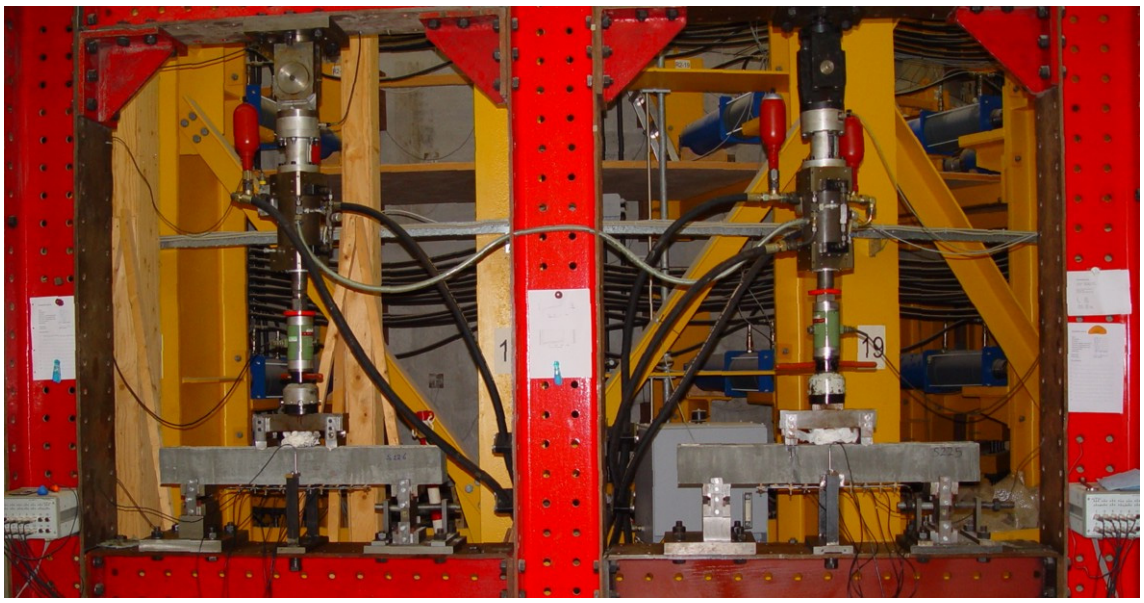

Figure 3.3: Overview of the experimental setup for the four-point bending tests.

3.2.1 Static tests

Tests on un-notched beams

A stiff steel test frame was used for the four point bending tests. The specimens were supported on steel bearings, one of them fixed and the other one being a roller support that allowed horizontal movements and rotation to occur freely, so that a restrained deformation due to torsion was avoided. The support load was distributed over 90 mm (width of the supporting steel plate). The beam dimensions were 125/125/1000 mm and the beams were tested at a span of 750 mm (Figure 3.4), loaded at their third points, meaning that a distance of 250 mm between the loading points was kept. The beam dimensions were chosen to be in analogy with the beams in the RILEM regulations for steel fibre reinforced concrete (TC162-TDF, 2002); there, beams are tested with a three point bending test at a span of 500 mm, have a cross-section of 150x150 mm with a 25 mm deep notch, so that an equal ligament height to the beams in the four point bending tests was obtained. Another common point between the four point bending tests and the test as described in the RILEM

recommendations is the distance between the loading points, in both cases being 250 mm.

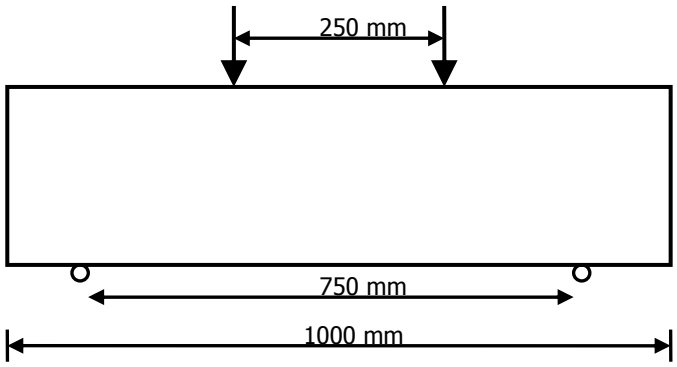

Figure 3.4: Beam dimensions for the four point bending test. Beams have a 125 mm square cross section; in case of notched tests, a 20 mm notch was cut at midspan.

The load was applied via a loading jack and measured by a load cell; the loading jack applied the force to a steel plate which distributed the load into the beam at a 250 mm distance. The load cell had a capacity of 100 kN. A hinge above the load cell prevented restrained deformations due to torsion. The beams were placed into the frame in the direction they were cast, meaning that the top surface during casting was the top surface of the experiment. At the top surface, two steel platens were glued on to the beam with a width of 40 mm, that distributed the applied load onto it.

The registered mid-span deflection was used as a control value for the static testing in a closed loop system. In order to measure the deflection, two LVDTs (linear variable displacement transducers) were placed at the bottom fibre at midspan at both sides of the beam. These LVDTs could register a maximum displacement of 10 mm. The average signal of the two was used to control the experiments, at a loading speed of 20µm/s. The deflection was measured as the registered vertical displacement of the bottom fibre with respect to the steel frame. A steel guiding frame was fixed to the testing frame on which the two LVDTs were placed. Two small steel strips were glued to the bottom fibre of the beam on which the LVDTs were placed to register deflections. It has to be noted that with this setup, if the crack occurs exactly at midspan, the glued steel strips could fall off and hinder the registering of the deflections. In case both steel strips would fall off simultaneously during a static deformation-controlled test, the test would abruptly be stopped. This however never happened during the experiments, since the steel strips also strengthen that part of the beam and therefore the major crack always formed next to the strips. The reason for choosing this guiding frame, rather than a glued frame around the beam to support the LVDTs, lies in the fact that such a frame would hinder a free deformation of the beam at repetitive loading at the chosen

frequency. It should be noted that two separate strips were glued to the beam and not a continuous one; this implies that still the crack can occur directly at midspan, and therefore will always be allowed to form at the weakest cross-section of the beam between the two loading points. With this setup, extraneous deformations are included, which can lead to an overestimation of deflections, which especially regards their initial values, while this difference diminishes for larger deflection values. This phenomenon is discussed with detail by Balaguru and Shah (1992). In any case, the fact that larger initial deflections could be measured with this setup is acknowledged but could not be avoided in this study since a different LVDT placement would hinder the operation of the fatigue tests.

Another set of a total of eight LVDTs was placed at the bottom fibre of the beam to measure the longitudinal displacement (and, indirectly, the total crack openings). Each LVDT could register a maximum displacement of 10 mm and was placed with a measuring length of 100 mm. There was an overlap of 50 mm between two adjacent LVDTs. Since the major crack after the peak load could form at a variable distance between the two loading points and was not predefined with a notch, it could happen that the crack formed directly under one of the fixation points of the LVDT glued to the beam and could therefore cause an LVDT to fall off; due to the 50 mm overlap at least one of the adjacent LVDTs would still register the displacements over the formed crack in case that happened. With this arrangement, the major crack could always be monitored. The total distance covered by these LVDTs was 450 mm around midspan. Figure 3.5 shows a beam in the testing frame and the LVDTs placed to register displacements. Also the auxiliary steel frame for the placement of the two LVDTs that measured the deflections is shown.

Tests on notched beams

For a limited number of tests on the HSFRC mixture only, notched four point bending tests were carried out. A 20 mm deep notch was cut at midspan with a diamond-edged saw. The notch depth was chosen to be 20 mm, so that the analogy between the notch and the ligament height (20/105) was similar to the same analogy in the RILEM three point bending tests (25/125). The deflections were measured in the same way as in the un-notched tests. The steel strip glued at the bottom fibre of the beam to support the tip of the LVDT was in that case glued just next to the notch, and again the average deflection signal served as a control signal for the deformation-controlled tests. The loading speed was kept at 20 μm/s.

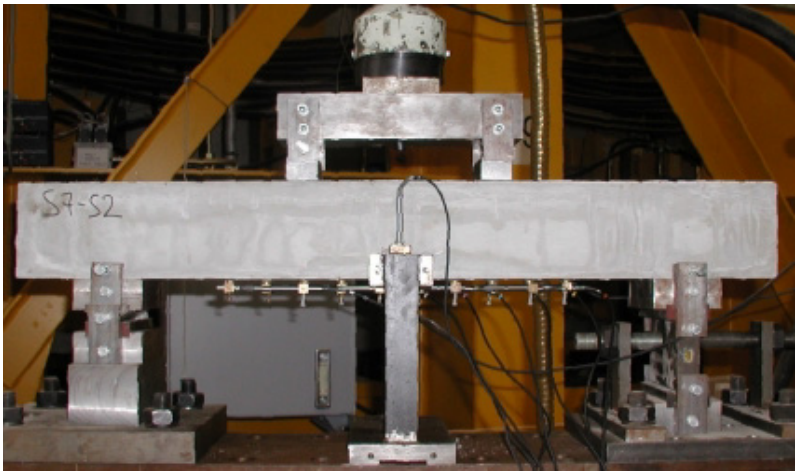

Figure 3.5: Beam in the testing frame for the four point bending tests. Visible are the load cell, the steel plate distributing the load onto the beam, the LVDT registering the deflection at midspan and its fixation system as well as the 8 LVDTs measuring the longitudinal elongation at the bottom fibre.

Since the notch predefines the crack formation, crack openings can be measured directly. Therefore, instead of placing LVDTs at the bottom fibre of the beam, four LVDTs were placed at both sides of the beams to measure the crack openings at the notch mouth and 10 mm above the notch mouth (this measurement will be referred to as 'notch tip' from now on) over measuring lengths of 100 mm. Additionally, two LVDTs were placed 30 mm below the top surface to register the displacements in a zone that experiences the transition from initially compressive and later tensile displacements. Two LVDTs with a larger accuracy that can register displacements up to 2 mm were placed at the top fibre of the beam to register the displacements in the compressive zone, again with a measuring length of 100 mm. Figure 3.6 shows the arrangement of the LVDTs on one side of the beam for the notched four-point bending tests; the same arrangement is placed at the back side of the beam.

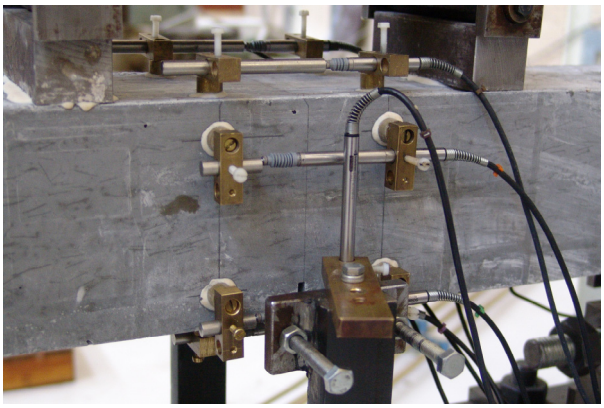

Figure 3.6: LVDT-placement for a notched four-point bending test.

3.2.2 Fatigue tests

The fatigue tests were in general performed on un-notched beams in the same testing frame and with the LVDTs arranged as already described for the static tests. Only for the HSFRC a limited series of notched fatigue tests was carried out in order to gather more information on the strain distribution and critical crack openings at fatigue failure; also in that case the same testing frame and LVDT arrangement was used as for the notched static tests. The testing procedure and data acquisition was identical for both notched and un-notched tests and will be described in the following.

The fatigue tests were load-controlled tests. Two load levels, a lower and an upper one, were predefined before each test. The upper value F_{max} was a certain percentage of the previously determined average static maximum load F_{static} for each mixture. The lower load value F_{min} was kept constant at 20% of the upper load value, meaning that the ratio R of the lower to the upper load was kept constant at 0.2 throughout the complete testing series. The load was applied gradually until the average, F_m, of the two levels and then a sinusoidal load was applied between these: a schematic representation of the applied load during a fatigue test is given in Figure 3.7. The testing frequency was 10 Hz. The chosen upper load levels for testing ranged between 50-90% of the average maximum static peak load, however most of the tests were performed in the range between 60-80%. An overview of all beams tested at different load levels for all three mixtures, including the notched HSFRC tests, is given in Table 3.2.

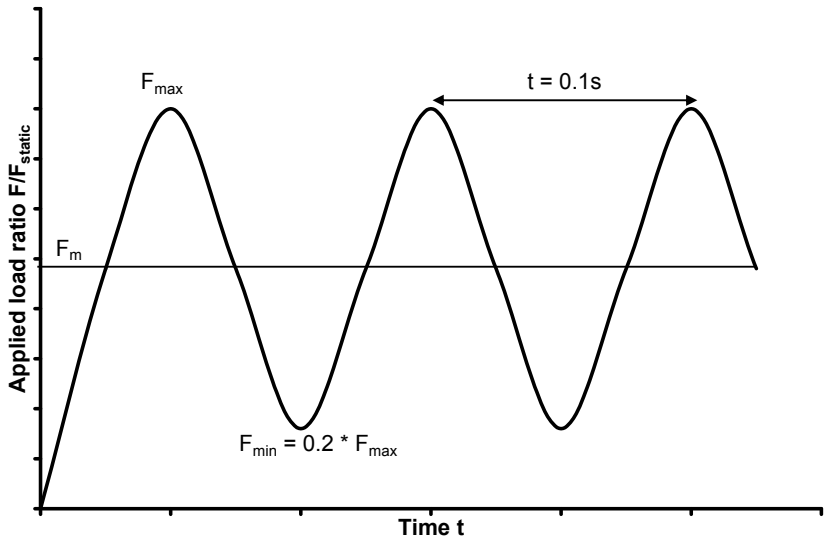

Figure 3.7: Schematic representation of the applied fatigue load.

A data acquisition computer programme was written in order to control the experiments and to obtain the measured displacements. Alarms were set that

stopped the testing if deformations exceeded pre-set limitations, or if the hydraulic pressure of the loading jack decreased. The average value and the amplitude of the registered displacement were saved once every minute (approximately every 600 load repetitions). The last values registered in case a test was stopped due to failure or a predefined number of load cycles where additionally saved.

Table 3.2: Overview of the fatigue experiments. The ratio R between the lower and the upper load level was kept constant at 0.2 for all tests.

	Beams tested per load level			
Upper load level	**BSI/CERACEM**	**HSFRC**	**hybrid HSFRC**	**notched HSFRC**
55%	5			
60%			6	3
65%	8		4	
70%	6	7	6	3
75%	5	4	6	
80%	6	7 (&3 at f=2Hz)	6	3
85%		7		
90%		6		

3.2.3 Combined durability-fatigue tests

Beams for bending tests and durability tests and cubes for standard strength tests were cast for a combined durability-fatigue testing programmes at the universities of Karlsruhe and Delft. In Delft, specimens were cast of the BSI/CERACEM mixture, while in Karlsruhe UHPC specimens were prepared; details on the mixtures found in Chapter 2. A brief overview of the experimental programme with regard to the tests on the beams is given in the following.

BSI/CERACEM beams

18 beams were prepared, consisting of: 6 beams for preliminary static and fatigue tests, 3 reference beams that were directly sent to Karlsruhe for freeze/thaw testing, 3 reference beams that were tested in Karlsruhe for chloride attack, 3 beams that were first subjected to 2 million load cycles at a load level of 50% of the average static material strength and where afterwards subjected to freeze/thaw cycles in Karlsruhe, and 3 beams that were also first subjected two 2 million load cycles at a load level of 50% and then subjected to chloride attack in Karlsruhe.

UHPC beams

12 beams were prepared, consisting of: 3 reference beams that were sent to Delft and were tested statically, 3 reference beams that were subjected to fatigue loading at upper load levels of 50%, 60% and 70% of the average static material strength, and 6 beams that were initially subjected to freeze/thaw cycles at Karlsruhe University and afterwards were sent to Delft for static reference testing of two

beams and fatigue testing of the other four beams at upper load levels of 50%, 60% and 70%. The beams subjected to fatigue loading, were first tested at an upper load level of 50% until failure or 2 million load cycles. In case they survived 2 million load cycles, then the upper load level was increased to 60%, and the beam was again tested until a maximum of 2 million load cycles. In case 2 million load cycles were survived, then the upper load level was increased to the final value of 70%. At this level, the beams were tested until failure.

3.3 Three point bending tests

A preliminary study on the mixture composition regarding its aggregate grading preceded the start of the test series for this PhD project. The study and its results have been reported elsewhere (Lappa et al., 2003a, Lappa et al., 2003b). In the scope of that study, three point bending tests have been carried out with specimens and setup in accordance with the RILEM regulations for steel fibre reinforced concrete (TC162-TDF, 2002). The same test set-up has been previously used by former researchers at Delft University of Technology (Kooiman (2000), Grünewald (2004), Markovic (2006) and Schumacher (2006)) and will not be given in detail here. The bending tests were performed on 150/150/600 mm beams at a 500 mm span, under deformation control by the measured notch tip opening at a loading rate of 50μm/s. These tests are mentioned here since in Chapters 4 and 6, the results will be presented for comparative purposes. The three point bending tests in this study were exclusively used on the HSFRC mixture. Also, it should be noted that for the hybrid HSFRC used in this study such results exist from the research of Markovic (2006). Figure 3.8 shows the dimensions of the three point bending tests, and Figure 3.9 is a photograph of the testing setup.

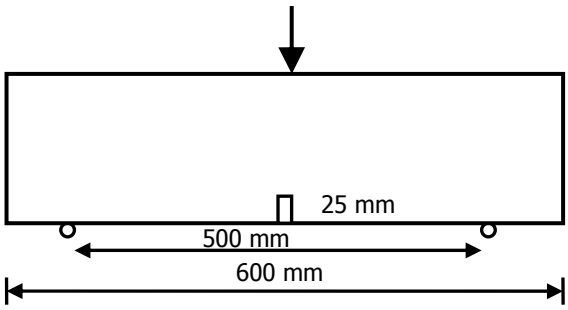

Figure 3.8: Dimensions of the three point bending tests. The beams have a 125 mm square cross-section.

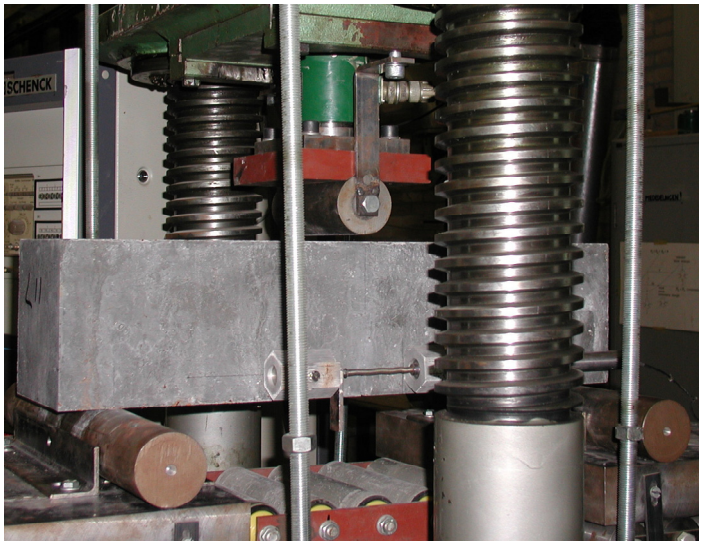

Figure 3.9: 3pt bending tests on notched beams in accordance with the RILEM guideline (TC162-TDF, 2002).

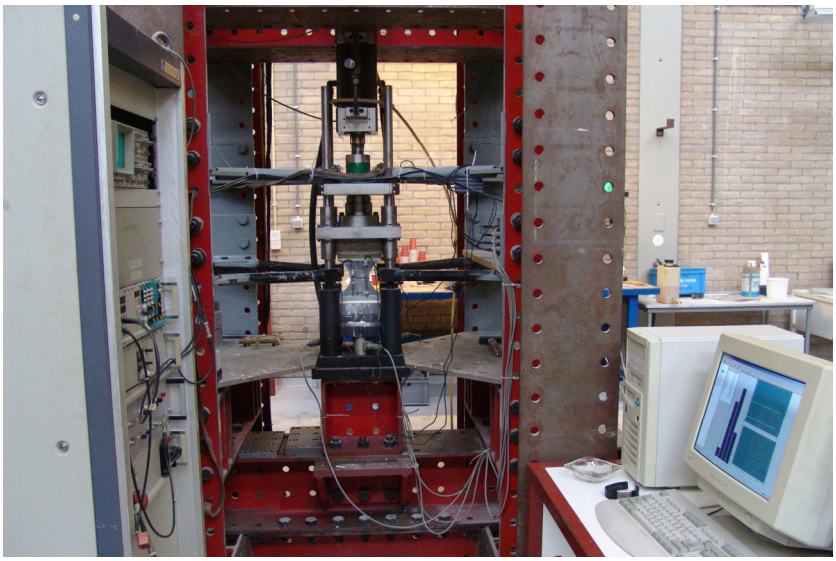

Figure 3.10:Testing facility for the uniaxial tensile tests

3.4 Uniaxial tensile tests

The uniaxial tensile tests were regarded to be necessary in order to evaluate the tensile load bearing capacity of the mixture and obtain appropriate material input parameters for modelling the structural behaviour. In this study, they were performed with the HSFRC mixture only. With the other two mixtures, no uniaxial tensile tests were planned since such tests had already been carried out by Markovic (2006) during his PhD research for the hybrid mixture with an identical test

setup, and by Jungwirth (2006) in the scope of his PhD thesis with a similar setup at the Ecole Polytechnique Fédérale de Lausanne. Therefore, for the tensile material input parameters of those two mixtures, appropriate results were available that replaced the need for own uniaxial tensile test results.

A testing facility for uniaxial tension was available at the laboratory (Figure 3.10). It is the same frame as described by Hordijk (1991), which was originally built in the 1970s but adapted throughout the years. This testing facility was used by Markovic (2006) for his PhD research on the tensile behaviour of high strength hybrid fibre reinforced composites and adapted for high strength concrete. In a preliminary numerical finite element study, he chose dog-bone shaped specimens as most appropriate for his mixtures and the testing frame. Also, after the first trial tests, he concluded that it is more efficient to cast longer specimens and cut off the ends to their final size, in order to avoid an altered fibre alignment at the edges due to boundary effects. He also recommended an additional stiffening of the edges of the specimens by steel strips in order to avoid failure outside the middle zone of the specimens. Since the HSFRC is of comparable strength to his mixtures, and the moulds used to cast the test specimens were still available in the laboratory, it was chosen to conduct the tensile tests in an identical way. In the following, the most important aspects of the testing frame, specimens and testing will be briefly explained. Figure 3.11 shows the test specimen dimensions, the dimensions of the moulds, and a photograph of the specimen in the loading frame.

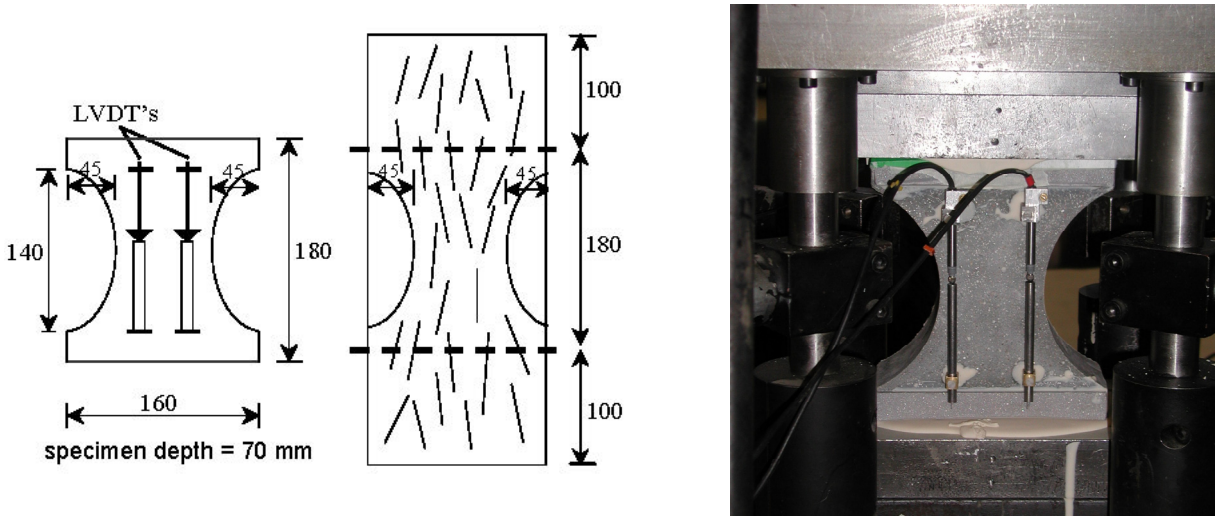

Figure 3.11 Test specimens after cutting, initial moulds (after (Markovic, 2006) and picture of a specimen glued to the loading platens of the testing frame.

The testing frame is a stiff frame with fixed end plates that does not allow any rotation. The specimen is cast in a longer and deeper mould than its end-size: the mould is 380 mm long and 100 mm deep, while the specimen is 180 mm long and 70 mm deep. The casts for these specimens are the only ones where timber moulds

instead of steel moulds were used. The longer ends and the top part of the specimen (30 mm from casting surface) are cut from the specimen approximately 21 days after casting. Further, the top and bottom zones of the specimens were stiffened by four steel strips; two of them were glued at the outside, and two in 20 mm deep grooves that were sawn into the specimen. Some specimens were prepared with a notch: in that case, when the specimen was cut into the right size, a 5 mm deep notch was cut from all four sides of the specimen. The specimens were glued into the testing frame.

The influence of the casting direction, or better said, the fibre orientation and alignment as a result of a different flow of concrete, was investigated by letting the concrete flow into the moulds once from its longer end (vertical cast) and once from the shorter end (horizontal cast), see Figure 3.12. If fibres would orient themselves with the flow direction, then the vertical cast should show a higher tensile strength than the horizontal one. However, since the HSFRC contains only 13 mm short fibres, this effect might not be as pronounced as with longer fibres.

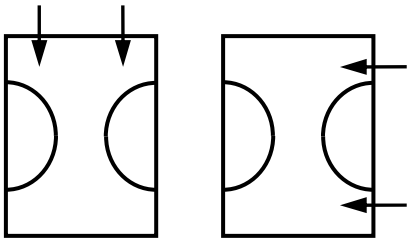

Figure 3.12: Vertical (left) and horizontal (right) casting direction of the tensile tests.

Three samples were tested for each testing parameter (casting method, notched or un-notched specimens). The total crack opening was registered by four LVDTs, two at each side at the front and back of the specimen. The LVDTs could register a maximum displacement of 2 mm and were placed over a measuring length of 110 mm. The tests were performed deformation controlled at a loading speed of 2µm/s; however, not the signal from the LVDTs was used as the control parameter but the displacement registered in the loading jack – in that way, the test could be continued even for displacements exceeding 2 mm and the complete tail of the stress-strain relation could be registered, at least quantitatively. It should be noted that with this testing arrangement, no snap back mechanisms can be recorded, since the displacements that control the experiment are registered with reference to the complete testing frame. It was still preferred to proceed in this way since this guaranteed a stable test.

At a later stage, it seemed necessary to repeat the tensile tests with a different measuring length: when the outcome of the experimental parameters was used as input in a material model in order to reproduce the results of the static bending tests, as will be discussed in Chapter 6, it seemed that the measured strain of the descending branch was too steep to satisfactorily model the test results. In the post-

peak stage, deformations localised at a single crack while the concrete around did not experience further increase of deformations. A 110 mm measuring length seemed too long to correctly measure the deformations in the postpeak stage. Therefore a new test series of three notched and three un-notched specimens was performed with a combination of one LVDT over a 35 mm long measuring length and one at 110 mm at each side, as shown in Figure 3.13. A 35 mm measuring length in this testing frame has already proven to be appropriate for plain concrete in order to obtain a characteristic stress-strain relation (van Mier, 1997).

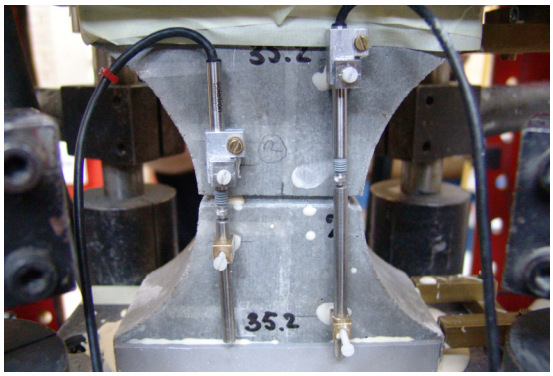

Figure 3.13 Notched tensile test specimen in testing frame with one LVDT over 35 mm measuring length and one at 110 mm on each side.

References

BALAGURU, P. N. & SHAH, S. P. (1992) *Fiber Reinforced Cement Composites*, McGraw-Hill, Inc.

GRÜNEWALD, S. (2004) Performance-based design of self-compacting fibre reinforced concrete. *PhD Thesis.* Delft University of Technology.

HORDIJK, D. A. (1991) Local approach to fatigue of concrete. *PhD Thesis.* Delft University of Technology.

JUNGWIRTH, J. (2006) Zum Tragverhalten von Zugbeanspruchten Bauteilen aus Ultra-Hochleistungs-Faserbeton. *Ecole Polytechnic Federale de Lausanne.* PhD Thesis Nr 3429 (2006).

KOOIMAN, A. G. (2000) Modelling Steel Fibre Reinforced Concrete for Structural Design. *PhD Thesis.* Delft University of Technology.

LAPPA, E. S., VAN DER VEEN, C. & WALRAVEN, J. C. (2003a) Self-compacting, high strength steel fibre reinforced mortar for pre-cast sheet piles. IN WALLEVIK, O. & NIELSSON, I. (Eds.) *3rd International Symposium on Self-Compacting Concrete.* Reykjavik, Iceland, RILEM Publications S.A.R.L.

LAPPA, E. S., VAN DER VEEN, C. & WALRAVEN, J. C. (2003b) High strength, self-compacting steel fibre reinforced mortar for precast sheet piles. Delft University of Technology.
MARKOVIC, I. (2006) High-Performance Hybrid-Fibre Concrete - Development and Utilisation. *PhD Thesis.* Delft University of Technology.
SCHUMACHER, P. (2006) Rotation Capacity of Self-Compacting Steel Fiber Reinforced Concrete. *PhD Thesis.* Delft University of Technology.
TC162-TDF, R. (2002) Recommendations of RILEM TC 162-TDF: Test and design methods for steel fibre reinforced concrete: bending test. *Materials and Structures,* 35**,** 579-582.
VAN MIER, J. G. M. (1997) *Fracture Processes of Concrete*, CRC Press, Inc.

4.

Behaviour under static loading: theoretical considerations and experimental results

This chapter shows the behaviour of high and ultra high strength steel fibre reinforced concretes under static loading. After theoretical considerations on the expected behaviour, as found in existing literature on comparable concrete mixtures, the experimental results on all static tests that were carried out in the scope of this study are presented and discussed. It will be shown that the materials tested in bending offer an improved bearing capacity compared to conventional plain concretes, and therefore enable a broad range of innovative applications. The steel fibres contribute significantly to the bearing capacity, and the extent of their contribution depends on their alignment and distribution. The latter is determined by means of image analysis on photographs of cut cross-sections of tested beams, that allows the determination of number and orientation of fibres on the basis of their size and cross-sectional shape. Another important aspect that will be discussed is the influence of the flowability and flow direction in the material's fresh state on the fibre distribution and orientation, and the implication on the mechanical properties and the behaviour of the test specimens. Finally, the results of the uniaxial tensile tests with the HSFRC mixture are presented and discussed. Especially the results of the uniaxial tensile tests will be used as input properties for material modelling in chapters 6 and 7. The results of the bending tests of all three mixtures will be compared to the outcome of the used analytical model in Chapter 6.

4.1 High performance concrete mixtures

Before presenting the results of the static tests, a brief introduction and literature review will be given here on high performance/high strength fibre reinforced concrete mixtures in order to present their general structural response and highlight

differences with conventional, un-reinforced concrete. Starting with some definitions: the term high strength concrete refers to mixtures with, as the name already implies, a high compressive strength, in general above 100 MPa. The term high performance implies that a concrete has certain improved performance characteristics, such as freeze-thaw durability, scaling resistance, abrasion resistance, chloride penetration, compressive strength, modulus of elasticity, shrinkage and creep. However, the term 'high performance fibre reinforced cement composite' is established since the series of workshops under the same name (Reinhardt and Naaman, 1992, Naaman and Reinhardt, 1996, Reinhardt and Naaman, 1999, Naaman and Reinhardt, 2003) and is defined as materials that have a pronounced strain hardening phase after the linear elastic phase, regardless of the actual compressive and tensile strength values. Figure 4.1 shows the definition of strain hardening/multiple cracking high performance fibre reinforced cement composites (HPFRCC) as opposed to conventional, softening, fibre reinforced concrete. In the present study, with the term 'high performance materials', hardening, not softening materials will be meant.

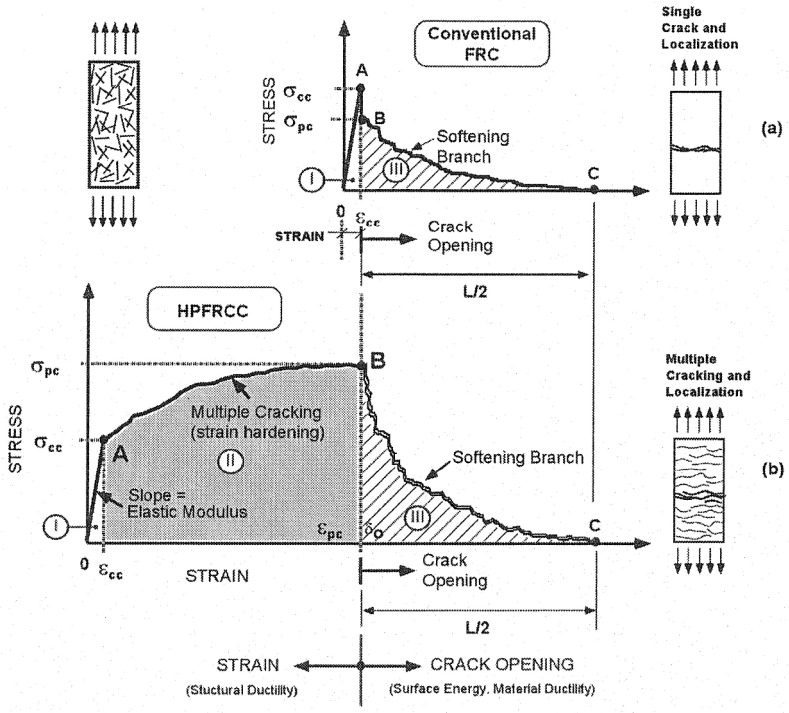

Figure 4.1: Definition of High Performance Fibre Reinforced Cement Composites, after Naaman (2003), opposed to 'softening' fibre reinforced concrete (FRC).

Depending on the fibre content in a mixture and their concentration and alignment in a structural element, different responses can be obtained; generally the fibres will always increase the deformation ability and ductility in a certain way. This increase can occur in the pre-peak or post-peak phase of the stress-strain or load-

deflection relation or in both. If a sufficient number of fibres is available, the bearing capacity is larger than the cracking load. When the load can be increased after first cracking, then the term 'hardening' is used. Depending on the fibre content, this hardening can occur in bending, in which case the material is defined as 'deflection hardening' material, or in uniaxial tension, in which case the definition is of a 'strain hardening' material. As a result of the possibilities of stress redistribution, in bending a lower fibre content is sufficient to achieve deflection hardening than in case of uniaxial tension. This implies that a tensile strain hardening material will implicitly be a deflection hardening material but not necessarily vice versa. A schematic overview of fibre reinforced composites and their possible stress-strain or load-deflection response was given by Naaman and Reinhardt (2005) and is presented in Figure 4.2.

On the definitions of strain hardening in uniaxial tension and deflection hardening in bending, it has to be noted that the strain hardening in tension is a better defined material property than the deflection hardening in bending. In bending, the dimensions of the specimen and the chosen setup also significantly influence the behaviour of a test specimen. A thin specimen, for example, is more likely to show deflection hardening than a thick one. In uniaxial tension, these effects are less pronounced.

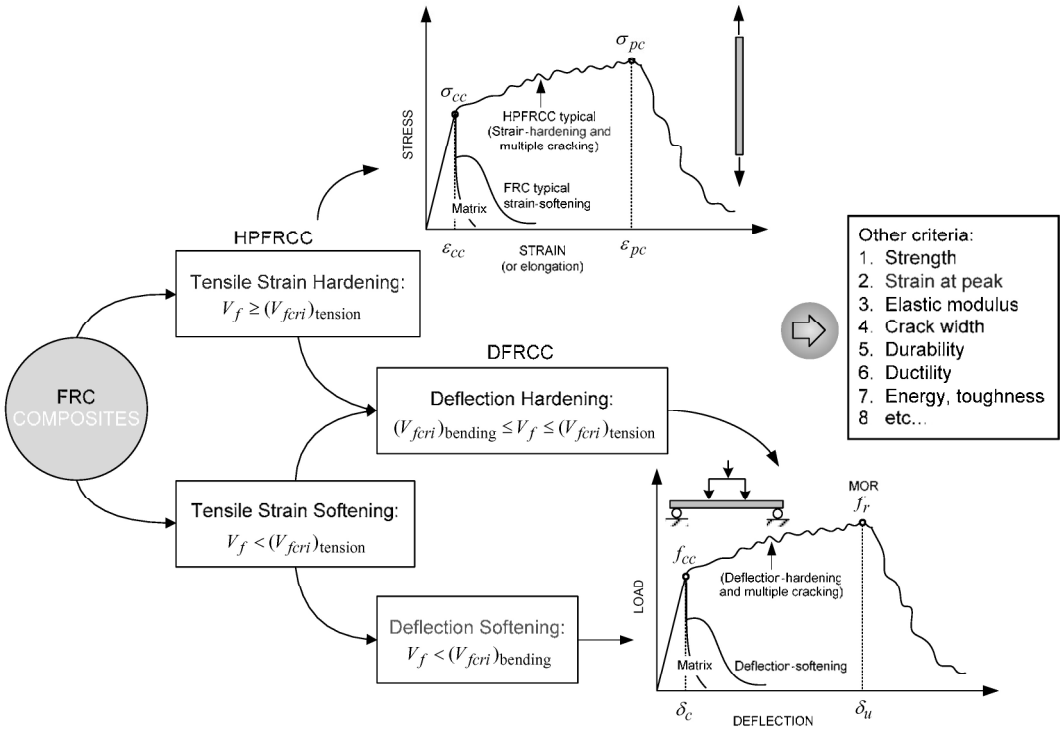

Figure 4.2: Classification of fibre reinforced composites (FRC) based on their tensile stress-strain response, after Naaman and Reinhardt (2005).

Ultra high strength (and high strength) mixtures can be tensile strain hardening mixtures but do not necessarily have to be so, depending on the strength of the matrix, the applied fibre content, and the fibre geometry. This fact is reflected in the French interim regulations (AFGC-SETRA, 2002) and in the proposed design diagram for the stress-strain relation; this includes a tensile strain hardening option for hardening materials but can also be in form of a 'conventional' softening stress-strain relation for non-hardening materials.

On the other hand, Victor Li and numerous researchers around him, (Li, 1993, Li et al., 1996, Li and Fischer, 2002, Li, 2004), have developed materials that they defined as 'engineered cementitious composites' (ECC), which are exclusively tensile strain hardening materials. Most ECC mixtures are of a rather low concrete strength, often around 35 MPa in compression. Consequently, with materials of such a strength class, a polyvinyl fibre addition of around 2% by volume is sufficient to provide a strain hardening material with a very ductile behaviour (the ultimate hardening ends at strains of up to 8‰). The hardening phase is normally characterised by the formation of a large number of cracks that are very densely aligned at a fine spacing (multiple cracking). These materials are mentioned here, since the tensile and bending behaviour of high and ultra high strength fibre reinforced concretes can be comparable to ECC materials if the fibre addition is sufficient to enable a tensile strain hardening. Figure 4.3 shows a typical stress-strain curve for ECC materials.

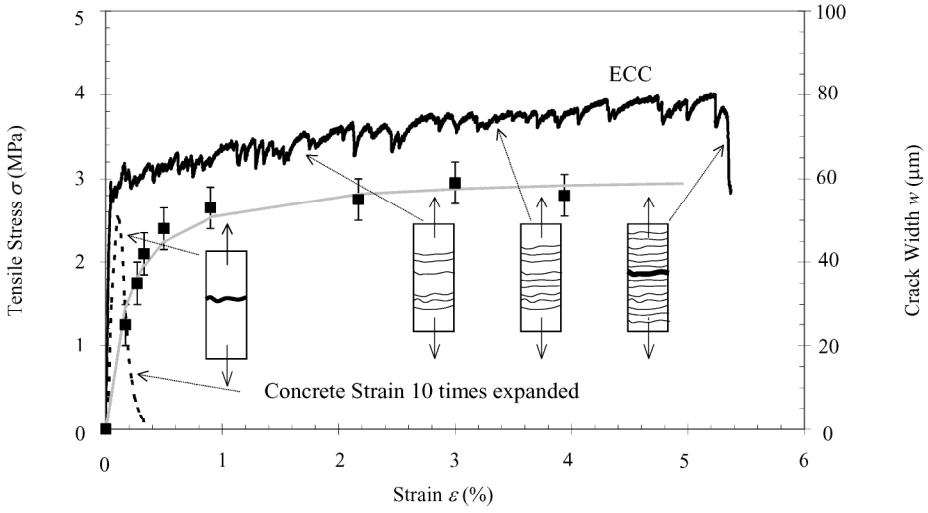

Figure 4.3: Typical stress-strain curve and crack width development of Engineered Cementitious Composites (ECC), after Li (2005).

As will be shown in the sequel of this Chapter, all mixtures used in this thesis were strain hardening mixtures and experienced the formation of multiple cracks before the peak load was reached, after which one major crack occurred due to

localisation and the material started unloading. In the following, this phenomenon of multiple cracking is evaluated from an energetic point of view.

4.1.1 Multiple cracking principle

The principle of multiple cracking lies on the assumption that, after the first crack has formed, the energy needed to let this crack grow is larger than the energy needed to form a new crack. The phenomenon of multiple cracking has been explained with an energy based approach by Aveston et al. (1971) for continuous fibre cementitious composites. This approach was later upgraded by Tjiptobroto and Hansen (1993) for composites with discontinuous random fibres (as are the fibre concretes of this research). Also Markovic (2006) used Tjibtobroto's and Hansen's approach to show that the concretes he developed with a combination of two different fibre types can have multiple-cracking abilities. In the following, the approach will be briefly presented and an evaluation for the mixtures used in this study will be performed.

An important assumption of the model is that the first crack that is created will eventually develop into a localised crack, the crack that will actually lead to failure. This assumption is however difficult to verify, since the multiple cracks are barely visible at their initiation.

Parameter identification:

The energy $E_{1\text{-}2}$ is the energy needed to form the first through crack and is defined as:

$$E_{1-2} = \Delta U_{f-mc} + \Delta U_{fr} + U_{db} \tag{4.1}$$

$\Delta U_{f\text{-}mc}$: increase of fibre strain energy by fibre bridging action of first crack;
ΔU_{fr}: frictional energy between fibres and concrete matrix;
U_{db}: debonding energy.

These three terms can be determined with the following expressions. First the term $\Delta U_{f\text{-}mc}$ can be determined with:

$$\Delta U_{f-mc} = \frac{V_{ef}}{E_f}\left[\frac{7}{48}\frac{\tau_f^2 L_f^3}{r^2} - \left(E_f \varepsilon_{mu}\right)^2 \frac{L_f}{4}\right] \tag{4.2}$$

V_{ef} is the effective volume quantity of fibres; $V_{ef}=\eta V_f$; η is the fibre orientation coefficient and V_f the applied fibre volume quantity of the fibres;
E_f is the modulus of elasticity of the fibres (E_f=210000 N/mm^2 for steel fibres);
L_f is the fibre length; r is the fibre radius;
τ_f is the average frictional stress at the fibre matrix interface; and

ε_{mu} is the strain at which the first through crack is formed (first bending point in uniaxial tensile stress-strain response.

The frictional energy ΔU_{fr} is defined by:

$$\Delta U_{fr} = \frac{V_{ef}\tau_f L_f^2}{4r}\left[\frac{\tau_f L_f}{3rE_f} - \frac{1}{2}\varepsilon_{mu}\right] \tag{4.3}$$

All terms in this equation have already been explained.

Finally, the debonding energy U_{db} is defined by:

$$U_{db} = \frac{V_{ef} L_f G_{II}}{r} \tag{4.4}$$

G_{II} is the fracture energy released at the fibre matrix interface during the debonding process. It can be calculated by the triangular surface area under the fibre pullout diagram $A^*_{debonding}$ and divided by the surface area of the fibre exposed to the action of the frictional stress A^f_{fr}. The latter will be calculated by using one half of the fibre length as an average debonding length.

The energy $E_2=E_3=\ldots=E_n$ is the energy required to create a new through crack and is defined by following equation:

$$E_2 = G_m V_m + \Delta U_{f-mu} - \Delta U_{fm} \tag{4.5}$$

With $G_m V_m$ being the fracture energy of the matrix needed to form a new crack surface, G_m the matrix fracture energy and V_m the matrix volume fraction ($V_m=1-V_f$).
$\Delta U_{f\text{-}mu}$ is the increase in the fibre strain energy as a result of crack bridging during multiple cracking, and
ΔU_{fm} is the decrease of the matrix strain energy.

The formula to determine the increase in fibre strain energy $\Delta U_{f\text{-}mu}$ due to crack bridging is given below:

$$\Delta U_{f-mu} = \frac{1}{24} E_f V_{ef} L_f \alpha(18 + 7\alpha)\varepsilon_{mu}^2 \tag{4.6}$$

$\alpha = E_m V_m / E_f V_f$ is the ratio between the matrix E-Modulus multiplied by its volume fraction and that of the fibres.

The decrease of the matrix strain energy ΔU_m can be obtained via:

$$\Delta U_m = \frac{11}{24} E_m V_m L_f \varepsilon_{mu}^2 \tag{4.7}$$

Based on the model's energy criterion, multiple cracking takes place as long as the energy $E_2=E_n$ needed to form a new crack is lower than the energy E_{1-2} needed to create and widen the first through crack. In order to ensure multiple cracking, a fibre volume fraction equal to or larger than the critical fibre volume quantity at which $E_2=E_{1-2}$ is required.

Markovic (2006) has already evaluated whether or not the hybrid HSFRC mixture in his study can form multiple cracking and shown that this can occur at a fibre volume of 1.5% (also his tensile tests proved this). This implies that one of the three mixtures of this study, the hybrid HSFRC, is a strain hardening material. This principle needs to be evaluated for the remaining two mixtures, the HSFRC and the BSI/CERACEM, which will be done in the following.

Parameters used for a quantitative calculation for the HSFRC mixture.

Determination of E_{1-2}:

E_f=210 000 N/mm^2, V_f=1.6%, but this parameter will be varied in the calculation (needed for the determination of V_{ef}), L_f = 13 mm, and r_f = 0.08 mm. The main unknown parameters are the fibre orientation factor η, the frictional stress τ_f, the strain at first cracking ε_{mu} and the fracture energy G_{II}.

Fibre orientation factor η:

This parameter can be varied. Image analysis of beam cross sections of this mixture showed little variation between the orientation factor of different beams: it was in the range of 0.7-0.8, showing that with the chosen casting methods the fibres were aligned preferably in favour of the bending test. More variation was found with regard to the actual number of fibres in a cross-section. In his thesis, Markovic (2006) varied the orientation factor from 0.5 (random orientation) to 0.8 (which was the orientation he observed from the image analysis) and 1.0 (perfect alignment of all fibres). Only small differences in the values of E_{1-2} and E_2 were observed between the orientation factors 0.8 and 1.0. Here, the orientation factor will be varied between 0.5 (unfavourable alignment) and 0.8 (alignment that corresponds to the values obtained with image analysis in this mixture).

Frictional stress τ_{fr}:

The frictional stress depends on the pull-out behaviour of the fibres in the matrix and can be determined by the frictional pull-out force P_d divided by the surface area of the fibre exposed to the frictional stress action A^f_{fr}:

$$\tau_{fr} = \frac{P_d}{A^f_{fr}} \tag{4.8}$$

For the surface area of the fibre, it is assumed that half of the fibre length is embedded in the matrix during the pull-out process, and its value can be determined by:

$$A_{fr}^{f} = 2\pi \cdot r \cdot \frac{L_f}{2} \qquad (4.9)$$

Assumptions have to be made for realistic values of the pull-out force, since no direct pull-out tests have been performed for this kind of fibre. Markovic (2006) performed pull-out tests for a fibre of the same length, but with a thicker diameter of 0.2 mm instead of 0.16 mm, so his fibres had a smaller fibre aspect ratio. The fibres were embedded in a similar high strength and dense matrix. He experienced a large scatter in his results. Therefore, he varied the fibre slip and corresponding pull-out force in his calculation, with an average value of P_d=15 N at a corresponding slip Δ_d=0.025 mm. Thinner fibres might show smaller pull-out forces since the frictional area around the fibre, increasing its pull-out resistance, is smaller. However, since no information on the pull-out of the used fibres is known, and the fibres' geometries are rather similar, the above mentioned average values of the frictional force P_d of Markovic's results were used.

The fibre matrix debonding energy G_{II}:
This value can be calculated with:

$$G_{II} = \frac{A^{*}_{debonding}}{A_{fr}^{f}} \qquad (4.10)$$

The parameter $A^{*}_{debonding}$ is the triangular surface area under the fibre pull-out diagram that corresponds to the fibre-matrix debonding phase, see Figure 4.4 (the pull-out force P_d is assumed to increase linearly with increasing slip Δ_d in the debonding phase, until the maximum fibre pull-out force is reached):

$$A^{*}_{debonding} = \tfrac{1}{2} \cdot P_d \cdot \Delta_d \qquad (4.11)$$

The average parameters from Markovic's calculation were used to determine this parameter, P_d=15N and was lowered to Δ_d=0.01mm because this is the most unfavourable case: higher slip values would provide steeper $E_{1\text{-}2}$ curves and therefore be in favour of the development of multiple cracking.

The strain ε_{mu} at which the first though crack forms:
This strain is obtained from the uniaxial tensile stress-strain relation: it is the point at which the first deviation from linearity is observed. In order to express the measured displacement during the test into a strain, the displacement δ_{mu} has to be divided by the measuring length l_m:

$$\varepsilon_{mu} = \frac{\delta_{mu}}{l_m} \tag{4.12}$$

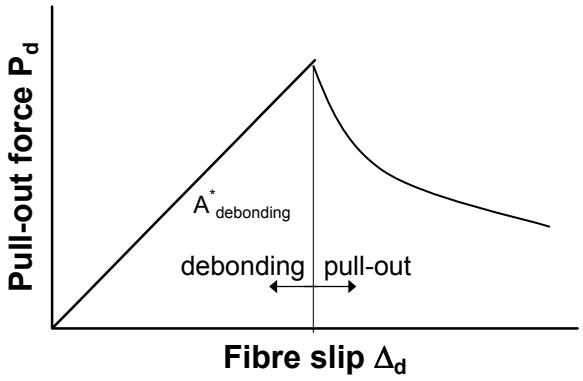

Figure 4.4: Schematic representation of the fibre pull-out force-slip response for straight fibres, with a distinction between the debonding phase (ascending branch) and the pull-out phase (descending branch).

Markovic (2006) varied this parameter for different fibre volume fractions, and also did tensile tests for different fibre volume fractions. In this study, only tests with one fibre volume fraction (1.6%) were performed, and the observed δ_{mu} was 0.015 mm resulting into a strain of 0.1‰. Since no other data is available, this strain value was assumed for different fibre volume fractions, and of course the most reliable result is obtained for the fibre volume of 1.6%.

Determination of E_2

Most parameters have already been identified, only the remaining ones are listed here:

Matrix volume fraction V_m: V_m=1-V_f depending on the fibre volume fraction.

G_m is the fracture energy of the matrix, obtained from tensile tests. No tests on plain concrete have been performed in this research project, but they have been performed by Markovic (2006) with a matrix of a comparable density and strength. A value of 0.108 N/mm was used for G_m, which will also be applied here. The parameter α, needed for the determination of $\Delta U_{f\text{-}mu}$, is the ratio between the E-moduli and volume fractions of the matrix and fibres. For the E-modulus of the matrix, a value of 45000 MPa was used.

When these input parameters are used, the values of $E_{1\text{-}2}$ and E_2 as plotted in Figure 4.5 are obtained for different fibre volume fractions and an assumed fibre orientation factor of 0.8. An orientation factor of 0.7-0.8 is believed to be a realistic value, as will also be shown by fibre counting with image analysis in subsection 4.4.

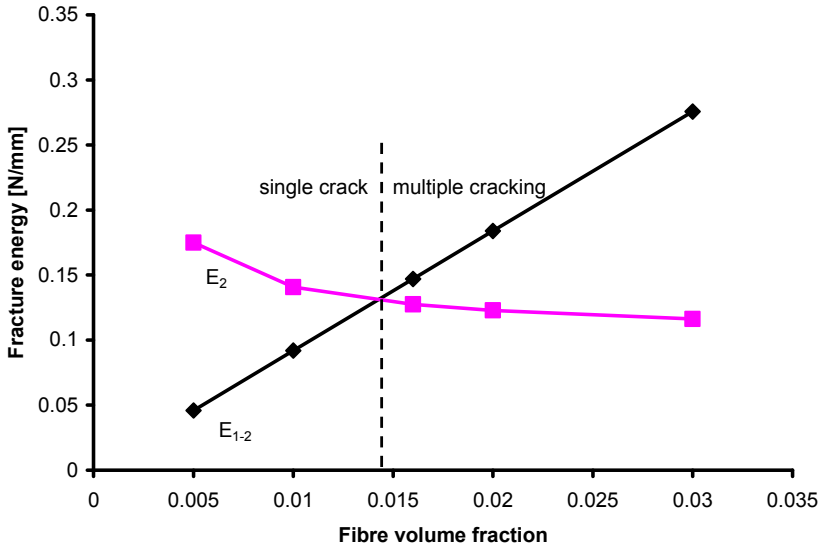

Figure 4.5: Evaluation of the multiple cracking condition with an energetic based approach in accordance with Tjiptobroto and Hansen (1993). The energy values have been determined for the HSFRC mixture with an assumed fibre orientation of 0.8.

As can be seen, multiple cracking can start from a fibre volume fraction of 1.5%, just below the applied fibre volume in the HSFRC of 1.6%. As will be shown in subsection 4.5 with the results of the performed uniaxial tensile tests, multiple cracking and strain hardening was actually observed for the applied fibre volume fraction of 1.6%.

Figure 4.6 shows the same energies determined for a fibre orientation factor of 0.5, considered to be a random fibre orientation. As can be seen, in that case multiple cracking would occur for fibre volume fractions above 2%.

Parameters used for a quantitative calculation for the BSI/CERACEM mixture.

As for the BSI/CERACEM, even more unknown parameters are encountered for the determination, since here not only the matrix is of a different strength and composition, with a maximum coarse aggregate size of 7 mm, but also the fibres are of different length and diameter, and no single fibre pull-out results have been reported up to now.

Nevertheless, an indicative calculation was performed. Regarding the parameters, following changes were made with respect to the HSFRC mixture: The matrix E-modulus was raised to 50000 MPa, the fibre length changed to 20 mm and the fibre diameter to 0.3 mm. The fibre orientation factor was set to 0.8. The matrix fracture energy was slightly increased from 0.108 N/mm to 0.120 N/mm.

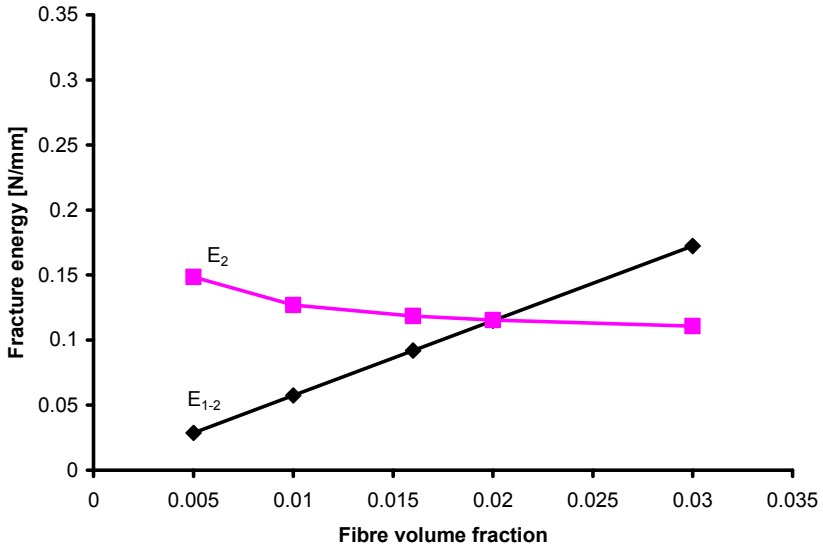

Figure 4.6: Same evaluation as in Figure 4.5, but with the energy values determined with an assumed fibre orientation of 0.5.

When keeping the same values of the pull-out force and corresponding slip at P_d=15N and Δ_d = 0.01mm, E_2 remains larger than E_{1-2} for fibre volume fractions up to 3% and therefore no multiple cracking would occur at the applied fibre volume fraction of 2.5%. Since multiple cracking occurred during the static bending tests, at least for the specimens cast with the 'flow' method, this indicates that not all parameters could be determined correctly. Markovic (2006) carried out pullout tests on fibres with a length of 13 mm and a diameter of 0.2 mm and found that a pullout force of 15 N can be a realistic value; the fibres in the BSI/CERACEM are 20 mm long and 0.3 mm thick so that they provide a greater surface area for bonding with the matrix, and a larger pullout force can be expected. To be more precise, the bonding area of Markovic's mixture would be $l_f/2*\pi*d_f$=6.5mm*π*0.2mm=4.08mm^2 while for the BSI/CERACEM that would result into 10mm*π*0.3mm=9.42mm^2. Thus, this area is approximately 2.3 times larger in case of the CERACEM; by assuming a constant bond strength τ_b for both mixtures, this means that the pullout force for the fibres of the BSI/CERACEM mixture can be expected to be up to 2.3 times higher than the one of Markovic's mixture, $P_d \leq$2.3*15N=35N. Figure 4.7 shows that for a pullout force of 30N and a bond slip of 0.25mm multiple cracking would occur for fibre volume fractions of at least 2%, therefore also for fractions of 2.5% as used in this study.

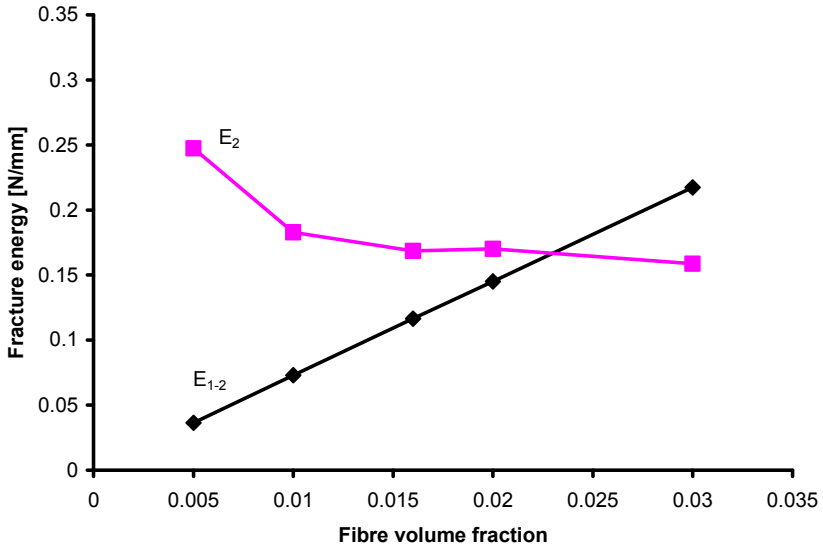

Figure 4.7: Multiple cracking evaluation with the energetic approach for the BSI/CERACEM.

Concluding remarks:

Since no fibre pull-out tests and plain matrix (without fibre reinforcement) tests have been carried out in this study, not all parameters needed to evaluate the multiple cracking phenomenon could be determined accurately and assumptions had to be made. However, it was possible to show that multiple cracking, at fibre volume fractions as used in the three mixtures, can actually occur based on the this model. The bending and tensile experiments showed that all three mixtures actually experienced multiple cracking, at least when appropriate casting methods had been used that provided a beneficial fibre alignment. In the following, the experimental results of the static structural tests will be given in detail.

4.2 Standard strength tests

As already mentioned in Chapter 3, each time a batch of concrete was cast for the preparation of test specimens for bending or uniaxial tension, also a set of six 100 mm cube specimens was produced in order to perform standard compressive and splitting tensile tests. In the following, the results of these standard tests will be briefly presented in order to provide an overview of the strength characteristics of the mixtures used. The average compressive and splitting tensile strengths $\bar{x}$, their standard deviation σ and the coefficient of variation V are listed in Table 4.1:

Table 4.1: Results of compressive/splitting tensile strength tests.

	Compressive strength			Splitting tensile strength		
	BSI/CERACEM	HSFRC	hybrid HSFRC	BSI/CERACEM	HSFRC	hybrid HSFRC
$\bar{x}$ [MPa]	217	146	131	28	20	20
σ [MPa]	13	5	6	3	2	2
V	6%	3%	4%	12%	9%	9%

The BSI/CERACEM mixture has the highest strength, but also the highest scatter. The other two mixtures have a lower scatter, and do not differ much with regard to the splitting tensile strength (they contain a comparable fibre volume fraction, but differ in fibre geometry). The scatter of the BSI/CERACEM in the compressive and splitting tensile strength, as expressed by the coefficient of variation of 6% and 12%, is still acceptable for laboratory concrete.

Although the compressive and splitting tensile strengths of the HSFRC and the hybrid HSFRC are in the same order of magnitude, the may differ significantly in the bending behaviour, and especially in the descending part of the load-deflection curve, as will be shown in the next section.

4.3 Bending tests

4.3.1 Three-point bending tests

The three-point bending tests were the first bending tests carried out with the scope of a preliminary study on mixture composition (Lappa et al., 2003b). Only the HSFRC mixture was calibrated with this method. Some results will briefly be mentioned here, mainly for comparing them with the four point bending tests reported in the subsection 4.3.2, but also in order to show the influence of the chosen casting method on the structural behaviour.

In brief, different trial mixtures were cast with different aggregate size distributions; from these, the best four were chosen and cast on a larger scale, to test their hardened state properties. One of these four mixtures is the HSFRC mixture, the main mixture in this research. Initially, cubes and prisms and a set of three beams were cast with the first two mixtures. The strength results were compared with those of a reference mixture, developed by Grünewald et al. (2000) by adapting a mixture originally developed by Sato et al. (2000). The beams were cast with a shovel, in accordance with the casting method proposed in the RILEM regulations (TC162-TDF, 2002), by placing a double volume of fresh concrete in the middle of the mould and a single volume at the ends. It should be noted that the researchers that worked on the RILEM regulations invented this casting method for concrete with a low workability that has to be compacted with vibration. For self-

compacting concrete they recommend to fill the moulds in one charge from one end of the mould, which will be referred to as the 'flow' method from now on (Vandewalle and Dupont, 2003). In any case, even though the hardened state properties regarding the compressive, splitting tensile strength and the E-modulus of the first two mixtures were in good agreement with the reference mixture, the flexural strength was significantly lower, as can be seen in Figure 4.9, where the average curves of the tested beams are shown. This is remarkable since all three mixtures were cast with the RILEM method and had identical fibre contents. This discrepancy highlighted the phenomenon that the production method is of significant importance for the structural behaviour. Grünewald cast the beams with a shovel placed very close to the mould. The beams cast for this research were cast with the shovel placed higher. According to Jungwirth (2006), a higher falling height can lead to an alignment of fibres in layers (Figure 4.8). In the beams prepared for the three-point bending tests, these layers of aligned fibres were perpendicular to the beam length and the fibre orientation was not favourable for the bending test. The fibre alignment and how it is affected by factors such as the casting method or formwork boundaries will be subject of further discussion in subsection 4.4.

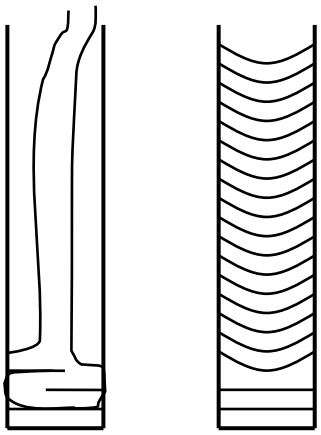

Figure 4.8: Alignment of fibres in layers due to a high falling height, here shown for the case casting of a column into vertical moulds, after Jungwirth (2006)

After these first results and observations, two more mixtures were cast with the 'flow' method; with this method, a better fibre alignment for the bending tests was obtained due to the fact that fibres orient themselves into the flow direction and also along the formwork boundaries, which is mainly an orientation along the beam length. The average curves of these mixtures were much closer to the reference mixture, one even reaching a higher strength (Figure 4.9).

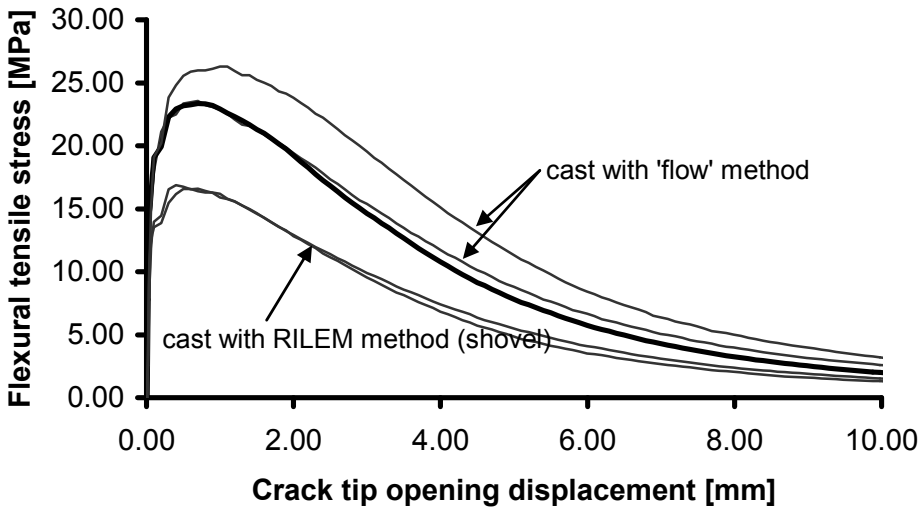

Figure 4.9: Influence of the casting method on the flexural behaviour. Results of the three point bending tests on HSFRC. Each curve represents the average of three beams. Two different casting methods are compared with the reference mixture by Grünewald et al. (2000), the bold black curve.

The results of these preliminary tests led to the following conclusions: all mixtures can be considered equivalent concerning their strength properties, as was shown by the tests on cubes and prisms. The differences in the bending behaviour can be traced back to the casting process and therefore the fibre orientation. Corresponding differences will be more pronounced in larger and deeper specimens, when the concrete actually has space to flow into the moulds, and primary and secondary flow patterns can form, as will be shown in more detail in subsection 4.4. The fibres affect the structural behaviour significantly; all curves shown in Figure 4.4 are representative curves for the material and the non-uniformity due to a different orientation, resulting from a different casting method, has to be considered in design of actual structural elements with such a self-compacting, fibre reinforced high strength mixture. For beams of the present dimension, the flow method is recommended because the concrete is easier and faster to cast, leads to a smaller and better controllable scatter within the beams of one test series, and is in agreement with the authors of the RILEM test regulations for self-compacting mixtures. It is also important to notice that an increase in strength, going along with a short hardening branch, is visible after the linear elastic stage, even though these were tests on notched beams.

4.3.2 Four-point bending tests

Before the results of the static bending tests on un-notched beams for each mixture will be given, some results concerning only the HSFRC mixture are given in order to

highlight the influences of a notch on the structural behaviour, and to compare the four- and three point bending tests. These comparisons are only possible for the HSFRC mixture, since for the other two mixtures, exclusively four point bending tests on un-notched specimens were performed.

Comparison of bending tests and specimens

The notch influences the structural behaviour by forcing the crack to form at a certain position. This weakening of the cross section forces deformations to localise at an early stage during the tests, at least when compared to un-notched tests. Therefore the 'deflection hardening' phase due to the formation of multiple cracks is hindered and not very pronounced in case of notched beams. The notch however does not necessarily correspond to the weakest cross-section: therefore even higher strengths can be obtained in the case of tests on notched specimens compared to un-notched ones, where deformations always localise at the weakest cross-section. Figure 4.10 shows the average deflection of the notched beams compared to the average deflection of the un-notched beams for the four point bending tests. All beams had the dimensions 1000/125/125 mm, and were tested with a span of 750 mm with the loads applied at the third points of the beams. The notched beams were provided with a 20 mm deep notch at midspan. In Figure 4.11, the average displacements at the notch tip and notch mouth are compared with the average displacement of the largest longitudinal elongation at the bottom fibre of the un-notched beams. When comparing crack openings and not the deflections, it can be seen that the difference in the structural behaviour between a notched and un-notched beam is not as pronounced as in case of the deflections. However, the curve shown here for the un-notched beams is the curve of the LVDT that registered the highest values; in the pre-peak phase, multiple cracks open along the entire beam span, and the total crack length would be the addition of all the small crack widths, a value which is very difficult to measure. Keeping that in mind, it is evident that the real crack width until peak load would be larger than the registered value here, and the strain hardening phase would be longer, so the total response would be in better agreement with the two curves shown for the deflection in Figure 4.10.

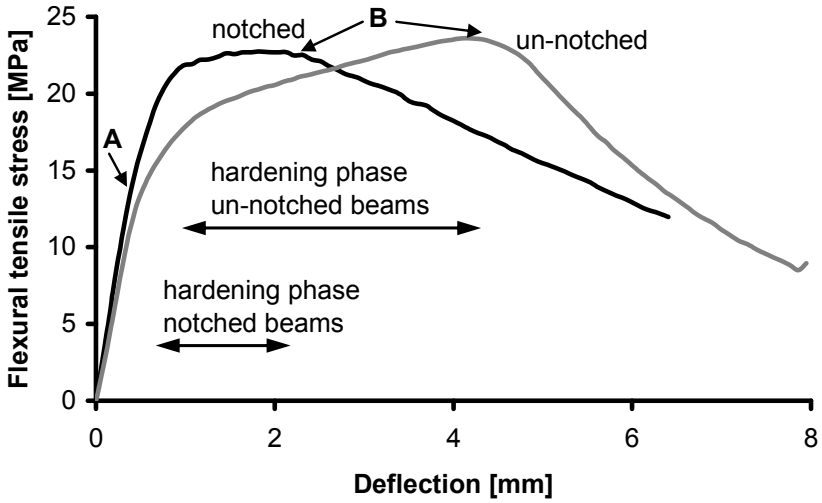

Figure 4.10: Average stress-deflection curves of notched and un-notched HSFRC beams. Beam dimensions: 125/125/1000 mm, span: 750 mm, notch: 20 mm. Point A indicates the point of crack initialisation, point B the end of the multiple cracking formation.

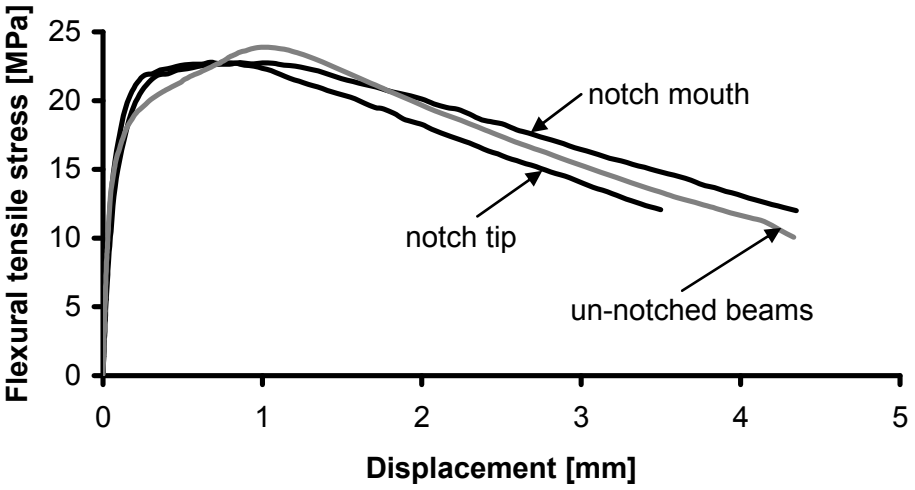

Figure 4.11: Average stress-elongation curves measured at the notch tip and notch mouth for the notched HSFRC beams, or the longitudinal displacement at the bottom fibre of the un-notched HSFRC beams.

On a number of notched specimens, also the strains at the compressive zone had been monitored in order to obtain information on the strain distribution throughout a static test. Results of the measured strain distribution will be mentioned in Chapter 6, where the measured strain distributions will be compared with the strain distributions calculated with the multi layer model.

Comparison between three and four point bending tests of HSFRC

As a final remark before showing the results of the static un-notched four point bending tests for the three mixtures, a comparison between all the tests on the HSFRC mixture mentioned before is shown in Figure 4.12. Beams tested in four-point bending had dimensions 1000/125/125 mm, a 20 mm deep notch at mid span and were tested at a span of 750 mm with the loads applied at the third points of the beam. The beams of the three-point bending tests had the dimensions 600/150/150 mm and were tested at a span of 500 mm (as recommended by RILEM (TC162-TDF, 2002)), and were provided with a 25 mm deep notch at midspan. Since the deflections were not registered during the three point bending tests, only the crack openings are compared. As can be seen, with the chosen dimensions of the test specimens similar responses are obtained with all three methods when the applied load is expressed in terms of the equivalent linear elastic flexural tensile stress. Also the linear elastic response is in very good agreement for all mixtures. However, as has been already mentioned, in case of the un-notched bending tests, the crack openings could only be registered indirectly, and the real crack opening would be larger in the pre-peak stage with a more pronounced hardening phase. The highest flexural stresses were obtained on the notched specimens in three-point bending; this is plausible since the notch is not necessarily located in the weakest cross-section, and in three-point bending a smaller part of the beam is subjected to the maximum bending moment compared to the four-point bending.

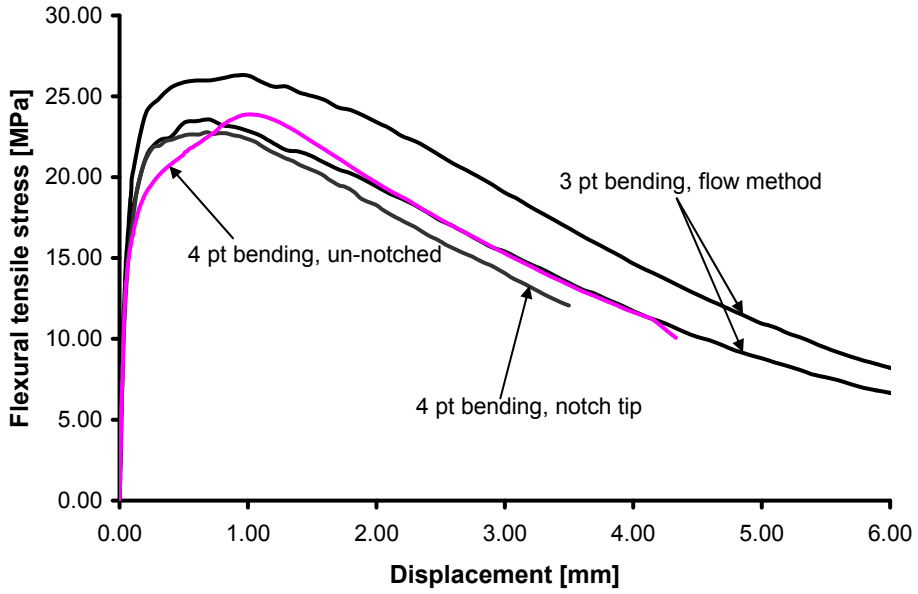

Figure 4.12: Comparison of the registered crack openings between the un-notched four point bending tests, notched four point bending tests and notched three-point bending tests. All beams were cast with the flow method.

A notch forces deformations to localise and predefines the crack path. Such a behaviour is not likely to happen in real structures. In order to estimate the overall structural behaviour of an element and test its ability to form multiple cracks in the pre-peak region and with that a hardening stage, tests on un-notched specimens are of advantage. However, in order to be able to measure the crack openings after the peak load, as soon as deformations localise into one major crack, tests on notched specimens are recommended. Measuring the crack openings can be essential for correctly modelling the stress-crack width relation. If the testing facilities and time allow, a combination of both testing methods, tests on un-notched specimens in order to obtain the pre-peak response including hardening, and tests on notched specimens for the post-peak response, might be the ideal way to test such high performance materials.

Results of static un-notched bending tests for all three mixtures

The main method in this research was the static four point bending test on on 1000/125/125 mm un-notched beams tested at a 750 mm span, and this was applied to all three mixtures in the study. The results can be found in detail in Lappa et al. (2005a). The main findings are listed in the following.

Figure 4.13 shows the results of the static bending tests for all four mixtures used in this study, the three main mixtures used for fatigue testing and also the UHPC mixture from Karlsruhe University (Scheydt, 2004) that was used for the joint durability/fatigue tests. The curves are given in form of an equivalent linear elastic flexural tensile stress in relation with the deflection. Each curve is the average of all beams tested under static loading for each mixture. All beams were cast by the 'flow' method. Eight beams were tested for each of the two high strength concretes, six beams for the ultra high strength concrete BSI/CERACEM, and three for the UHPC mixture. In Table 4.2, the average peak load and corresponding stress of all beams of one mixture and their coefficient of variation are listed for the three main mixtures of this study (BSI/CERACEM, HSFRC and hybrid HSFRC).

Table 4.2: Average peak loads, corresponding stresses and coefficients of variation for the static bending tests.

	BSI/CERACEM	HSFRC	Hybrid HSFRC
Number of tested beams	6	8	8
Peak load [kN]	77.7	62.1	50.4
Flexural strength [MPa]	29.9	23.9	19.3
Standard deviation [MPa]	3.2	2.0	1.4
Coefficient of variation	11%	8%	7%

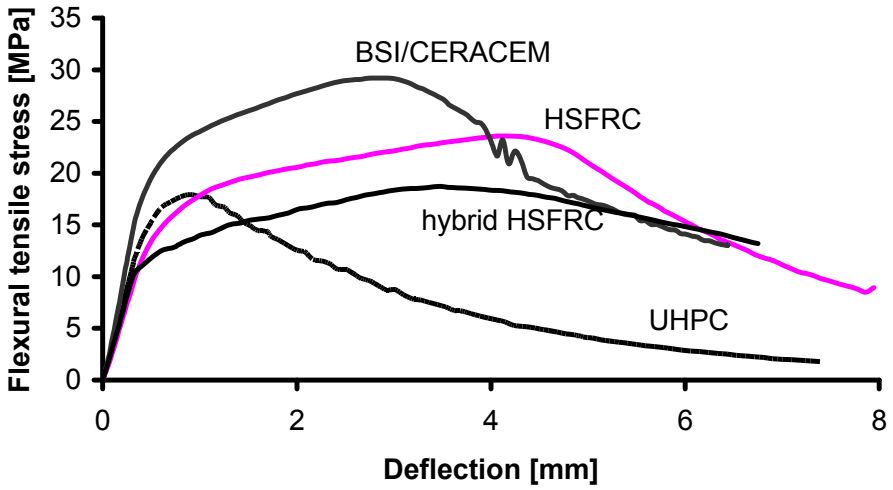

Figure 4.13: Average static stress-deflection curves of beams made of the four concrete mixtures used in this study.

As can be seen, the specimens made of the two HSFRC mixtures show a comparable initial stiffness and are in good agreement in the linear elastic part until initial cracking. This is expected considering the fact that both mixtures have a similar dense matrix of the same strength, and contain a similar volume of fibres. The stiffness of the BSI/CERACEM is higher than that of the HSFRC; due to the Bauxite aggregate addition this material reaches an elastic modulus of approximately 50 GPa opposed to 40-45 GPa for the two HSFRCs. All three mixtures show a significant load increase after first cracking, showing deflection hardening. This is associated with the formation of many microcracks that are barely visible; up to that moment no crack localisation had occurred yet. The load could be increased up to deflections of 3 mm and even larger.

The response of the UHPC mixture from Karlsruhe was added in Figure 4.13 in order to further highlight the hardening phase. The UHPC is an ultra high strength concrete reinforced with 2.5 vol.% of the shortest fibres used in this study, namely 8 mm, with 0.175 mm diameter in cross-section (more details on the mixture compositions can be found in Chapter 2). Due to their shorter length and therefore lower fibre aspect ratio, a fibre addition of 2.5% is not sufficient to obtain a pronounced deflection hardening behaviour. Moreover, while the BSI/CERACEM and the two HSFRC are self-compacting, the UHPC is compacted by vibration; pull-out tests on single fibres have shown that a self-compacting matrix results into higher bond stresses (Holschemacher and Klug (2005), Markovic (2006)), so that the three self-compacting mixtures can exhibit a higher pull-out resistance, which acts in favour of the development of a hardening phase.

With regard to the response of the mixtures tested in a bending test on un-notched specimens, it should be noted that the descending branch of the hybrid

HSFRC is less steep, since the 60 mm long fibres can bridge larger crack openings while the 13 mm long fibres of the HSFRC and 20 mm long fibres of the BSI/CERACEM are better able to bridge microcracks in the prepeak region.

Figure 4.14 shows that the peak flexural stress can be directly related to the amount of fibres present in the cross-section close to the crack leading to failure, by plotting the average flexural strength of each mixture against a dimensionless fibre factor. This factor is introduced in order to compare fibres of different geometry, and can be obtained by a multiplication of the fibre volume fraction V_f with the fibre aspect ratio, which is the ratio between the fibre length l_f and the fibre diameter d_f. The scatter in the value of the maximum flexural tensile stress is indicated by error bars.

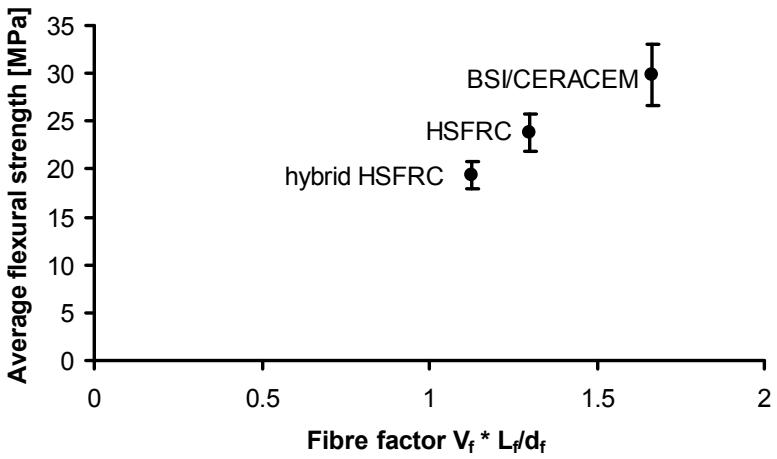

Figure 4.14: Relation between the maximum flexural tensile strength and the fibres present in each mixture.

4.4 Image analysis

Fibres are crucial for the tensile load bearing capacity of a fibre reinforced material and the more fibres present and aligned in loading direction in a cross-section, the higher will be the crack bridging resistance and load bearing capacity. Therefore, often the fibres in the testing specimens have been counted in order to quantify and evaluate the structural behaviour of fibre reinforced concrete.

Different methods can be used in order to count fibres in a structural element, test specimen or a cross-section. These methods include wash-out tests (Alfes, 2006), that imply that after mixing the concrete, a mould is filled, to be emptied over a sieve while the concrete is still flowable. After washing out the coarse aggregates and fibres that remain on the sieve, the steel fibres can be separated from the aggregates with a magnet, and by counting and weighing them, the fibre

concentration in the mixture can be evaluated. Such an approach will not be followed in this thesis; the fibre concentration will only be evaluated on hardened concrete, on parts of previously tested specimens. Also, wash-out tests cannot provide information on the fibre orientation in a specimen, but only their concentration. However these tests are often used as a quality control test by contractors at the construction site. Additionally, with suitable wash-out tests segregation effects of aggregates on fibres in a matrix can also be studied (Lowke et al., 2003).

As already mentioned, the fibre dispersion was not evaluated on concrete in the fresh state, only on parts of previously tested specimens. Of course, one possible method is to manually count the fibres present in the fracture surface of a test specimen, as has for example been done by Soroushian and Lee (1990) and Kooiman (2000). This, however, is a very time consuming and strenuous task for the rather high fibre additions in the mixtures used in this research. Also, due to the fact that short, thin fibres have been used, especially in the HSFRC mixture, fibre concentrations above 30 fibres/cm^2 can occur at the applied fibre volume fraction of 1.6%, making a manual count almost impossible. Therefore a different, more automated method had to be chosen.

Other common methods are based on counting on images of sections of a specimen and not on the specimen itself; these images could be X-rays (Stroeven et al., 1978, Kasperkiewicz et al., 1978), photographs of microscopical images (Eberhardt and Clarke, 2001), or simple photographs of cross-sections (Schönlin, 1988). On these images, the fibres can again be counted manually, as has been done by Grünewald (2004) on X-ray images, or digitally with appropriate image analysis software (Mlekusch, 1999). For this research, photographs were taken of beam cross-sections which later were analysed with the image analysis software package Optimas (Media Cybernetics, 1999).

Additional possible methods for counting fibres, which were however not applied to this research, are non-destructive methods on whole specimen parts. These include alternating current (AC) impedance spectroscopy (Özyurt, 2006) and computerised tomography (CT) imaging (Farhat et al., 2006), which can provide information on the steel fibre concentration in mixtures. It should be noted that both techniques cannot give information on the actual short fibre alignment and concentration but more globally, on their concentrations in the mixture. In the case of CT scans these can be shown in the form of contour-plots (Farhat et al., 2006). However, these rather costly techniques were not applied in this research since already sufficient information on the fibre alignment was obtained by the image analysis of the cut cross-sections.

Before presenting the results of the fibre count by image analysis performed in this study, background information on the theory and methodology will be given. Image analysis can be a useful tool to study micro-structural characteristics of various

materials and has been utilised in various fields, including medicine, biology, engineering and material science. Image analysis implies that various measurements are performed on images; most of the time a 3D structure is evaluated, where the images only represent a section plane through the structure. For a general overview of possible measurements on images, the representation of 3D shapes in a 2D image, and counting techniques of areas and points on images, general stereology textbooks are available such as Russ and Dehoff (2000).

In concrete, image analysis on photographs, X-rays, on light microscopy or scanning electron microscopy (SEM) images have been applied in order to evaluate the porosity of a mixture (Ye, 2003), aggregate and fibre distributions in a mixture, fibre orientation, and the mineral composition of a mixture, among others. An overview of possible uses of image analysis in civil engineering, and for cement and concrete in particular, is given by Chermant et al. (2001). A number of researchers have used image analysis in order to count fibres in fibre reinforced concrete (Akkaya et al., 2000, Grünewald, 2004, Özyurt, 2006, Markovic, 2006). In the following, the used technique will be briefly explained. The determination of the number and orientation of short fibre reinforced composites on an image of a cross-section has been described in detail by Mlekusch et al., (1999), Mlekusch (1999), Eberhardt and Clarke (2001) and Eberhardt et al. (2001). For the determination of an actual fibre orientation factor representing the complete image observed, the technique as described by Schönlin (1988) and applied by Grünewald (2004) and Markovic (2006) has been used.

Fibres in cross-sections will be generally visible with an elliptical form. In the ideal case, when the fibre is perpendicular to the cross-section, it will be visible as a full circle, otherwise as an ellipse. In case an ellipse is visible, the minor axis *b* corresponds to the fibre diameter, while the major axis *a* is the visible length of the fibre on that plane. Two angles exist that characterise the fibre direction: the in-plane angle φ and the out-of-plane angle θ; all definitions are shown in Figure 4.15. The out-of-plane angle θ gives an indication of the fibre alignment with regard to the loading direction; in that case, a perpendicular out of plane direction ($\cos\theta=1$) would imply a perpendicular alignment to the loading direction and a preferable alignment with regard to the load bearing and crack bridging ability of the fibre. The in-plane direction φ is equal to the orientation of the ellipse major axis *a* with respect to an arbitrary in-plane direction (Eberhardt and Clarke, 2001) while the out of plane angle θ can be determined from the major, *a*, and minor, *b*, axis length of the fibre in the cross-section:

$$\theta = \arccos(b/a) \tag{4.13}$$

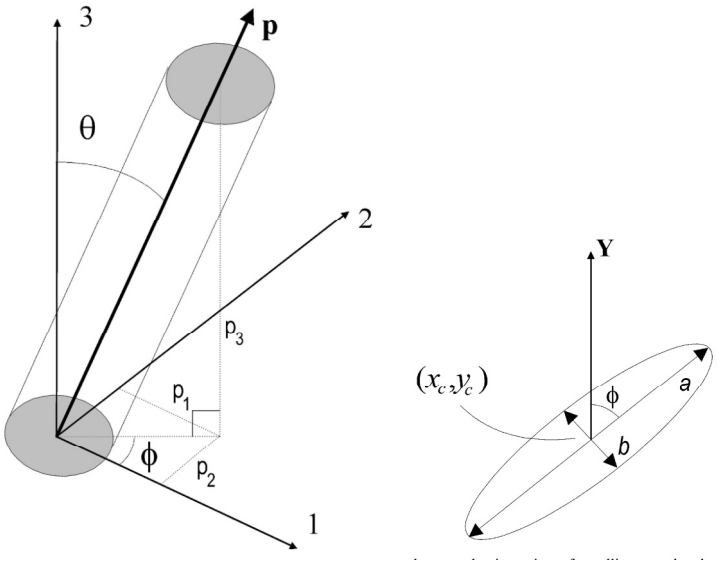

Figure 4.15: Left: fibre in a 3D space; visible are the in- and out-of-plane angles φ and θ. Right: definition of an ellipse with its center point, major and minor axis and in-plane angle (after Eberhardt and Clarke (2001))

Note that there is an orientation ambiguity when determining the orientation angles from the image of one cross-section only (see Figure 4.16): fibres with orientations (θ, φ) and (θ, φ+π) are indistinguishable, the analysis of three perpendicular cross-sections is needed for a complete evaluation of the fibre orientation. However, with regard to the fibre crack bridging ability in the beams of this study, the response of fibres orientated with (θ, φ) and (θ, φ+π) would be equal. Therefore it is sufficient to only regard one cross-section for each beam and the fibres' out-of-plane angles in order to derive information on the fibre orientations.

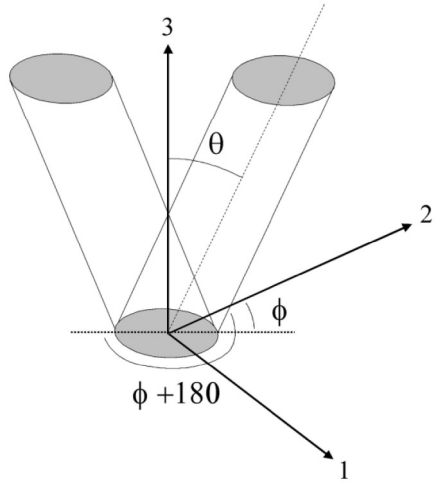

Figure 4.16: Unambiguity in determining the fibre orientation from a single cross-section (after Eberhardt and Clarke (2001))

The total number of fibres N in a cross section can be determined by adding up all visible ellipses and circles. A dimensionless orientation factor η, giving an indication on the average orientation within a cross-section, can either be determined by comparing the counted number of fibres N to the theoretical number of fibres N_f [1/mm^2] that should be present according to the applied fibre volume fraction in the mixture, or via the out-of-plane angles determined for the single fibres in the cross-section.

The first method, has been applied by Soroushian and Lee (1990) and is given by the following equation:

$$\eta = N_f \cdot \frac{A_f}{V_f} \qquad (4.14)$$

With A_f [mm^2] being the cross-sectional area of the fibres, $\pi d^2/4$, d [mm] the fibre diameter, and V_f [-] the volume fraction of fibres in the concrete.

The second method to determine the orientation factor, via the fibres' out-of-plane angle, can be determined with the next equation (Schönlin, 1988). This is the method applied in this study:

$$\eta = \frac{1}{N} \cdot \sum_{i=1}^{N} \cos\theta_i \qquad (4.15)$$

In the above equation the number of fibres N [-] is the total number of fibres counted in the cross-section via image analysis.

Tested beams of all three mixtures were cut 1-2 cm behind the fracture surface and pictures were taken of the cross-sections using a camera with flash. Since the concrete absorbs the light of the camera flash but the steel fibres reflect it, the steel fibres are easily distinguishable on the images and a colour threshold can be set in order to count and determine the fibre orientation with the image analysis software 'Optimas' (Media Cybernetics, 1999). The results of the image analysis of the BSI/CERACEM will only be presented briefly here since they have been given in detail in Lappa et al. (2004a).

The fibres counted in all cut cross-sections of the HSFRC are shown in Figure 4.17 plotted on normal probability paper. The assumption of a normal distribution of the fibres in the beams is valid. Behloul (1996) also assumed a normal distribution in his PhD thesis on another industrial ultra high strength concrete, DUCTAL. The same distribution can be assumed for the BSI/CERACEM and the hybrid HSFRC mixture: the probability plots are included in Lappa et al. (2005a).

Figure 4.18 shows the fibres present in beams tested under static loading in relation to the static flexural tensile strength, for the BSI/CERACEM and HSFRC. A direct relation was observed for the BSI/CERACEM, and also the HSFRC beams tend to show higher strengths a larger number of fibres, even though the relation is not

so direct. Since the scatter in the HSFRC beams was much lower and a much smaller range of strengths was obtained at testing, it is more difficult to obtain a direct relation between the number of fibres and the flexural tensile strength. The results of the BSI/CERACEM include beams produced with two different casting methods.

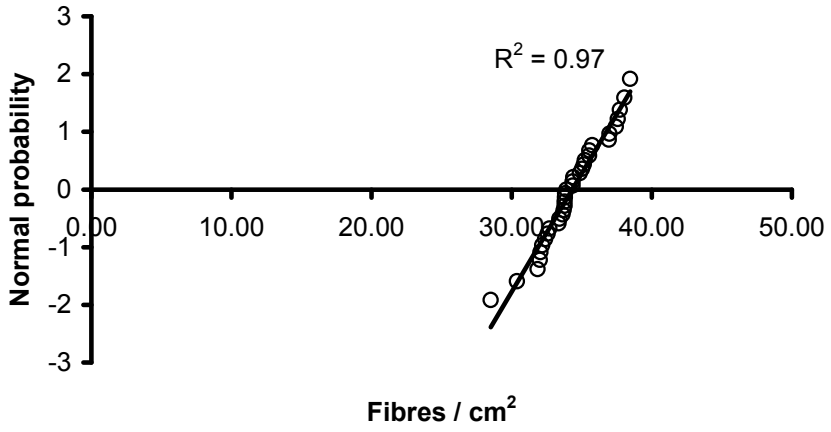

Figure 4.17: Fibres/cm^2 counted in cross-sections of HSFRC beams. Average value:34 fibres/cm^2 with a coefficient of variation of 6%.

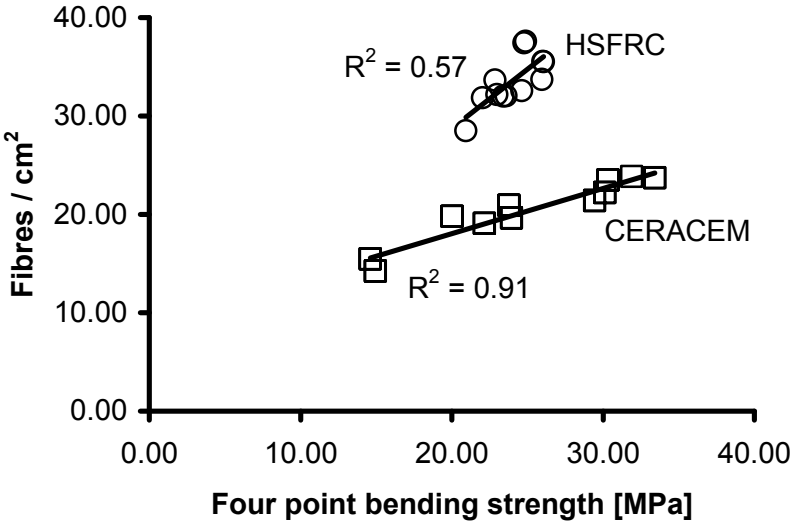

Figure 4.18: Fibres in beam cross section of the beams tested under static loading in relation with the static flexural tensile stress fort the BSI/CERACEM and HSFRC beams subjected to four-point bending.

For the hybrid HSFRC mixture, the results of the image analysis in terms of a relation between the number of fibres in a cross-section close to the fracture surface and the corresponding static flexural strength can be seen in Figure 4.19. One of the images used for the fibre count provided a very low number of fibres in comparison

to the other images: 10.61 fibres/cm^2 had been counted in the bottom half of the beam, which is a lower value compared to the average number of value of 11.82 fibres/cm^2 by a factor of 1.5 times the standard deviation. In this count, both the hooked-end longer fibres and the straight smaller fibres have been regarded. A relation between the number of fibres in a cross-section and the static flexural strength can only be obtained if that particular image with this low amount of fibres is left out. In Figure 4.19 the regression lines of the fibre count are given, once when the critical image with low fibre amount is taken into account (black line and square markers) and once when it is left out (grey line and 'x' markers).

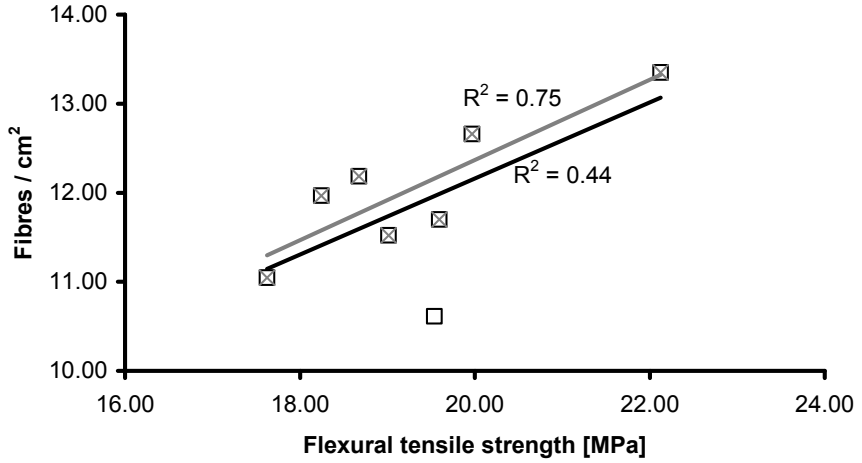

Figure 4.19: Fibres in beam cross section in relation with the static flexural tensile strength for the hybrid HSFRC, once including the smallest value (black) and once without it (grey).

Figure 4.20 shows the orientation numbers determined for beams of all three mixtures tested under static loading. The orientation number does not correlate to the static flexural tensile strength or the production method, but is more or less constant for beams of one mixture at values in the range of 0.7-0.8. These values show that the fibres were not aligned randomly, but had a main orientation direction, and that was perpendicular to the fracture surface, so that the fibres could bridge appearing cracks. Detailed results regarding the amount of fibres counted in the top and bottom half of a beam cross-section for each mixture and their orientation number are included in Lappa et al., (2005a).

The fibre count by image analysis resulted into an average value of 19.14 fibres/cm^2 for the BSI/CERACEM, 34.33 fibres/cm^2 for the HSFRC and a total of 11.88 fibres/cm^2 for the hybrid HSFRC. The latter value is composed out of 10.02 fibres/cm^2 of short and 1.86 fibres/cm^2 of long fibres. Ideally, if all fibres would be aligned perpendicular to the cross-section (orientation factor 1.0), all fibres would be visible as circles. This theoretical maximum amount of fibres can be determined for

each mixture by determining the area of one single fibre, and by multiplying this value by the fibre volume fraction of the mixture and the cross-sectional area of the beam. In that way, 35.37 fibres/cm^2 should be ideally present in the BSI/CERACEM, 79.20 fibres/cm^2 in the HSFRC and 18.18 fibres/cm^2 in the hybrid HSFRC (15.92 fibres/cm^2 of short fibres and 2.26 fibres/cm^2 of long fibres). Therefore, with image analysis 54% of this ideal number of fibres was obtained for the BSI/CERACEM, 43% for the HSFRC, and 65% for the hybrid HSFRC.

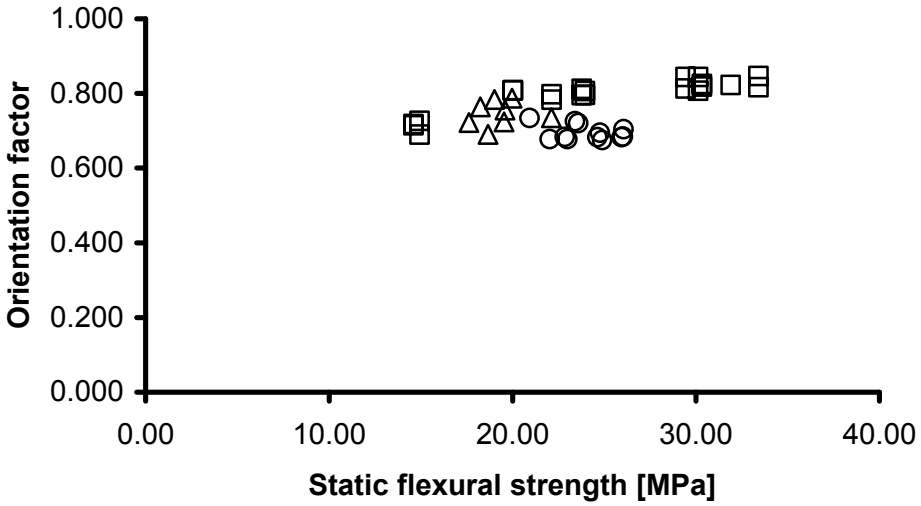

Figure 4.20: Orientation number in relation to the flexural tensile strengths of beams tested under static loading made of BSI/CERACEM (squares,) HSFRC (circles) and hybrid HSFRC (triangles).

Factors influencing the fibre alignment

The main factors responsible for the fibre alignment in a section are the boundaries of formwork, the flow direction of concrete, gravity and vibration. Since all mixtures examined here are self-compacting, orientation due to vibration can be ruled out. The orientation along formwork boundaries (wall-effect) is a very dominant factor for these beams, since the beams are cast in separate small moulds and that implies that a considerable part of the cross-section is influenced by the formwork boundaries. However, the smaller the fibre length, the smaller the area affected by the wall-effect, which is mainly present at lengths approximately one time the fibre length. Therefore, this effect should be the least visible for the HSFRC and the most for the long fibres in the hybrid HSFRC. Also gravity effects can occur; the fibre count showed that for the BSI/CERACEM and HSFRC, approximately 55% of the fibres were situated in the bottom half of the beam and 45% in the top part. For the hybrid HSFRC this ratio was almost equal to 50%.

It was already mentioned in section 4.3.1 that the casting method influences the fibre alignment; therefore the falling height and the flow possibilities and direction of

the concrete in the mould as related to the chosen casting method, casting direction and mould, are factors that influence the fibre alignment. Therefore, the fibre alignment and orientation can differ significantly in beams cast horizontally or vertically, as has been reported by Stiel et al. (2004), with vertically cast beam elements showing lower strengths and deformation abilities in their flexural behaviour due to poorer fibre alignment. Also in the beams cast for this study a tendency of fibre alignment due to the concrete flow was observed. In this case all beams were cast horizontally: therefore a beneficial alignment with regards to their bending behaviour could be achieved. The chosen beam dimensions however also enabled a secondary, circular flow in the mould, and an alignment of fibres along with this flow could be observed as the concrete was flowing from the top to the bottom of the mould. For this secondary flow to develop, a certain filling height is needed; in the lowest layers, the fibres are well orientated mainly due to the wall effect, while in the higher layers the fibres are also orientated along this secondary flow, showing a larger fibre spacing and positions less perpendicular to the beam cross section compared to the fibres present in the bottom part. Figure 4.21 shows the assumed fibre alignment for the beams cast with the 'flow' method, showing the influence of the primary flow on the left, along the beam length, and of the circular secondary flow, as can be seen on the right, from the top to the bottom of the beam. Arrows indicate the point where the concrete is poured into the mould and the primary and secondary flow directions. Also Lyslo Døssland (2006) reported similar flow patterns while casting large-scale walls of self-compacting fibre reinforced concrete. Figure 4.22 highlights the effect of the secondary flow, by showing the fibre alignment as observed on the fracture surface of an actual cross-section of a tested beam and schematically reproducing the fibre alignment over the cross-section.

It has been shown that for the beams cast in this study, the fibres were aligned mainly perpendicular to the fracture surface, especially in the bottom layers of concrete in a beam. Since the top side of the beam in the mould was also the top side of the beam in the testing apparatus, this means that fibres were able to bridge cracks and have a beneficial effect on the load bearing capacity of the beams. Beams cast in a different way or tested upside down would perform differently. These effects have to be taken into account when designing actual structural elements out of such materials. The French interim design regulations for ultra high strength concrete show one possibility how these effects can be included (AFGC-SETRA, 2002): A factor 1/K was introduced to take fibre orientation effects into account, which expresses the greatest observed deviation from the mean. In order to determine appropriate values for K, it is advised to use test specimens from representative models of the actual structure. Different K factors should be used depending on the element shape and production method, so that different values for thick or thin beams, slabs or columns apply.

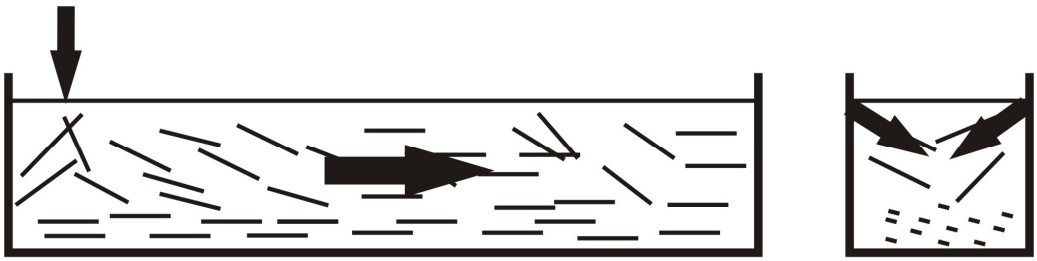

Figure 4.21: Illustration of fibre alignment due to primary and secondary flow.

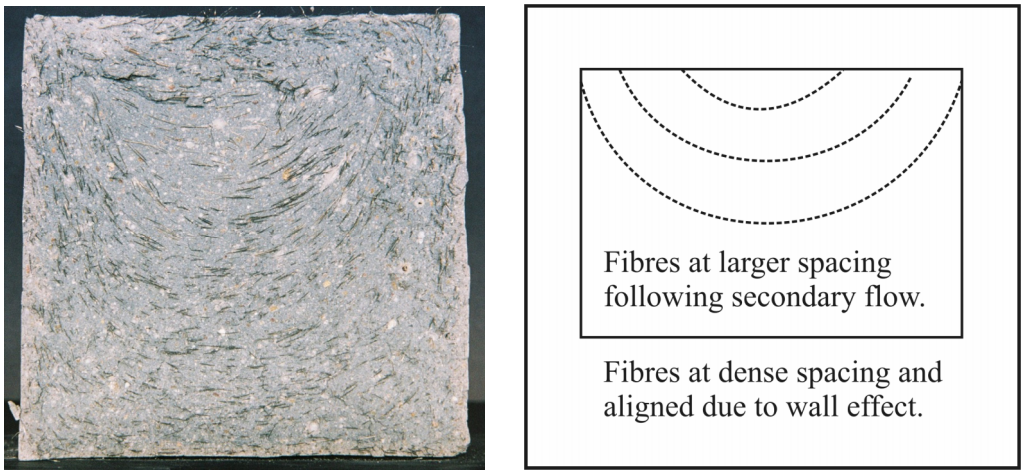

Figure 4.22: Fracture surface of a tested beam and schematic representation of the fibre alignment in the cross-section.

A final remark on the fibre alignment and concentration; up to now, the fibre concentration had mainly been evaluated for cross sections close to the fracture surface, but for the BSI/CERACEM a small study to evaluate the fibre concentration at different cross-sections along the beam length was performed on five beams that were cast only for this purpose. All five beams were cast out of the same batch of concrete. They were cast with the 'flow method' and the coordinate x=0 indicates the end of the mould from which the concrete was placed into it. The beams were cut at distances 125, 375, 500, 625 and 875 mm from that point. Figure 4.23 shows the results from the image analysis on the cross-sections; also the orientation numbers were determined but little variation was found between them. The orientation number can be regarded a constant along the beam length with values just above 0.7. As can be seen, for most of the beams, the number of fibres decreased with increasing distance from the casting point with a 'dip' in the middle. One would expect a constant decrease; however, since the BSI/CERACEM mixture was not so workable, the concrete was placed at its opposite end during casting and this could be an explanation for this increase in fibre concentration.

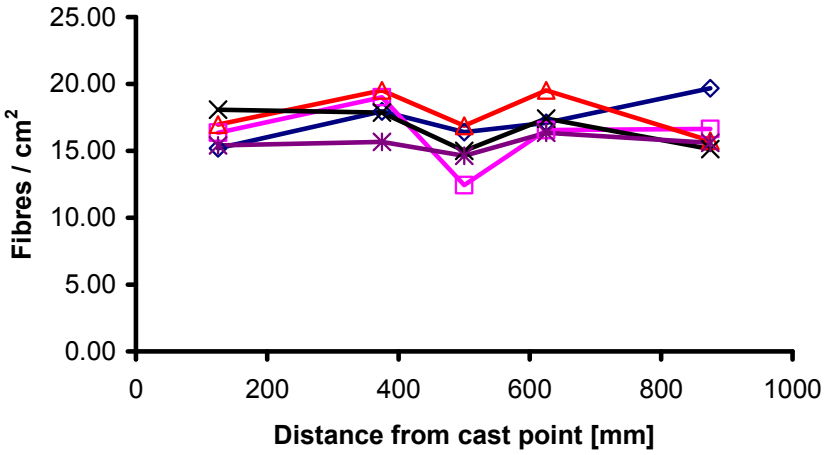

Figure 4.23: Fibre concentration along the beam length for BSI/CERACEM beams.

4.5 Tensile tests

Tensile tests were performed with the HSFRC mixture only with the intention to use the results as material input parameters in Chapters 6 and 7. At the Stevin Laboratory of Delft University, tensile tests on high strength fibre concrete had been already carried out by Markovic (2006), and the same specimen size, testing facility and procedure was chosen for the tests of this study. Initially, a series of six un-notched and six notched dogbone specimens was tested. The testing was as described by Markovic (2006), with four LVDTs placed as a set of two on each side over a measuring length of 110 mm in order to measure the displacements. Of the six un-notched and notched specimens, three were cast with a horizontal pouring direction of the concrete into the mould and three with a vertical one (Figure 3.12, Chapter 3). The results of all tensile tests are given in Table 4.3, they include the results for horizontal and vertical casting directions (marked with H or V respectively) and the results of the additional series with a measuring length of 35 mm (grey values). In the following, the main observations of the tensile tests will be presented.

It was expected that the specimens, which were cast vertically, would behave better than those cast horizontally. The main reason for this expectation is that fibres have a tendency to align with the flow, so that the ones cast vertically are more in line with the direction of the tensile load, than the ones cast horizontally. It should be noted that also the front and backside of each specimen can have different fibre orientations: one side was the bottom surface of the mould, were a preferable orientation for testing due to fibre alignment along the formwork boundary can occur. The other side was cut with a diamond edge saw since the moulds were

30 mm wider than the depth of the specimens. Therefore, a more random alignment can be expected at that side.

Table 4.3: Results of the uniaxial tensile tests. H or V indicate a horizontal or vertical casting direction. Grey values: additional series with 35 mm measuring length.

notched specimens			un-notched specimens		
Cast V/H	**Force [kN]**	**Stress [Mpa]**	**Cast V/H**	**Force [kN]**	**Stress [Mpa]**
H	35.99	10.00	H	43.02	8.78
H	32.47	9.02	H	37.65	7.68
H	37.35	10.38	H	39.01	7.96
V	42.09	11.69	V	46.582	9.506530612
V	35.25	9.79	V	40.918	8.350612245
V	40.43	11.23	V	46.3867	9.466673469
V	46.92	12.69	V	45.12	9.05
V	44.87	12.30	V	49.56	10.00
V	38.77	10.73	V	49.90	10.16
average	**39.35**	**11.91**	**average**	**48.19**	**9.74**
st dev	**4.69**	**1.04**	**st dev**	**2.67**	**0.60**
COV	**12%**	**9%**	**COV**	**6%**	**6%**

The considerations on the fibre alignment are evaluated in Figure 4.24 and Figure 4.25. Figure 4.24 shows the average curves of three specimens cast vertically and horizontally, and the total average of both curves. On the left part, the average curves for the un-notched specimens are shown, and on the right part the average curves of the notched specimens. As can be seen, the vertically cast specimens showed a slightly better tensile response by reaching higher strengths, than the horizontally cast specimens, which can be explained by a more beneficial fibre alignment for the vertically cast specimens due to fibre alignment in flow direction. Figure 4.25 shows the differences in fibre alignment within one specimen, by showing all measurements of the four LVDTs at both sides of a specimen. The LVDTs placed at the side that was cut with a saw show larger displacements than the ones placed at the side that was the bottom part of the mould, thus showing a 'wall effect'. The fibre alignment at the formwork boundary is beneficial for the tensile tests, since more fibres can bridge the crack opening, and this is the reason why smaller crack openings are registered on that side compared to the opposite side, the cut side, which had a more random fibre orientation.

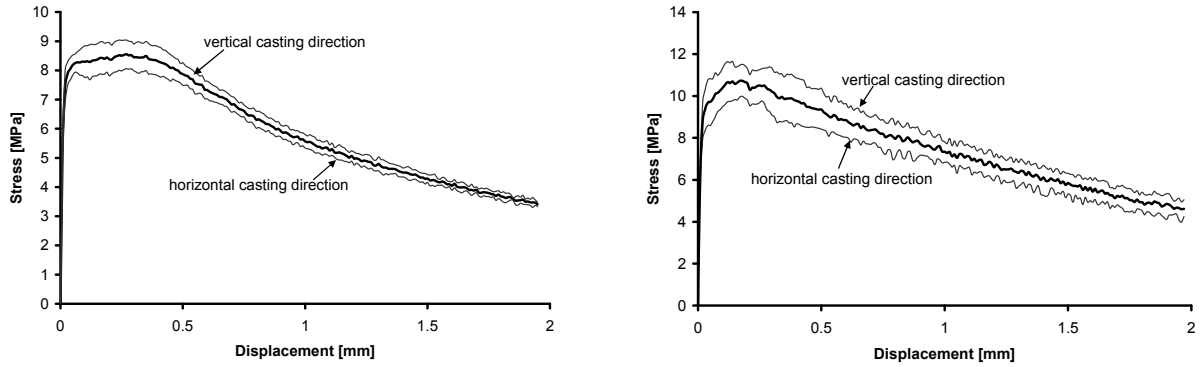

Figure 4.24: Influence of the casting direction on the uniaxial tensile response. Shown are the average curves of three specimens and their overall average. Left: un-notched specimens; Right: notched specimens.

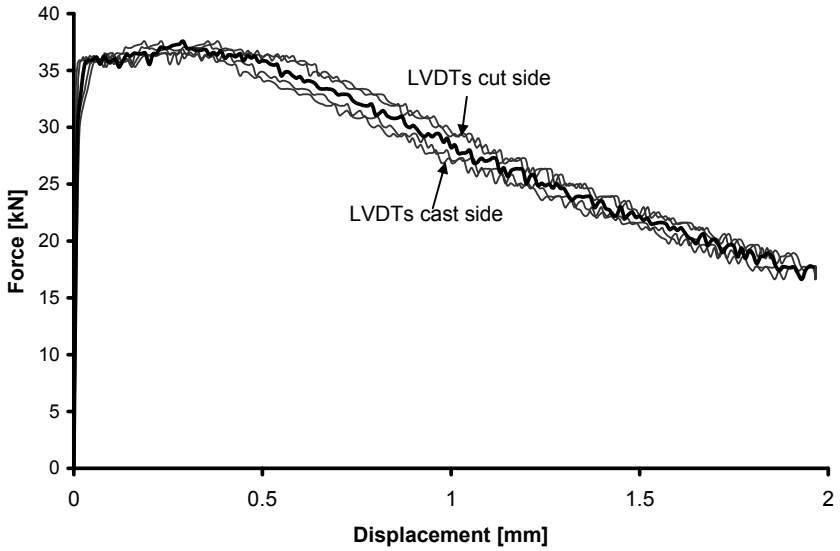

Figure 4.25: Individual LVDT-measurements during a uniaxial tensile tests; the LVDTs at the cut side of the specimens registered larger displacements opposed to the LVDTs at the cast side.

As can already be observed in Figure 4.24, the notch influences the structural response in uniaxial tension in a similar way as observed in the bending tests. Figure 4.26 highlights the influence of a notch by comparing only the average curves of all six specimens of a notched and un-notched test series regardless their casting method. It should be noted that the material shows strain hardening also in uniaxial tension and not only in bending. Therefore it can be classified as a 'high performance' material in accordance with the definition of high performance fibre reinforced cementitious composites by Naaman and Reinhardt (1996). This strain

hardening is longer for un-notched specimens (horizontal distance AC in Figure 4.26), meaning that the crack localisation into one single crack occurs later, since multiple cracking is not hindered by a notch that predefines the crack path and forces cracks to localise early. The notched specimens reach higher tensile stresses (not loads), since the notch is not necessarily located at the weakest cross-section of the specimen. The onset of initial cracking, that is the transition from the linear elastic to the strain hardening or multiple cracking phase, is identical for both notched and un-notched specimens (point A in Figure 4.26). As a final remark, note that the dogbone shaped specimen already has a reduced cross-section in its middle part, and so it already predefines the crack location. Therefore, the use of a notch in a dogbone specimen can be questionable. Indeed, the notched specimen tests were not carried out in order to use their load-displacement response as a characteristic curve for the tensile load bearing capacity of the material but in order to obtain a stable descending branch (stress-crack width relation) after crack localisation at postpeak. Only the curve obtained from the un-notched specimens will be used as input for the material model in Chapters 6 and 7.

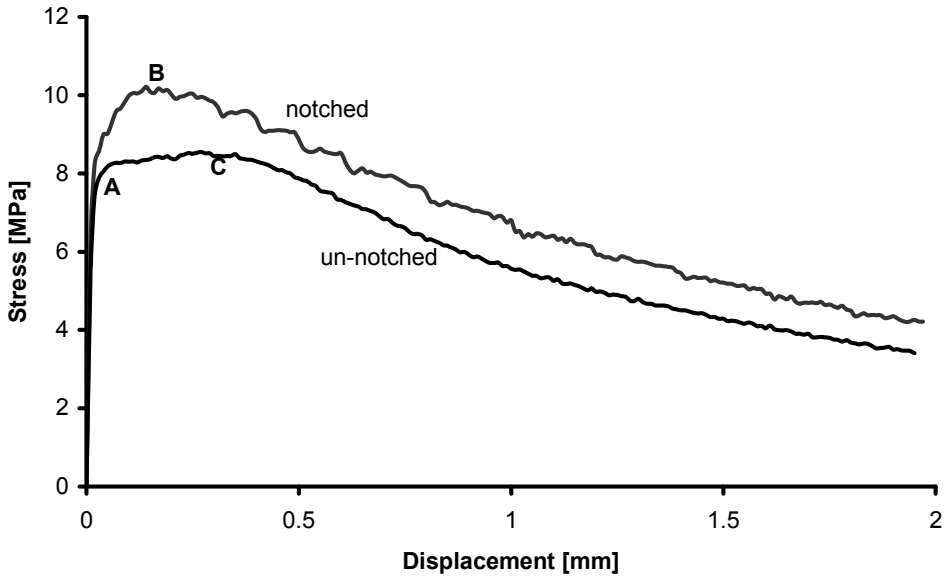

Figure 4.26: Comparison of average structural response of notched and un-notched dogbone specimens subjected to uniaxial tension. The average curves given are the overall averages of all six specimens of both casting methods. Marked are the initial cracking phase (point A), and the end of the multiple cracking phase (point B in case of notched specimens and point C in case of un-notched ones).

When examining material properties by experimental research, and the possibility to perform both notch and un-notched tests is given, it can be advantageous to perform both: the un-notched tests can provide information for the stress-strain behaviour of the material up to the peak load, and the notched test can

be used in order to obtain a stress-crack width relation at postpeak. This approach was also followed by Jungwirth (2006). Further, in case of notched specimens, the major crack was straighter, since its crack path is predefined by the notch, than in case of un-notched specimens, as can be seen in Figure 4.27. Figure 4.28 shows the fracture surface of an un-notched tensile test, where a number of fine cracks is visible below the main fracture surface and also pulled-out fibres on the fracture surface.

Figure 4.27: The main crack in a notched and an un-notched specimen.

Figure 4.28: Crack surface of an un-notched tensile specimen; visible are pulled-out fibres and fine distributed cracks close to the main crack surface

In the following, the results of an additional testing series with measuring length over 35 mm and 110 mm will be discussed. This testing series was necessary in order to evaluate assumptions of crack localisations that were made after using the previous test results as input to model the results of beams (see Chapter 6). On each

side of the specimens, one LVDT was placed with a 35 mm measuring length and one with 110 mm; three notched and three un-notched specimens were tested. The results, regarding the registered peak force and strength values, for this additional series can be taken out of Table 4.3, while in the following paragraphs the results will be discussed with respect to the measured displacements and resulting strains.

Figure 4.29 shows an example of registered displacements and their equivalent strains during an un-notched tensile test; on the left, the stress-displacement relation is given and on the right, the stress-strain relation with displacements divided by their corresponding measuring length. The black curves correspond to LVDTs that measured over a length of 35 mm, the grey ones over 110 mm. The equivalent measurements for notched specimens can be seen in Figure 4.30. Figure 4.29 shows that in this particular case, one of the two LVDTs with a measuring length of 35 mm was placed outside the formation of the major crack: therefore unloading and a decrease of displacements was registered after the peak load (Figure 4.31). This happened with all three tested specimens, however fortunately the other LVDTs always bridged the crack even those with the 35 mm measuring length, so that always at least one postpeak measurement over the major crack was obtained with this length. This problem did not occur in case of the notched specimens, since the notches predefined the crack position and therefore the major crack was always bridged by both LVDTs over the shorter length.

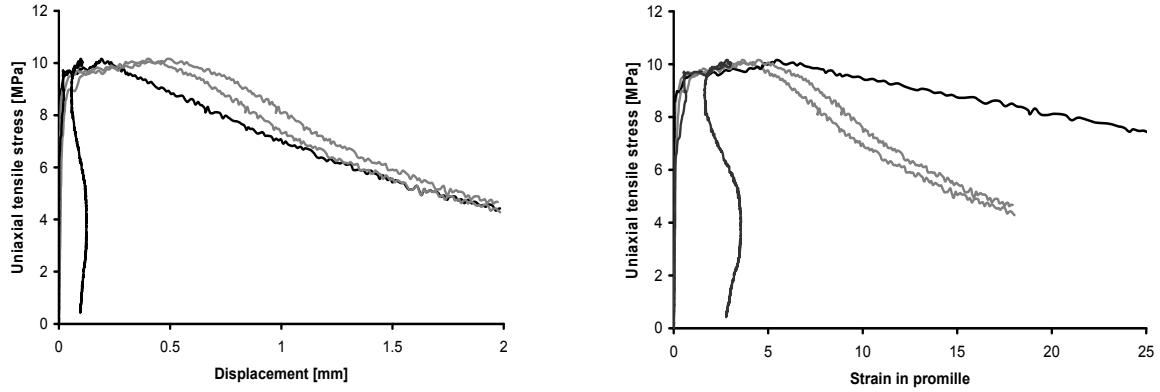

Figure 4.29: Examples of un-notched tensile tests with 35 mm (black lines) and 110 mm (grey lines) measuring lengths respectively, showing stress-displacement (left) and stress-strain (right) curves.

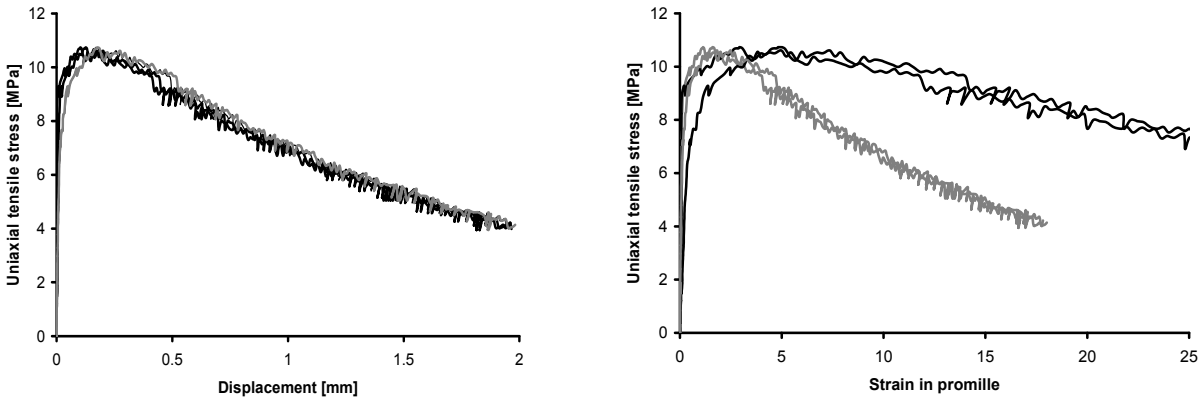

Figure 4.30: Examples of notched tensile tests with 35 mm (black lines) and 110 mm (grey lines) measuring lengths respectively, showing stress-displacement (left) and stress-strain (right) curves.

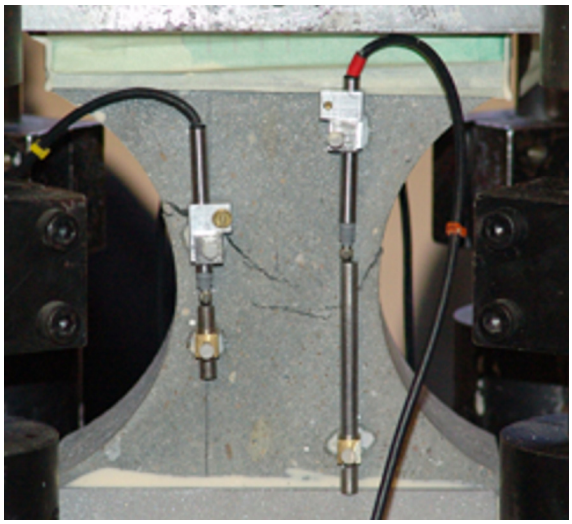

Figure 4.31: Un-notched tensile test with LVDTs with measuring lengths of 35 mm and 110 mm; in this case, the LVDT over 35 mm was not bridging the main crack on the shown side of the specimen.

Figure 4.29, Figure 4.30 and Figure 4.31 indicate that the previously mentioned assumptions on crack localisation after the peak load were valid: A more ductile descending branch (in terms of a stress-strain relation) can be regarded as a representative postpeak stress-strain relation, and it will be shown in Chapter 6 why this assumption was of importance. This is further demonstrated by the following figures which show the mean curves of all three specimens rather than the results of a single tests. Figure 4.32 shows the average curves of three un-notched specimens as registered by LVDTs over 35 mm (black curves) and 110 mm (grey curves), as a stress displacement diagram (left) and as a stress-strain diagram (right). Equivalent results can be seen in Figure 4.33 for the three notched specimens. As can be seen,

similar displacements have been registered, and the main difference lies in the descending branch of the stress-strain relation, which is much more 'ductile' when a shorter measuring length is used, verifying the assumptions that led to this testing series. The choice of a 35 mm measuring length has been proven to be a reasonable value for plain concrete (van Mier, 1997) and can therefore also be used for fibre reinforced concrete.

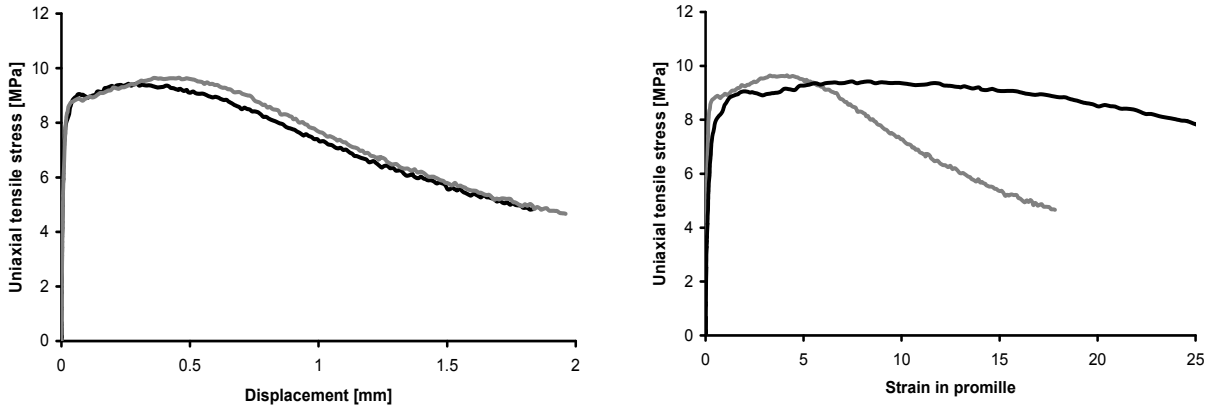

Figure 4.32: Average stress-displacement relation (left) and stress-strain relation (right) as the average of three un-notched specimens determined by measuring over 35mm (black curves) and 110 mm (grey curves).

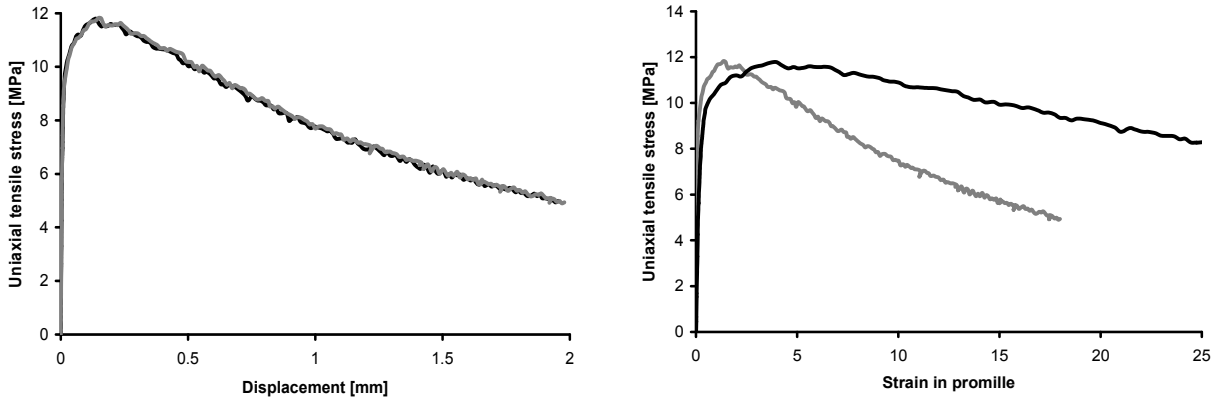

Figure 4.33: Average stress-displacement relation (left) and stress-strain relation (right) as the average of three notched specimens determined by measuring over 35mm (black curves) and 110 mm (grey curves).

Finally, the results of this additional testing series with different LVDT arrangements are compared with the results of the previous testing series in Figure 4.34. Shown are the individual results of a set of three specimens per series and their average (in bold). In black, the curves of initial testing series is shown, which are the average of all four LVDTs placed with a measuring length of 110 mm. Only

the results of the specimens cast vertically are shown, since this was the casting method also used for the additional testing series. In grey, the results of the additional series are shown. The curves shown are the average of the two LVDTs over 110 mm, since the 35 mm ones cannot serve for comparison in terms of a stress-strain relation. As can be seen, the additional testing series reached slightly higher strengths, however the scatter and difference is within reasonable limits between the cast batches of fibre reinforced concrete and the observed strength differences can be considered negligible.

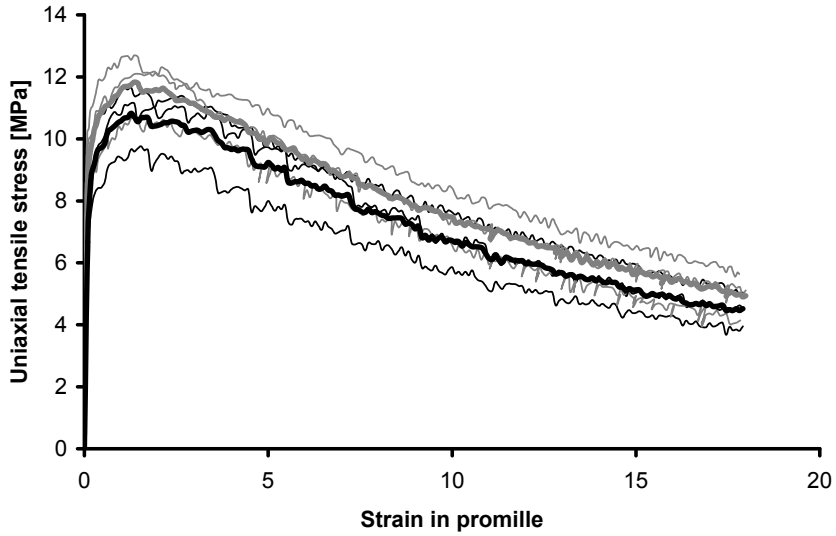

Figure 4.34: Comparison between the initial test series (black curves) and the second test series with different measuring length arrangement (grey curves).

Concluding remark on uniaxial tensile tests

Concluding, the following observations and main findings can be drawn from the performed uniaxial tensile tests: First of all, with the chosen testing method a stable tensile test, both for notched as well as un-notched specimens, could be performed. The results of the tensile tests show that the HSFRC, at least with the chosen fibre volume fraction, casting method, and moulds and specimen sizes used, a strain hardening material reaching high peak tensile strength values (for a cementitious material). This strain hardening phase, or yield plateau, is better visible in case of un-notched tests where more possibilities for the formation of multiple cracks are given. The notch predefines the crack location, and forces deformations to localise into a single crack at an earlier stage. The casting method has an influence on the fibre orientation: a preferred orientation with the flow was observed: also a strong influence of the orientation along the formwork boundaries was present. If a more random orientation is desirable, it is recommended to cut the specimen from all sides out of a larger element. In this testing series, specimens were cut from three of the four sides, and the fourth, un-cut size, showed always smaller displacements due to

a better fibre alignment along the formwork boundary in the tensile loading direction.

The measuring length is an important parameter for the evaluation of tensile test results and has to be chosen carefully. In this case, a length of 110 mm was not accurate enough in order to measure the crack localisation at postpeak and corresponding unloading of the concrete outside the major crack. A 35 mm length is more appropriate in order to accurately measure the postpeak displacement. The difference between the two lengths, in terms of stress-strain, is not as pronounced in the pre-peak phase, since multiple cracks open almost uniformly at a dense spacing over the complete 110 mm length.

4.6 Conclusions

An overview of the complete static experimental programme was given, including three- and four point bending tests, notched and un-notched, and uniaxial tensile tests. The following main statements can be derived from the experiments performed:

- All three mixtures allowed further load increase after the first cracking load was reached; they can be classified as deflection hardening materials but also strain hardening materials in uniaxial tension.
- The flexural tensile strength depends on the applied fibre volume fraction in the mixture (when the mixtures are compared generally among each other) and on the amount of fibres present in the critical beam cross section (when individual beam results of one mixture are compared). The effect of the fibre concentration in a cross-section on the strength is more pronounced than that of the fibre orientation. Of course, this statement is only valid within this testing series, with the chosen testing method and production and casting method of the test specimens, that all had a preferred fibre alignment and a rather uniform fibre orientation within all beams of a mixture.
- The strain or deflection hardening and the multiple cracking formations are better visible in case of un-notched test specimens. However, tests on notched specimens can give a good description of the descending branch and the crack opening of the major crack. For a good evaluation of the material behaviour for multiple cracking materials, it is advisable to perform both notched and un-notched tests, if possible.
- Factors that influence the fibre orientation in these self-compacting mixtures, were the flow direction (both primary and secondary), the flow along formwork boundaries (wall-effect), gravity effects (segregation), as well as the falling height of the concrete poured into the moulds. Whether or not a secondary flow is present depends on the specimen height and width; the

effect will be more pronounced for larger specimens, while only primary flow and wall effects will occur in case of thin sections.
- A stable uniaxial tensile test could be performed, and a measuring length of 35 mm was more appropriate in order to register crack openings after crack localisation at post-peak.

References

AFGC-SETRA (2002) Béton fibrés a ultra-hautes performences, recommandations provisoires.

AKKAYA, Y., PELED, A. & SHAH, S. P. (2000) Parameters related to fiber length and processing in cementitious composites. *Materials and Structures,* 33**,** 515-524.

ALFES, C. (2006) Stahlfaserbeton - Neue Ansätze zur Qualitätssicherung. IN FISCHER, H. B. (Ed.) *16th International Conference on Building Materials (IBAUSIL).* Weimar, Germany, F.A. Finger-Institut für Baustoffkunde, Bauhaus Universität Weimar.

AVESTON, J., COOPER, G. A. & KELLY, A. (1971) Single and Multiple Fracture. The properties of Fibre Composites. *Conference Proceedings of National Physical Laboratory.* IPC Science and Technology Press Ltd.

BEHLOUL, M. (1996) Analyse et Modelisation du Comportement d'un Materiau a Matrice Cimentaire Fibree a Ultra Hautes Performances (Beton des Poudres Reactives). *Phd Thesis.* Ecole Normale Superieure du Cachan.

CHERMANT, J. L., CHERMANT, L., COSTER, M., DEQUIEDT, A. S. & REDON, C. (2001) Some fields of application of automatic image analysis in civil engineering. *Cement & Concrete Composites,* 23**,** 157-169.

EBERHARDT, C. & CLARKE, A. (2001) Fibre orientation measurements in short-glass-fibre composites. Part I: automated, high-angular-resolution measurement by confocal microscopy. *Composites Sciences and Technology,* 61**,** 1389-1400.

EBERHARDT, C., CLARKE, A., VINCENT, M., GIROUD, T. & FLOURET, S. (2001) Fibre-orientation measurements in short-glass-fibre composites - II: a quantitative error estimate of the 2D image analysis technique. *Composites Sciences and Technology,* 61**,** 1961-1974.

FARHAT, F. A., NICOLAIDES, D., KANELLOPOULOS, A. & KARIHALOO, B. L. (2006) High Performance fibre-reinforced cementitious composite (CARDIFRC) - Performance and application to retrofitting. *Engineering Fracture Mechanics,* In press, corrected proof.

GRÜNEWALD, S. (2004) Performance-based design of self-compacting fibre reinforced concrete. *PhD Thesis.* Delft University of Technology.

GRÜNEWALD, S., BOLO, T., VAN DER VEEN, C. & WALRAVEN, J. C. (2000) Performance-based design of a high strength self-compacting fibre reinforced mortar. *Stevin-report no 25.5-01-30.* Delft University of Technology.

HOLSCHEMACHER, K. & KLUG, Y. (2005) Pull-out behaviour of steel fibers in self-compacting concrete. *4th International RILEM Symposium on Self-Compacting Concrete.* Chicago, USA.

JUNGWIRTH, J. (2006) Zum Tragverhalten von Zugbeanspruchten Bauteilen aus Ultra-Hochleistungs-Faserbeton. *Ecole Polytechnic Federale de Lausanne.* PhD Thesis Nr 3429 (2006).

KASPERKIEWICZ, J., MALMBERG, B. & SKARENDAHL, A. (1978) Determination of Fibre Content, Distribution and Orientation in Steel Fibre Concrete by X-Ray Technique. IN SWAMY, R. N. (Ed.) *Testing and Test Methods of Fibre Cement Composites.* The Construction Press, UK.

KOOIMAN, A. G. (2000) Modelling Steel Fibre Reinforced Concrete for Structural Design. *PhD Thesis.* Delft University of Technology.

LAPPA, E. S., BRAAM, C. R. & WALRAVEN, J. C. (2004a) Static and fatigue bending tests on ultra high strength fibre reinforced concrete. Delft University of Technology.

LAPPA, E. S., BRAAM, C. R. & WALRAVEN, J. C. (2005a) Flexural performance of high and ultra high strength fibre reinforced concrete - overview of static and fatigue experimental program. Delft University of Technology.

LAPPA, E. S., VAN DER VEEN, C. & WALRAVEN, J. C. (2003b) High strength, self-compacting steel fibre reinforced mortar for precast sheet piles. Delft University of Technology.

LI, V. (2004) Strategies for High Performance Fiber Reinforced Cementitious Composites Development. IN AHMAD, S., DI PRISCO, M., MEYER, C., PLIZZARI, G. A. & SHAH, S. (Eds.) *Fiber reinforced concrete from theory to practice.* Bergamo, Italy, Starrylink Editrice Brescia.

LI, V. (2005) Engineered Cementitious Composites. IN BANTHIA, N., UOMOTO, T., BENTUR, A. & SHAH, S. P. (Eds.) *3rd International Conference on Construction Materials: Performance, Innovations and Structural Implications (ConMat '05) and Mindess Symposium.* Vancouver, Canada, The University of British Columbia, Canada.

LI, V. C. (1993) From Micromechanics to Structural Engineering - The Design of Cementitious Composites for Civil Engineering Applications. *Journal of Structural Mechanics and Earthquake Engineering JSCE,* 10**,** 37-48.

LI, V. C. & FISCHER, G. (2002) Reinforced ECC - An Evolution from Materials to Structures. *1st fib-congress - concrete structures in the 21st century.* Osaka.

LI, V. C., MIHASHI, H., WU, H. C., ALWAN, J., BRINCKER, R., HORII, H., LEUNG, C., MAALEJ, M. & SANG, H. (1996) Micromechanical models of mechanical response of HPFRCC. *High Performance Fiber Reinforced Cement Composites 2.* Ann Arbor, RILEM International S.A.R.L.

LOWKE, D., WIEGRINK, K. H. & SCHIESSL, P. (2003) A simple and significant segregation test for SCC. IN WALLEVIK, O. & NIELSSON, I. (Eds.) *3rd*

International Symposium on Self-Compacting Concrete. Reykjavik, Iceland, RILEM Publications S.A.R.L.

LYSLO-DOSSLAND, A. (2006) Walls of self-compacting fibre reinforced concrete (in Norwegian). NTNU Trondheim University of Technology.

MARKOVIC, I. (2006) High-Performance Hybrid-Fibre Concrete - Development and Utilisation. *PhD Thesis.* Delft University of Technology.

MEDIA CYBERNETICS, L. P. (1999) Optimas. 6.5 ed.

MLEKUSCH, B. (1999) Fibre orientation in short-fibre-reinforced thermoplastics II. Quantitative measurements by image analysis. *Composites Sciences and Technology,* 59**,** 547-560.

MLEKUSCH, B., LEHNER, E. A. & GEYMAYER, W. (1999) Fibre orientation in short-fibre-reinforced thermoplastics I. Contrast enhancement for image analysis. *Composites Sciences and Technology,* 59**,** 543-545.

NAAMAN, A. E. (2003) Engineered Steel Fibers with Optimal Properties for Reinforcement of Cement Composites. *Journal of Advanced Concrete Technology,* 1**,** 241-252.

NAAMAN, A. E. & REINHARDT, H. W. (1996) Characterization of High Performance Fiber Reinforced Cement Composites - HPFRCC. IN NAAMAN, A. E. & REINHARDT, H. W. (Eds.) *High Performance Fiber Reinforced Cement Composites 2 (HPFRCC 2). 2nd International RILEM workshop.* Ann Arbor, USA, RILEM Publications 31, E. & FN Spon.

NAAMAN, A. E. & REINHARDT, H. W. (Eds.) (1996) *High Performance Fiber Reinforced Cement Composites: HPFRCC 2*, RILEM Publications 31, E. & FN Spon.

NAAMAN, A. E. & REINHARDT, H. W. (Eds.) (2003) *High Performance Fiber Reinforced Cement Composites - HPFRCC 4*, Pro 30, RILEM Publications S.A.R.L.

NAAMAN, A. E. & REINHARDT, H. W. (2005) Proposed classification of HPFRCC composites based on their tensile response. IN BANTHIA, N., UOMOTO, T., BENTUR, A. & SHAH, S. P. (Eds.) *3rd International Conference on Construction Materials: Performance, Innovations and Structural Implications (ConMat '05) and Mindess Symposium.* Vancouver, Canada, The University of British Columbia, Canada.

ÖZYURT, N. (2006) Correlating Fiber Dispersion, Rheology, and Mechanical Performance for Fiber-Reinforced Cement-Based Materials. *Institute of Science and Technology.* Istanbul Technical University.

REINHARDT, H. W. & NAAMAN, A. E. (Eds.) (1992) *High Performance Fiber Reinforced Cement Composites,* London, RILEM Publications 15, E. & FN Spon.

REINHARDT, H. W. & NAAMAN, A. E. (Eds.) (1999) *High Performance Fiber Reinforced Cement Composites (HPFRCC 3)*, Pro 6, RILEM Publications S.A.R.L.

RUSS, J. C. & DEHOFF, R. T. (2000) *Practical Stereology,* New York, Kluwer Academic/Plenum Publishers.

SATO, Y., VAN MIER, J. G. M. & WALRAVEN, J. C. (2000) Mechanical characteristics of multimodal fibre reinforced cement based composites. IN ROSSI, P. & CHANVILLARD, G. (Eds.) *International RILEM symposium on Fibre Reinforced Composites (BEFIB 2000).* Lyon.

SCHEYDT, J. (2004) Dauerhaftigkeit von ultrahochfestem Beton. *Institut für Massivbau und Baustofftechnologie.* Karlsruhe University.

SCHÖNLIN, K. (1988) Ermittlung der Orientierung, Menge und Verteilung der Fasern in faserbewehrtem Beton. *Beton und Stahlbetonbau,* 83**,** 168-171.

SOROUSHIAN, P. & LEE, C. D. (1990) Distribution and Orientation of Fibers in Steel Fiber Reinforced Concrete. *ACI Materials Journal,* 87**,** 433-439.

STIEL, T., KARIHALOO, B. L. & FEHLING, E. (2004) Effect of casting direction on the mechanical properties of CARDIFRC. IN SCHMIDT, M., FEHLING, E. & GEISENHANSLÜKE, C. (Eds.) *International Symposium on Ultra High Performance Concrete.* Kassel, Germany, Kassel University Press GmbH.

STROEVEN, P., DE HAAN, Y. M., BOUTER, C. & SHAH, S. P. (1978) Pull-out tests on Steel Fibres. IN SWAMY, R. N. (Ed.) *Testing and Test Methods of Fibre Cement Composites.* The Construction Press, UK.

TC162-TDF, R. (2002) Recommendations of RILEM TC 162-TDF: Test and design methods for steel fibre reinforced concrete: bending test. *Materials and Structures,* 35**,** 579-582.

TJIPTOBROTO, P. & HANSEN, W. (1993) Tensile Strain Hardening and Multiple Cracking in High-Performance Cement-Based Composites containing discontinuous Fibers. *ACI Materials Journal,* 90**,** 16-25.

VAN MIER, J. G. M. (1997) *Fracture Processes of Concrete*, CRC Press, Inc.

VANDEWALLE, L. & DUPONT, D. (2003) Bending Test and Interpretation. IN SCHNÜTGEN, B. & VANDEWALLE, L. (Eds.) *Test and Design Methods for Steel Fibre Reinforced Concrete - Background and Experiences -.* Bochum, Germany, RILEM publications S.A.R.L.

YE, G. (2003) The Microstructure and Permeability of Cementitious Materials. *PhD Thesis.* Delft University of Technology.

5.

Behaviour under fatigue loading: theoretical considerations and experimental results

This chapter provides an overview of the results of the fatigue experiments. Fatigue four point bending tests were performed on un-notched beams of all four mixtures of this study, and a limited series of fatigue four point bending tests on notched beams was performed for the HSFRC mixture. The results will initially be presented in the form of S-N lines, which can be used for fatigue verifications in design guidelines and regulations. In analogy to the presentation of the static test results, again special attention will be given to the fibres and their contribution to the fatigue test results. In this chapter, also the results of a limited microscopical study are included. Additional experimental observations will be discussed, such as the influence of the applied upper load level on the deformation and the influence of the loading frequency on the number of cycles to failure and deformations. The function of the static load-displacement curve as a possible envelope curve for the fatigue displacements will be discussed, as well as the presence of a fatigue limit, which is defined as an upper load level below which the material can survive an unlimited number of load repetitions. All the above considerations will help to understand the failure modes and mechanisms under fatigue loading conditions, an area where at present further insight and research is still necessary. Finally, the results of a joint durability-fatigue experimental programme will be presented.

5.1 Literature review –fatigue of (fibre) concrete

Fatigue of plain concrete

Fatigue of concrete has been investigated more intensively from 1970 up to the present date, since fatigue was by then recognised as a possible failure mode in structures subjected to repeated and reversed loading such as bridges or offshore

structures. A brief overview of contributions that led to the present knowledge will be given here.

Holmen (1979) studied the compressive fatigue behaviour of plain concrete. He was the first to measure deformations and show the deformation evolution during a fatigue test, also known as the cyclic creep curve (Figure 5.7). Further, his extensive experimental programme provided relations between the applied stress ratio as a percentage to the static strength and the number of cycles to failure (S-N or Wöhler curves). He fitted curved lines to his testing data rather than straight lines, however for concrete and similar cementitious materials often straight lines on a semilogarithmic scale are used to present the data, especially in codes and standards as in the Model Code (MC90, 1993). Holmen further evaluated the effect of damage accumulation by variable amplitude fatigue loading in order to check the applicability of a linear damage accumulation as stated in the Palmgren-Miner rule (Palmgren, 1924, Miner, 1945) and found that a higher applied stress level, followed by a lower one, has a larger detrimental influence on the fatigue life, than a lower stress level followed by a higher one, the so-called sequence effect. Further studied were the decrease of stiffness during fatigue loading and the increasing fatigue life with decreasing amplitude (influence of the lower load level). Also Oh (1991a) found that the loading sequence, but also the load magnitude, influence the fatigue life of test specimens, and modified the cumulative damage theory of Palmgren-Miner in order to take these effects into account.

Fatigue data is usually presented as a relation between the applied stress ratio S of the upper load level divided by the static strength and the total number of loading cycles, N. The total number of loading cycles N a specimen can survive up to failure will also be denoted as the 'fatigue life' of a specimen in this chapter. In an S-N relation, the influence of the lower stress level can be included as a third variable (Aas-Jakobsen, 1970, Tepfers and Kutti, 1979) in the following form:

$$S = \frac{\sigma_{\max}}{f_{cm}} = 1 - \beta(1 - R) \cdot \log N \tag{5.1}$$

In this equation, R is the ratio between the applied maximum and minimum stress level, and the factor β is a material constant that was found to have values in the range of 0.064-0.08 for compression, while the equation has also been verified for tension with a factor of β=0.0685 by Tepfers (1982). Hsu (1971) established different S-N relationships for low, high and ultra high cycle fatigue and added the parameter T, the loading duration, as an independent parameter into the relationship. As Cachim (1999) already concluded, Hsu's work shows that a simple relationship between the applied stress and fatigue life is very difficult to obtain. The relation between the stress and fatigue life is normally obtained by regression analysis of the experimental data and the results are often given within 90% or 95% confidence limits, as has been done by Cornelissen and Reinhardt (1984). Either a power law or a logarithmic law are recommended for the best-fit relation by regression analysis; the power law has the property of an infinite N when S turns

zero, while the logarithmic law gives a finite value for N in that case, and is therefore only valid for a certain range of S values (Cachim, 1999).

Apart from regression analysis of experimental data, S-N relations can also be obtained by statistical analysis of the data; in that way these relations can be given for different failure probabilities, so-called S-N-P curves. One function often used in that purpose is the two parameter Weibull distribution (Oh, 1991b, Singh and Kaushik, 2003) with the distribution function and its shape parameters determined separately for each load level. Apart from the Weibull distribution, the log-normal distribution has been used, for example by Saito and Imai (1983), who performed uniaxial tensile fatigue tests. Another alternative is the McCall model (McCall, 1958) which, among others, has been used by Holmen (1979) and Do et al. (1993).

The above mentioned research and methods were mainly performed on compressive fatigue tests; however also the tensile and flexural tensile fatigue behaviour has been studied. Cornelissen and Reinhardt (1984) studied the effect of various minimum stress levels and the influence of the moisture content by testing dry and wet concrete, where wet concrete had significantly shorter fatigue lives compared to dry concrete. Stress reversals, meaning load cycles that change from compressive into tensile loading or vice-versa, have a detrimental effect on the fatigue performance on concrete and are significantly reducing the fatigue life; this effect has been studied by Cornelissen and Timmers (1981) and the findings have been summarised in form of a Goodman diagram for concrete (Cornelissen and Siemes, 1985). The tensile fatigue behaviour has further been studied by Hordijk (1991), who expressed the cyclic tensile stress-strain relation in form of a continuous function model, and Kessler-Kramer (2002) who mainly performed deformation-controlled uniaxial tensile fatigue tests and derived a rheological cyclic stress-strain model.

The flexural tensile fatigue behaviour has mainly been evaluated by fatigue bending tests on small beams or prisms. Cornelissen and Reinhardt (1984) showed that the secondary strain rate (the strain rate during the second, stable part of the cyclic creep curve) correlates strongly with the number of cycles to failure. Subramaniam et al. (2000) performed flexural fatigue three-point bending test on notched beams and analysed the results with a fracture mechanics based approach; they found a correlation between the fatigue life and the effective crack length.

A problem in evaluating fatigue test results is the great scatter that normally accompanies the data. The main reason behind this is the scatter in the static material strength (CEB, 1988); therefore, the exact value of the applied upper load level cannot be directly determined and this already implies a scatter in the results. Moreover, another reason for scatter in fatigue testing can be the strain-rate sensitivity of concrete and cementitious materials, since fatigue testing can be at rates up to 2000 times higher than that of the static testing (Issa and Shafiq, 1999).

Fatigue of fibre reinforced concrete and special cementitious composites

The fatigue behaviour of fibre reinforced concrete has been investigated by numerous researchers, in terms of compression, tension and bending. An overview is given by Barr and Lee (2003), who collected the results of several researchers and derived linear regression lines of plain concrete and for fibre reinforced concrete with fibre contents of 0.5% and 1% for compression and bending. The fatigue behaviour of fibre reinforced concrete has been found similar or even better than plain concrete, but it can also result into a degradation of fatigue life (Cachim, 1999) due to a possible introduction of additional flaws in concrete by the fibres. A positive influence of fibres on the fatigue behaviour is more pronounced in case of bending or tension than in compression. This trend was also evident from the linear regression lines of the experimental data in the literature examined by Barr and Lee (2003). Since the scatter of fatigue experiments can be related to a great extent to the scatter in the static strength within a mixture, and since the scatter in FRC is usually larger than that of plain concrete at least for tension and bending, it is evident that the scatter in fatigue of FRC can be even larger than that of plain concrete.

Not many contributions exist on fatigue of special cementitious materials, such as strain hardening normal strength fibre concretes (the so-called 'engineered cementitious composites' ECC), and on high and ultra high strength concretes with and without fibre addition. An experimental and numerical study on the flexural fatigue behaviour of ECC has been performed by Suthiwarapirak (2003). They found that crack openings and deflections were increasing with increasing upper load level (Figure 5.1), while for conventional fibre concretes without strain hardening often the opposite is the case, larger displacements are obtained with decreasing upper load levels, supporting the envelope curve concept. Also, they found a bilinear S-N relationship, in a form that is more common for metallic materials, to be more suitable to describe the tests results, while for conventional fibre concretes a linear relationship is better suitable. Figure 5.2 shows the derived S-N line for the ECC, compared to those of two polymer fibre reinforced mortars, that had a lower fibre reinforcement and, consequently, no multiple cracking and strain hardening characteristics.

The following fatigue tests have been reported on high, and mainly ultra high strength concrete: Do et al. (1993) performed fatigue tests on high strength concrete without fibre reinforcement, and found that the failure strain was independent of the stress level and close to the static strain at peak load, whereas in normal strength concrete the fatigue failure strains can be higher than the static strain at peak. A limited study on the compressive behaviour of ultra high strength fibre concrete has been performed by Fehling et al. (2005), who found similarities in the fatigue behaviour of UHPC and plain normal strength concrete in compression. Studies on the flexural fatigue behaviour of ultra high strength fibre reinforced concrete have been performed by Parant (2004), who found a considerable scatter

when the fatigue life was related to the characteristic static peak value of the flexural strength but a much better relation between the initial fatigue deformation and the corresponding static values (Figure 5.3). Behloul et al. (2005) performed a limited study on an industrial ultra high strength concrete (Ductal), mainly in order to verify the fatigue verification as defined in the French interim design regulations (AFGC-SETRA, 2002). Farhat et al. (2007) performed flexural fatigue tests with CARDIFRC, an ultra high strength fibre reinforced concrete which has recently been developed at Cardiff University. Small beams with CARDIFRC had a very high scatter and a rather poor fatigue performance. However, an additional testing series was performed on thin slabs, rather than small beams, where a more aligned and uniformed fibre distribution could be achieved. Then, the fatigue performance was much better: for upper load levels below 80% of the average static strength no failure occurred.

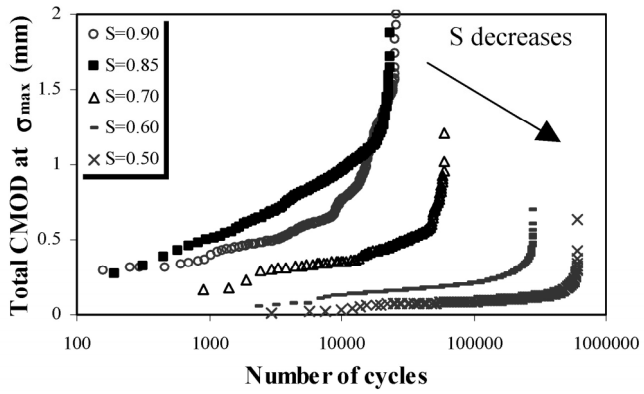

Figure 5.1: Influence of the upper load levels on the maximum deflections for ECC specimens, after Suthiwarapirak et al. (2002).

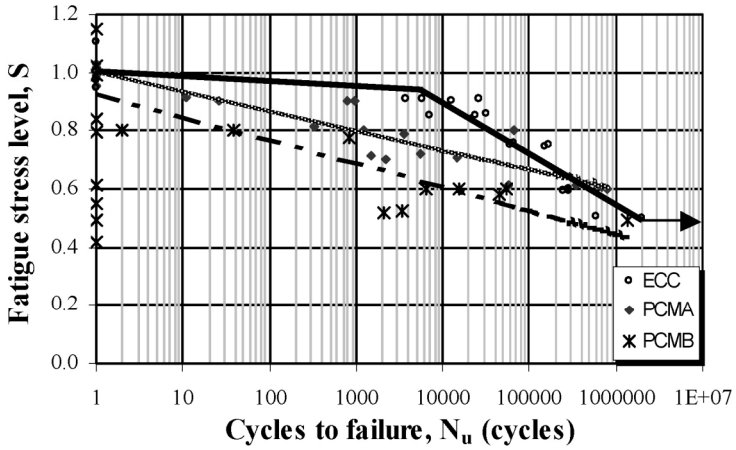

Figure 5.2: S-N lines for the ECC and for two polymer fibre reinforced mortars that have no strain hardening/multiple cracking characteristics, after Suthiwarapirak et al (2002).

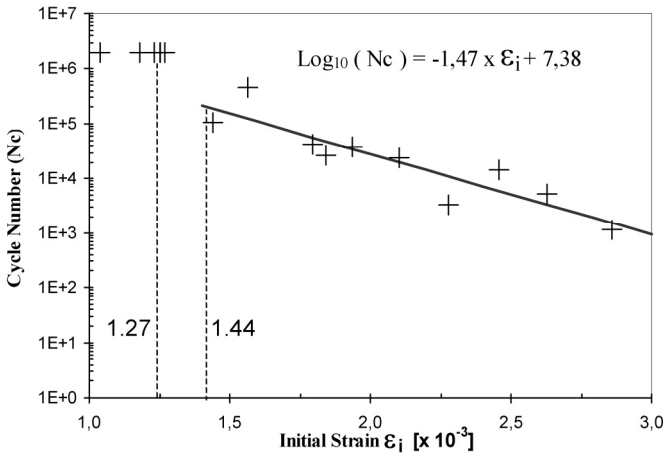

Figure 5.3: Relation between initial strain and fatigue lives for CEMTEC$_{multiscale}$ composites, after Parant et al. (2004).

5.2 Fatigue behaviour of the tested high strength mixtures

5.2.1 Standard strength tests and influence of testing

100 mm cubes were cast together with the beams, and a set of three was always tested at an age of 28 days in order to obtain the compressive and splitting tensile strength values. Detailed results of these standards test will not be provided here; they can be taken from Lappa et al. (2005a). The average results are listed in Table 4.1 of Chapter 4. This table includes the results of cubes that were cast in batches of beams intended for fatigue loading.

Most of these standard strength tests were performed at an age of 28 days; however, especially for the HSFRC mixture, also tests at different ages were performed in order to study the time-dependent strength development. Especially the strength development for ages of 28-90 days is of interest with regard to the fatigue testing programme: as was already mentioned in Chapter 3, due to the long duration of fatigue tests, not all beams could be tested at an age of 28 days, and in general the age of the beams at fatigue testing could be from 28 up to 90 days. The strength increase from 28-90 days, especially in the flexural strength, was concerned negligible. The following results will support this assumption.

High strength concrete develops its strength rapidly in the first week after casting and no significant strength increase is observed between 28-90 days. Figure 5.4 shows the development of the compressive strengths from an age of 1 day up to 90 days as tested on 100 mm cubes from two batches cast of HSFRC. The cubes of the first batch were tested after 1,2,7 and 28 days; the cubes of the second batch were tested at 28, 56 and 90 days. Three cubes were tested at each age, and the

average of the three is shown in the graph. As can be seen, the strength increase is limited after an age of 28 days, and also not so pronounced between 7 and 28 days. This difference is even less in case of the splitting tensile strength: Figure 5.5 shows that the splitting tensile strength development has finished after an age of 7 days, there was no significant increase observed after 28 days. The steel fibres of the mixture contribute are mainly responsible for the (splitting) tensile strength and the fibres do not change their strength properties in time.

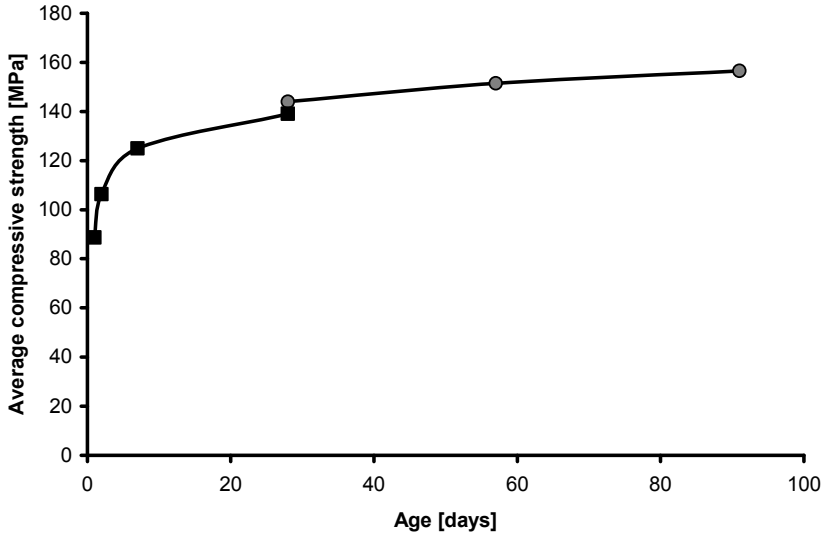

Figure 5.4: Average compressive strength tested on 100 mm cubes at different ages; Marked with squares are the results of one batch of HSFRC tested at 1, 2, 7 and 28 days. Marked with circles are the results of a batch of HSFRC tested at 28, 56 and 90 days.

Since the flexural tensile strength is mainly affected by the tensile strength of the mixture, also here it is expected that this development will not show a significant increase with time, especially not for higher ages than 28 days, due to the fact that also here the steel fibres in the mixture are directly influencing this value. This assumption was supported experimentally for the HSFRC mixture. A series of four static tests was performed at an age of approximately three months after casting. These beams were also, just like beams tested statically at an age of 28 days, removed from the fog room at an age of 25 days and stored in the laboratory until testing. No significant strength or difference in the shape of the load-deformation curve could be observed, as can be seen in Figure 5.6 where the average stress-deflection curves of eight beams tested at an age of 28 days and of the four beams tested at 90 days are shown. The average flexural tensile strength of all beams tested at an age of 28 days was 23.9 MPa with a coefficient of variation of 8%, while the average stress of the four beams tested at an age of 90 days was 24.3 MPa with a coefficient of variation of 4%. Together, the average value of the stress of all

beams of the HSFRC mixture at different ages is 24 MPa with a coefficient of variation of 7%.

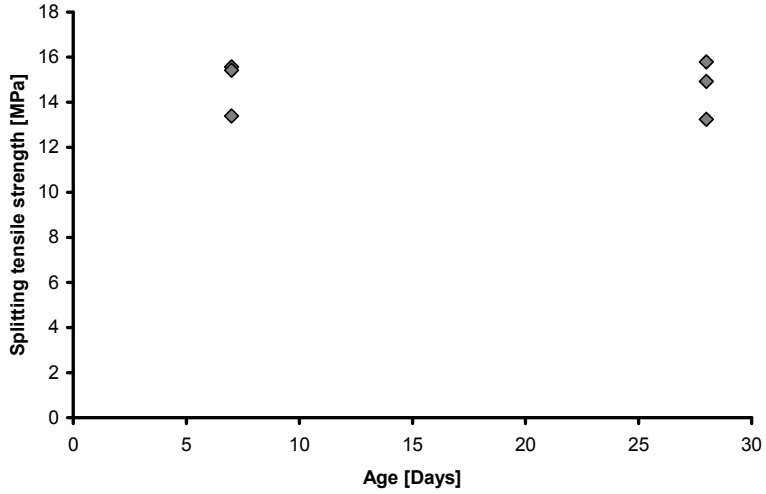

Figure 5.5: Splitting tensile strength of one batch of HSFRC after 7 and 28 days.

All the above considerations justify the chosen arrangement of the fatigue experiments which lead to differences in the time of testing in the range of 28-90 days, but as can be seen this has little effect on the structural material response for this type of high strength fibre reinforced mixtures.

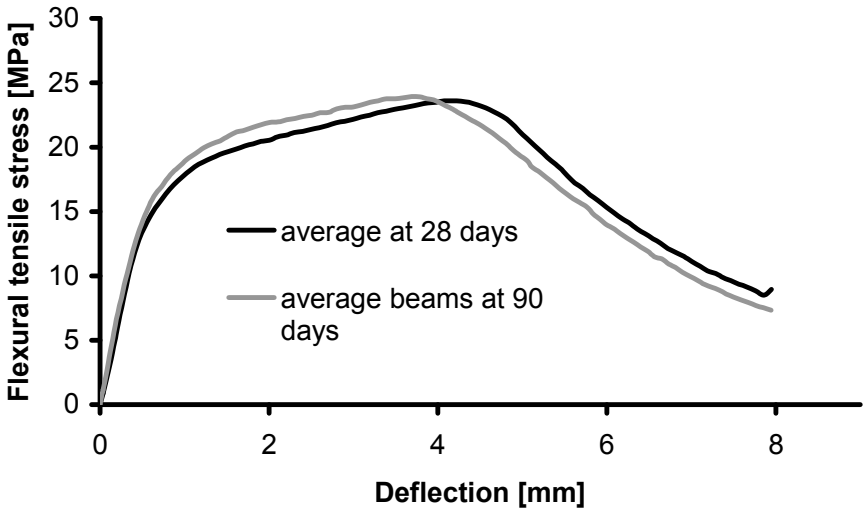

Figure 5.6: Average curves of statically tested beams after 28 days (average of 8) and after 90 days (average of 4).

5.2.2 Fatigue four point bending tests on un-notched beams

As a first approach, the results of the three mixtures tested under fatigue loading will first be presented as S-N lines, showing the relation of the applied upper stress level, expressed as a ratio of the material's static strength S, and the number of load repetitions to failure N. However, the first two figures presented here, show what is actually measured during each fatigue test and are representative curves for the behaviour of each tested beam under fatigue loading:

Figure 5.7 shows the average deflection evolution during the experiment as measured by the two LVDTs at midspan of the beam that measure the deflection. This is the curve of a hybrid HSFRC beam that was tested at an upper load level of 75% of the average peak load of statically tested beams of the same mixture (S=0.75), and which failed at 72035 load cycles. The three characteristic stages during the fatigue experiments are visible: a first initial stage, where the deformations increase rapidly, followed by a second stage, where the deformations increase gradually at a constant rate and finally a last stage, where the deformations increase rapidly again and the specimen eventually fails. In Figure 5.8, the deformations of the same beam are shown but a logarithmic scale was used for the number of load repetitions. It can be seen that the increase of the deflection in the first two stages of the fatigue experiment can be considered linear when using a logarithmic scale.

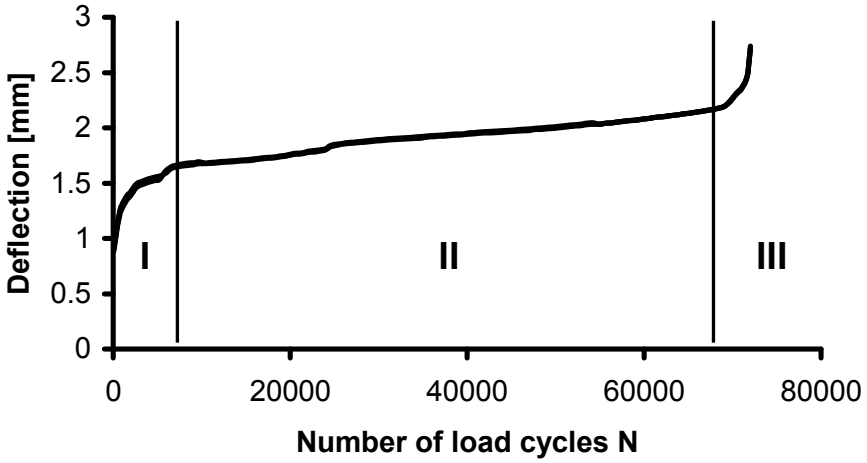

Figure 5.7: Characteristic fatigue curve showing the deflection increase with increasing number of load cycles.

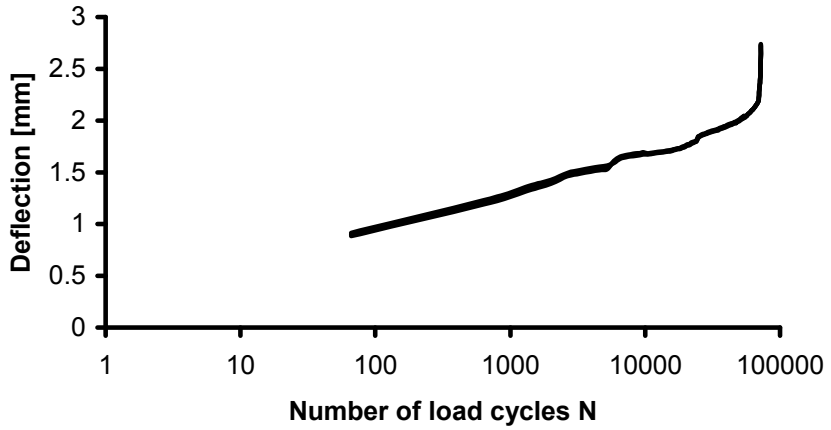

Figure 5.8: The curve of Figure 5.7, with the number of cycles on a logarithmic scale.

Table 5.1, Table 5.2 and Table 5.3 show the number of cycles to failure corresponding to each applied load level for the BSI/CERACEM, the HSFRC and the hybrid HSFRC respectively. The average number of cycles per load level given in the tables is calculated without including the specimens that did not fail up to ten million load cycles. The scatter is high, which is a common problem in interpreting fatigue experiments, and evokes the need for a logarithmic scale for the data. In the tables, the average numbers of each load level are given (bold values); however, specimens that did not fail up to 10 million load cycles (run-out specimens) are not included in this number. The italic values given in the last row of each table give the average number of cycles when the run-out specimens are taken into account. Of course, this is not a real average number, however this numbers give a better indication of the trends observed during the experiments.

The fatigue results presented in the Tables 5.1-5.3 are also presented in the form of S-N curves in Figure 5.9, Figure 5.10 and Figure 5.11 for each mixture. Due to the high scatter in the results it is difficult to present lines directly from the experimental data. Presented are the lines corresponding to a linear regression line of the average of the logarithms of each number of cycles to failure for each tested load level. Two lines are presented: a black line corresponding to the average of all failed specimens, and a grey line, where also the specimens that did not fail up to ten million load cycles have been taken into account when calculating the average. Whether or not the run-out specimens should be included for the determination of S-N lines and the average fatigue life per load levels is debatable. As Cachim (1999) states, omitting run-out specimens would underestimate the real number of cycles to failure, while including them would provide safer S-N lines since most specimens were able to withstand larger numbers of cycles. Therefore, the run-out specimens are often included in the analysis.

Table 5.1: Number of load cycles to failure for each load level for the BSI/CERACEM.

Stress ratio	**0.55**	**0.65**	**0.70**	**0.75**	**0.80**
Fatigue life N	30559	*)	*)	22443	*)
	479509	307	26013	29295	313
	2392819	5304	31384	124003	6199
	4975486	9204	58523	163931	6206
	10000000	17626	22587	170771	7694
		97569	686008		21212
		10000000			
		10000000			
Average	**1969593**	**26002**	**164903**	**102089**	**8324**
with 10mil	*3575674*	*2875716*	*164903*	*102089*	*8324*

*) Specimens showed rapid failure, less than 50 load cycles.

Table 5.2: Number of load cycles to failure for each load level for the HSFRC.

Stress ratio	**0.70**	**0.75**	**0.80**	**0.85**	**0.90**
Fatigue life N	3721710	155200	40151	2876	764
	10000000	744089	477648	7987	856
	10000000	1811576	490075	119679	2469
	10000000	10000000	1640586	391133	3568
	10000000		2259480	1104037	16265
	10000000		3135639	4655284	44862
	10000000		10000000	4890594	
Average	-	**903622**	**1340597**	**1595941**	**11464**
with 10mil		*3177716*	*2577654*	*1595941*	*11464*

Table 5.3: Number of load cycles to failure for each load level for the hybrid HSFRC.

Stress ratio	**0.6**	**0.65**	**0.7**	**0.75**	**0.8**
Fatigue life N	542703	10000000	3325	72035	1135
	2796879	10000000	49402	138153	13701
	4087983	10000000	102222	288403	20064
	6085655	10000000	119229	433416	37274
	10000000		190500	469774	39252
	10000000		10000000	532318	146328
Average	**3378305**		**92936**	**322350**	**42959**
with 10mil	*5585536*	-	*1744113*	*322350*	*42959*

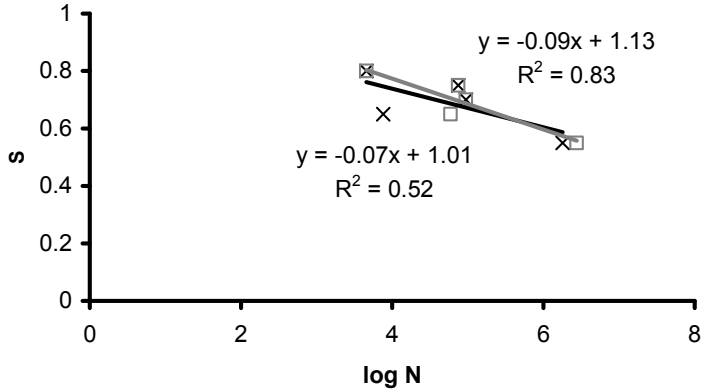

Figure 5.9: S-N lines for the BSI/CERACEM mixture. In grey, the fatigue life for each load level is determined including the specimens that did not fail up to 10 million load cycles.

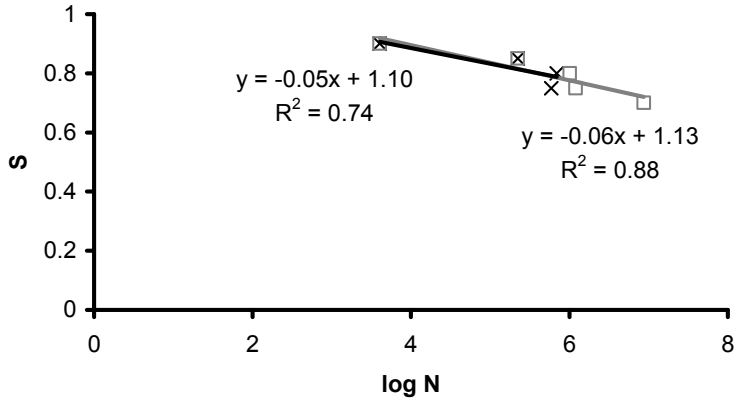

Figure 5.10: S-N lines for the HSFRC mixture.

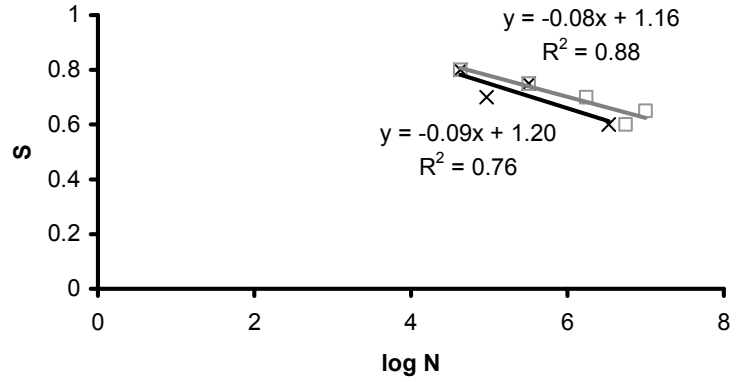

Figure 5.11: S-N lines for the hybrid HSFRC mixture.

The graphs all have in common that none of them provides a perfect fit, but a certain trend for a straight line on a semi-logarithmic scale can be seen. Also, the correlation is much better when the specimens that did not fail at ten million load cycles are included. The BSI/CERACEM shows the least favourable fatigue performance of the three examined mixtures; not only regarding the scatter, but also in terms of number of load repetitions that can be sustained at a certain percentage of the material's static strength. For example, the BSI/CERACEM can survive 10^6 load cycles at a stress level of approximately 60% of the static material strength, opposed to 75% for the HSFRC and 65% for the hybrid HSFRC. As a reminder, this was the mixture that had the highest scatter in the static test results, and it is only logical that this mixture will show an even larger scatter in the fatigue results and therefore a less favourable fatigue performance. It was also the mixture with the lowest workability and flowability in the fresh state; the fresh state properties are therefore important for the material's performance in the hardened state. Two more reasons for the higher scatter of this mixture are: the fact that it was the first mixture tested and some initial problems regarding the testing setup and procedure had to be solved; the fact that this is the only coarse aggregate mixture, and therefore a fatigue aggregate debonding could further shorten the fatigue life. Nevertheless, in terms of absolute fatigue performance, the BSI/CERACEM can endure more load cycles at a higher load, since this concrete is of considerably higher strength than the other two mixtures. On average, the BSI/CERACEM beams survived 10^5 load cycles at a load of 58 kN (corresponding to a flexural tensile stress of 22 MPa), which was assumed to be a load level of 75% of the static peak load. The highest load level tested for the HSFRC was 90%, at a load of 56 kN (corresponding to a flexural tensile stress of 21 MPa), and the average fatigue life was 11000 cycles, an order of a magnitude less.

The mentioned 'absolute' fatigue performance, meaning the number of load repetitions to failure that each beam survived at a certain value of the upper load, is additionally given in Figure 5.12, which shows the number of cycles to failure for each tested beam together with the regression line obtained from the average at each load level for all three mixtures. The regression line for the BSI/CERACEM is omitted due to the mixture's high scatter. The graph shows, that the already mentioned superior fatigue performance of the BSI/CERACEM in terms of absolute load is strictly speaking only valid for higher load levels. At upper load values of approximately 50 kN, the fatigue life of the BSI/CERACEM approach the one of the HSFRC; this is due to the fact that the HSFRC did not reach failure at loads lower than 70% of its material strength, while this was the case at 50% for the BSI/CERACEM.

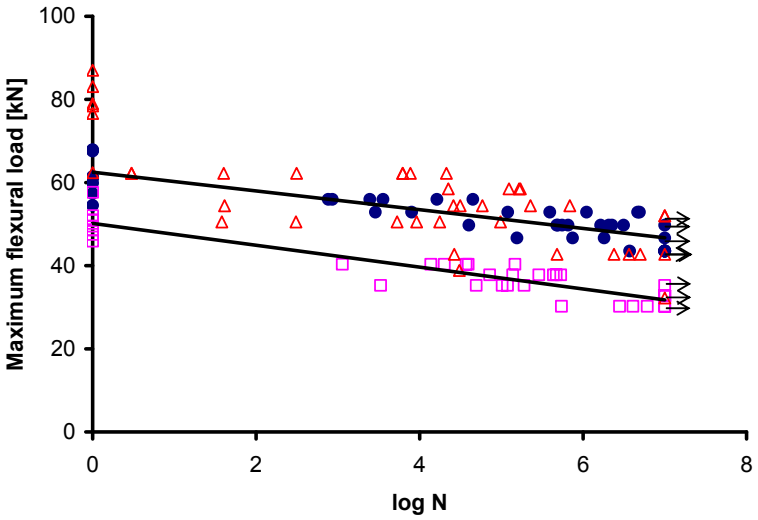

Figure 5.12: Fatigue test results shown as a relation between the applied upper load and the fatigue lives of all tested beams: BSI/CERACEM is marked by triangles, HSFRC by circles and the hybrid HSFRC by squares. Static tests are included, and arrows indicate run-outs.

Figure 5.13 shows the results of Figure 5.12, but in terms of the applied stress ratio S rather than the upper load level. These two figures serve mainly comparative purposes of the three mixtures. The shown regression lines in Figure 5.13 are the least squares linear regression lines of Figure 5.9, Figure 5.10 and Figure 5.11, as obtained from the averages including run-out specimens, since these lines provided a better fit of the experimental results. For the sake of comparison, regression lines as obtained by Barr and Lee (2003) for flexural fatigue of plain and fibre reinforced concrete with a 1% fibre content are also shown; they compared experimental data from eight different researchers for plain concrete and from three researchers for the 1% FRC, even though different setups and specimen dimensions were used, and derived linear least squares regression lines from the available data. Comparing these lines with the fatigue data of the performed study, it can be seen that the data is close to the line given for plain concrete. While Barr and Lee (2003) found higher fatigue lives with increasing fibre content, only the HSFRC confirms this trend in this study.

Another way for an evaluation of he fatigue performance of the mixtures in this study is by comparing the slope of the regression lines of the three mixtures to the term β(1-R) of equation 5.1. The factor β would be 0.07 for the HSFRC, 0.08 for the hybrid HSFRC and 0.11 for the BSI/CERACEM for a stress ratio R=0.2. The values for the two HSFRCs are close to the reported values for plain concrete in compression of 0.064-0.08, whereas only the BSI/CERACEM has a steeper slope of the S-N line due to the high scatter of this mixture. Concluding, it can be said that the fatigue

behaviour of these new materials is, in general terms, comparable to that of plain concrete.

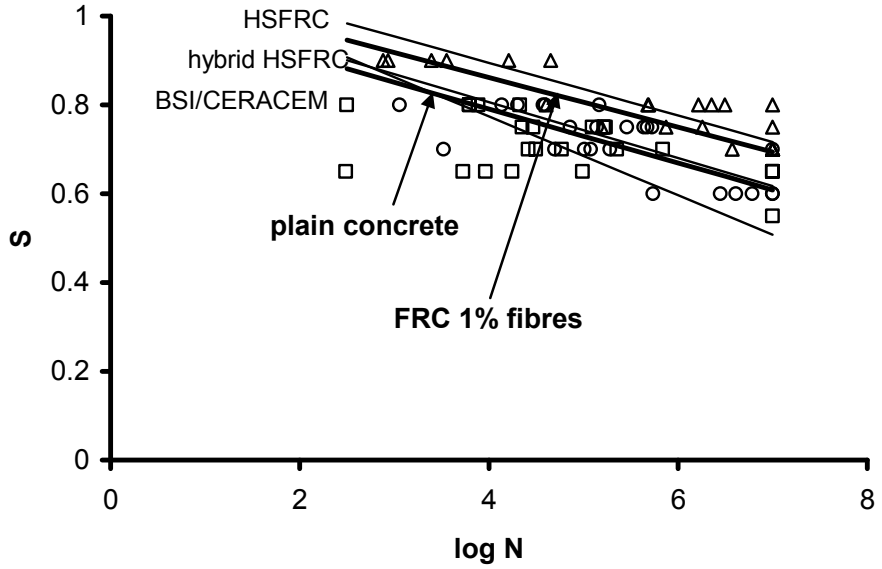

Figure 5.13: Fatigue performances of the three mixtures, experimental data and regression lines for the HSFRC (triangles), hybrid HSFRC (circles) and BSI/CERACEM (squares). For comparison, linear regression lines as provided by Barr and Lee (2003) for flexural fatigue of plain and fibre reinforced concrete with 1% fibre volume content are given.

As a final, general remark on the fatigue tests on un-notched beams, a statistical analysis was performed with the data of all mixtures, and a two parameter Weibull distribution was used to model the fatigue behaviour and obtain probabilistic S-N relations. These results can be found in Lappa et al. (2005a).

5.2.3 Fatigue four point bending tests on notched beams

A limited number of fatigue four point bending tests on notched beams were performed, with the HSFRC mixture only. These tests were intended to provide information on the strain distribution during testing: therefore, LVDTs were also placed on top of the beams to measure the deformations in the compressive zone. The strain measurements will be provided in Chapter 7, when they will be compared to calculated strains as obtained from the proposed fatigue material model. Here, an overview of the tests and the results will be given. As already stated, it was a limited test series, so that the results are not as representative as the tests on un-notched beams, which are statistically more representative. For a thorough statistical analysis of the results, even for the un-notched beams, more specimens would be necessary but this would extend the time frame and the scope of this study.

An overview of the results is given in Table 5.4, where the results of the tested beams per load level are presented. Three load levels, 60%, 70% and 80%, were applied. At 80%, two additional beams were tested, but these results cannot be included into the series since failure occurred due to setup and software problems (they were the first notched beams tested and the setup had to be adjusted accordingly). The number of cycles to failure, the average deflection at failure, the crack opening displacement at the notch tip at failure, and the strain (in promille ‰) at failure are given. Figure 5.14 shows these results as an S-N plot; the hollow markers show the individual beam tests, while the solid ones are the average of the three beams tested at each load level.

Table 5.4: HSFRC notched fatigue tests results overview:

Stress level	N	Deflection [mm]	COD notch tip [mm]	Millistrain comp. zone [‰]
60%	8400551	1.23	0.52	1.640
	10000000	0.83	0.16	0.643
	4653893	1.80	0.58	1.724
Average	**7684815**	**1.29**	**0.42**	**1.336**
70%	5807438	0.84	0.28	0.607
	4870225	1.55	0.73	1.663
	3741702	1.50	0.60	1.764
Average	**4806455**	**1.30**	**0.54**	**1.345**
80%	4739436	1.40	0.55	1.575
	11818	1.75	0.79	2.242
	87	2.30	1.12	2.876
Average	**1583780**	**1.82**	**0.82**	**2.231**

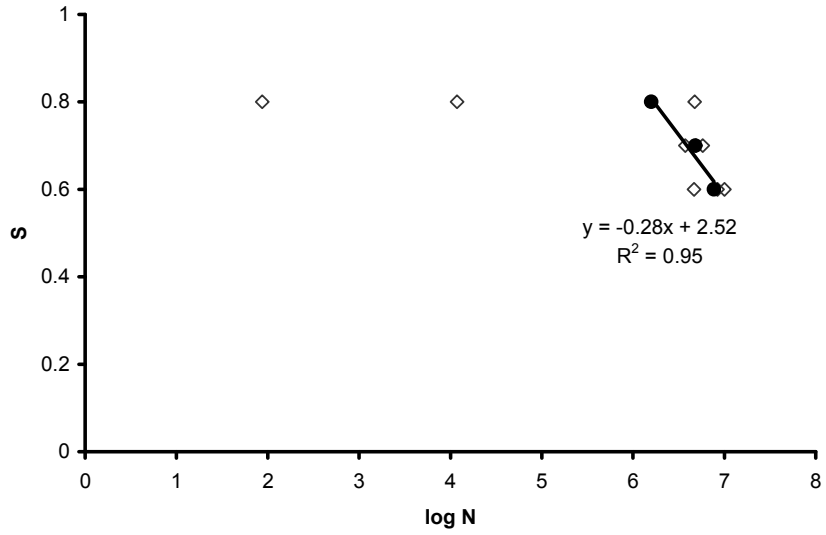

Figure 5.14: S-N plots of the notched fatigue tests; the hollow markers are the individual tests while the solid ones are the average per load level.

As can be seen in Table 5.4, these results show some trends within this limited series. Deformations are increasing with increasing upper load level: this shows that also here, the static curve cannot function as an envelope curve for fatigue displacements at failure, just as was also the case with fatigue tests on un-notched specimens. The scatter was highest for the load level of 80%. Often in fatigue tests the highest scatter is obtained for the highest load levels tested and the lowest for the lower load levels (Holmen, 1979, Do et al., 1993, Zhang and Stang, 1998), which was also the case here. The first (and only) specimen to survive 10 million load cycles without failure was at an upper load level of 60%; for the un-notched HSFRC beams, this occurred already at 70%. However, this difference is not surprising since the notch already predefines the crack path and deformations localise earlier, leading to an earlier failure compared to tests on un-notched beams. Also, the multiple cracking phase, which allows further deformation increase and ductility in the pre-peak region, cannot be as pronounced as was observed in tests on un-notched beams in case of notched beams. By comparing the slope of the regression line (S-N line) of Figure 5.14 with the slope of the line of the un-notched tests in Figure 5.10, it can be seen that a steeper line is obtained for the notched HSFRC specimens. Again, this can be explained by the fact that the notch forces deformations to localise earlier, and therefore an inferior fatigue performance is obtained, compared to un-notched beams. For design purposes, the S-N lines derived from un-notched specimens are more suitable, since real structural elements are not normally provided with notches. The S-N line given for the notched beams is only indicative since the testing series was rather small.

5.3 Fibre count by image analysis

The procedure to count the fibres and determine their orientations in cross-sections close to the fracture surface of the beams has already been reported in Chapter 4. In this section, some additional observations regarding the fibres in the beams tested under fatigue loading will be given. One of the main problems in interpreting the fatigue results is the scatter, and this is related to the fact that the exact static material strength of each tested beam is not known. Therefore, the scatter in the static material strength is highly responsible for the scatter in the fatigue performance. This implies that if the actual strength of each tested beam can be determined, the fatigue results could be 'corrected' in accordance to the actual loading ratio and then the scatter should be minimised.

Even though in theory it can be possible to use the relations between the fibres in the critical cross-section and static strength from the fibre count to estimate the actual material strength of the beams to adjust the experimentally found S-N lines, this correction proved to be difficult for the three main mixtures of this study. It was not possible to determine S-N lines with that method that were better, or in any case

more reliable, than the ones obtained by the average values of the beams tested for each load level. One of the reasons that this correction was not possible is the fact that except for the BSI/CERACEM, for the other two mixtures no direct relation was obtained from the fibre count. But even the better relation between fibres and the static strength of the BSI/CERACEM, did not provide more definite S-N relations than the original test data. In fact, the 'corrected' S-N relation correlates to a lower extent for this mixture compared to the other two. This implies that the amount of fibres in the critical cross section is not the only factor determining fatigue failure. Figure 5.15 up to Figure 5.17 show the corrected results after the fibre count. The specimens that did not fail at ten million cycles are included in the graphs. The corrected results of all three curves are slightly better than the results of all individual beams without the corrections, so they indicate that a 'correction' with the applied method improves the crude fatigue results. However, due to limitations of the method only an indication of the improvement can be given here rather than the exact determination of the S-N lines.

Even though the fibre count did not give definite answers for fatigue, it was useful in order to study the fibre orientation, and for comparing the fibre concentrations in all the beams, and in order to study possible segregation effects. Detailed results of the image analysis are given in Lappa et al. (2005a). In Chapter 4, effects of the flow on the fibre orientation were discussed and it was shown that with the chosen beam dimensions and fibre geometries, alignments due to primary and secondary flow can occur. The density of the fibre spacing decreases and the orientation is inferior with increasing distance from the bottom fibre of the beam. This means that during a fatigue experiment, only the bottom part of the beam has the best fibre alignment to bridge cracks which increases the strength and deformation ability, and the influence of the fibres is less pronounced for the upper part of the beam. It is possible that the influence of the fibres on the fatigue behaviour is more evident if thin slabs, where the fibres will be more uniformly aligned and better able to bridge cracks, were chosen as test specimens rather than the beam dimensions used in this study. This could be of interest for such high performance materials, since they are suitable for thin overlays or slender structures, as first applications show, and therefore thin slabs could be more representative for the typical cross-sections of such materials. This assumption, of a better fibre orientation and improved fatigue performance in case of thin slabs rather than small beams, was verified by another study at Cardiff University as reported by Farhat et al. (2007) for the ultra high strength cement composite CARDIFRC. Fatigue tests on small beams (100/100/500 mm) and thin slabs (360/90/35 mm) were performed; the scatter in the small beams was very high, but much lower for the thin slabs. The thin slabs had a good fatigue performance with no failure up to 10 million load cycles at an upper load level of 80%. They attributed the difference in fatigue behaviour between the beams and slabs mainly to the fibre orientation and distribution, which was evaluated with CT imaging; a much better fibre distribution could be obtained

for the thin slabs. However, their study is not completely comparable to the mixtures of this thesis since CARDIFRC is a vibrated concrete and not a self-compacting mixture. The observed minor fibre distribution of the CARDIFRC small beams could partly also be attributed to the used high compaction frequency of 100 Hz which proved to be hindering a uniform fibre distribution, while a lower frequency was subsequently chosen for the thin slabs.

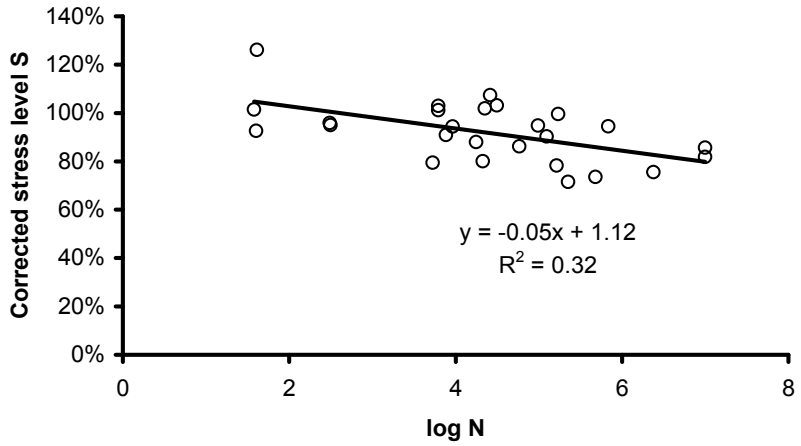

Figure 5.15: ‚Corrected' S-N lines from the result of the fibre count for the BSI/CERACEM mixture.

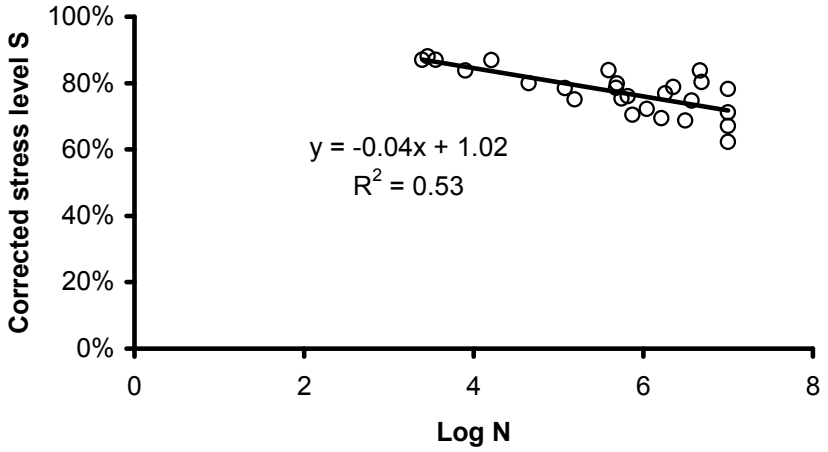

Figure 5.16: ‚Corrected' S-N lines from the result of the fibre count for the HSFRC mixture.

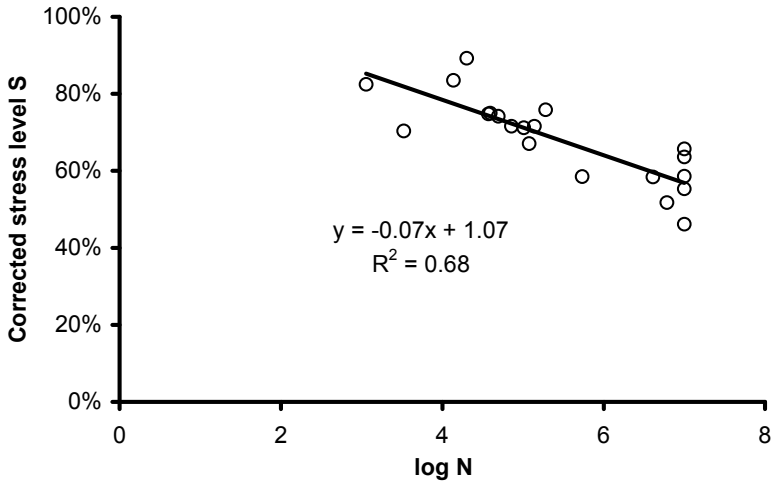

Figure 5.17: ‚Corrected' S-N lines from the result of the fibre count for the hybrid HSFRC mixture.

5.4 Microscopical observations on the material structure

Microscopy has been a useful tool for studies on both natural and artificial materials and can also be used in the field of concrete in order to provide information on clinker, cement, aggregates or for information on deterioration and failures (St John et al., 1998). In concrete, universal polarising microscopes, fluorescent microscopy as well as scanning electron microscopes have been successfully used in that purpose. Fluorescent microscopy is a useful tool in order to determine the porosity, estimate the water/cement or water/binder ratio and observe crack patterns. In order to use it, it is necessary to impregnate the concrete with a thin epoxy containing a fluorescent dye. In this limited study, polarising microscopy and fluorescent microscopy have been used to evaluate the quality of the cementitious matrix and the effect of fatigue loading on the cement microstructure.

Three thin sections were prepared out of the tested specimens, one out of each concrete mixture, and impregnated with a fluorescent epoxy resin. The sections were regarded under plain-polarised, cross-polarised and ultraviolet light under magnifications of 25 and 100 times. In that way, additional information on the mixture compositions and their properties could be obtained, which form a useful addition to the information gathered by examining the fresh and hardened state properties. From the fresh-state results on workability, mentioned in the previous section, one can easily conclude that the BSI/CERACEM is slightly inferior to the other two HSFRC mixtures, but as will be shown in this section, this statement is

reversed under the microscope, making the mixture superior to the other two HSFRC.

In the following, a brief overview of the observations on the mixtures with the microscope will be given. All three thin sections were prepared from specimens previously tested under fatigue loading: the BSI/CERACEM was tested at an upper load of 58.5 kN (75% of the assumed static strength) and failed after 124001 load cycles. The HSFRC was loaded with an upper load of 56 kN (90% of the static strength) and failed after 856 load cycles. The hybrid HSFRC was tested at 35 kN (70% of the static strength) and failed after 49402 load cycles. Therefore, all thin sections were taken from significantly damaged specimens.

The thin section of the BSI/CERACEM specimen was the most visibly damaged of the three: thin cracks were dispersed at a regular pattern throughout the complete slice, Figure 5.18. Moreover, the same figure shows that cracks were partially also going through the aggregates: these are mainly the sand aggregates, since Bauxite was used as coarse aggregate, which has a very high strength and it is unlikely that the cracks would propagate through it. The cracks could propagate through the sand aggregates due to the high strength of the matrix. In case of a normal strength matrix, this would not have been the case and the cracks would form around the aggregates. The mixture has a low water-to-binder (w/b) ratio and therefore the matrix, when observed under UV light, has a very dark colour due to its high density and low porosity. Throughout the entire section a uniform w/b factor was present. There were no variations in the colour of the matrix, not even at 'outer' parts closer to the surface of the specimens; this means that a very stable matrix is obtained with no microbleeding or other flaws. Also the air content was very low; not many and only small air pores could be seen. The only 'flaw' that could be observed was in the embedment of the steel fibres: sometimes air was entrapped around a fibre, which can be seen in Figure 5.19 at the lower right part of the visible fibre, and there were also parts where a local fibre clustering was visible. This local fibre clustering is not necessarily the result of a poorer workability and flowability in the fresh state: this was the only mixture with a rather coarse aggregate and the aggregates can hinder a uniform fibre distribution.

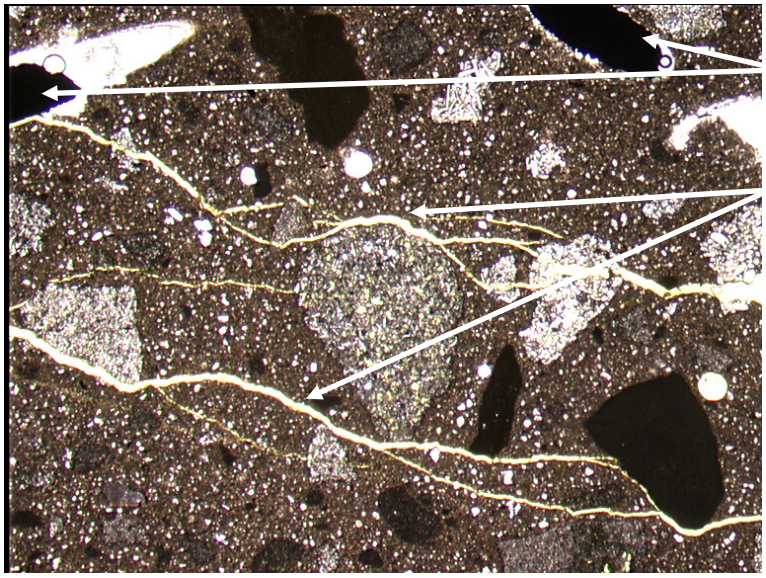

Figure 5.18: Visible cracking in the BSI/CERACEM, visible under plain polarised light, with cracks partially crossing the aggregates. The dimensions of the image are 5.4 x 3.5 mm (25x magnification).

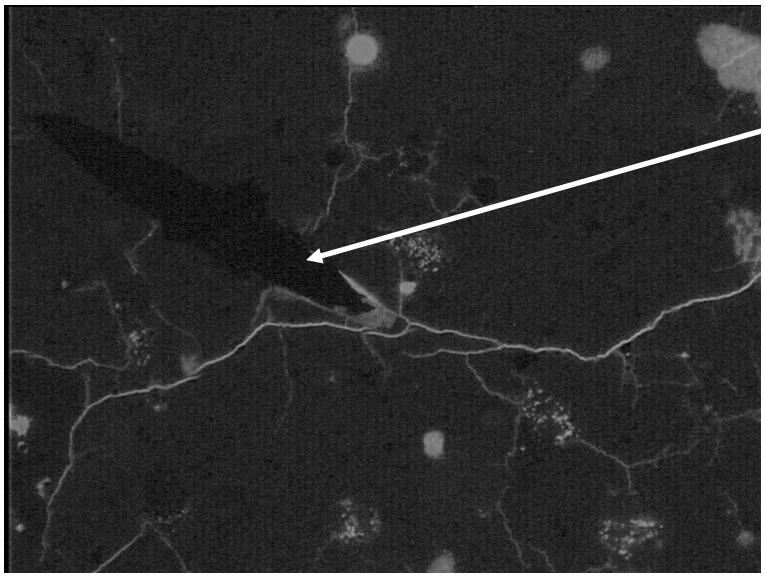

Figure 5.19: Image of the BSI/CERACEM under UV light, magnification 25x. Fine cracking is visible and a steel fibre. The dimensions of the image are 5.4 x 3.5 mm.

Both HSFRCs showed a lower quality of the matrix with regard to the BSI/CERACEM as seen under the microscope. More heterogeneity was visible, especially regarding the air content and the w/b ratio. Compared to the BSI/CERACEM, more air was entrapped: the air percentage could locally be above 5%, while the measured value of 3 or 3.5% during the cast reflects the overall average value of the mixtures. The w/b ratio was less evenly distributed in the

mixture: this is evident by the differences in the darkness of the cement paste, lighter areas are representing a higher (local) w/b ratio. Toward the outer layer, the cement paste is much lighter than at the inner parts, which is due to microbleeding toward the surface. Figure 5.20 shows this effect for the HSFRC mixture: on the left, an image from the inner part of the slice is shown, which shows local inhomogeneities in the w/b ratio, and on the right a part of the same slice is shown close to the beam surface, which has a much higher local w/b ratio.

Additionally it is worth mentioning that apart from the observed inferior matrix qualities of the two HSFRCs compared to the BSI/CERACEM, some advantages were observed: The bond between the steel fibres and the matrix was apparently better, at least within the observed thin sections. The two following figures, Figure 5.21 and Figure 5.22, show parts where steel fibres were visible. Less air compared to the BSI/CERACEM is present around the fibres.

Less cracks are visible in the observed slice of the HSFRC, and even though the part of the hybrid HSFRC shown in Figure 5.22 is visibly cracked, the whole thin section is less cracked compared to the one of BSI/CERACEM. However, all slices were taken from specimens that showed failure under fatigue loading, and regarding the loading percentage and the fatigue life of the specimens, the HSFRC should be the most damaged specimen of all, but here the opposite was the case. This could indicate two things: either the BSI/CERACEM is more prone to fatigue damage compared to the two HSFRCs, which could be the case since the fibres do not seem to be embedded with a perfect bond into the matrix, or the BSI/CERACEM shows a more uniformly distributed cracking throughout a larger part of the beam, while the damage is much more localised and concentrated at one specific part of the beam for the two HSFRCs. More specimen parts have to be observed with the microscope in order to obtain a generalised conclusion, but it is very likely that the answer lies in a combination of the two explanations.

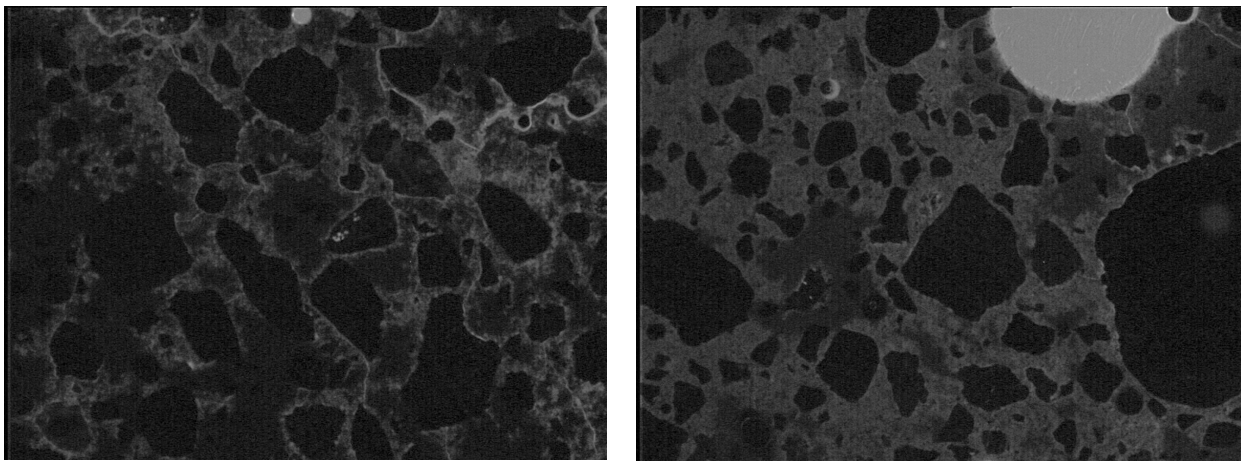

Figure 5.20: Image of the HSFRC mixture at different zones showing variability in w/c factor. 25x magnification, the dimensions of the image are 5.4 x 3.5 mm.

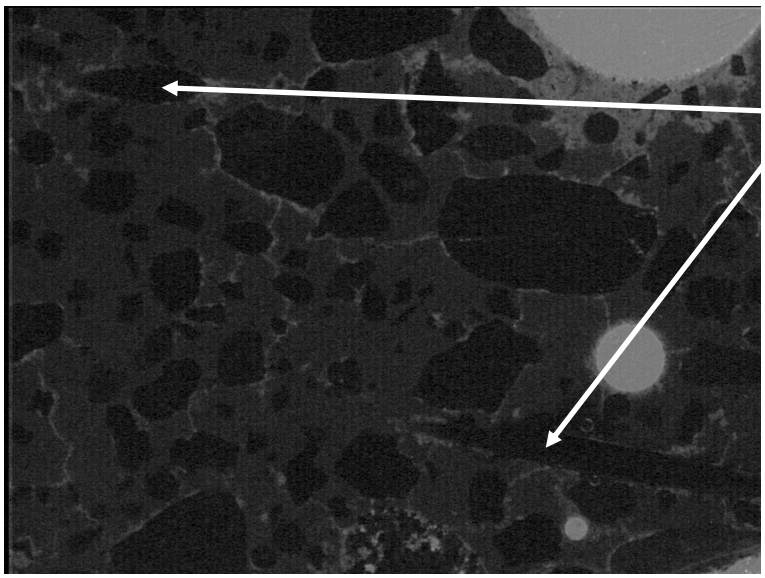

Figure 5.21: Part of an HSFRC slice under UV light, with two steel fibres visible. The dimensions of the image are 5.4 x 3.5 mm.

Concluding, the microscope is a useful instrument in order to gather additional information on the mixture composition and damage mechanisms that are not visible from the fresh and hardened state results alone. The fresh state properties already showed that the fibres were more evenly distributed and more stable embedded in the two HSFRC mixtures. This is supported by the fact that 'air pockets' around steel fibres were not as pronounced in these two mixtures under the microscope compared to the BSI/CERACEM, neither local fibre clustering, which was however the case in the slice taken out of the BSI/CERACEM. Even so, the quality of the matrix of the BSI/CERACEM is better compared to the HSFRC, as a more homogeneous cement matrix with a stable w/b factor was visible. A point for further research would be to optimise the three mixtures. The goal should be to improve the flowability of the BSI/CERACEM so that the fibres can be better distributed and embedded into the matrix, and to improve the composition of the cement, fillers and additives of the two HSFRCs in order to obtain a homogeneous microstructure of the matrix, but without altering the fresh state properties and by maintaining the good workability of the mixtures.

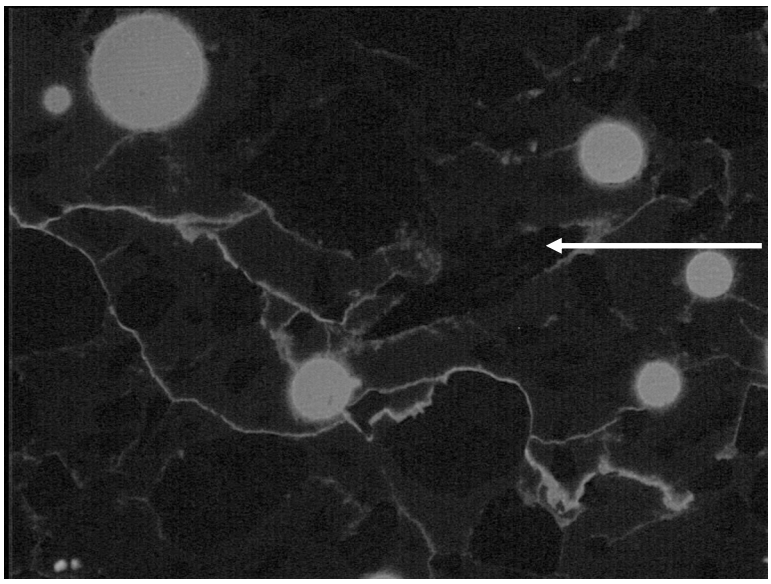

Figure 5.22: Part of the hybrid HSFRC under UV light, with a short fibre visible. Also visible are fine cracks due to fatigue loading and air voids. Image dimensions: 5.4 x 3.5 mm.

5.5 Discussion

5.5.1 Fatigue loading on cracked/un-cracked specimens

Fatigue loading can have a different impact on cracked or uncracked specimens. The static bending tests showed that the 'hardening' branch of the load-deflection curves starts at values between 60-65% of the peak load for the BSI/CERACEM beams and between 55-60% for the two hybrid mixtures. This means that most of the beams tested under fatigue loading were under loads corresponding to the phase where the specimen has been visibly cracked from the static action of the loading, even though the cracks have not localised yet. It is possible that beams that are loaded at upper load levels corresponding to the first stage of the static load-deflection curves, before the 'hardening' branch has been reached do not fail up to ten million load cycles. Due to the scatter in the results this assumption cannot be verified through this test series. What also cannot be ruled out is the fact that the failure mechanisms differ for a greater amount of initial cracking and a lower one.

Whether or not the specimen is extensively cracked or not due to the initial loading at a certain load level can not only influence the total fatigue life, but also the main mechanism leading to failure. Possible failure mechanisms can be: a gradual fatigue crack growth of existing cracks with increasing number of load repetitions, or fatigue crack initiation, meaning a gradual formation and opening of

new cracks during the fatigue loading process. At high fatigue load levels, where many cracks have already formed during the initial loading process, fatigue crack growth might be the main mechanism leading to failure. On the other hand, at lower levels, where the specimen has not experienced an extensive initial cracking, fatigue crack initiation can be responsible for failure. Suthiwarapirak et al. (2004) performed fatigue tests with an engineered cementitious composite (ECC), a ductile, multiple cracking fibre reinforced material. The crack pattern at lower fatigue crack level was less pronounced compared to higher levels. Moreover, at lower levels the average fatigue life was shorter than that of a fibre concrete without strain hardening. They conclude that multiple cracking characteristics are less pronounced at lower load levels, which implies a more brittle type of failure. These assumptions could not be verified in this study, but they could also neither be ruled out. However, if this phenomenon is valid for the mixtures of this study, it could be one more explanation why the static load-deflection curve cannot function as an envelope curve to predict failure, see also section 5.5.4.

5.5.2 Influence of the (upper) load level

Presence of a fatigue limit

While in metals a certain fatigue limit exists, that is a certain load (or stress) level below which no failure is reached in fatigue loading, the existence of such a limit has not been proven yet for concrete. The experimental data of this study on un-notched tests are also not suitable to prove (or rule out) the existence of such a limit. Specimens did not fail at ten million cycles at upper load levels of approximately 50-55% for the BSI/CERACEM, 65% for the hybrid HSFRC and 70% for the HSFRC. Especially for the BSI/CERACEM the presence of the fatigue limit cannot be verified due to the high scatter. Only the best workable mixture, the HSFRC, with the lowest scatter in mechanical properties, indicates the presence of a fatigue limit; this implies that if the scatter in mechanical properties can be reduced for the other two mixtures, more reliable observations on the presence of a fatigue limit could be given.

Even though a fatigue limit has not been verified for concrete, such a limit is often used for practical purposes in codes and regulations. A limit of 50-60% is accepted for plain concrete (CEB, 1988). The experimental results cannot indicate a more precise fatigue limit. Therefore, the current fatigue codes of practice seem also appropriate for these high performance fibre concretes as well. A fatigue limit of 50% is advised in the Japanese tentative guideline (JSCE, 2005) for design and construction of Engineered Cementitious Composites (ECC).

Influence of the upper load level on fatigue deformations

In order to compare the evolution of the deflection with increasing number of cycles during the fatigue experiment for each load level, an average curve of the individual

beam results was made for each mixture and load level for all un-notched fatigue tests. For that purpose, the individual curves were normalised, meaning that the number of cycles during the experiment n were divided by the numbers of cycles at failure N. This was necessary since even within each load level, the number of cycles at failure varied significantly. With the help of these normalised curves, the influence of the upper load level on the deformation can be shown.

Figure 5.23, Figure 5.24 and Figure 5.25 show the curves for the load levels tested for the three mixtures. It can be seen that in general terms, all curves show the visible three stages of the fatigue experiments, and the second stage takes part of more than 80% of the total fatigue life. Moreover, the curves also show that higher upper load levels lead to higher deformations, this fact is best seen in Figure 5.23 for the BSI/CERACEM mixture.

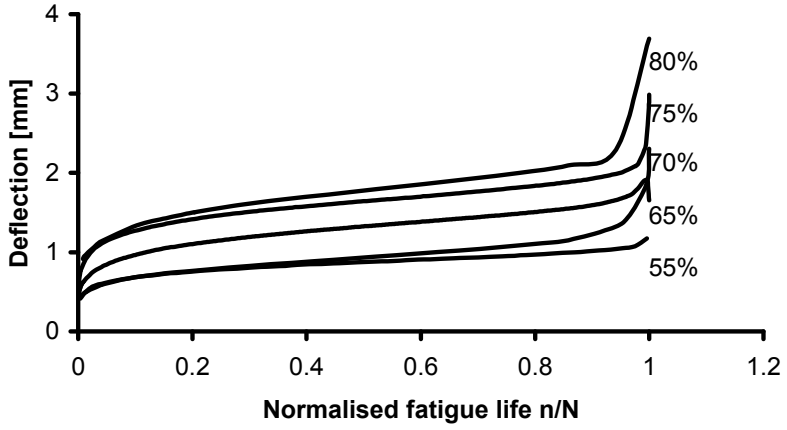

Figure 5.23: Average deflection during a fatigue experiment of all beams tested at a certain load level for the BSI/CERACEM mixture.

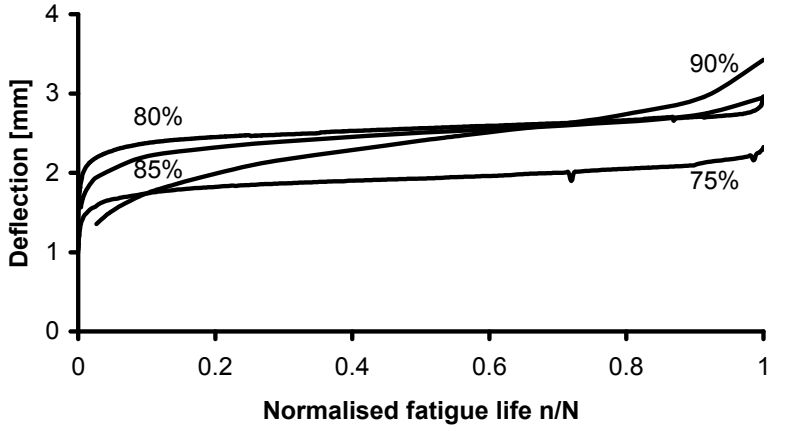

Figure 5.24: Average deflection during a fatigue experiment of all beams tested at a certain load level for the HSFRC mixture.

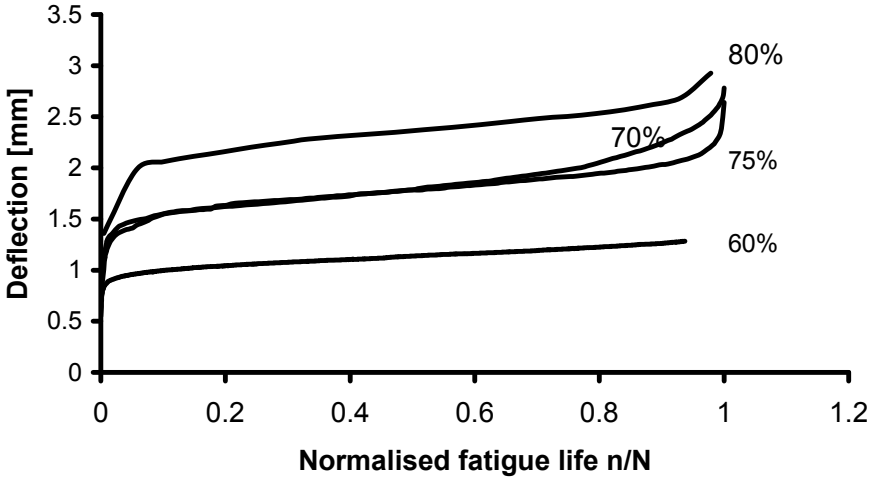

Figure 5.25: Average deflection during a fatigue experiment of all beams tested at a certain load level for the hybrid HSFRC mixture.

Figure 5.26, Figure 5.27 and Figure 5.28 compare the deflection evolution during fatigue life between the three concrete mixtures for a similar load level. Since each mixture had a different average static strength, the same load level does not correspond to the same upper load. It can be seen that the average deflections at a certain load level between the two HSFRC mixtures correspond better together than the BSI/CERACEM. This is due to the fact that the static strengths of these two mixtures and their stiffness were more or less in the same range. The fact that the deflections of the BSI/CERACEM at a certain load level are lower than for the other two mixtures, is mainly due to its very high stiffness, reflected in the value of the Young's modulus of around 50 GPa, thus resulting in smaller deflections even when the absolute load value was significantly higher compared to the other two mixtures.

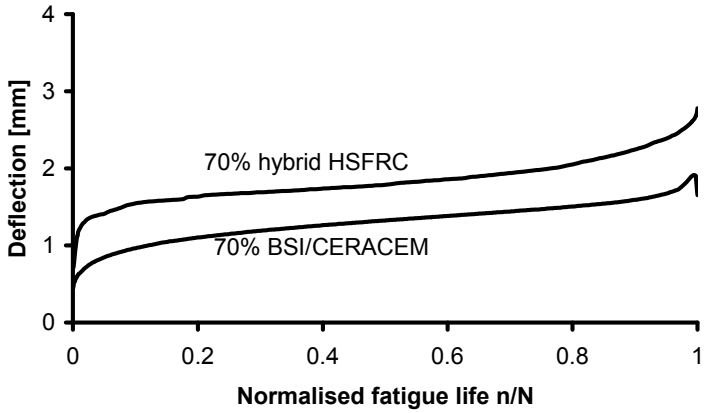

Figure 5.26: Average deflection during a fatigue experiment of BSI/CERACEM and hybrid HSFRC beams tested at an upper load level of 70%.

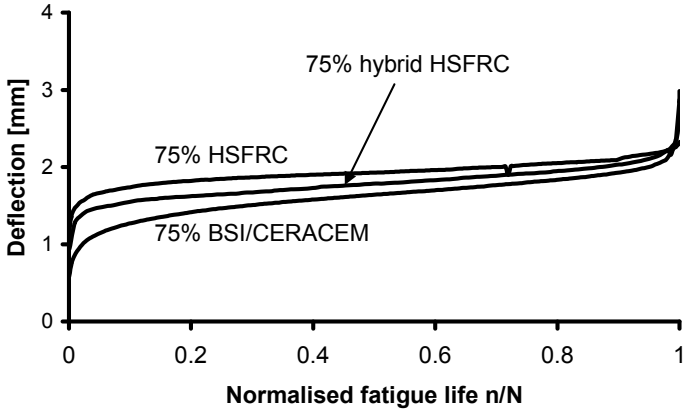

Figure 5.27: Average deflection during a fatigue experiment of BSI/CERACEM, HSFRC and hybrid HSFRC beams tested at an upper load level of 75%.

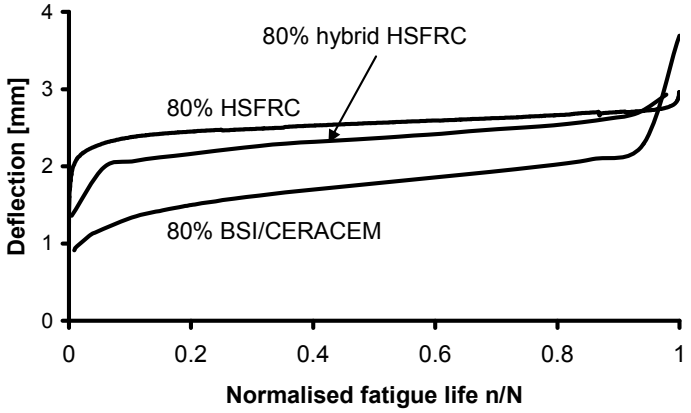

Figure 5.28: Average deflection during a fatigue experiment of BSI/CERACEM, HSFRC and hybrid HSFRC beams tested at an upper load level of 80%.

Relations between the deflection evolution and failure

There is a unique relation between the slope of the deflection development at the second stage of the fatigue experiment (the deflection increase rate) and the number of cycles to failure. This relation is presented in Figure 5.29 (for the un-notched beams), and it is linear on a logarithmic scale. All three mixtures are included in the graph: the relation is therefore independent of the concrete mixture (though related to the specimens' dimensions and the testing method). Such a linear relation is in accordance with earlier findings on flexural fatigue of plain concrete (Cornelissen and Reinhardt, 1984).

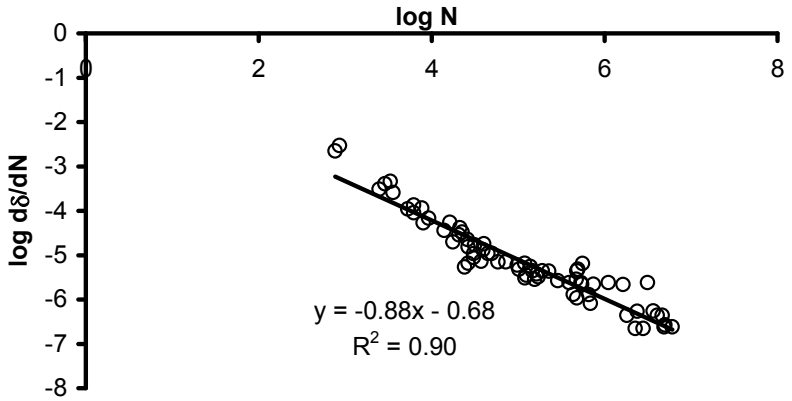

Figure 5.29: Relation between the rate of deflection increase in the second stage of the fatigue experiment and the number of cycles to failure. Beams of all three mixtures are included in the graph.

The same relation can be plotted for the rate of the crack opening increase in the second stage of the experiment, see Figure 5.30. However, the crack openings were only measured indirectly as the longitudinal elongation of the bottom fibre of the beams. In the graph, the rate is shown for the LVDT of each beam that showed the largest values of these elongations. Independent of the concrete mixture, for beams that had a fatigue life of over 10^5 load cycles, this rate could not be determined, since the slope of the deformation increase was very close to zero, at least with the chosen measurement arrangement.

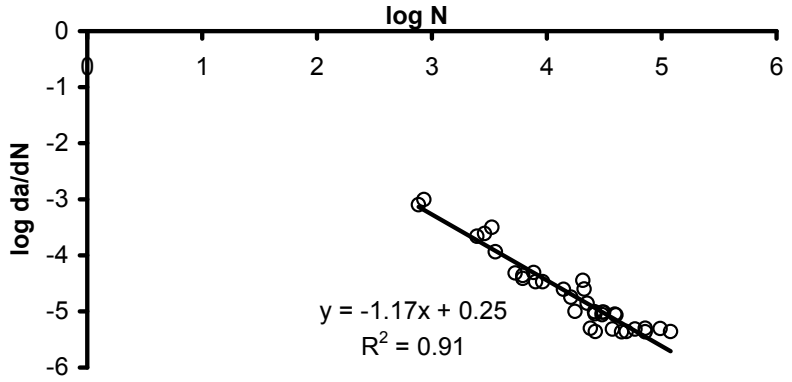

Figure 5.30: Relation between the rate of the deformation increase of the greatest longitudinal deformation (crack opening) measured vs. the number of cycles to failure for beams of all three mixtures with a fatigue life smaller than 10^5.

As was the case in the tests on un-notched beams, also for the tests on notched beams a relation between the slope of the deflection of the second stage of the fatigue experiment and the number of cycles to failure, on a double-logarithmic

scale, is found, as can be seen in Figure 5.31. Since only one of the beams survived 10 million load cycles, it is not possible to draw conclusions on the presence of a possible fatigue limit or other type of threshold for tests on notched specimens.

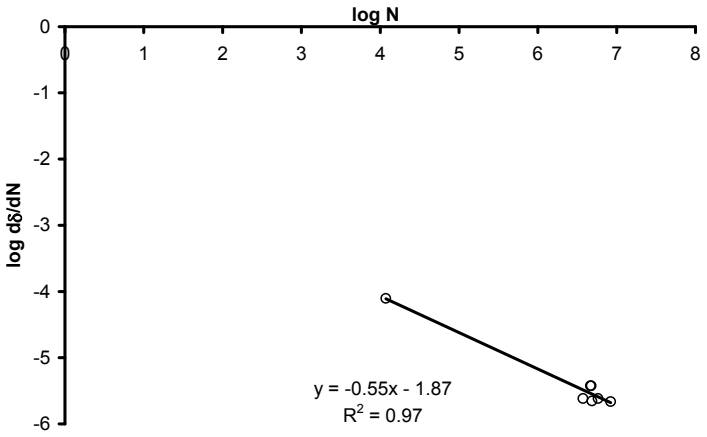

Figure 5.31: Relation between the slope of deflections in the second stage of a fatigue tests and the number of cycles to failure.

During the tests on notched beams, the crack opening could be directly measured, and also strains in the compressive zone were measured at the top surface of the beam. This enabled more precise conclusions on the strain distribution in the beam during the fatigue load duration; these results will be presented in Chapter 7 together the calculated strains with the proposed fatigue material model.

In the literature, a relation between the initial deformation, at the beginning of the fatigue experiment when the loading is applied, and the number of cycles to failure has been documented by Parant (2004), for an ultra high strength composite with a very high fibre content ($CEMTEC_{multiscale}$). Figure 5.32 shows the initial deflection in relation with the number of cycles to failure for the un-notched beams of this study. Only for the two high strength concretes, not for the BSI/CERACEM, such a relation was observed. A clear deformation threshold was only observed for the HSFRC mixture (see Figure 5.33). There, beams that did not fail before reaching ten million load cycles, had initial deformations much smaller than the ones of beams that did fail during the experiments. For the hybrid HSFRC this threshold was less pronounced, but still present, since there was an overlap between the beams that did not fail up to ten million load cycles and three beams with a rather high fatigue life, exceeding one million load cycles (log N>6), see Figure 5.34. Taking into account the fact that both HSFRC mixtures showed this deformation threshold, this would additionally support the presence of a fatigue limit for at least these two mixtures.

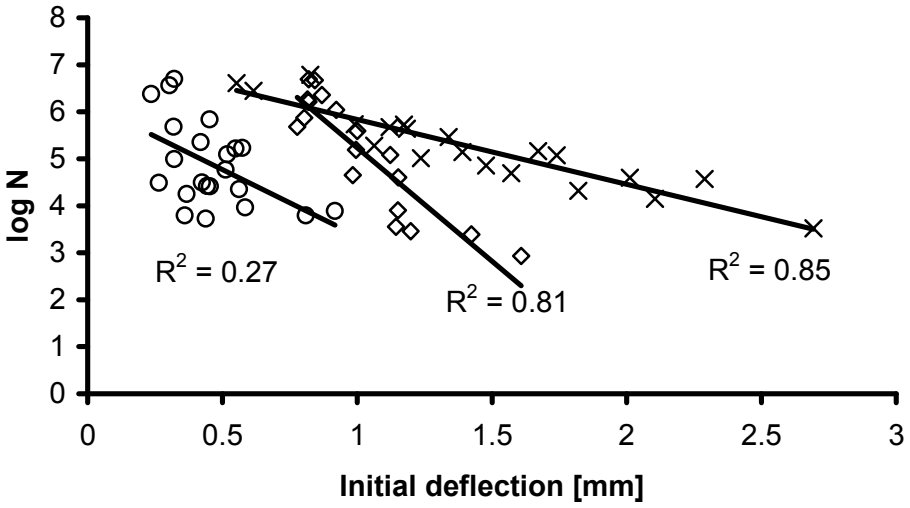

Figure 5.32: Initial deflection at the beginning of the fatigue experiment vs.the logarithm of the number of cycles to failure.

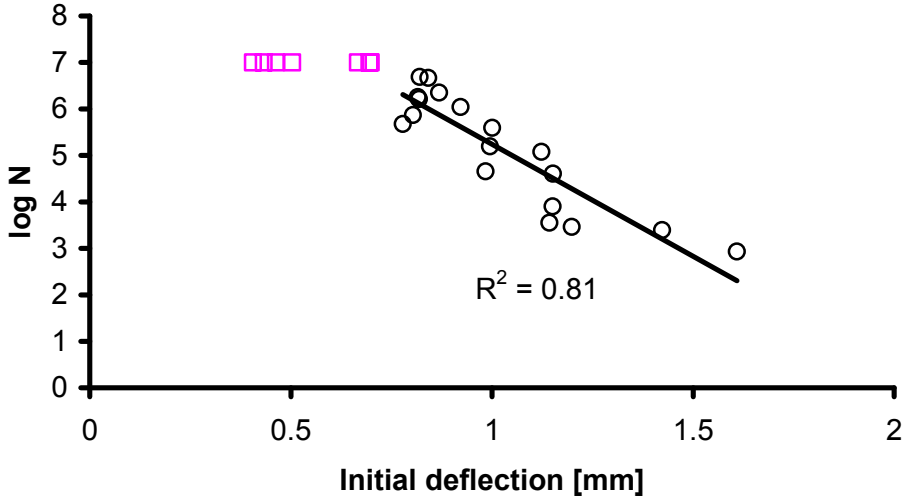

Figure 5.33: Initial deflection vs. logarithm of fatigue life for the HSFRC mixture. Beams that did not fail up to ten million load cycles are marked with squares.

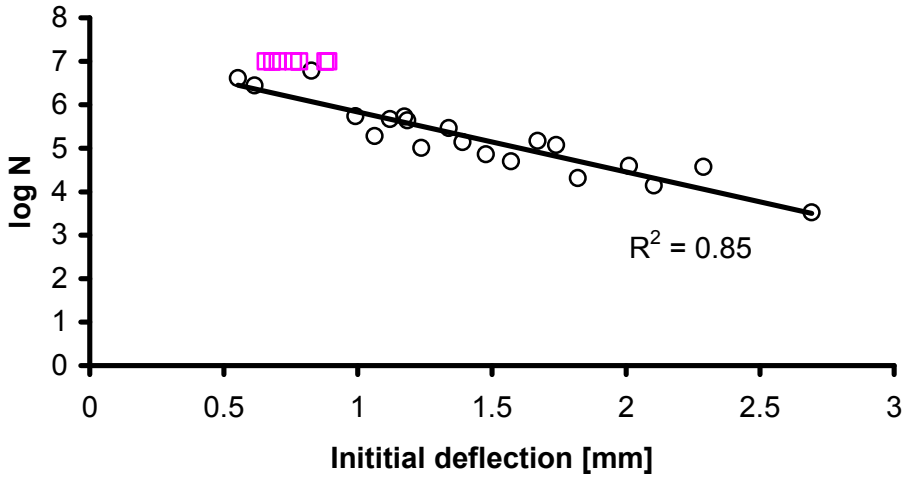

Figure 5.34: Initial deflection vs. logarithm of fatigue life for the hybrid HSFRC mixture. Beams that did not fail up to ten million load cycles are marked with squares.

5.5.3 Influence of the testing frequency

Concrete fatigue is usually tested at frequencies of 1-2 Hz and up to 20 Hz. The testing frequency has an effect on the fatigue behaviour; however these effects are more pronounced at higher upper load levels S≥0.75 (Cornelissen, 1986) or at very low frequencies of less than 1 Hz (Arthur et al., 1982). For load levels S<0.75, it is believed that the effects of testing frequencies in the range of 1-20 Hz are negligible (CEB, 1988). The main visible effect of a higher testing frequency is an overestimation of the fatigue life for higher (S>0.75) upper load levels (Holmen, 1979). Also, overheating of a specimen can occur at high testing frequencies (CEB, 1988); however, possible overheating seems to affect mainly reinforced concrete specimens rather than un-reinforced plain or fibre concrete.

The fatigue tests of this study were all performed at a frequency of 10 Hz. This might be a rather high frequency for concrete, however frequencies of up to 12 Hz have been applied previously to test flexural fatigue of concrete and fibre reinforced concrete (Suthiwarapirak et al., 2004), (Singh and Kaushik, 2000). The frequency was chosen since it was decided to test specimens up to 10 million load cycles. A lower frequency of 2-3 Hz, which is more common in concrete fatigue experiments, would have the negative consequence of very time-consuming tests and also a higher influence of time-dependent behaviour such as creep on the results.

Three HSFRC beams were tested under a frequency of 2 Hz at an upper load level of 80% of the static strength, a load level that had also been applied to seven beams of the same concrete at a 10 Hz frequency. Figure 5.35 shows the results of five of the beams tested at 10 Hz (black lines) and the three beams tested at 2 Hz (grey lines). The 2 Hz-beams failed at 555277, 656777 and 2064448 load cycles,

resulting in an average of 1092167 load cycles, compared to an average number of 1340597 load cycles of the seven beams at 10 Hz. For fatigue, these two average values, at 2 Hz and at 10 Hz, are comparable values. Since a logarithmic scale is used for fatigue results, the beams tested at 2 Hz had an average fatigue life of logN=6.04, and the beams tested at 10 Hz had a fatigue life logN=6.12, on a logarithmic scale. Therefore, from these limited number of tests, it can be concluded that the fatigue life, meaning the number of load repetitions to failure, is independent of the loading frequency, at least for the upper load level of S=0.8 that was examined in this case. The lower frequency had more influence on the deformations: one of the beams tested at 2 Hz shows similar values of the average deflection with the beams tested at 10 Hz, while the other two show significantly smaller deflections. Figure 5.36 shows the average deflection corresponding to the fatigue life of the beams tested at 2 Hz, 10 Hz, and the average of all. From the limited number of tests performed here, it seems that a higher frequency leads to larger deflections, at least at the tested high upper load level of 80% (or in other words, the higher frequency results in a higher stiffness degradation and higher deformations). As can be concluded by the above observations, the HSFRC was tested at a load level S=0.8>0.75 and according to the observations of previous researchers, a smaller fatigue life should be obtained for a lower frequency. However, this cannot be confirmed by the tests carried out in this study.

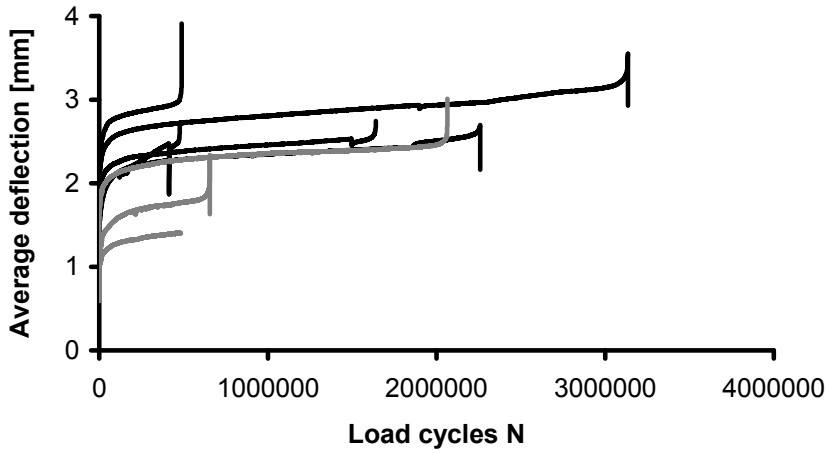

Figure 5.35: HSFRC Beams tested at un upper load level of 80% of the static strength at a frequency of 2 Hz (grey lines) and 10 Hz (black lines).

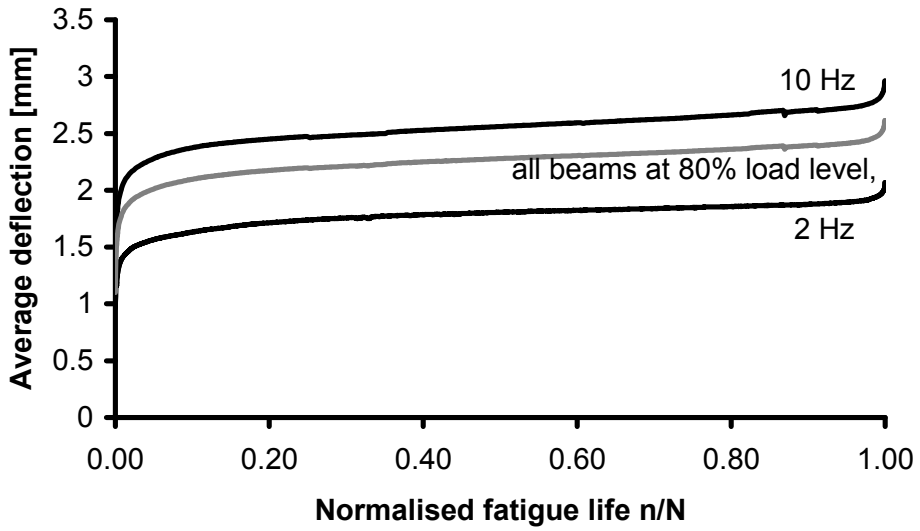

Figure 5.36: Average deflection evolution of HSFRC beams tested at 80% at a frequency of 2 Hz, 10 Hz and the average of all beams of the load level regardless the frequency.

5.5.4 On the static response serving as envelope curve

For concrete and fibre reinforced concrete under fatigue loading, a commonly used approach is that of the static structural response serving as an envelope curve for fatigue loading and determining the onset of fatigue failure. This implies that as soon as fatigue deformations reach the corresponding value of the deformation for the same load level at the descending branch of the static response, as is schematically shown in Figure 5.37, then fatigue failure occurs. Even though the concept probably applies for concrete in compression, it is still questionable whether or not this concept applies for concrete in bending, and for high and ultra high strength concrete in general. In the following, evidence and contradictory proof on this concept will be given as found in the literature.

The static load-deflection curve from a bending tests has been found to serve as an envelope for fatigue deformations by Zhang and Stang (1998), Zhang et al. (1999) and Cachim et al (2002). Zhang et al. (1999) state that the crack mouth opening (CMOD), and fatigue crack length, as a failure criterion in a flexural test, will be smaller than the values that can be attained under monotonic conditions. Subramaniam et al. (2000) also found that the values of the deflection and crack openings at fatigue failure do not match the static curve, but found larger crack openings and deflections at fatigue failure compared to the static ones. They suggest that only an envelope in terms of the effective crack length is valid, however the crack length is difficult to measure. Kessler-Kramer (2002), who performed load-

controlled fatigue bending tests as well as load and deformation controlled uniaxial tension fatigue tests for normal and high strength concrete, found that the differences between static and fatigue deformations are the more pronounced the larger the numbers of load cycles up to failure were. In some cases, a slightly different failure criterion has been found valid: Fatigue failure is observed to occur when the fatigue displacement value reaches the value that corresponds to the static displacement at peak load, and not the static displacement at the corresponding load level of the descending branch in the postpeak stage. This was the case in Do et al. (1993) for compressive fatigue tests with high strength concrete, even though they state that for normal strength concrete the fatigue failure strain would always be larger than the static peak strain, and in Balász (1991) for the slip deformation for bond fatigue between concrete and rebars.

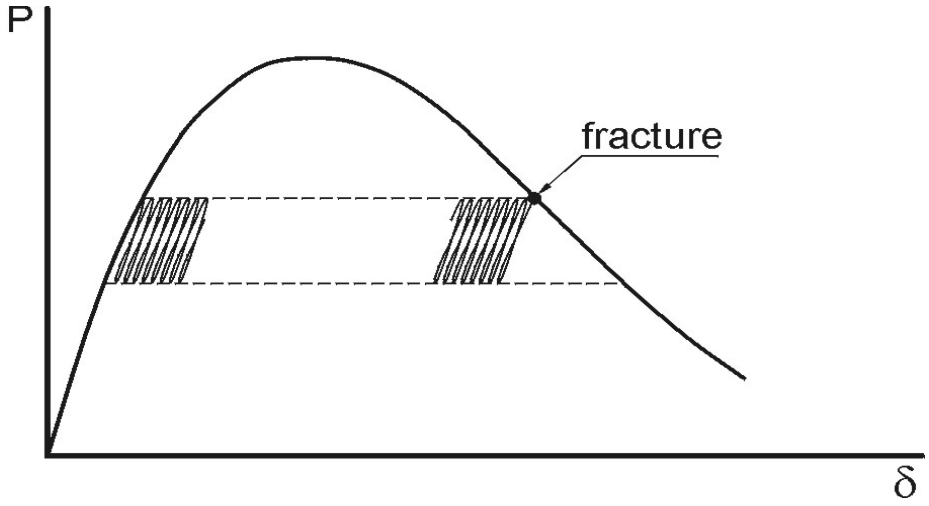

Figure 5.37: Principle of the static structural response serving as an envelope for fatigue deformations.

In the following, whether or not the static response can function as an envelope will be evaluated for the mixtures of this study as observed in the performed experiments. Figure 5.38, Figure 5.39 and Figure 5.40 show the normalised static load-deflection curves for each of the tested concretes, and the value of the deflection of the fatigue beams tested to failure at the corresponding load level. For all concretes, only the higher load levels (from 75% and higher) showed deflections comparable to the corresponding deflection of the static curves at the same stress level on the descending branch of the curves; for lower stress levels, the deformations at failure were significantly smaller than the corresponding values of the static curves.

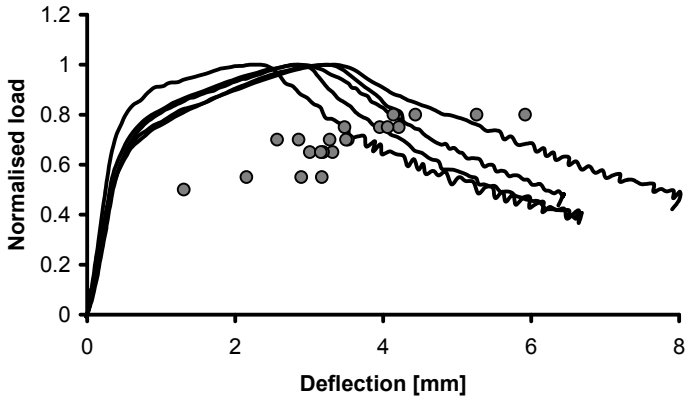

Figure 5.38: Normalised static load-deflections curves and deflections at fatigue failure for the BSI/CERACEM beams.

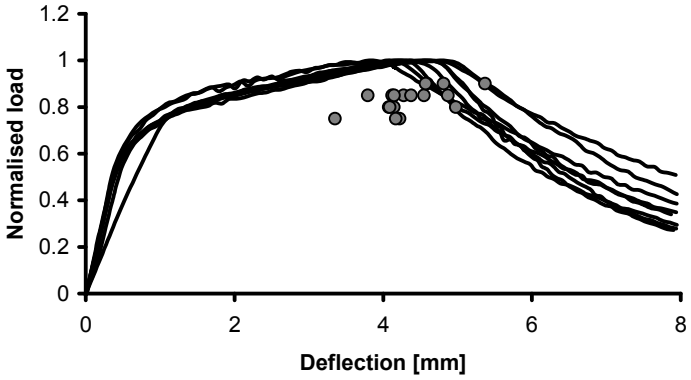

Figure 5.39: Normalised static load-deflection curves and deflections at fatigue failure for the HSFRC beams.

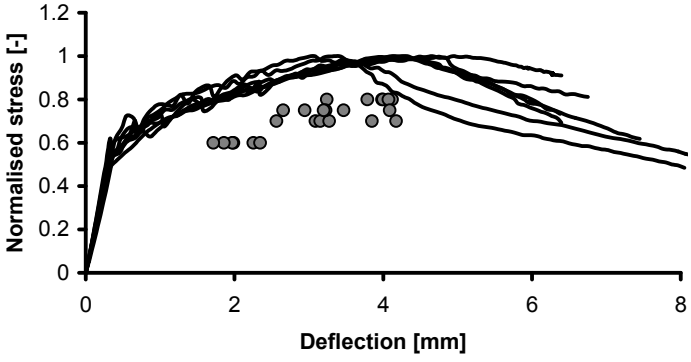

Figure 5.40: Normalised static load-deflection curves and deflections at fatigue failure for the hybrid HSFRC beams.

As already mentioned before, for flexural fatigue both supportive and contradictory evidence has been found for the envelope curve concept regarding the deflections and crack openings. Especially recent publications (Suthiwarapirak et al., 2004),(Subramaniam et al., 2000) have shown that the envelope curve in bending is not valid, at least not in terms of deflection. The static curve served as an envelope in terms of compliance, that is the inverse of the stiffness, or the effective crack length (Subramaniam et al., 2000). Neither the compliance nor the effective crack length were measured in the static and fatigue testing series in this study so this cannot be verified here.

Suthiwarapirak (2004) observed similar results as in this study, with deflections that were dependent on the upper load level and the deflections at higher stress levels better corresponding to the static response as an envelope during their fatigue testing of ECC. At high fatigue load levels, most cracks were formed during the first load repetitions, and fewer new cracks formed during testing up to failure. At these load levels, the fatigue crack growth is most likely the dominant failure mechanism opposed to fatigue crack initiation. At lower load levels, where the applied load does not provoke extensive cracking in the initial load repetitions, multiple cracking was much less pronounced and in fact fatigue crack initiation will become responsible for failure. They conclude that multiple cracking characteristics are less pronounced at lower load levels, which implies a more brittle type of failure and can explain the smaller deflections compared to the corresponding static ones on the descending branch at the same load, and this can also be the case for the materials tested in this study.

5.6 Joint durability-fatigue testing series

Within this study a joint fatigue-durability testing series was performed, under collaboration with the concrete technology group of the University of Karlsruhe, in Germany. This joint research will be completed with the PhD work of Dipl.-Ing. Jennifer Scheydt on durability of ultra high strength concretes. Ultra high strength concretes are considered very durable materials due to their dense compositions and low porosity, which makes it very difficult for fluids and acids to penetrate. The work at Karlsruhe University will result in a thorough evaluation of the durability of these materials. Here, only a brief overview of their experimental programme will be given, focused on the joint experimental part of both research projects. In a way, the two subjects, fatigue and durability, are closely related: Fatigue can be regarded as the mechanical durability of a material with regard to external loading conditions, while durability, in its classical sense as the freeze thaw and chloride attack resistance, as the environmental durability of a material, its resistance against continuous detrimental effects from the environment.

In Karlsruhe, a number of ultra high strength mixtures have been developed (Scheydt, 2004) for the study on durability. These include coarse aggregate ultra high strength mixtures, with a maximum aggregate size of 8 mm, and mortars. The mixtures can be heat treated to reach even higher compressive strength, and reach compressive strengths of 180-220 MPa, depending on the actual mixture composition and curing conditions. The research programme at Karlsruhe University for durability includes experimental testing series on carbonation, chemical attack, chloride penetration, and frost- and de-icing salt resistance. In addition, parameters that influence the durability, such as the microstructure of the material and its transport parameters are studied. Regarding the microstructure, the methods used to obtain the needed information include thermogravimetry, x-ray diffraction, microscopy and porosity measurements. For the determination of the transport parameters, tests for the gas permeability, diffusion and capillary suction are carried out. An overview of the research project in Karlsruhe and first results is given by Herold and Scheydt (2006).

Within the joint fatigue-durability testing series, two concrete mixtures are regarded: the BSI/CERACEM used in this study and cast at Delft University, and one of the coarse ultra high performance mixtures from Karlsruhe University, denoted in this study as UHPC. Information on the mixture compositions of both mixtures can be taken from Chapter 2. Both concretes have in common a compressive strength of approximately 200 MPa, a steel fibre addition of 2.5 vol.%, and a similar maximum aggregate size, 7 mm in the BSI/CERACEM and 8 mm in the UHPC.

In Delft, 18 beams were prepared from the BSI/CERACEM mixture for the durability-fatigue testing series. Six beams were used for preliminary static and fatigue tests. Six beams were sent as reference beams to Karlsruhe, without being subjected to any loading in Delft. Three of them were intended for freeze-thaw testing in Karlsruhe and three for chloride attack. The remaining six beams were first subjected to a fatigue preloading in Delft before being sent to Karlsruhe. After being subjected to the fatigue loading, in Karlsruhe three of these beams were intended for freeze-thaw testing and three for testing against chloride attack. The results on these pre-damaged beams can in that way be compared to the reference beams that were not pre-damaged by fatigue.

In Karlsruhe, 12 UHPC beams were prepared for the common testing series. Six beams were sent directly to Delft as reference beams. Three of them were tested statically up to failure in order to determine their average peak load, which is used to determine the value of the upper load level for the fatigue tests. The remaining three reference beams were then subjected to fatigue flexural loading. The other six beams cast in Karlsruhe were first subjected to a freeze-thaw attack. They were subjected to 200 freeze-thaw cycles before being sent to Delft for further testing. Of these, 2 beams were tested under static loading, in order to verify the value of the upper load level for fatigue testing and to see the effect of the freeze-thaw damage on the static material behaviour. The remaining four beams were then subjected to

fatigue loading. In the following subsections, the main findings of this joint testing series will be mentioned, focussing on the static and fatigue bending tests in Delft. The results of the durability tests will be reported by Jennifer Scheydt and will be included in her own PhD work.

5.6.1 Results of the tests on the BSI/CERACEM mixture

Six BSI/CERACEM beams were prepared for preliminary static and fatigue tests, three beams were tested statically and three were subjected to fatigue loading. The static tests were performed in order to determine the average peak load and compare this to previous results of the same mixture, and use these results to determine the upper load level for the fatigue tests. These preliminary tests were necessary, since a different batch of the premix was used than in the static tests with the BSI/CERACEM mixture, as reported in Chapter 4. The three reference beams had an average peak load of 62.5 kN (corresponding to a flexural tensile stress of 23.9 MPa), and together with the previously tested static beams of the same mixture this resulted into an overall average of 64.5 kN (corresponding to a flexural tensile stress of 24.8 MPa). This total average was considered to be a better suitable value, representing the complete scatter of the mixture, and was set as the reference value for the upper load level of the fatigue tests. The remaining three beams of the preliminary testing series were subjected to fatigue loading, in order to verify the assumption that upper load levels of 50% and 60% would not result into failure before two million load cycles, which was the case.

After these preliminary static tests, the fatigue pre-damaging was performed on beams that would afterwards be subjected to freeze-thaw attack or chloride attack in Karlsruhe. Fatigue tests on BSI/CERACEM, as reported in section 5.2.2, showed that for this mixture, a fatigue life of at least 10 million cycles can be expected for upper load levels lower than 60%. The fatigue pre-damage for the beams intended for joint fatigue-durability testing should result in cracking, but not complete failure of the beam. Therefore, it was chosen to subject these beams to upper load levels not higher than 60% of the average static load. Of the six beams sent to Karlsruhe for the combined loading series, four were tested at an upper load level of 50% and two at an upper load level of 60%, where all six beams were tested up to two million load cycles. None of these beams failed after this fatigue loading.

In Karlsruhe, these pre-damaged six beams were subjected to further durability tests together with the six reference beams of the same mixture, that were not previously subjected to fatigue loads. Three of the reference beams and three of the pre-damaged beams were subjected to freeze-thaw cycles, and the other three of the reference beams and the pre-damaged beams were subjected to chloride attack. At the time this thesis was written, not all of the experimental series had been completed. Therefore here only preliminary results, and only on the freeze-thaw attack, can be given. Initially, the dynamic Young's modulus of the beams was tested before the freeze-thaw attack with a non-destructive ultrasonic method. Almost no

difference was observed between the reference and the pre-damaged beams, which shows that the fatigue cycles at the chosen upper load level did not change the static load bearing capacity significantly. A higher fatigue load level might have been more appropriate. However, as has been stated before, at a higher load level it is very likely that beams would fail before reaching two million load repetitions, and this was not desired. The results of the freeze-thaw testing series so far showed that after 175 temperature cycles, both the reference and the pre-damaged beams did not change their dynamic Young's modulus significantly, and did not show any sign of spalling on the surface.

5.6.2 Results of the tests on the UHPC mixture

A total of 12 UHPC beams were sent to Delft, consisting of six reference beams that had not been subjected to any kind of damage, and six beams that had been subjected to 200 freeze-thaw cycles in Karlsruhe. Of the six reference beams, three were tested under static loading, to determine their static load bearing capacity. Of the six pre-damaged beams, two were subjected to static loads, in order to evaluate the effect of the freeze-thaw attack on the static load bearing capacity. All remaining beams were tested under fatigue loading.

The three reference beams subjected to static loading had an average peak load of 47.0 kN, which corresponds to a flexural tensile strength of 18.0 MPa, with a low scatter, the coefficient of variation being 4%. The average flexural stress-deflection curve of this mixture is shown in Figure 4.13 in Chapter 4. The two pre-damaged beams had peak loads of 53.6 kN and 47.6, which correspond to flexural tensile strengths of 20.6 MPa and 18.3 MPa. The initial stiffness of the pre-damaged and the reference beams was identical. The flexural strength of the pre-damaged beams was even slightly higher than the average of the reference ones. This can be due to the fact that the pre-damaged beams were tested at an age of 513 days, while the reference ones were tested at an age of 92 days. However, as was already discussed in Chapter 4, these high strength mixtures develop their strength mainly in the first 28 days and little difference is observed between the 28 day strengths and at later ages. Also, the overall average of all 5 statically tested beams of the UHPC mixture results into a load of 48.4 kN, which corresponds to a flexural tensile stress of 18.6 MPa, with a coefficient of variation of 7%. Such a coefficient of variation is a reasonable scatter for fibre reinforced concrete, and this indicates that the results of the two pre-damaged beams are most likely within the natural scatter of the static strength of this mixture. The results of the static tests on pre-damaged and reference beams show that the freeze-thaw attack did not affect the static load bearing behaviour.

Three reference beams and four pre-damaged UHPC beams were subjected to fatigue loading. Since no other fatigue tests had been performed with this mixture, and at the time of the fatigue testing on the reference beams the effect of the 200 freeze-thaw cycles on the load bearing capacity of the beams was not known, it was

decided to initially subject every beam to two million load cycles at an upper load level of 50% of the average static load. In the case a specimen did not fail, the load was increased to 60%, and if possible also to 70%, up to a maximum of two million load cycles at each upper load level. All three reference beams could be subjected to two million load cycles at an upper load level of 50% without failure. Two of the three also survived two million load cycles at 60% without failure, one of them failed at this load level after 5314 load cycles. The remaining two beams failed at a load level of 70%, at 12442 and 41694 load cycles. The four UHPC beams that had been previously subjected to 200 freeze thaw cycles were subjected to fatigue loading, in the same way as the reference beams at load levels of 50%, 60% and 70%. The upper load level was defined in that case as the average of the three reference beams and the two predamaged beams (48.4 kN) that had been tested under static load. All four beams could be subjected to two million load cycles at an upper load level of 50% without failure. Two of the four failed after the upper load was increased to 60%, at 316620 and 1180827 cycles. The other two failed after the upper load was increased to 70%, at 341 and 4048766 cycles. These results show that the freeze-thaw attack had no observable influence on the fatigue load bearing capacity of the UHPC mixture.

5.6.3 Concluding remarks on the joint durability-fatigue research

Even though this joint experimental series was rather limited with regard to the number of specimens, the results show that both ultra high strength mixtures, the BSI/CERACEM and the UHPC, are mixtures with an excellent durability. After 200 freeze thaw cycles, the surface of the beam was still intact, without any signs of spalling. Only steel fibres that were positioned on the surface, had rusted, but as the results of the static and fatigue testing show, this is limited to only these fibres on the surface and has no effect on the static or fatigue load bearing capacity.

A difficulty in this joint testing series was finding an appropriate level of pre-damage that would lead to a different durability or load bearing capacity with regard to the reference beams. This is mainly due to the high durability of the material, but it also shows that the chosen testing procedure had its limitations in order to evaluate the combined effect of environmental loading, such as freeze thaw and chloride attack, and fatigue loading. As a recommendation for further research, a testing series on simultaneous fatigue/durability loading might be more suitable. A different experimental setup is needed in order to perform fatigue tests in a climate room simultaneously with freeze-thaw cycles. However, since fatigue tests are usually performed at periods of one cycle every 0.1 second or up to every 0.5 second (corresponding to 10-2 Hz), and freeze-thaw cycles at 1 cycle every day, this implies that not many freeze-thaw cycles can be performed during the fatigue testing, and with these durable materials it is questionable if such a testing series would provide more information than the results shown in this study.

5.7 Points for further research

The performed experimental programme and its results is a valuable contribution to the evaluation of the (flexural) fatigue behaviour of high strength fibre reinforced cement composites. Even so, there are still a number of parameters that could not be examined thoroughly due to time constraints within this research. These will be listed in the following and are interesting points for further future research, and necessary in order to get a complete overview of the fatigue behaviour of such mixtures. The aim of this additional research would be to have a better understanding of fatigue failure processes; with that achieved, the design and building codes could be adapted and a more efficient material use and a safer design can be possible that would fulfil the demands of future increasing live loads or design for a longer lifetime of a structure.

First of all, the microscopical observations show that a study on further improvement of the mixture compositions might be advisable in order to further improve the quality of the binder and the fibre-matrix interface that might result into a better fatigue performance. On the one hand, the two HSFRCs are very workable mixtures, but the binder is not always of a homogeneous quality, a point for further improvement. However, the workability and flowability properties should remain unaltered. Further, even though the binder quality is good in case of the BSI/CERACEM, there were air pockets between the fibre and the matrix, and local fibre clustering was observed. Also the reduced workability in the fresh state indicates that the used fibre type and geometry is not so suitable at this high volume fraction in order to provide a good workability. Therefore, there might be either a suitable fibre type (possibly with a slightly shorter length), or a lower fibre volume fraction, that can provide a better workability. The aim should be to improve the workability, and bond between the fibre and the matrix, but to keep the strength values in the hardened state at the values obtained in this study. With an improved workability, it is expected that the mixture's fatigue performance will improve as well. Moreover, since the performed microscopical study was of a limited range, with only one specimen of each mixture, another point for further research is a larger study with more specimens that can provide stronger conclusions and more information on the fatigue damage mechanisms on a microscale.

In this study, constant amplitude fatigue tests were performed with a lower-to-upper load ratio R=0.2. The influence of the lower load level for different loading values R has still to be evaluated experimentally. Only repeated loading with no stress-reversals has been studied. As has been shown by Cornelissen and Siemes (1985), stress reversals can have a detrimental effect on the fatigue lives, and differences exists in case of compressive-tensile or tensile-compressive fatigue loading. These are also additional points of interest. However, the present testing setup does not allow stress reversals therefore a new testing setup would have to be built for such tests.

For a complete overview of the fatigue behaviour of the materials studied, additional testing series of compressive fatigue and uniaxial tensile fatigue as well as compressive-tensile fatigue have to be performed. For a better micromechanical evaluation, static and repeated cyclic single fibre pull-out tests could provide insight in the fibre bridging degradation at fatigue loading; however, these tests are difficult to perform especially for the smallest, 13 mm long fibres used in this study that have a diameter of only 0.16 mm. Further, deformation controlled uniaxial tensile fatigue tests, as have been performed by Zhang et al. (2000) and Kessler-Kramer (2002), would provide insight in damage mechanisms, and a more precise parameter identification for fatigue material models. Also, the effect of the fibres might be better visible in case of thin slabs, which would allow a more uniform and better fibre orientation, so that the effect and benefit of the fibre addition on the fatigue behaviour could be better evaluated.

The moisture content can influence the fatigue performance and it has been found that wet concrete has a worse fatigue performance than dry concrete (Van Leeuwen and Siemes, 1979). The influence of the moisture content was not in the scope of the present study, and its influence was minimised by keeping the same curing and drying conditions of the testing specimens. However, a further point to investigate is whether the use of completely sealed specimens could additionally minimise the influence of the moisture content and further reduce the scatter of the fatigue testing series. Moreover, actual structures suffering from fatigue, as bridges, are affected by rain and humidity of the environment and this fact has to be accounted for in design. This evokes the need for a testing series under 'environmental' conditions under different moisture contents and gradients to account for environmental effects.

Finally, a point for further experimental research is a better evaluation of fatigue loading on pre-cracked specimens, especially for fibre reinforced concrete, as fibres become effective after the first cracking of the matrix. For that, specimens should be first statically pre-loaded up to a certain crack width and then unloaded again; afterwards, the fatigue loading should be applied. Such experiments have been performed for the industrial UHPFC mixture DUCTAL by Behloul et al. (2005); however, they did not study the failure mechanisms but used the experiments to verify that the fatigue verifications, as provided in the French interim regulations for UHPC provides a safe design of structures.

5.8 Conclusions

Fatigue tests have been performed on three different high strength steel fibre reinforced mixtures at different (at least four) load levels, with a constant upper-to-lower load ratio of 0.2 and at a frequency of 10 Hz. The upper load was set to a

percentage of the previously determined static load, ranging from 50% up to 90%. From the observed results, the following can be concluded:

- A better workability in the fresh state leads to less scatter in the material's mechanical properties and therefore also reduces the scatter in the fatigue properties. The HSFRC mixture has the best workability and flow ability in the fresh state, and this was also the mixture that has the most favourable fatigue performance, especially when the upper load level is related to the peak load of the static tests.
- Even though high and ultra high strength materials show improved material properties regarding static strength values and durability, such an improvement is not visible for fatigue properties. Of the three mixtures tested here, only the HSFRC showed an improved fatigue performance with regards to plain concrete, showing no failure for upper load levels lower than 70%. The BSI/CERACEM, the ultra high strength mixture of this study, which was the mixture with the highest compressive and flexural tensile strengths, had an inferior fatigue performance with regard to the two HSFRC, showing that strength alone is not an indication of a material's fatigue performance.
- In fatigue, the fibre orientation and concentrations seem to be of less importance, at least compared to the role of these parameters in the static performance. Therefore, the material's performance could not be significantly improved by applying a correction on the basis of the results of the fibre count in cross-sections close to the fracture surface. The microscopic study showed that the bond between the matrix and the fibres was not as good as for the HSFRC, and this mixture had also the worst fatigue performance, which suggests that fibre (de)bonding is of greater importance than their alignment in fatigue. Moreover, the results of the fibre count and the microscopy study show that fatigue failure mechanisms are influenced by a number of parameters. The fibres alone cannot provide definite answers, even though in the observed static bending behaviour, a direct relation between the fibres in the cross section and the static strength was found.
- The fatigue results show a considerable scatter, which makes the results difficult to interpret. However, S-N lines were shown with the average number of cycles of failure for each load level. When the specimens that did not show failure up to ten million load cycles were included in the average, a better correlation between the stress ratio and number of cycles to failure was obtained for all three mixtures.
- The microscopic observations show that a better bond between fibres and matrix exists for the two HSFRC mixtures than for the BSI/CERACEM mixture. However, the quality of the binder is more homogeneous for the BSI/CERACEM and shows variability in the local w/c ratio and air content for the two HSFRCs.
- Regarding the presence of a fatigue limit, the HSFRC did not show failure at loads corresponding to less than 70% of the static material strength, and also the

initial deformation of the beams that did not fail were significantly lower than the values of beams that failed. Such a deformation threshold was also observed for the hybrid HSFRC mixture. Conclusions on the presence of a fatigue limit or deformation threshold for the BSI/CERACEM cannot be drawn.

- A unique relation for all three mixtures existed between the slope of the deflection at the second stage of the experiments and the number of cycles to failure. This relation was linear on a double logarithmic scale. The two high strength mixtures additionally showed a relation between the initial deflection when the load was initially applied, and the number of cycles to failure.
- The static load deflection curve does not function as an envelope curve for the fatigue experiments. At least it does not fit in terms of deflection, crack openings or compressive strains, since all these deformations depend on the applied upper load level, and higher deformations were observed for higher upper load levels.
- The testing frequency affects mainly the deformations and stiffness degradation and has less influence on the number of load cycles to failure at a certain load level.
- Fatigue tests on notched beams of the HSFRC mixture showed an inferior fatigue behaviour compared to un-notched ones since the notch forces deformations to localise at an earlier stage.
- The joint fatigue-durability testing series shows that these materials have a high durability, and almost no significant damage can be observed after 200 freeze-thaw cycles.

References

AAS-JAKOBSEN, L. (1970) Fatigue of Concrete Beams and Columns. *Bulletin No 70-1, Div. of Concrete Structures.* NTH University of Trondheim.

AFGC-SETRA (2002) Béton fibrés a ultra-hautes performences, recommandations provisoires.

ARTHUR, P. D., EARL, J. C. & HODGKIESS, T. (1982) Corrosion Fatigue in Concrete for Marine Applications. IN SHAH, S. P. (Ed.) *Fatigue of Concrete Structures.* Publication SP-75, American Concrete Institute.

BALÁSZ, G. L. (1991) Fatigue of Bond. *ACI Materials Journal,* 88**,** 620-629.

BARR, B. I. G. & LEE, M. K. (2003) Dynamic Analysis of Cracked Sections (Literature Review). *Test and Design Methods for Steel Fibre Reinforced Concrete Brite-EuRam Project BRPR-CT98-0813 (DG12-BRPR), Final Report, Sub-task 5.3.*

BEHLOUL, M., CHANVILLARD, G., PIMIENTA, P., PINEAUD, A. & RIVILLION, P. (2005) Fatigue Flexural Behaviour of Pre-cracked Specimens of Special UHPFRC. *ACI Special Publication, Volume 228.* American Concrete Institute.

CACHIM, P. B. (1999) Experimental and numerical analysis of the behaviour of structural concrete under fatigue loading with applications to concrete pavements. *PhD Thesis.* Faculty of Engineering of the University of Porto.

CACHIM, P. B., FIGUEIRAS, J. A. & PEREIRA, P. A. A. (2002) Numerical modelling of fibre-reinforced concrete fatigue in bending. *International Journal of Fatigue,* 24**,** 381-387.

CEB (1988) Fatigue of Concrete Structures - State of the Art Report. *Bulletin d'Information No 188.* Comite Euro-International du Beton.

CORNELISSEN, H. A. W. (1986) State-of-the-art report on fatigue of plain concrete. *Report 5-86-03.* Delft University of Technology.

CORNELISSEN, H. A. W. & REINHARDT, H. W. (1984) Uniaxial tensile fatigue failure of concrete under constant amplitude and programme loading. *Mag. of Concrete Research,* 36**,** 216-227.

CORNELISSEN, H. A. W. & SIEMES, A. J. M. (1985) Plain concrete under sustained tensile or tensile and compressive fatigue loadings. *BOSS Conference.* Amsterdam, Elsevier Science Publishers.

CORNELISSEN, H. A. W. & TIMMERS, G. (1981) Fatigue of plain concrete in uniaxial tension and in alternating tension-compression. Experiment and results. *Report 5-81-7.* Delft University of Technology.

DO, M. T., CHAALLAL, O. & AÏTCIN, P. C. (1993) Fatigue behaviour of high-performance concrete. *Journal of Materials in Civil Engineering,* 5**,** 96-111.

FARHAT, F. A., NICOLAIDES, D., KANELLOPOULOS, A. & KARIHALOO, B. L. (2007) High performance fibre-reinforced cementitious composite (CARDIFRC) - Performance and application to retrofitting. *Engineering Fracture Mechanics,* 74**,** 151-167.

FEHLING, E., SCHMIDT, M., TEICHMANN, T., BUNJE, K., BORNEMANN, R. & MIDDENDORF, B. (2005) *Entwicklung, Dauerhaftigkeit und Berechnung Ultrahochfester Betone (UHPC). Forschungsbericht DFG FE 497/1-1*, Kassel University Press GmbH, Kassel.

HEROLD, G. & SCHEYDT, J. (2006) Development and durability of ultra high performance concretes. *Concrete Plant & Precast Technology (BFT),* 10/2006**,** 4-14.

HOLMEN, J. O. (1979) Fatigue of Concrete by constant and variable amplitude Loading. *PhD Thesis, Bulletin No 79-1.* NTH University of Trondheim.

HORDIJK, D. A. (1991) Local approach to fatigue of concrete. *PhD Thesis.* Delft University of Technology.

HSU, T. T. C. (1971) Fatigue of plain concrete. *ACI Journal,* 78**,** 292-304.

ISSA, M. A. & SHAFIQ, A. B. (1999) Fatigue Characteristics of Aligned Fiber Reinforced Mortar. *Journal of Engineering Mechanics,* 125**,** 156-164.

JSCE (2005) Tentative Guideline for Design and Construction of Engineering Cementitious Composites ECC (Draft). Japanese Society of Civil Engineers (JSCE). JSCE TC 334.

KESSLER-KRAMER, C. (2002) Zugtragverhalten von Beton unter Ermüdungsbeanspruchung. *PhD Thesis.* Universität Karlsruhe (TH).

LAPPA, E. S., BRAAM, C. R. & WALRAVEN, J. C. (2005a) Flexural performance of high and ultra high strength fibre reinforced concrete - overview of static and fatigue experimental program. Delft University of Technology.

MC90 (1993) Model Code 1990. CEB Bulletin d'Information No 203 ed., Comite Euro-International du Beton CEB-FIP.

MCCALL, J. T. (1958) Probability of Fatigue Failure of plain Concrete. *ACI Journal,* 55**,** 233-244.

MINER, M. A. (1945) Cumulative Damage in Fatigue. *Journal of Applied Mechanics,* 12**,** 159-164.

OH, B. H. (1991a) Cumulative damage theory of concrete under variable amplitude fatigue loadings. *ACI Materials Journal,* 88**,** 41-48.

OH, B. H. (1991b) Fatigue-life distributions of concrete for various stress levels. *ACI Materials Journal,* 88**,** 122-128.

PALMGREN, A. (1924) Die Lebensdauer von Kugellagern. *Zeitschrift Verein Deutscher Ingenieure,* 68**,** 339-341.

PARANT, E. (2004) Mecanismes d'endommagement et comportements mecaniques d'un composite cimentaire fibre multi-echelles sollicitations severes: fatigue, choc, corrosion. *PhD Thesis.* Ecole Nationale des Ponts et Chaussees.

PARANT, E., ROSSI, P. & BOULAY, C. (2004) Fatigue behaviour of new ultra-high performance cement composite. IN M. DI PRISCO, R. F., G.A. PLIZZARI (Ed.) *6th International RILEM Symposium on Fibre Reinforced Concrete (FRC), BEFIB 2004.* Varenna, Lake Como, Italy, RILEM Publications S.A.R.L.

SAITO, M. & IMAI, S. (1983) Direct Tensile Fatigue of Concrete by the Use of Friction Grips. *ACI Journal,* 80**,** 431-438.

SCHEYDT, J. (2004) Dauerhaftigkeit von ultrahochfestem Beton. *Institut für Massivbau und Baustofftechnologie.* Karlsruhe University.

SINGH, S. P. & KAUSHIK, S. K. (2000) Flexural Fatigue Life Distributions and Failure Probability of Steel Fibrous Concrete. *ACI Material Journal,* 97**,** 658-667.

SINGH, S. P. & KAUSHIK, S. K. (2003) Fatigue strength of steel fibre reinforced concrete in flexure. *Cement and Concrete Composites,* 25**,** 779-786.

ST JOHN, D. A., POOLE, A. B. & SIMS, I. (1998) *Concrete Petrography*, Arnold.

SUBRAMANIAM, V. K., O'NEIL, E. F., POPOVICS, J. S. & SHAH, S. P. (2000) Crack Propagation in Flexural Fatigue of Concrete. *Journal of Engineering Mechanics,* 126**,** 891-898.

SUTHIWARAPIRAK, P. (2003) Fracture mechanics based fatigue life analysis of RC bridge slabs repair by fiber cementitious materials. *PhD Thesis.* The University of Tokyo.

SUTHIWARAPIRAK, P., MATSUMOTO, T. & KANDA, T. (2002) Flexural Fatigue Failure Characteristics of an Engineered Cementitious Composite and Polymer Cement

Mortars. *JSCE Journal of Materials, Concrete Structures and Pavements,* 57**,** 121-134.
SUTHIWARAPIRAK, P., MATSUMOTO, T. & KANDA, T. (2004) Multiple Cracking and Fiber Bridging Characteristics of Engineered Cementitious Composites under Fatigue Flexure. *Journal of Materials in Civil Engineering,* 16**,** 433-443.
TEPFERS, R. (1982) Fatigue of plain Concrete subjected to Stress Reversals. IN SHAH, S. P. (Ed.) *Fatigue of Concrete Structures.* American Concrete Institute.
TEPFERS, R. & KUTTI, T. (1979) Fatigue Strength of plain, ordinary and lightweight Concrete. *ACI Journal,* May 1979**,** 635-652.
VAN LEEUWEN, J. & SIEMES, A. J. M. (1979) Miner's rule with respect to plain concrete. *HERON,* 24**,** 1-34.
ZHANG, J. & STANG, H. (1998) Fatigue Performance in Flexure of Fiber Reinforced Concrete. *ACI Materials Journal,* 95**,** 58-67.
ZHANG, J., STANG, H. & LI, V. C. (1999) Fatigue life prediction of fiber reinforced concrete under flexural load. *International Journal of Fatigue,* 21**,** 1033-1049.
ZHANG, J., STANG, H. & LI, V. C. (2000) Experimental Study on Crack Bridging in FRC under Uniaxial Fatigue Tension. *Journal of Materials in Civil Engineering,* 12**,** 66-73.

6.

Modelling the static bending behaviour

This chapter focuses on the modelling of the static material behaviour in bending. An equilibrium based analytical model is used, and the calculated material behaviour is compared to the experimental results. Suitable tensile input was provided directly from uniaxial tensile test results. For the HSFRC mixture, these tensile tests were performed within this study, while for the other two mixtures results available from other researchers were used. As will be shown in the case of the HSFRC mixture, the model can reproduce the results of three point bending tests on notched beams, four point bending tests on both notched and un-notched beams, and the results can be shown either as the predicted crack openings or the deflection. Predicting the inelastic part of the deflection with the multi-layer model is a point of special attention, especially in case of un-notched beams. It will be shown that this can be done either by rigid body kinematics, in accordance with the relation between the crack opening and the deflection as confirmed by the experimental results, or by appropriate adaptations of the model that hold for a multiple-cracking material. This chapter further shows that the results of the uniaxial tensile tests can be used as input for calculating the flexural response. A short parameter study shows the influence of input parameters on the model predictions. The strain distributions over the beam height will be discussed by comparing the calculated strains to the experimentally measured ones.

6.1 Overview: Aspects of concrete material modelling

Concrete is a complex multi-phase material with numerous parameters influencing its structural response. With the term 'concrete', in this section not only conventional concrete but all kinds of cementitious materials, including high strength/high performance fibre reinforced materials, will be addressed. Different material models exist to describe its material behaviour. The number of parameters that directly influence the concrete behaviour depends on the chosen observation scale, that means whether a macro-, meso- or microscale is used. In the following, a brief

overview of concrete material models will be given, for compression and tension, even though focus will be set on the tensile model, and differences between high strength concrete to normal strength concrete, and fibre reinforced concrete to concrete without fibres will be highlighted wherever appropriate. Reinforced concrete, as in cementitious materials with steel bar (rebar) reinforcement, will not be included, since this is not in the scope of the present study.

6.1.1 Concrete in compression

Models for concrete in compression are representative material relations based on observations of deformation-controlled specimen testing. Concrete is, compared to metals, a brittle material, and can experience sudden and explosive failure under certain loading conditions. In general, the higher the concrete strength, the more brittle the material behaviour will be. The term brittle may need further explanation, since also concrete can, when tested with a suitable testing setup and appropriate specimen size show sufficient deformation ability in a deformation controlled test for a controlled failure. In principle, every material tested in a deformation controlled way can show four distinct stages in its stress-strain relation. The first stage is a continuous increase of the load and deformations, without the development of permanent deformations when the load is removed (linear elastic stage). The second stage is a stage of additional load increase with increasing deformation, with the difference that in this stage, permanent (plastic) deformations have been formed (hardening stage). The third stage is a fast decrease in the load with increasing deformations. This is the first part of the material's softening relation, that is unstable and not easy to control during the test. The final and fourth stage is the second part of the softening relation, where the load drops at a slower rate with increasing deformation, and this part of the test can be performed in a stable, controlled way. Depending on the material, these four phases might differ in their length for certain materials it is possible that certain phases might be missing completely. In concrete, all four stages are visible, even though the deformation ability, described as the area below the last two of the four stages, below the softening part of the stress-strain relation, might be very limited for certain mixture compositions. This is the reason why for design purposes, these last two phases can be omitted from the stress-strain relation.
The addition of fibres can increase the deformation capacity of concrete and can therefore increase the area under the softening part of the stress-strain relation, therefore for such materials, it is more common to define a softening part in material input stress-strain relations used in material models or for structural design. Of course, concrete is not a homogeneous or isotropic material. Therefore, different material input relations for different loading directions can be defined. However, using an anisotropic material relation is not in the scope of this study: here only material input relations in the main loading direction will be discussed.

The simplest relation for the elastic part of the stress-strain relation is a linear elastic material input relation (on a macroscale). Instead of a linear elastic material input, a nonlinear elastic relation could also be implemented. In design codes, often a parabolic relation is used (prEN1992, 2001). After the linear elastic stage, the material can still increase its load bearing capacity in the second, hardening stage, which is however already accompanied by the formation of permanent deformations. This stage can be accounted for in material input by introducing a 'yield plateau', and therefore a linear elastic-ideal plastic material input relation for concrete, to model this observed deviation from linearity close to failure and also parts of the softening relation. If the concrete's deformation capacity is sufficient to allow a post-peak softening part, as can be the case in fibre reinforced concrete, this can be implemented by linear, multi-linear, hyperbolic or other appropriate softening relations. In actual building codes, as for example the Eurocode 2 (prEN1992, 2001), the stress strain relation for concrete in compression (for normal strength, plain concrete) can be modelled in two ways. Both can be used as equivalent idealised material models: a parabolic relation followed by a straight ideal plastic 'yield plateau', and a linear elastic relation followed by a straight 'yield plateau' (Figure 6.1).

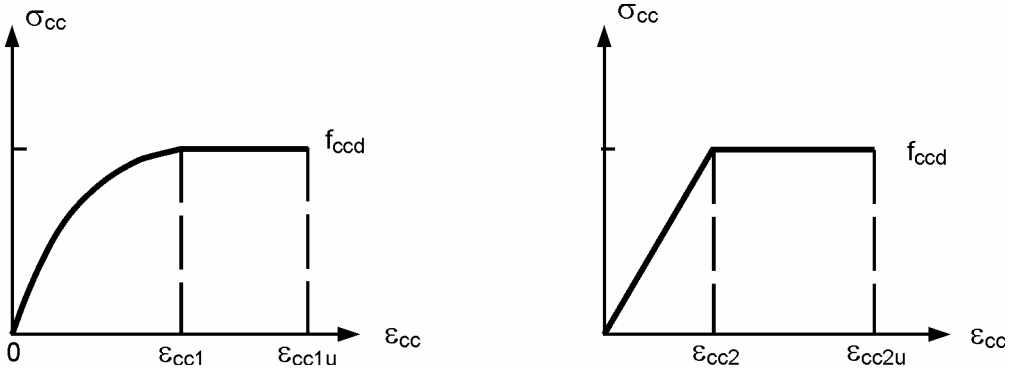

Figure 6.1: Design stress-strain relation for concrete in compression in EC2 (prEN1992, 2001). Left: parabolic model; right: bi-linear model

For certain purposes, especially in research, macroscale models might not be sufficient in order to understand and reproduce concrete compressive behaviour, therefore micromechanical models might be more appropriate. These models do not consider concrete as a continuum, but account for the interaction of the cement matrix and the aggregates (and fibres, if appropriate). These models, however, are not within the scope of the present study.

The higher the concrete strength, the more linear the stress-strain relation is up to the peak load during a deformation-controlled strength test. Therefore, a linear stress-strain relation up to the peak load makes sense in case of ultra high strength concrete. In case of no fibre reinforcement, it might be more appropriate to omit any softening relations due to the brittleness of this material. In case a fibre reinforcement is applied, a softening relation or 'yield plateau' would be more

appropriate. In the few codes and design guidelines that exist so far, the German tentative guideline for UHPC (DAfSTB, 2005) includes a transition from high strength concrete to ultra high strength concrete with a parabolic stress-strain relation, that becomes a linear relation for concrete strength classes beyond 180 MPa. After the peak load, a 'yield plateau' is included to provide some deformation capacity in the post-peak part, and the length of this plateau is defined by the ultimate compressive strain limit, see Figure 6.5. The French interim regulations (AFGC-SETRA, 2002) consider a linear elastic compressive relation up to a peak load with no further softening or yield plateau for the serviceability linear state, and a linear relation including a 'yield plateau' for the ultimate limit state (Figure 6.6).

6.1.2 Concrete in tension

The tensile load bearing capacity and its modelling play an important role in this study, as (flexural) tensile, and not compressive, failure was always the principal failure mode of all test specimens. In recent years, developments in fracture mechanics and material technology stimulated the generation of more advanced and accurate models, especially for concrete subjected to tension. Also, advances in fracture mechanics and the adaptation of existing fracture mechanics models for metals to concrete provided a better understanding of cracking and stress transfer in cracks and resulted into suitable models. As is the case in compression, also in tension models for the macro-, meso- and microscale exist.

Macroscale concrete tensile models usually consist of an elastic and an inelastic part; for conventional normal strength concrete, the inelastic part is an appropriate postpeak softening relation. The postpeak ductility and deformation capacity depend on the matrix composition, the bond between the aggregates, and, in case of fibre reinforced materials, on the fibre amount, geometry and bond between the fibres and the matrix. On the macro and mesoscale, two different approaches exist for modelling the postpeak response: it can be expressed in terms of a stress-strain relation, an approach often followed in design regulations, or in terms of a stress-crack width relation, an approach that gradually enters design regulations and is quite common in concrete material modelling for research purposes.

The pre-peak concrete tensile response is usually represented as a linear stress-strain relation, and in the following, models for the post-peak softening part will be discussed. Strain hardening materials, that allow an additional load increase after the end of the linear elastic phase has been reached, are rather new (in concrete) and their description differs from normal concrete. Suitable material input for such kind of materials will be discussed later, after the softening models have been discussed. Also hardening materials experience a softening stage after the peak load has been reached. Therefore, the same softening models and approaches can be used for both strain hardening and strain softening materials in the postpeak region.

Softening relations for concrete and cementitious materials without fibres

As already mentioned, the softening part of the tensile relation can be expressed by either a stress-strain relation, or in terms of a stress-crack width relation. For concrete, Hilleborg et al. (1976) in their Fictitious Crack Model (FCM) split the stress-crack opening displacement as measured in a uniaxial tensile test into a linear stress-strain relation up to the peak load (and for the un-loading part of the concrete outside the major crack) and a stress-crack width relation for the softening behaviour in the cracked section, Figure 6.2. In his model, stresses can still be transferred across the crack in the cohesive zone from the fictitious crack tip, that is not visible, up to a certain critical crack width w_0, Figure 6.3. Further to the stress-crack width model of Hilleborg, the crack band model for plain concrete, was developed by Bažant and Oh (1983). In their model, a zone with very fine distributed cracks lies ahead of the crack tip, that is the fracture process zone, Figure 6.4. The width of that zone is used in order to translate deformations into a stress-strain relation for this zone rather than stress-crack width relations that refer to an infinitely small width (the crack). This model is better suitable for implementation into finite element codes, where it is usually called the smeared crack approach. On the basis of a defined fracture process zone, a stress-crack width relation can always be converted into a stress-strain relation, when a 'characteristic length' or 'influence length' is introduced, that can translate the crack width into a strain. Finding a suitable length, that gives reliable results for calculations with numerical finite element models and analytical models, is an important condition in order to obtain consistent material modelling.

Regardless whether a stress-crack width or a stress-strain approach is followed, in both approaches similar shapes can be used to describe the postpeak softening relation. For concrete and similar cementitious materials, Hordijk (1991) derived a function that was in accordance with experimental results, which has by now been implemented into a number of finite element codes. Other possibilities for fitting functions would be a power law function, or even simpler relations such as linear, bi-linear and multilinear softening relations.

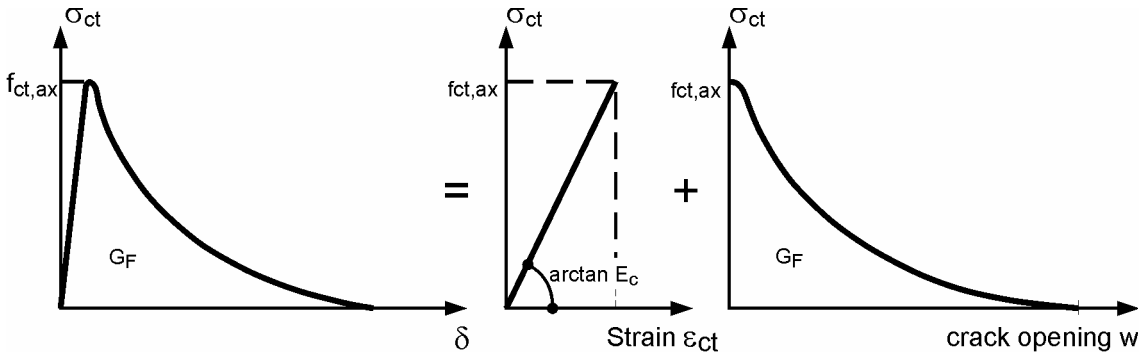

Figure 6.2: Fictitious crack model; measured σ-δ relation separated into a σ-ε and a σ-w relation after Hilleborg et al. (1976).

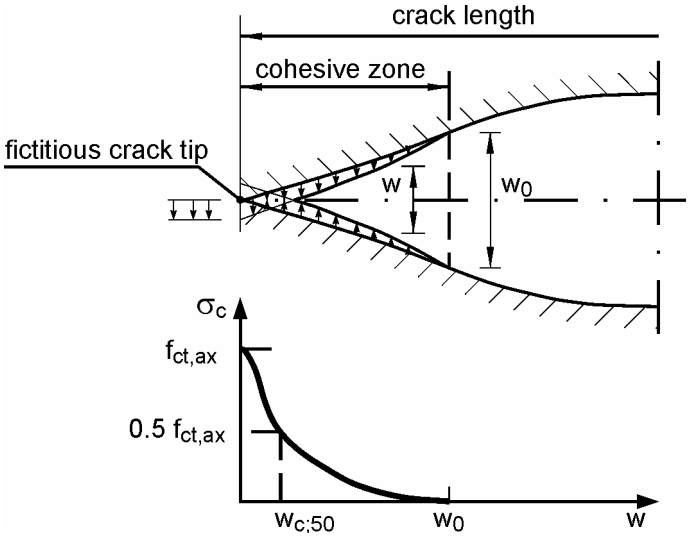

Figure 6.3: Fictitious crack model for concrete after Hilleborg et al. (1976) with fictitious crack tip definition.

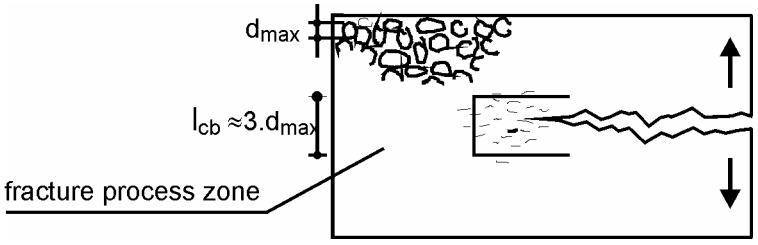

Figure 6.4: Definition of the crack band and the fracture process zone after Bažant and Oh (1983).

Softening relations for (steel) fibre reinforced cementitious composites

The simplest way to include the fibre action into a tensile input relation on a macroscale, is by adjusting the stress-strain or stress-crack width relation to account for the effects of the fibres on the structural response. Depending on the fibre type, geometry, strength and the matrix properties, fibres can either be activated in the prepeak part, bridge microcracks and therefore increase the peak strength, or increase the ductility and deformation capacity by allowing higher stresses in the postpeak range and thus increase the area beneath the stress-crack width or stress-strain relation. The first fibre benefit, the increase of the peak load, is mainly in case of short steel fibres, while the increased ductility in the postpeak range mainly occurs in case longer steel fibres are used. Regarding ultra high strength concrete, such a design approach, with a linear stress-crack width relation for the postpeak stage (Figure 6.5), is proposed for design in the ultimate limit state in the tentative German design rules for ultra high strength concrete (DAfSTB, 2005).

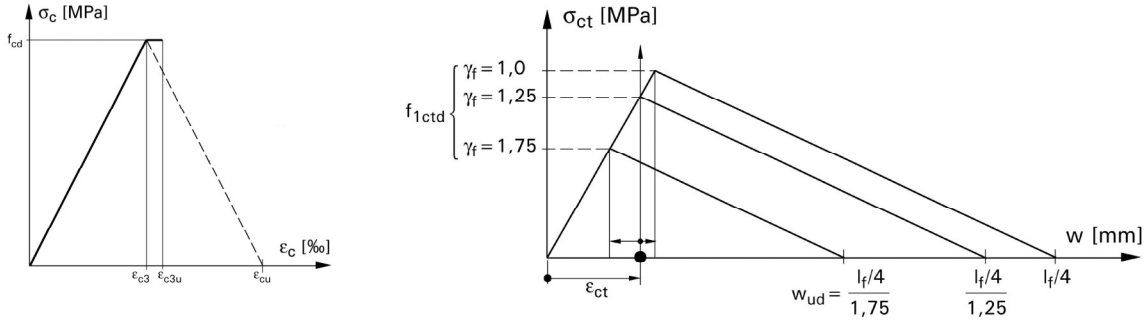

Figure 6.5: Input in compression (left) and tension (right) for design in the ultimate limit state (DAfSTB, 2005).

In the models quoted previously, fibre reinforced concrete is regarded as a homogeneous material on a macroscale, which is of course a simplification of the real material behaviour, although such an approach is often sufficient to describe a structural material response. In case more precise modelling is needed, different relations for different loading directions can be applied in case of inhomogeneities (such as a preferred fibre orientation). Also, meso- and microscale models can be applied. For fibre reinforced concrete (without strain hardening), Li et al. (1993) developed a model based on Hilleborg's fictitious crack model, but with the stress-crack width relation divided into terms that account for aggregate bridging in plain concrete, and fibre bridging based on the pull-out behaviour of a single fibre, with the overall response being a superposition of the two.

Multiple cracking, strain hardening materials and their material input

The phenomenon of multiple cracking and strain hardening has already been discussed in Chapter 4, at least from a phenomenological point of view. The main difference of such materials to pure strain softening materials is the strain hardening phase up to the peak load, before deformations eventually localise into a single crack at the postpeak part.

The simplest way to implement the hardening phenomenon on a macro scale, is by introducing a simplified linear strain hardening phase beyond the linear elastic phase, in terms of a stress-strain hardening relation. In case a stress-crack width and not a stress-strain relation is used, it is more common to speak of crack widths only in the softening part of the relation, meaning that the hardening phase is included as a non-elastic part in the stress-strain relation. Even though the specimen is cracked in the hardening phase, these (multiple) cracks are barely visible and barely measurable, which makes them unsuitable for the definition of a stress-crack width relation. Such an approach was also followed in this study, which seems reasonable since the cracks during the hardening phase were barely visible. In case larger crack widths are observed in the multiple cracking phase, it may be wiser to define a linear elastic stress-strain relation, followed by a multi-linear stress-crack width relation, in which the first part is a hardening relation with increasing stress

and the second part is a softening relation after the peak. Such an approach was adapted by Yang and Fischer (2005) for ECC materials.

A macroscale approach, usually in terms of a global stress-strain relation, with first a strain hardening part followed by a softening relation, is up to now followed in the few available design regulations, such as the interim French regulations (AFGC-SETRA, 2002). The schematic material input relation for design of strain hardening ultra high strength fibre reinforced concretes, with a linear part and a 'yield plateau' in compression, and a bilinear softening relation after strain hardening, is schematically shown in Figure 6.6. For the serviceability limit state, the relation can be simplified into an ideal linear elastic part in compression, and with a linear, instead of a bi-linear, softening part in tension. The Japanese tentative guideline for the design with ECC (JSCE, 2005) has an ideal elastic part (yield plateau) after the linear elastic part, and no softening relation, for design in the ultimate limit state.

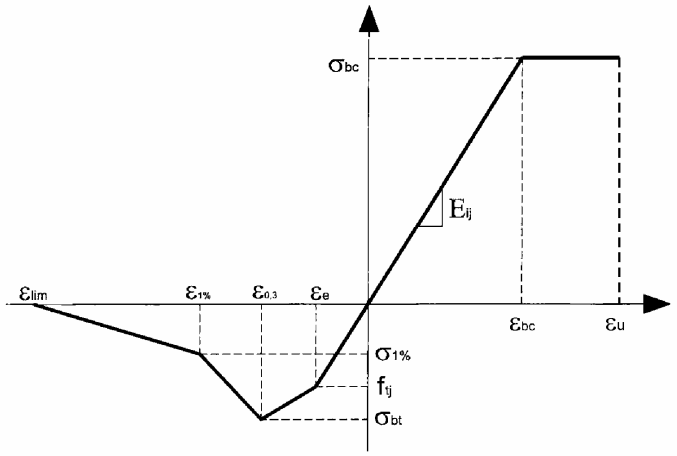

Figure 6.6: Material input relation for design with ultra high strength fibre reinforced concretes in the ultimate limit state (AFGC-SETRA, 2002).

On a micromechanical basis, microscale models have been developed that describe stress concentrations as derived from initial matrix flaws, and debonding, bridging and pull-out of a single fibre. Further, on a meso scale the propagation of a single crack bridged by many randomly oriented fibres can be described, as well as the multiple cracking process, as an interaction of initial flaws and microcracks together with opening, closing and sliding of cracks, all this in a representative small part of the material, a representative volume element. All this knowledge can improve the final material model on the macroscale that functions as a material model for the complete structural response. For ECC, such a multiscale approach, with representative relations from the micro- up to the macroscale, have recently been proposed by Kabele (2007) and Dick-Nielsen (2006). Also, an analytical model for ECC, that shows the multiple cracking development by a set of linearly aligned springs, has been developed by Yang and Fischer (2006).

Concluding, it can be seen said that for both compression and tension, simple and more advanced material models exist for the behaviour of concrete and similar cementitious composites. The simpler models regard concrete as a homogeneous material on a macroscale, the more advanced ones regard properties on a meso- or even microscale. Strain hardening cementitious materials need an appropriate modification of the tensile material input relation on the chosen observation scale. However, the outcome of all models and the reliability of these results always depend on the input parameters. The output can only be reliable as long as the input parameters can be determined with accuracy. For some of the advanced material models, the input parameters can only be determined by extensive experimental testing, which might be hindering for large scale structural applications.

6.1.3 Modelling the flexural response of un-reinforced beams

In order to model the experimentally observed bending behaviour of concrete beams, finite-element modelling as well as analytical equilibrium based approaches can be applied. Often only bending tests have been performed with a (fibre) reinforced cementitious composite, and only splitting tensile tests and compressive cube or cylinder tests for input parameters of the matrix; while the compressive cube or cylinder test might give a suitable approximation of the material compressive input relation, this is not the case in the splitting tensile test, which can only indicate the peak tensile load. Therefore, an inverse analysis is often used, in order to derive a suitable complete tensile material input relation, representative for the material behaviour as observed in a bending test.

The inverse analysis is a modelling procedure, first defined by Roelfstra and Wittmann (1986). It consists of three levels. The first, input level, assumes a certain stress-strain or stress-crack width relation of the material that is used as a first approximation. The second, numerical level, computes the flexural response of a beam in accordance with its geometry, boundary conditions and material. The third level consists of an accuracy check; the deviation between the calculated and experimental results is obtained, and if this deviation is above certain tolerances then the analysis is repeated with a modified tensile input relation. In this way, the procedure is repeated until an acceptable tolerance is obtained, and this provides the characteristic tensile material input relation for the cementitious composite. The second, numerical level of the inverse analysis can be performed with finite element models, but also analytical equilibrium based models, like the multi layer model of Hordijk (1991) or the model of Østergaard (2003), can be used.

In this study, not only bending tests, but also tensile tests have been performed or exist from other researchers (Jungwirth, 2006, Markovic, 2006) for the materials used. Therefore, no inverse analysis was performed, but a more straightforward approach was followed. The applicability of the experimentally obtained uniaxial tensile relation was controlled by using it as an input relation and calculating the flexural response of a beam of dimensions equivalent to the tested specimens. The

analytical model of Hordijk (1991) was used, because it is simple but at the same time reliable, can be easily implemented, and the effects of each input parameter directly evaluated.

In the following, in Section 6.2, the principles of the multi-layer model will be explained, while Sections 6.3, 6.4 and 6.5 will show the input parameters for the HSFRC, the BSI/CERACEM and hybrid HSFRC respectively, focussing mainly on the tensile material input. In Section 6.6, a short parameter study will be performed for the HSFRC mixture only in order to evaluate and highlight the influence of different material and model input parameters on the structural response; and in Section 6.7 the modelled and measured strain distributions in the tensile and compressive zone of the beam will be compared in case of notched beams of a four point bending test. Finally, in Section 6.8, an alternative will be shown for modelling the deflection of a multiple-cracking material, which is not based on rigid body kinematics but with a modified tensile material input.

6.2 Multi-layer model for the flexural response of beams

The analytical model used for the reproduction of the experimental results of the bending tests is an equilibrium based multi-layer beam model as developed by Hordijk (1991). Kooiman (2000) has already shown that the model is appropriate for modelling the flexural response of fibre-reinforced concrete beams and, therefore, not only plain concrete, and Grünewald (2004) further used it for self-compacting fibre reinforced concrete. As will be shown here, with appropriate modifications the model is also suitable for the materials used in this research, high strength concrete with strain hardening in tension, for three and four point bending tests on notched and un-notched specimens.

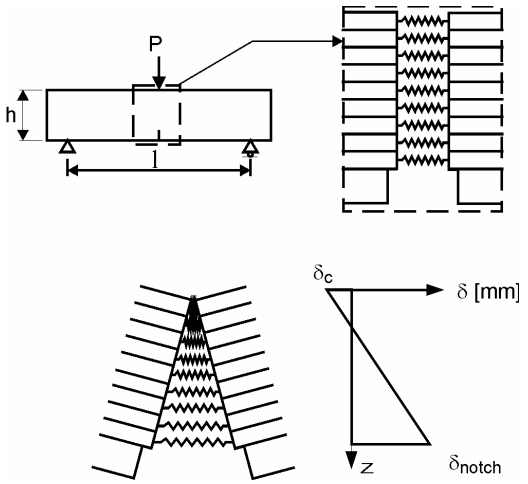

Figure 6.7: First principle of the multi-layer-model (Hordijk, 1991): division of the beam in two halves, connected with springs.

The model is based on three basic principles:

First, it is assumed that the beam is divided into two halves which are connected by springs, Figure 6.7. In case the beam has a notch, the springs are only present above the notch at the effective beam height. Each spring represents the behaviour of a small layer of a beam, and a linear strain distribution is assumed over the effective beam height.

Second, the strain in each spring corresponds to the average deformation in each layer (at mid-height of each layer). From this strain distribution the corresponding stresses in each layer (spring) are calculated with stress-displacement relations defined as input parameters of the model (Figure 6.8). From these stresses, normal forces and bending moments are determined for each layer, and by summation of all layers internal normal forces and bending moments for the complete beam cross section are determined. Since the model is applied to pure bending without external normal force, the total normal force derived from the summation of all layers has to be zero. This is the equilibrium condition the model is based on. The total inner bending moment, that results after the equilibrium condition is met, has therefore to be equal to the external bending moment resulting from the applied load to the beam. From the bending moment the applied load can be determined by equilibrium conditions on a simply supported beam, P = 4*M/L in case of three point bending tests (the load equals four times the moment divided by the span length).

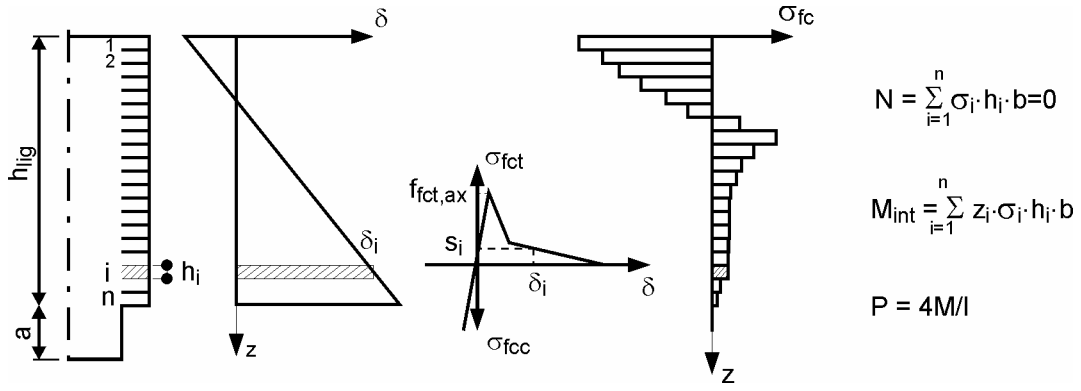

Figure 6.8: Second principle of the multi-layer model: Constitutive material input relation for each layer and force equilibrium conditions in order to define the strain distribution in the beam.

Third, an incremental procedure is applied in order to model the applied load-displacement relation as performed in a bending test. Therefore, the (tensile) strain at the bottom layer of the beam (or at notch tip in case of a notched beam) is increased in small steps. After each step, the corresponding maximum compressive strain at the top layer is determined in an iterative procedure under the condition that the total inner normal force is zero. The strain in the intermediate layers is distributed linearly between the two maximum tensile and compressive strain values

at the outer layers. By combining the resulting applied load and corresponding displacement at each step, the total load-displacement relation is determined and the results of the numerical simulation can be compared to the experimental results.

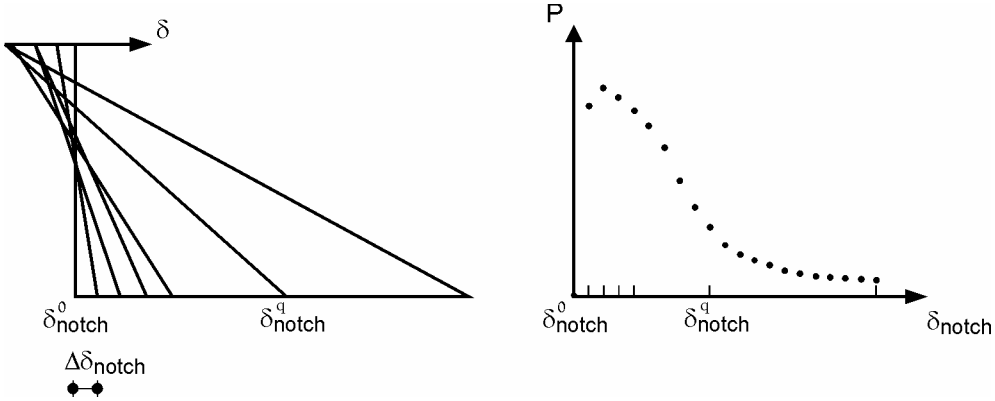

Figure 6.9: Third principle of the multi-layer model: incrementally increasing the strains at the bottom fibre and by force equilibrium the total beam response of the flexural test is followed.

The model is applicable for simply supported beams since the assumption of a linear tensile and compressive stress distribution is valid at midspan, as long as a sufficient distance from its supports is provided.

6.3 Modelling the HSFRC beams

The HSFRC mixture was considered the main mixture of the study; therefore, the modelling of beams of this mixture will be studied in more detail than the other two mixtures. Moreover, this is the only mixture where not only four point bending tests on un-notched beams were performed, but also three and four point bending tests on notched beams. This fact enables an evaluation of the model and its input parameters on more than one structural element, and tests the suitability of the tensile input, as obtained by the uniaxial tensile tests, for all cases. The principles of the model have already been discussed in section 6.2; in the following, the input parameters will be specified, especially the compressive and tensile stress-strain and stress-crack width relations.

6.3.1 Three point bending tests on notched beams

The model was first tested on the three point bending tests on notched beams (of dimension 150/150/600 mm, with a 25 mm deep notch, span length 500 mm), since it could be directly compared to results of Kooiman (2000) and Grünewald (2004), who used the same model in their study on beams of fibre reinforced concrete and self-compacting fibre reinforced concrete, respectively. Both researchers had mainly

normal strength mixtures and not high strength mixtures, with different fibre contents of mainly longer hooked-end fibres, with a length of at least 30 mm. Therefore, not all input parameters of their mixtures were applicable for the HSFRC, which is of a different strength class but has also a different fibre reinforcement of straight short steel fibres. These short fibres have a different effect on the structural response, by mainly increasing the peak tensile load rather than increasing the ductility in the postpeak part.

Two general input parameters are the number of layers and the influence length l_i, which allows a transformation of the stress-crack width relation into an equivalent stress-strain relation. In accordance with Kooiman's and Grünewald's simulations, the total number of layers was chosen to be n=500, meaning that each layer had a thickness of 0.25 mm covering the total ligament height above the notch of 125 mm. The influence length, an important parameter of the model, was introduced by Hordijk (1991) to represent the length of the fracture zone, the part of the beam replaced by springs. In a way, this is comparable to the width of the crack band in the model of Bažant and Oh (1983). A suitable value for this length was found to be $0.5h_{lig}$=62.5mm in case of the three point bending tests (Kooiman, 2000). The influence of this parameter and results of simulations with other values than one half of the ligament height will be further discussed in section 6.6.

Input parameters for compression

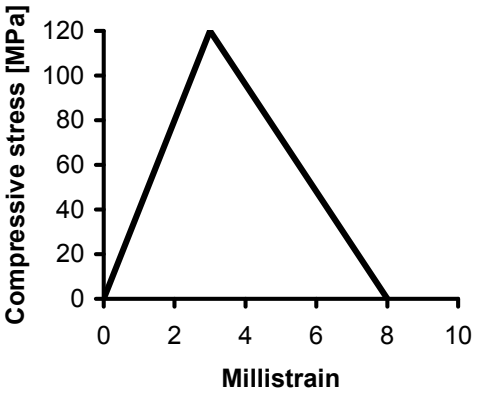

Figure 6.10: Compressive stress-strain relation for the HSFRC mixture

A simplified bi-linear stress-strain relation was defined for the compressive behaviour: the compressive stress increases linearly up to a compressive strength of 120 MPa up to a limit of 3‰, resulting into a Young's modulus of 40 GPa. The chosen strength value corresponds to the average compressive strength tested on concrete cubes, and the inclination of the compressive stress-strain relation was also verified by compressive tests on prisms. A linear descending branch was assumed up to an ultimate compressive strain of 8‰. Kooiman and Grünewald had used an ultimate compressive strain of 10‰ in their calculation, but for the HSFRC mixture

8‰ is more appropriate due to the reduced deformation ability given by the higher strength and shorter fibres of this mixture. The input stress-strain relation is shown in Figure 6.10.

Input parameters in tension

The tensile input parameters were based on the response as obtained from the performed uniaxial tensile tests. Initially, only the results from the first series of tests, with a measuring length of 110 mm, were available (Chapter 4). As a first approach, the curve obtained from the uniaxial tensile tests obtained from un-notched dogbone specimens were used as input, as shown on the left part of Figure 4.24. The response was simplified into a suitable stress-strain relation, for which three stages were implemented: a linear elastic part up to the linear elastic tensile strength and strain, with an identical stiffness as already defined in compression; a linear hardening branch that enables further stress increase up to a certain strain limit and corresponds to the multiple cracking phase of the material, and finally a stress-strain relation approximated by a linear relation from the peak stress value down to zero at an ultimate strain value. This last part, the linear softening stress-strain relation, is equivalent to a stress crack width relation. Strains can be obtained by dividing the crack widths with the influence length, which is set to half of the beam height above the notch, l_i=62.5 mm. Here, only a linear softening branch was implemented, and not a bi-linear one as Kooiman and Grünewald used in their simulations; for high strength concrete with short straight fibres, a linear descending branch can be sufficient in order to model the flexural response, since the short fibres contribute more in the prepeak part of the tensile strength rather than increasing the deformation capacity in the postpeak part. Linear softening relations were also found to be suitable for ultra high strength concretes without coarse aggregates (Xiao et al., 2004). From the modelled strain distribution with the multi-layer model, the tensile strains were converted into crack openings by multiplication with the influence length, and then the load (or flexural tensile stress) crack opening relation of the model could be compared to the experimental results of the bending tests.

Figure 6.11 shows the simplified tensile input in terms of a stress-strain relation (left), and the results of the multi-layer model (MLM) compared to the average experimental curve of the notched three point bending tests (right). As can be seen, even though in the prepeak part agreement was found between the model and the experiment, a much steeper descending branch was predicted with the model than found in the bending tests. One possible explanation for this discrepancy could lie in different fibre orientations and distributions between the bending tests and the uniaxial tensile tests; also, the fact that a bending test allows more stress redistributions and is more stable to perform than a uniaxial tensile tests could play a role. However, these assumptions cannot explain the significant difference as observed between the modelled and experimentally found descending branch alone.

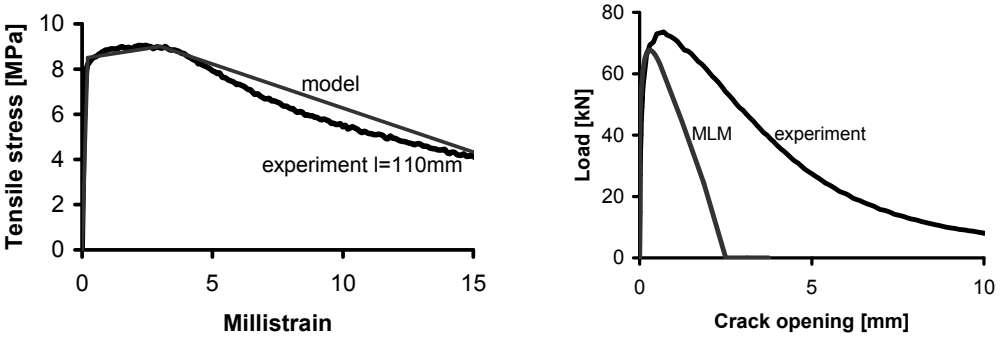

Figure 6.11: Tensile input in accordance with the tensile test and a measuring length of 110 mm (left); outcome of the response for the three point bending test (right).

The most plausible explanation between the differences in the modelled and experimentally obtained descending branch of the bending tests was assumed to be the chosen measuring length of 110 mm. Up to the peak load, during the linear elastic and the strain hardening phase, multiple cracks are distributed uniformly throughout the specimen and the choice of a measuring length does not affect the resulting stress-strain curve significantly, since all parts of the specimen experience similar stresses and strains. However, after the peak, the deformations localise into a single crack. Therefore, only a small part of the specimen is experiencing an elongation while other parts of the specimen, outside the crack, are actually unloading and closing the cracks that had previously formed. This implies that at postpeak, the registered deformation over a 110 mm measuring length was assumed to be mainly the opening of the major crack, which would justify the use of a smaller measuring length for better representation of the crack opening in terms of strain. With a smaller measuring length, the registered deformations would correspond to larger strains and would therefore result in a more ductile descending branch, which could provide a better input relation for the bending tests. A second test series of three notched and three un-notched dogbone specimens with measuring lengths of 35 mm and 110 mm (at each side of the specimen) was performed to verify this assumption. The results of this additional series were discussed in Chapter 4, and as can be seen in Figures 4.32 and 4.33, the above assumptions could be verified since deformations did localise after the peak load. While LVDTs with both measuring lengths measured similar deformations, the corresponding stress-strain relations, especially in the postpeak part, differ significantly for both measuring lengths.

Therefore, after the additional tensile test series was performed, the response of the un-notched specimens as a stress-strain response with a 35 mm measuring length were used for the tensile material input relation. For the descending branch, again a linear descending branch was chosen, with three variations: up to limit crack widths of $w_c=l_f/4$, $w_c=l_f/3$ and $w_c=l_f/2$. After a crack width of one half of the fibre length, it is assumed that no further stresses can be transmitted across the cracks,

since the fibres would have been completely pulled out of the matrix. In reality, most of the fibres will have been pulled out already at smaller crack widths, which makes a limit crack width of one third or one fourth of the fibre length more realistic. Figure 6.12 shows the modified tensile input after the additional tensile test series with a measuring length of 35 mm. On the left, the response is shown in terms of a stress crack width relation, an all three variations of the softening branch are shown. As can be seen, while for a critical crack width of $l_f/4$, the experimental results and simplified curve are in good agreement, at least in terms of the area below the stress-crack width response (fracture energy), for larger critical crack widths the ductility of the postpeak response is overestimated, and a bilinear, rather than a linear input, would be more suitable if these larger crack widths are chosen for the material input. On the right in the figure, the complete input is shown in terms of an overall stress-strain relation, and the simplified input curves, with their three variations of the descending branch, are shown and compared to the test results with respect to measuring lengths of 110 mm and 35 mm.

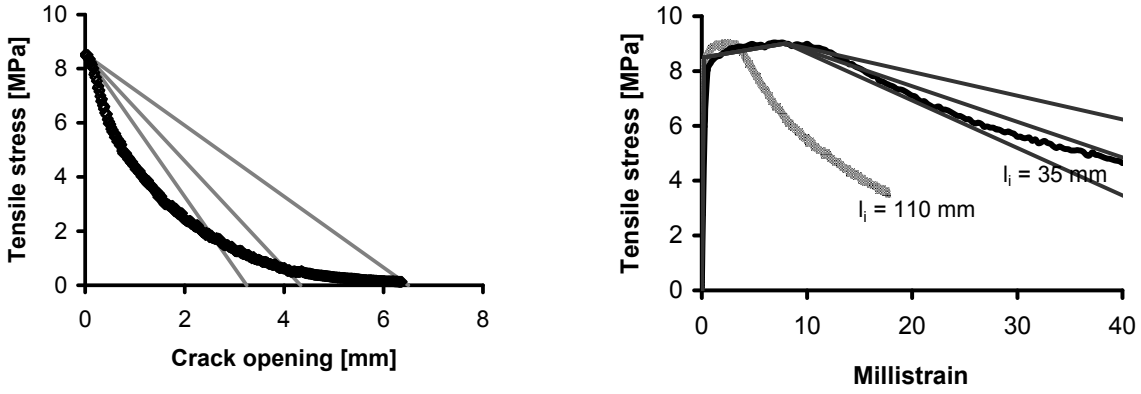

Figure 6.12: Modified tensile input. Left: stress-crack width relation, simplified linear relations to crack widths of $l_f/4$, $l_f/3$ and $l_f/2$. Right: Tensile response with 110 mm and 35 m measuring length and simplified input corresponding to the 35 mm measuring length.

The results of the simulations can be seen in Figure 6.13. As can be seen, a much better agreement is found between the simulated and experimental results when the tensile input corresponding to a 35 mm measuring length is used. For the three point bending tests, the linear softening up to a crack width of $l_f/3$ gives the best approximation of the experimental results, but also a crack width of $l_f/4$ is in good agreement within the range of the scatter of the individual beam results. The average peak load is approximated very well with the chosen input parameters.

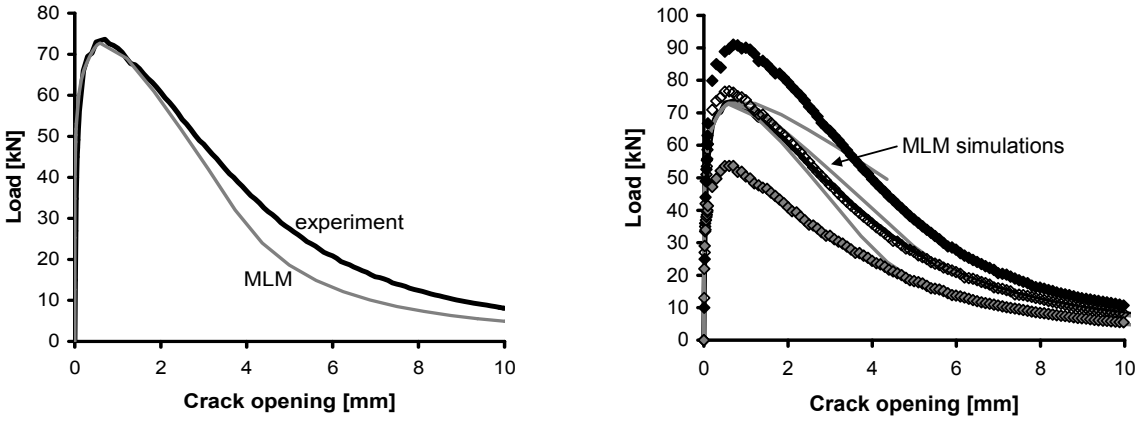

Figure 6.13: Simulated beam response with the multi-layer model (MLM). Left: Average experimental curves and simulation up to a crack width of $l_f/4$. Right: Individual exp. curves of the testing series and simulations for crack widths $l_f/4$, $l_f/3$ and $l_f/2$.

6.3.2 Four point bending tests on notched beams

Crack openings

The model, as first used for the three point bending tests, predicts the crack openings of the beams at a bending tests quite well; therefore, the following step was to use the same model for the four point bending tests on notched beams with respect to crack openings. The beams were of dimension 125/125/1000 mm, with a 20 mm deep notch at midspan, and were tested at a span length of 750 mm, loaded at their third points. Regarding the input parameters, the same input as described for the three point bending test was used: 500 layers were chosen over the ligament height above the notch of 105 mm, so that the height of each layer was 0.21 mm. The influence length was set to one half of the ligament height; as in the case of the three point bending tests, in the case of the notched four point bending tests this results to $l_i=0.5h_{lig}=52.5$ mm. The force equilibrium condition, that was used in order to derive the applied load as derived from the obtained internal bending moments that was found to fit an assumed linear strain distribution and corresponds to a zero internal normal force, had to be adjusted to fit the equilibrium conditions of a simply supported beam under four point bending, P=6*M/l (was P=4*M/l in case of three point bending). All other input parameters were set to the same values as described for the three point bending tests, with the compressive relation as given in Figure 6.10, a tensile stress-strain relation with a strain hardening part corresponding to the results of the un-notched uniaxial tensile tests as measured with a measuring length of 35 mm and a linear stress-crack width opening relation (descending branch) up to ultimate crack widths of $w_c=l_f/4=3.25$ mm. $w_c=l_f/3=4.33$ mm and $w_c=l_f/2=6.5$ mm (Figure 6.12).

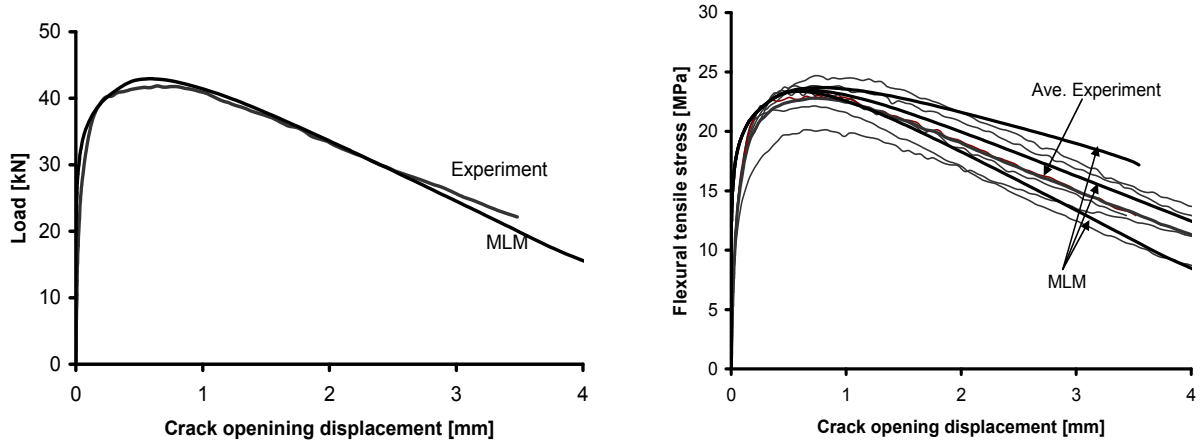

Figure 6.14: Modelled response of the notched four point bending tests with regard to the crack opening displacement. Left: average experimental curve and MLM simulation with $w_c=l_f/4$; right: Individual beam responses and average curves, and MLM simulations for $w_c=l_f/4$, $w_c=l_f/3$ and $w_c=l_f/2$.

Figure 6.14 shows the results of the simulated crack openings of the notched four point bending tests compared to the average experimental curve (on the left) and to the individual beam test results (right). The simulation with a critical crack width of one fourth of the fibre length fits the average curve of the experiments the best (Figure 6.14, left) while also a critical crack width of one third of the fibre length is within reasonable scatter in accordance with the performed beam tests. A critical crack width of one half of the fibre length overestimates the crack bridging ability in the descending branch; but for such a crack width, as can be seen in the left part of Figure 6.12, the fracture energy is overestimated with a linear descending branch and a bi-linear or other relation seems more appropriate for simulations up to that crack width. Nevertheless, the simulations show, that also for the four point bending tests on notched beams, the tensile input, as obtained from uniaxial tensile tests with a 35 mm measuring length, is suitable for modelling the bending tests. A linear descending branch was found to be appropriate, and critical crack widths of one fourth or one third of the fibre length seem appropriate for the HSFRC mixture. In the following, the adaptation of the model in order to reproduce the deflections of the bending tests will be discussed, and from now on an ultimate crack opening of one fourth of the fibre length will be used in the tensile input relation.

It should be noted that it was chosen to use critical crack widths as one of the tensile input parameters; this crack widths are then transferred into strains by division with the influence length, which is defined in relation with the ligament height of the beam. The four point bending tests on un-notched beams and the three point bending tests have a ligament height of 125 mm, the four point bending tests on notched beams of 105 mm; therefore, the input stress-strain relation is different in the postpeak descending branch for the four point bending tests on

notched beams. However, with the chosen beam and notch dimensions, the differences in the stress-strain relation are not so pronounced. In both cases, good agreement for the stress-strain curve from the uniaxial tensile tests with a 35 mm measuring length, and the simplified input stress-strain relation with a linear descending branch up to a limit crack width of $l_f/4$, is found.

Table 6.1: Input parameters of the notched bending tests on HSFRC

General model parameters	
Number of layers	500
Influence length, 0.5*hlig [mm]	52.5
Compression	
Bi-linear compressive relation	
Compressive strength [MPa]	120
Linear elastic strain limit [promille]	3
E-Modulus [GPa]	40
Ultimate limit strain [promille]	8
Tension	
Strain hardening and linear descending branch	
Linear elastic tensile strength [MPa]	8.5
Linear elastic tensile strain [promille]	0.2
Hardening strength [MPa]	9
Hardening strain [promille]	8
Ultimate crack width [mm] = L_f /4	3.25

The input parameters, as described here, with a limit crack width of 3.25 mm, being one fourth of the fibre length, are the main input parameters that will be used as a basis for modelling the response of the deflections of notched and un-notched bending tests with this mixture, and as the basic input for the parameter study dealt with in section 6.6. An overview of the main input parameters is given in Table 6.1.

Deflections

The model predicts the strain distribution along the beam under the condition of a zero normal force, and from the tensile strain during each iteration the crack opening can be determined by multiplication with the influence length l_i. It was also desirable to predict the deflections with the chosen model, and this will be discussed in the following, here for the case of the four point bending tests on notched beams. That deflections can be modelled with the multi-layer model was already shown by Hordijk (1991) in case of normal strength un-reinforced concrete; he computed the deflections as derived from an elastic part, that is derived from the resulting applied load obtained from force equilibrium on a simply supported beam from the resulting inner moment during each step of the iterative modelling procedure, and an inelastic part, that was computed from kinematic conditions on the beam. A similar approach is followed in this study; the main issue is to find an appropriate kinematic condition

for the inelastic deformations. In the following, all model input parameters are as listed in Table 6.1.

The elastic deflections can be determined related to the applied total load F, the span length l, the elastic modulus E and the second moment of inertia I, with the following equation, which is valid for the deflection at midspan for a simply supported beam under four point bending:

$$\delta_{el} = \frac{23}{1296} \cdot \frac{Fl^3}{EI} \tag{6.1}$$

When the second moment of inertia is expressed by the beam width b and its height h ($I=bh^3/12$), the equation (6.1) becomes:

$$\delta_{el} = \frac{23}{108} \cdot \frac{Fl^3}{Ebh^3} \tag{6.2}$$

In order to model the deflections, and especially the inelastic deflections, an appropriate kinematical relation was sought in order to model the deflections from the crack openings. As has been shown by the work of the RILEM task group on fibre reinforced concrete (Barr and Lee, 2003), the crack openings *w* and the deflections δ are related to the beam span L and the depth around which the beam rotates H (by rigid body kinematics, through the following equation:

$$\frac{\delta}{w} = \frac{L}{4} \cdot \frac{1}{H} \tag{6.3}$$

This equations holds for small rotation angles ϕ, where $\tan\phi = \sin\phi = \phi$. The definitions of the rotation angle ϕ and the rotation depth H can be seen in Figure 6.15, in the case of three point bending, and are valid also for four point bending. The critical parameter in this equation is the rotation depth H which is not a constant value. In order to get an estimation of appropriate values of H during the bending tests, the ratio between the deflection and crack opening measured at the crack mouth at the bottom fibre of the beam during a test were plotted against the deflection evolution, Figure 6.16. The rotation H is increasing during a bending test; this can be seen by the decrease of the δ/w ratio with increasing deflection, and from equation (6.3) it is clear that this ratio is inversely proportional to H. There is a physical explanation for this: the beam starts to rotate as soon as it is cracked, and the larger the crack length, the more the beam can rotate, therefore the larger the value of H. For large crack widths and openings, close to failure, it is assumed that the crack has evolved almost through the complete beam, thus H equals the full beam height. For notched beams, the beam height of 125 mm (plus 5 mm distance between the beam end and the fixation of the LVDT measuring the crack mouth opening) and the span of 750 mm applies for the right part of equation (6.3), the ratio of δ/w equals 1.4; this value is indicated by the straight line drawn into Figure 6.16. As can be seen, this is the value the curves tend to approach at larger deflections in the postpeak region. The continuous decrease of the curves towards

that value indicates the gradual increase of the crack length and therefore also the height H, by a gradual widening of the crack already initiated by the notch.

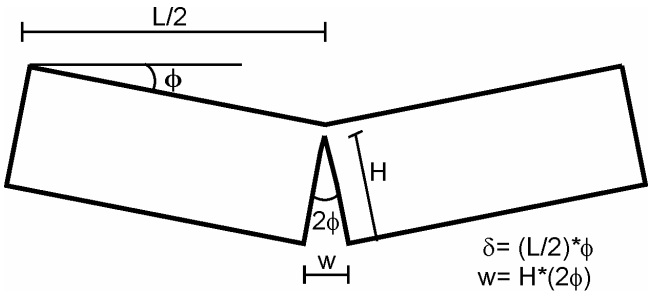

Figure 6.15: Definition of the rotation depth H.

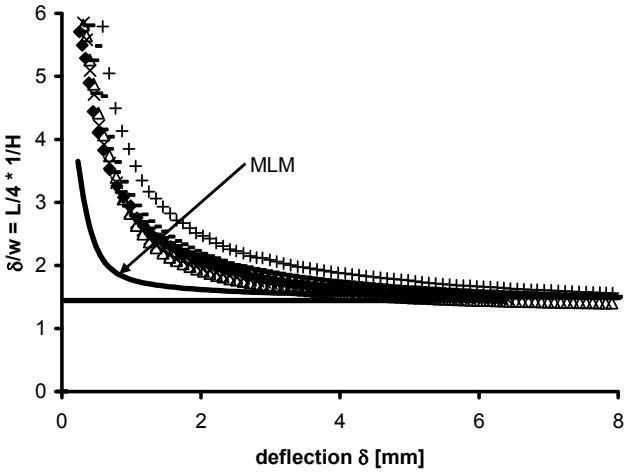

Figure 6.16:Ratio between the deflection and the crack width for different deflection values during four point bending tests on notched beams. The results of the tested beams, shown with markers, are compared with the results of the multi layer model.

The results of the multi-layer simulations, with the deflections modelled from the linear elastic deflections (equation (6.1)) added with the deflections from the kinematical relation, depending on the crack openings, as given in equation (6.3), are shown in Figure 6.17. As can be seen, the model can predict the deflections in the pre- and postpeak region of the bending tests in good agreement with the chosen input parameters. The value of the rotation depth H is in fact the depth of the tensile zone of the beam height during each simulation step; its inverse evolution (δ/w = L/4*(1/H)) can be seen in Figure 6.16 together with the experimental results.

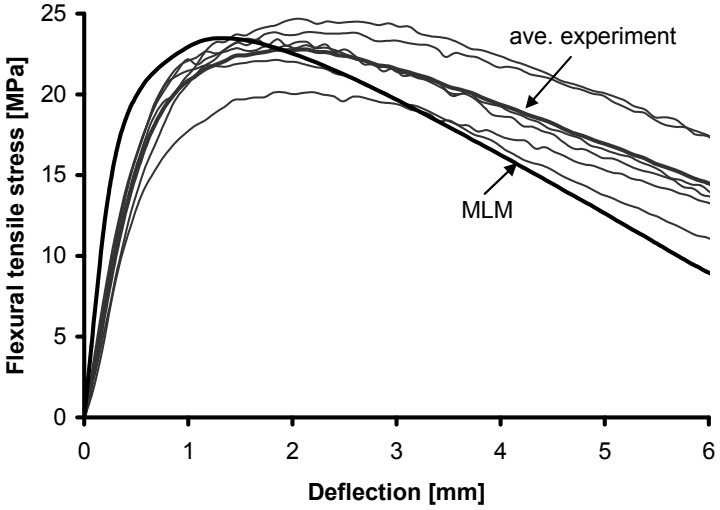

Figure 6.17: Modelled deflections and experimental results of the notched four point bending tests.

6.3.3 Un-notched four point bending tests

Crack openings

The same methodology as described above was followed to model the crack openings of the four point bending tests. Therefore, 500 layers were used over the complete beam height of 125 mm resulting into a layer thickness of 0.25 mm. An influence length of l_i=0.5h=62.5 mm was used for the transformations of strains into crack openings. Except for the influence length of 62.5 mm, all other input parameters are as listed in Table 6.1.

Figure 6.18 shows the results of the multi-layer model and the experiments. As can be seen, again the input is able to reproduce the experimental results with good agreement. It has to be mentioned that the measured crack openings of the experimental results are not the real crack openings, it is not possible to directly measure the crack openings since the crack path is not predefined by a notch. Therefore, the curves shown here are the ones of the LVDTs at the bottom of the beam, which registered the largest deformations. Also, it should be noted that the multi-layer model is strictly speaking only valid for calculating the opening of one major crack at midspan, and is therefore more appropriate for notched beam tests. However, its use in this study is justified by the fact that after the peak load, deformations always localised into a single crack: single crack failure always occurred.

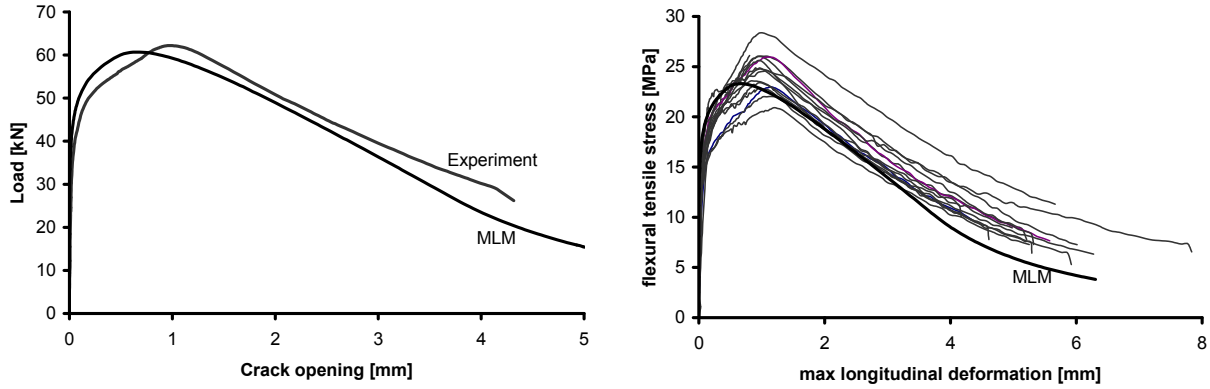

Figure 6.18: Modelled and experimental crack openings of the un-notched four point bending tests; left: average exp. curve, right: individual beam results.

Also, the experimental results were compared with respect to the distance from midspan where the critical crack formed, and average curves were determined for each group; when these curves are compared, in terms of normalised curves with the stress divided by the peak value, little difference in the bending behaviour can be observed (Figure 6.19); therefore validating the use of a model that implies a crack opening of one single crack at midspan.

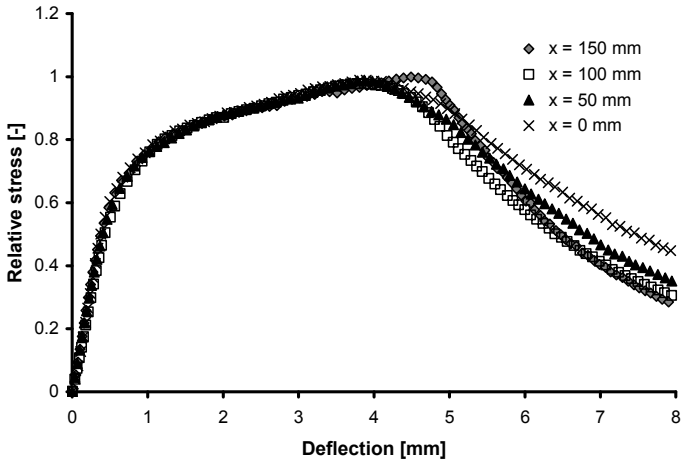

Figure 6.19: Normalised average stress-deflection curves; each average curve is for beams with the same approximate distance x to midspan where the critical crack formed.

Deflections

The same approach as described for the notched beams was followed to model the deflections of the un-notched beams, with the deflections being composed of an elastic component and an inelastic one. However, in case of the un-notched beams the deflection hardening is a critical issue; in order to find an appropriate kinematic relation for its implementation, the deflection-crack opening ratio of the beam tests

was plotted for different deflection values as obtained during a bending tests, in order to evaluate the applicability of equation (6.3). This plot is shown in Figure 6.20.

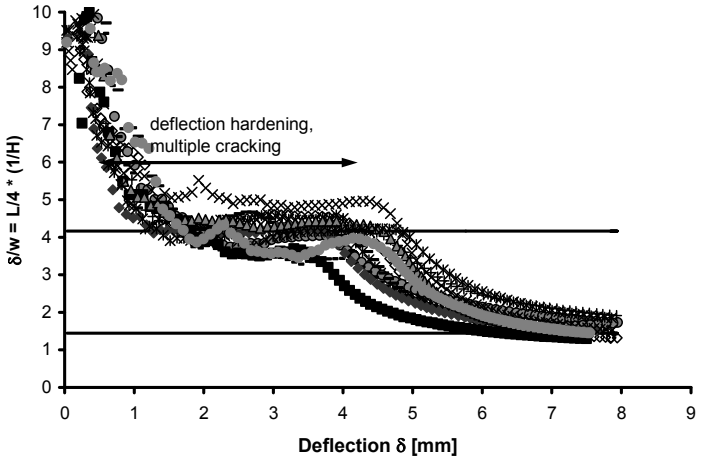

Figure 6.20: Ratio between the deflection and the crack width for different deflection values during four point bending tests on un-notched beams.

As can be seen in Figure 6.20, the δ/w ratio and by consequence also the rotation depth H evolves differently in case of un-notched beams: As the deflection increases, there is first a gradual drop of the ratio, implying an increase of H, just as in the case of the notched beams. The beam starts to crack and the rotation depth gradually increases with increasing crack length. However, the ratio reaches a 'plateau' during the deflection hardening phase, which was not the case for notched beams. This implies that the beam rotation stabilises at a certain fixed value. Assuming that the first crack formed will be the critical crack leading to failure, as already assumed in the multiple cracking energy approaches in Chapter 4, in this phase the critical crack is stabilised and its length is not growing, since the energy needed to form additional cracks is lower than that needed to further open the critical crack. Consequently, more and more cracks are generated in this phase. At the end of this phase, the critical crack will widen further, so that the rotation depth H will start to increase again. In Figure 6.20, the line drawn at the height of the plateau formed during the hardening phase corresponds to a value for H of 40 (+5) mm from the bottom of the beam, one third of its total height of 125 mm. For larger deflection values, the ratio eventually approaches values equivalent to H=(125+5) mm, indicated by the second straight line, as was also the case in the notched tests.

Figure 6.21 exemplary compares the deformations registered by the eight LVDTs placed at the bottom of one beam with the ratio between the deflection and crack openings, as measured for that same beam. As can be seen, initially, for deflection values up to approximately 4 mm, all LVDTs at the bottom fibre show similar

elongation, implying a regular micro-crack pattern in the beam, during the complete deflection hardening phase. After that, at post-peak, one single crack opens, that is registered by two of the eight LVDTs, while the other six start unloading, therefore showing smaller deformations values. The transition from the multiple cracking phase, which corresponds to the deflection hardening stage, to the single crack localisation occurs where the 'plateau' in the deflection-crack opening ratio ends.

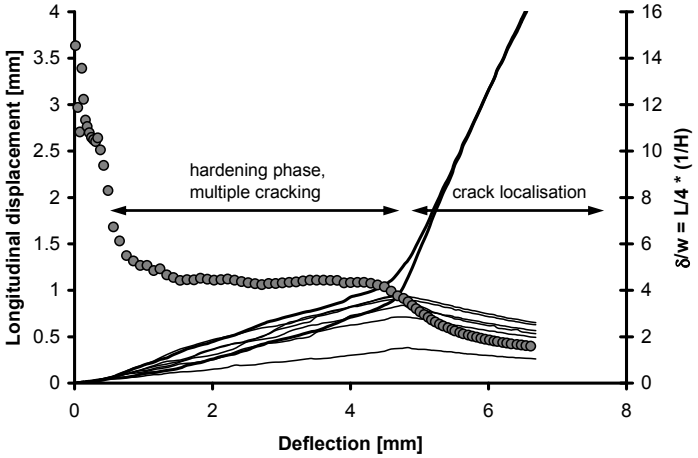

Figure 6.21: Comparison of the longitudinal displacements, as registered by 8 LVDTs at the bottom of one beam, and the ratio between the deflection and crack openings, which is marked with circles.

This observed stabilisation of the rotation depth H at 40 mm, before the crack localises, was implemented into the multi-layer model in case of un-notched beams for the duration of the hardening phase, up to a certain value of the crack opening. Following the hardening phase and forced rotation height, a variable rotation height H in accordance with the height of the compressive zone was used for larger crack openings and so for the descending branch of the load-deflection curve with crack localisation into one single crack. In that way, it is possible to simulate not only the crack openings but also the deflections of an un-notched bending tests, as can be seen in Figure 6.22.

Concluding, it was shown that also for the un-notched bending tests of the HSFRC mixture, the crack openings could be modelled with the input as derived from the uniaxial tensile tests. Moreover, the same input parameters were suitable in order to model notched three point bending tests, notched four point bending tests and un-notched four point bending tests of this study. In order to use the model for deflections of a bending tests, and especially in order to model the inelastic part of the deflections, a kinematic approach given by equation (6.3) was followed. The rotation depth H is a variable in this equation, and its value has been validated by the performed bending tests; for un-notched tests, it was found that this value remains fixed at approximately 40 mm from the bottom of the beam during the

deflection hardening phase. When this phenomenon was implemented into the model, the multi-layer model can be used to model the deflection of un-notched bending tests.

It can be argued whether the followed approach is suitable for modelling the behaviour of un-notched beams, especially with regard to the deflection. Naturally the model is better suitable for notched beams, but its applicability in this case is validated by the crack localisation in one crack after the peak load. However, the chosen approach for the determination of the deflection with the fixed rotation depth, even though verified by the experimental results, remains a curve fitting approach. Equations (6.1) and (6.2) describe the linear elastic part of the deflection, while equation (6.3) is valid for the deflection in the last phase, after the major crack has been formed and localised, so the relation for the hardening stage is missing in this approach. In section 6.8, some additional modifications of the model are shown, that enable a better approximation of the deflection without the implementation of a fixed rotation depth. These modifications will only be shown for the un-notched HSFRC beams in four point bending.

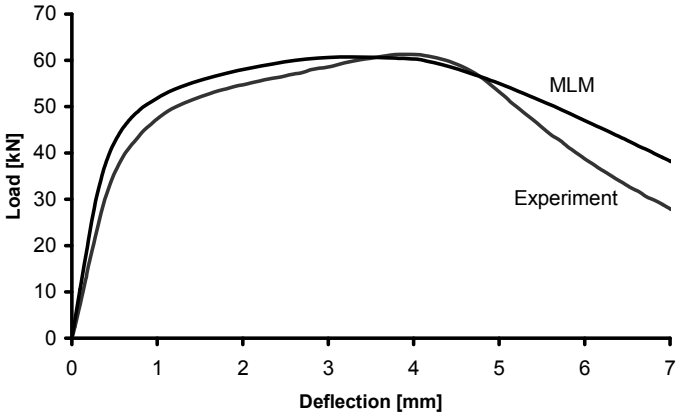

Figure 6.22: Modelled and average experimental deflections of the four point bending tests on un-notched beams.

6.4 Modelling the BSI/CERACEM beams

In the following, the static response of the BSI/CERACEM beams will be approximated by the multi-layer model. For this mixture, only four point bending tests on un-notched beams were performed; and as was already mentioned, the applicability of the multi-layer model is better suitable in case of notched beams. Also, in this case no own uniaxial tensile tests were performed. However, in his PhD thesis, (Jungwirth, 2006) performed uniaxial tensile tests and defined a stress-strain

and stress-crack width relation that fitted his experimental results. This relation will be used to model the bending tests with this mixture.

The BSI/CERACEM is the mixture of this study that had the largest scatter in the static and fatigue test results; therefore, the individual strength values, but also the stress-deflection relation, varied significantly during this series. For example, in Chapter 4 the average curve of the deflection of all beams cast with the flow method was shown (Figure 4.13) while the three BSI/CERACEM beams, cast at a later stage, that were intended for the joint durability/fatigue experiments with the University of Karlsruhe, had a significantly lower average flexural tensile strength, as can be seen in Figure 6.23, where these two average curves are compared. This is mentioned in order to highlight the fact that already when the same mixture (but a different batch of the premix binder material) was cast in the same laboratory, with identical casting methods, different material responses were obtained. Therefore, the results of Jungwirth (2006), cast in a different laboratory, with a separate batch of the premix material, with not necessarily the same casting procedure as used in this study, and with specimens of different dimensions, might result in a different response when used as input for the multi-layer model.

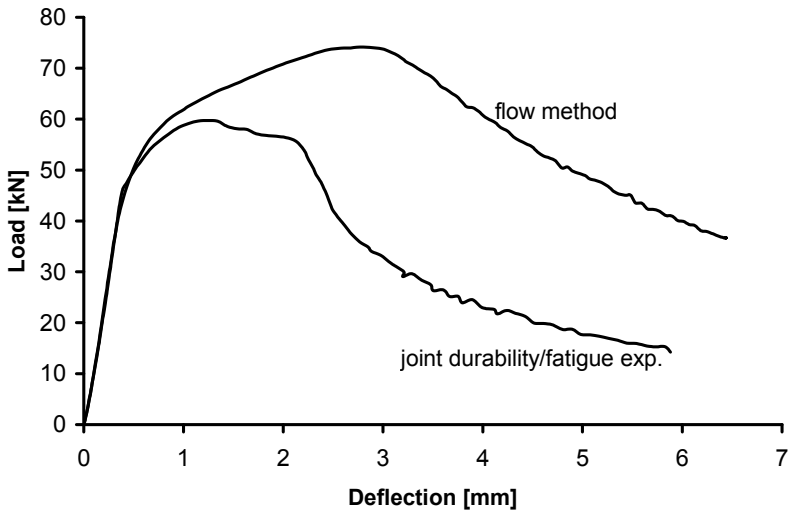

Figure 6.23: Average curves of the BSI/CERACEM beams, one of the beams of the initial testing series, the other for the beams cast for the joint durability/fatigue tests. In both cases, the flow method was used for casting the test specimens.

In his PhD thesis, Jungwirth used exactly the same material and developed a stress-strain relation with a hyperbolic softening relation in accordance with the results of his uniaxial tensile tests. Here, his relations will be tested in order to see if they provide a suitable input for the static modelling of the bending tests of this study: In the multi-layer model, again 500 layers were implemented over the beam height of 125 mm, and an influence length of 62.5 mm ($0.5*h_{lig}$) was chosen.

In compression, a bi-linear compressive relation was used in the form of the relation shown in Figure 6.10 for the HSFRC. Therefore, the stresses increase linearly up to a compressive strength of 190 MPa at a strain of 3.2‰, with an E-modulus of 60 GPa (these values were also used by Jungwirth for the same mixture). After the peak stress has been reached, the stresses are assumed to decrease linearly to zero at an ultimate strain of 8‰. The same ultimate strain as for the HSFRC mixture was used, even though this mixture is of a significantly higher strength, which can reduce the deformation capacity, however this is counteracted by the longer fibres in this mixture, which makes the ultimate strain of 8‰ a reasonable value.

In tension, the relation as defined by Jungwirth is applied: initially the stresses and strains increase linearly with the same E-modulus as in compression, up to a linear elastic tensile strength of 8.9 MPa at a strain of 0.15‰. After that, a strain hardening up to a strength of 9.7 MPa and a strain of 2.5‰ occurs. Then, softening occurs up to a critical crack width of w_c=10 mm, which corresponds to one half of the fibre length. Jungwirth (2006) defined a hyperbolic softening relation according to:

$$\sigma(w) = f_{ct,hard} \cdot \left(\frac{a}{\frac{w}{w_c} - b} + c \right) \tag{6.4}$$

The parameters a, b, c are experimental parameters that fit best the obtained uniaxial softening curve. The parameters that provided the best fit to Jungwirth's uniaxial tensile tests were: a=0.2, b=-0.171 and c=-0.170. The tensile input relation for the BSI/CERACEM, as defined by Jungwirth (2006) and implemented into the multi-layer model, can be seen in Figure 6.24 as a stress-strain relation up to the peak load and a hyperbolic stress-crack width softening relation.

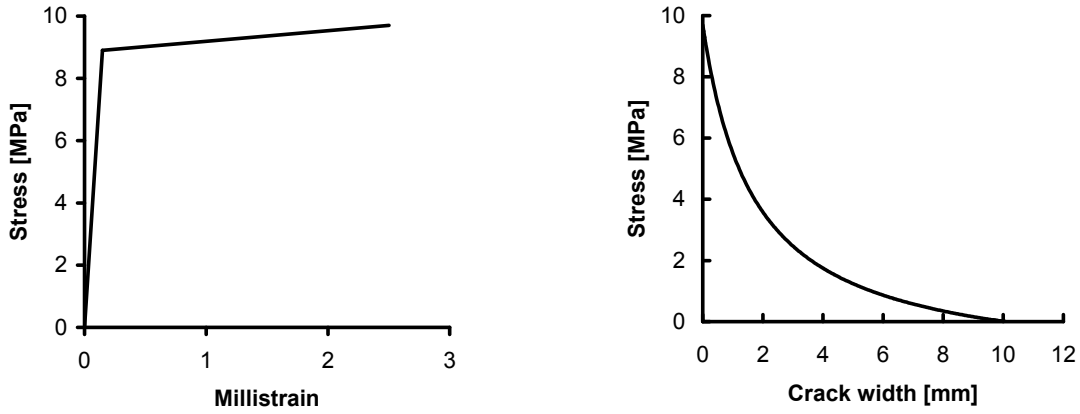

Figure 6.24: Tensile input relation for the BSI/CERACEM, after (Jungwirth, 2006).

The results of the multi-layer model can be seen in Figure 6.25, with respect to the crack openings (left) and deflections (right). The results of the model are shown together with the two average curves as already shown in Figure 6.23, that is the average curve of all beams cast with the flow method of the initial testing series and the ones for the additional series for joint fatigue/durability experiments. It should be noted that the experimental crack opening was not registered directly, but the curves derived from the LVDT at the bottom, that registered the largest displacement, are shown. Also, for the inelastic deflections of the four point bending tests, the same approach as for the HSFRC mixture was followed, with a fixed rotation height in order to model the hardening part. As can be seen, Jungwirth's tensile input corresponds better to the average curves of the joint durability/fatigue experiments, which had significantly lower strengths than the first series with the flow method. Considering the fact that the input relation was derived from tensile tests performed at another laboratory, and for a mixture that was already known to show considerable scatter in its material properties, it can be concluded that the model can reproduce the flexural response within acceptable tolerances. Also in this case, a tensile input with relations obtained from uniaxial tensile tests was suitable for modelling the flexural response of the beams of this study.

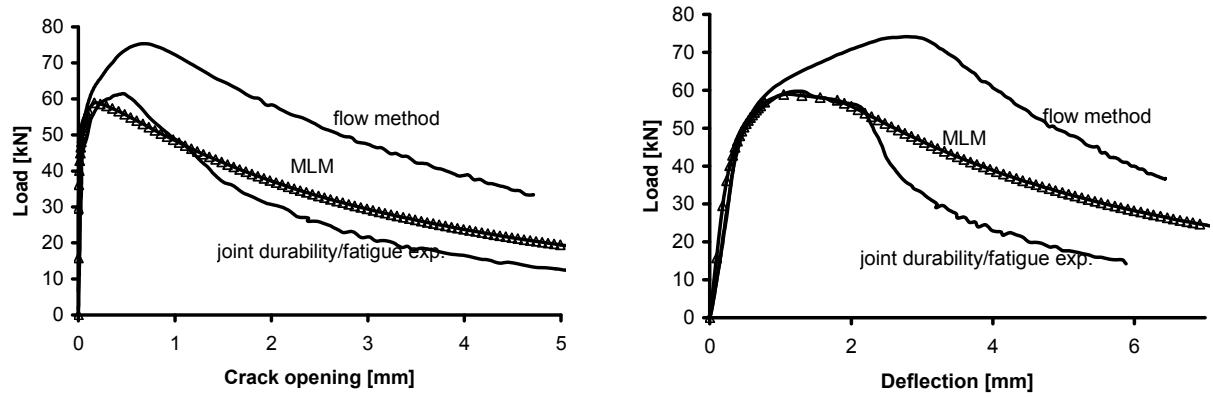

Figure 6.25: Modelled flexural response of the BSI/CERACEM; left: load-crack opening relation; right: load-deflection relation..

6.5 Modelling the hybrid HSFRC beams

As already mentioned, only four point bending tests on un-notched beams have been performed with the hybrid HSFRC mixture. However, Markovic (2006) performed three point bending tests on notched beams and uniaxial tensile tests with the same setup, as used for the HSFRC mixture in this study. Here, first Markovic's three point bending tests and then the four point bending tests of this study will be modelled

with the input derived from Markovic's uniaxial tensile tests (Page 91, Markovic, 2006). In both the three and four point bending tests, 500 layers were used over the beam height of 125 mm and an influence length of $0.5*h_{lig}$=62.5 mm. Regarding the compressive input, a relation similar to the one shown in Figure 6.10 was chosen, since both the HSFRC and the hybrid HSFRC are comparable in terms of strength and stiffness: a linear ascending branch up to the compressive strength of 120 MPa at a strain of 3‰, resulting into an elastic modulus of 40 GPa, and a linear descending branch up to an ultimate strain of 10‰. The ultimate strain of 10‰, rather than 8‰, was chosen, since this mixture contains longer fibres and therefore an increased deformation capacity in the descending branch, at least when compared to the mixtures with only short fibres, can be assumed. Anyhow, the chosen value is not relevant in this case, since both values are not reached in the simulation.

The tensile input is based on the results of Markovic (2006) from un-notched dogbone shaped specimens, as presented in Figure 3.20 b) in his thesis for the stress-strain relation up to the peak load (deformations were transferred into strains by division with the measuring length of 110 mm), and in Figure 4.28 of his thesis for the stress-crack opening relation in the postpeak stage. The input relation is shown in Figure 6.26, as a stress-strain relation with a linear elastic part and a strain hardening part, and a postpeak stress crack-width relation that was simplified into a bi-linear relation. Bi-linear relations are more suitable for composites that contain longer fibres, since larger crack-openings can be bridged, and a linear relation up to these crack openings would significantly overestimate the fracture energy of these mixtures. The hybrid HSFRC mixture contains 1% of 60 mm long fibres with an aspect ratio of 80 (diameter 0.75 mm); the same kind of fibre has also been used in the mixtures of Kooiman (2000). Therefore, the following parameters were used: an ultimate crack width of $w_0=l_f/2$=30 mm, a critical crack width at the intersection point of the bi-linear relation changes of $w_c=w_0/6$=5 mm, and a stress s_c at the intersection point of $s_c=0.2*f_{ct}=0.2*12$ MPa=2.6 MPa. These values seemed more appropriate for these kind of fibres according to Kooiman (2000), but also fitted the stress-crack width relation as given by Markovic (2006) in Figure 4.28 of his thesis.

Figure 6.27 shows the results of the multi layer model compared with the input after Markovic (2006), for the case of the three point bending tests on notched beams. These tests were performed in his study and the results are presented in Figure 3.13 of his thesis. As can be seen, the tensile input derived from the tensile tests is suitable for reproducing the results of the three point bending tests, as was the case for the HSFRC mixture. Both the model and the experimental results predict flexural tensile stresses in the range of 30 MPa.

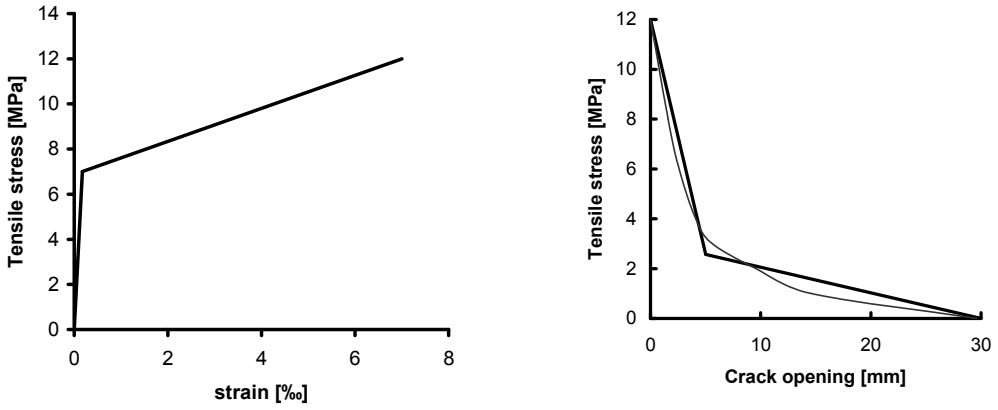

Figure 6.26: Tensile input for the hybrid HSFRC beams based on uniaxial tensile tests of un-notched dogbone specimens performed by (Markovic, 2006).

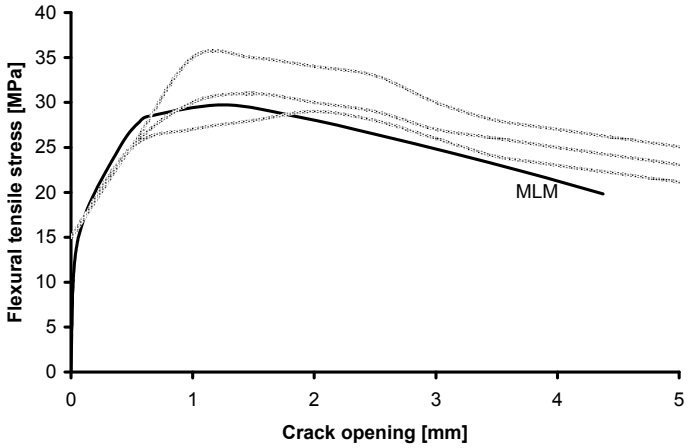

Figure 6.27: Modelling notched three point bending tests of hybrid HSFRC

Next, the four point bending tests on un-notched beams of this study were modelled with the same input parameters. The results are presented in Figure 6.28, as a stress-deflection relation (left) and a stress-crack opening relation (right). The deflections are determined by a linear elastic part, equation (6.1), and an inelastic part based on kinematic relations, equation (6.3), with an implemented fixed rotation depth of 40 mm during the deflection hardening, as already described for the other two mixtures. As can be seen in Figure 6.28, the curve of the multi-layer model, even though of a comparable shape with the experimentally observed curves, overestimates the load bearing capacity of the beam, and predicts flexural tensile stresses of 30 MPa rather than values close to 20 MPa, as were obtained by the experimentally tested beams. This shows that the tensile input, as derived from Marcovic's tensile tests, seems suitable for reproducing the results of his own bending tests (Figure 6.27), while a lower peak tensile strength has to be assumed

for the hybrid HSFRC beams of this study; the possible reasons for this discrepancy will be discussed in the following.

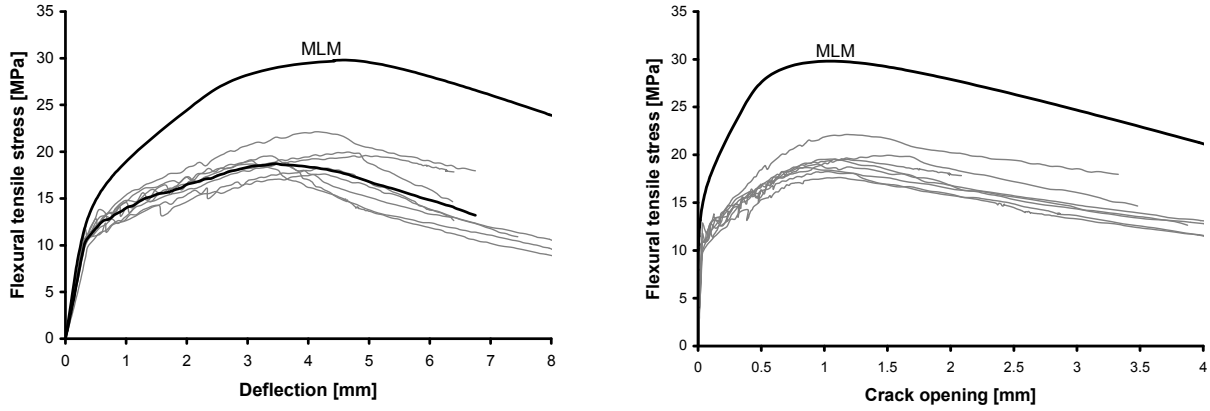

Figure 6.28: Results of the multi-layer model for the hybrid HSFRC beams.

Possible reasons behind the discrepancy of the modelled and experimental data, while using the tensile input as derived from Marcovic's tensile tests, can be the quality of the binder materials, differences in the casting methods and productions of test specimens and curing conditions, and in the fibre orientations and alignment. For the observed differences in the flexural tensile strength in the order of 10 MPa, the main parameter has to be the fibre concentration and alignment, which can result from different casting and production methods of the test specimens. Markovic cast all his testing specimens with a shovel, by placing thin layers of the fresh concrete into the moulds. As he mentions (and is schematically visualised in Figure 3.23 of his thesis), in this way fibres are oriented in the direction of these thin layers. In case of his bending and tensile tests, this resulted into a very favourable direction regarding the crack bridging ability of the fibres. Markovic also counted the fibres with image analysis: for his beam specimens, he counted 8.2 fibres/cm^2 of short fibres with an orientation number of 0.7, and 1.4 fibres/cm^2 of long fibres with an orientation number of 0.9; for his tensile tests, he found 11.9 fibres/cm^2 of short fibres with an orientation of 0.8 and 1.5 fibres/cm^2 of long fibres with an orientation number of 0.9.; these numbers confirmed the preferable fibre alignment as a result of the casting method, and show a slightly better fibre alignment for the tensile tests than for his flexural tests. The beams of this study were cast with the 'flow' method, as has already been discussed in Chapter 4. This method allows two different flow directions, primary and secondary, of the fibres, so that the fibres can be aligned in both of these flow directions. The average fibres and their orientation numbers, as counted with image analysis, were 10.6 fibres/cm^2 of short fibres with an orientation of 0.8, and 1.7 fibres/cm^{2}of long fibres with an orientation of 0.7, which confirm a less beneficial fibre alignment, especially regarding the orientation numbers of the long fibres, for the beams of this study. As can be seen in Figure 6.29, when the values of the linear elastic tensile strength and the hardening strength are reduced

by 70% in the tensile input, while all other input parameters are left unaltered, then the model, even though it still overestimates the average response of the beams, lies within the obtained scatter of the individual test results. A reduction of 60% would lead to an even better agreement, but a reduction of 70% is in better agreement with the observed differences in the fibre orientation, as observed by Markovic and the results of this study.

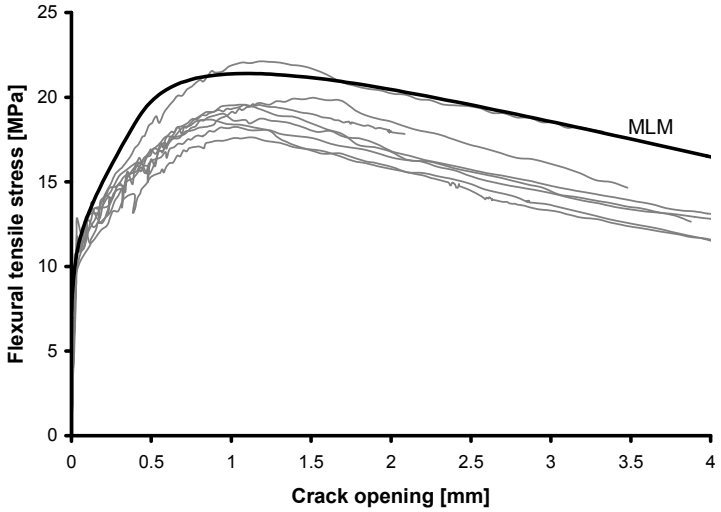

Figure 6.29: Modelled flexural response of the hybrid HSFRC beam with the input strengths in the tensile region reduced by 70%.

Concluding, it was shown that the tensile input for the hybrid HSFRC, could reproduce the three point bending tests on notched beams but was not found as suitable for the four point bending tests on un-notched beams, even though the same mixture composition was used for these beams, but a different casting method. This further shows that for real structural elements in building practice, different structural responses can be obtained depending, among others, on the production method. This has to be accounted for in design. A possible method is described in the French interim design regulations (AFGC-SETRA, 2002), with a reduction factor K to account for fibre orientation effects, and by using different K values for different structural element shapes.

6.6 Parameter study

The results of a brief parameter study, performed in order to evaluate the influence of different input parameters, will be presented here. This parameter study was performed for the HSFRC mixture, the main mixture in this study, and for the notched four point bending tests, since the multi-layer model is more appropriate for the case of notched beams, even though it was shown here that with appropriate

assumptions, also the un-notched bending tests could approached with the model. Basis of the parameter study is the input relation as described in section 6.3.2, with the input parameters listed in Table 6.1, apart from certain parameters which were altered in the scope of the parameter study.

Influence of the main model parameters: number of layers, influence length

The multi-layer modelling procedure, as developed by Hordijk (1991), has two important parameters, that are independent on the input of the material properties, and affect the accuracy of the model predictions: the number of layers n and the influence length l_i.

The number of layers was kept constant at n=500 and was not altered in the scope of this parameter study. Kooiman (2000) showed that the number of layers has an influence on the predicted peak load; a higher peak load is predicted for a lower number of layers. However, no significant difference was observed between 500 and 1000 layers. Therefore, 500 layers seemed a reasonable value with respect to the accuracy of the results and the computational time. Since in this study, similar or identical effective beam heights applied (125 mm and 105 mm, in Kooiman's case always 125 mm), the choice of 500 layers is justified for the desired model accuracy.

An important parameter for the multi-layer model is the influence length, that transforms deformations (of the compressive zone) and crack openings (in the tensile zone) into strains. The same length is used to transform compressive and tensile transformations into strains in this case, and for the main calculations this length was set to one half of the effective beam height as was found appropriate by previous researchers that have used the model (Hordijk (1991), Kooiman (2000) and Grünewald (2004)). Hordijk physically described the influence length as the length of the fractured zone that is replaced in the model by springs; another way of visualising this length is in the analogy to the effects (as described in Chapter 4) of the measuring length for deformation measurements in experimental testing.

Figure 6.30 shows the calculated response of the notched HSFRC beams under four point bending for influence lengths from a minimum value of 10 mm up to 105 mm: the latter value corresponds to the complete ligament height of the beam. The in-between values of 35 mm, 52.5 mm (standard value in most of the calculations of this study) and 70 mm correspond to one third, one half and two thirds of the ligament height. As can be seen, the two extreme values of 10 mm and 105 mm show failure in the cross-section for the modelled range of crack openings. In case of l_i=10 mm, the cross-section fails since the ultimate compressive strain limit was reached in the cross-section. In the model, the compressive deformation capacity of the beam depends on the choice of the influence length ($\delta=l_i*\varepsilon$); for such a small influence length, a compressive failure can only be avoided if a larger deformation capacity would be provided in tension, which would not correspond to the tensile input as observed in uniaxial tensile tests. However, since no compressive failure was observed during the experiments, an influence length of 10 mm does not

seem suitable for a correct reproduction of the experimental data. The failure in the cross-section for l_i=105 mm is a tensile one, the limit crack width was reached. The tensile deformation capacity is influenced by the choice of the influence length, as is the case in compression, but also on the ultimate crack width, which is larger with increasing fibre length. A larger value for l_i results into larger deformations at the elastic limit and when the hardening strength is reached, but into a smaller limit crack width, since the crack widths are defined by the strains divided by l_i. This means that after the peak load, less deformation capacity is available in the tensile zone with increasing values of l_i, which results into failure in the cross section for a length of 105 mm for the chosen mixture input properties.

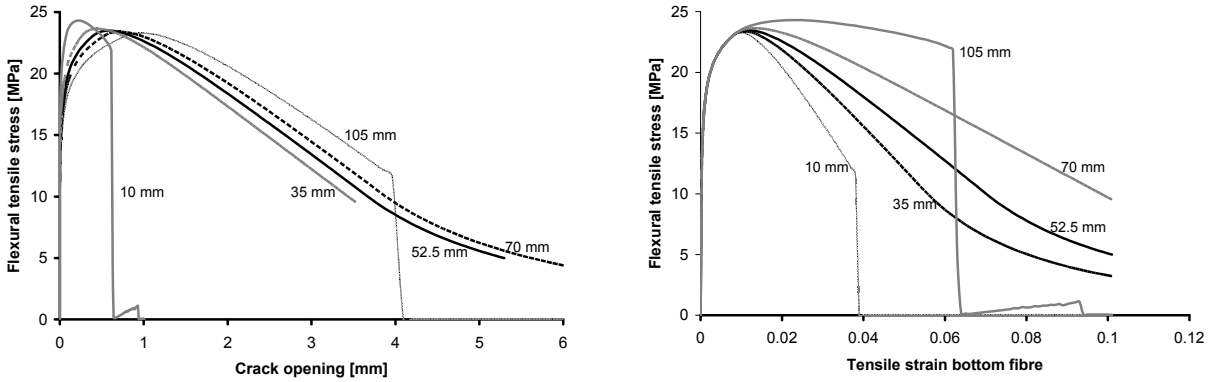

Figure 6.30: Effect of the influence length on deformations (left) and tensile strains (right).

Figure 6.30 shows the results of calculations with variations of values for the influence length l_i with respect to deformations (crack openings) on the left and the maximum strains in the tensile zone (bottom fibre) on the right, with respect to the flexural tensile stresses as obtained by the load derived from equilibrium conditions with the resulting inner bending moment. As can be seen, the peak stress (load) is influenced by this value and higher strengths are obtained for lower values of l_i., This influence is not so pronounced (in this case ranging from 23.3 MPa up to 24.3 MPa). However, as was already discussed for the two extreme values previously, the choice of l_i influences the deformation capacity of the cross-section, and this is more evident for the stress-strain relation rather than the stress-crack width relation. In general terms, the overall deformation ductility increases with increasing l_i, although the limit crack width decreases with increasing l_i. These considerations show, that the influence length is an important parameter of the model. For good accuracy, a realistic and appropriate value has to be chosen. The chosen value of $0.5*h_{lig}$ has also been found suitable by Pederson (1996) who compared similar calculations to finite element calculations. A similar modelling procedure is also recommended for inverse modelling in the French interim regulations for ultra high strength concrete (AFGC-SETRA, 2002): there, $2/3*h_{lig}$ is recommended for the influence length, that

corresponds to a length of 70 mm in the case of the notched beams under four point bending. As can be seen in Figure 6.30, the difference between the predicted response for 70 mm and 52.5 mm is not very pronounced, so that again the chosen value seems to be justified also in comparison with recommendations and findings of other researchers. The influence of l_i will be discussed further in section 6.7.

Influence of the compressive input relation

In all simulations, a simplified bilinear compressive input relation was used, as shown in Figure 6.10. Other input relations are possible, for example an elastic-ideal plastic relation, as is often applied in design codes. Therefore, in order to evaluate the influence of the compressive input relation on the model predictions, simulations with variations in the compressive input relations were performed for the HSFRC mixture for notched four point bending tests. Two variations were implemented, shown in Figure 6.31: The first variation is an ideal linear elastic compressive behaviour, with an unlimited tensile load bearing capacity, and a stiffness of 40 GPa as in the original relation. The second variation is an elastic-ideal plastic relation, with the initial elastic relation as in the original relation, up to a strength of 120 MPa at a strain of 3‰. After that, the strength remains constant at 120 MPa up to an ultimate strain of 5‰.

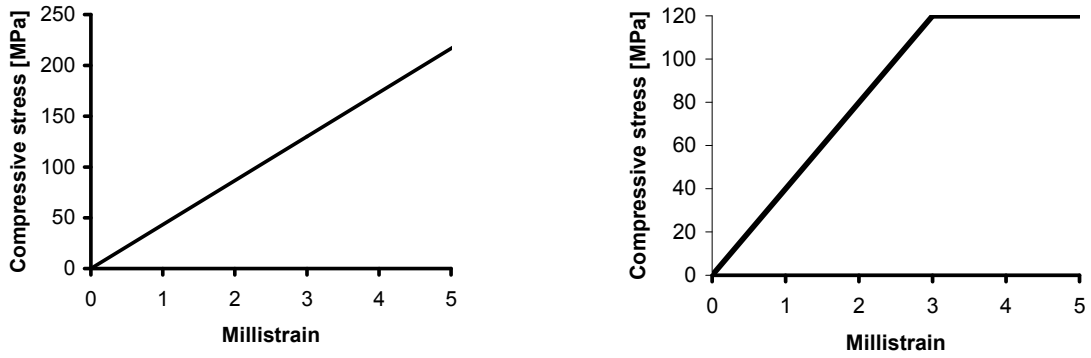

Figure 6.31: Variations of the compressive input behaviour

The results of these two variations are shown together with the results of the original model for the mixture (originally shown in Figure 6.14) in Figure 6.32. As can be seen, these variations in the input relation have no visible influence on the model predictions, which justifies the use of a simplified bilinear compressive relation. The three calculated curves are almost identical, and can hardly be distinguished in the figure.

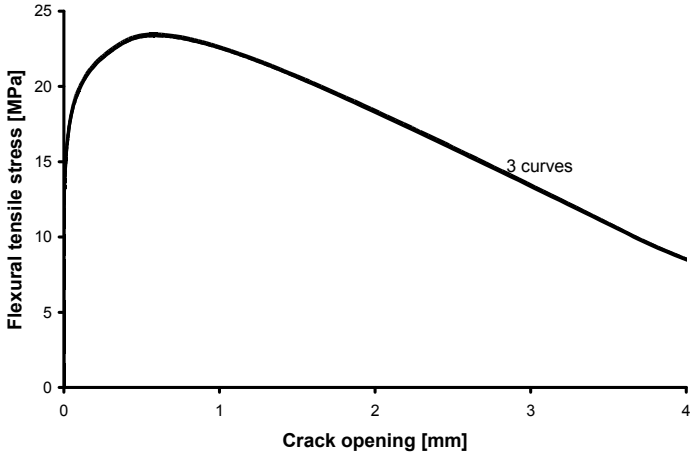

Figure 6.32: MLM predictions for variations in the compressive input relation of HSFRC

Figure 6.33 shows that variation of the compressive strength in the range of 80-150 MPa while the ultimate strain is kept constant at 8‰ (on the left), and a variation of the ultimate compressive strain limit from 6-10‰ while the compressive strength is kept constant at 120 MPa (on the right), have no significant effect on the outcome of the multi-layer model. In both cases, the value of the elastic modulus was left unaltered at 40 GPa. Therefore, by changing the value of the compressive strength, the value of the linear elastic strain limit changes in compression. In the case of a compressive strength of 80 MPa, not enough deformation capacity is given in the cross-section, and the cross-section fails; however, this strength value is not realistic for that mixture, which shows strengths of at least 100 MPa when tested on 150 mm cubes.

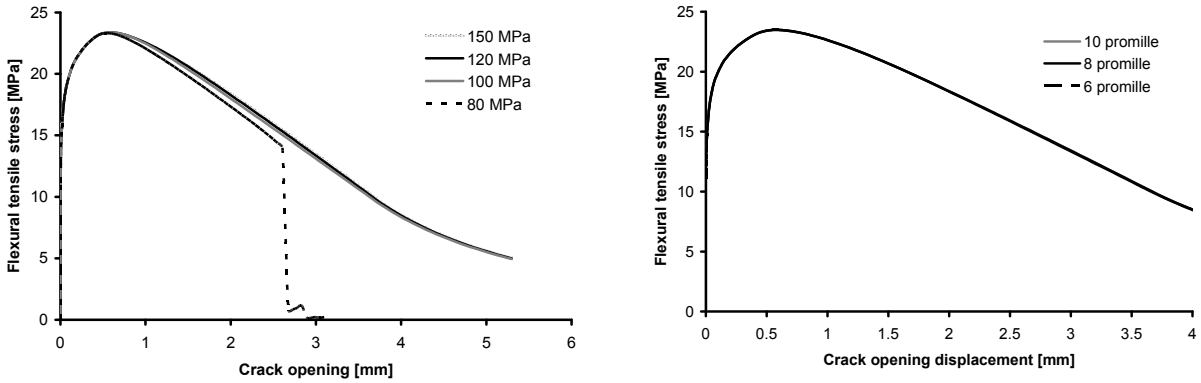

Figure 6.33: Influence of the compressive strength (left) and the ultimate compressive strain limit (right) on the model predictions.

Influence of the (linear elastic) stiffness

In all the previous variations of the model input parameters, the E-modulus was left unaltered; here, the effect of this parameter is examined in the following

simulations. Figure 6.34 shows the effect of the stiffness, which varied from 30 GPa up to 50 GPa, on the outcome of the multi-layer model. As can be seen, the effect is better visible in the stress-deflection relation than in the stress-crack opening relation, where clearly the stiffness influences the first part of the relation, as anticipated. In the simulations, only the linear elastic stiffness and corresponding strain limits, in tension and compression, were altered, while the hardening strain limits and strengths were kept constant. Therefore, the slope of the hardening in tension and of the bilinear softening in compression changes, and this can be seen as minor differences in crack openings and deflections after the linear elastic part of the model. The effect of the stiffness on the peak flexural tensile strength value, at least in the studied range, is negligible.

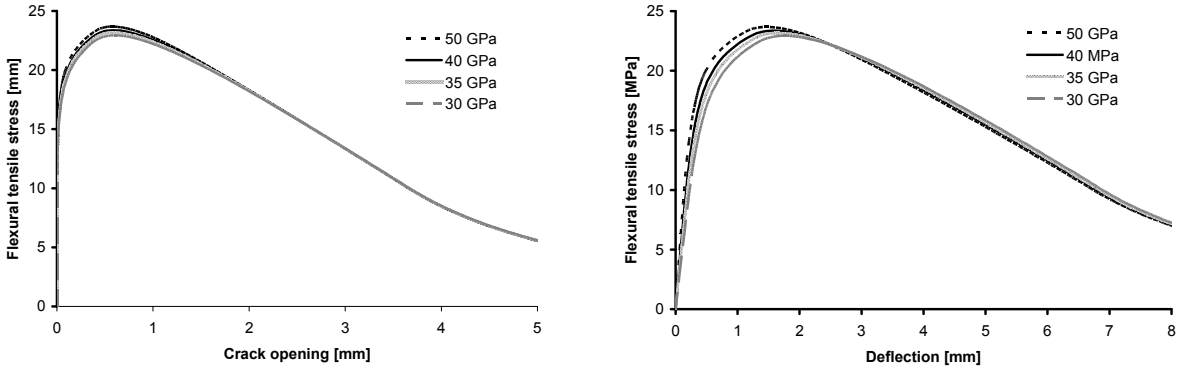

Figure 6.34: Effect of the stiffness on the multi-layer model predictions

Influence of the tensile input relation

It was shown that a linear stress-crack width relation provides a good prediction of the experimental results; however previous researchers, who modelled fibre reinforced concrete (though with different fibre geometries) with the same multi-layer model used bi-linear relations (Kooiman, 2000, Grünewald, 2004). The possible use of a bilinear relation is discussed here. In the bi-linear input relations of Kooiman and Grünewald, the ultimate crack width was varied between one fourth and one half of the fibre length, and the critical crack width at the intersection point was varied between one fifth of the ultimate crack width and one seventh of it. Therefore, simulations were performed for two extreme cases as input: a critical crack width of one seventh the ultimate crack width (0.46 mm) with an ultimate crack width of one fourth of the fibre length (3.25 mm), and a critical width of one fifth of the ultimate (1.3 mm) at an ultimate crack width of one half of the fibre length (6.5 mm). The stress values at the intersection point is, in accordance with Kooiman's and Grünewald's input model, set to a value of 30% of the tensile strength. Figure 6.35 shows, on the left, these two extreme stress crack width relations, opposed to a linear relation up to an ultimate crack width of one fourth of the fibre length; on the right, the outcome of the model predictions is shown together with the experimental results. As can be seen, with a bilinear input relation

the model predicts for the descending part lower stresses than in the experiments. Only if a higher stress is entered at the intersection point, a better fit of the experimental results is obtained; however, by raising this value, the bi-linear relation is approaching the shape of the linear relation, and this justifies the use of a simple linear relation for the HSFRC mixture. A linear relation for mixtures with longer fibres, such as the other two mixtures in this study, is not appropriate, since due to the larger ultimate crack widths, that correspond to longer fibres, the fracture energy of these mixtures would be significantly overestimated.

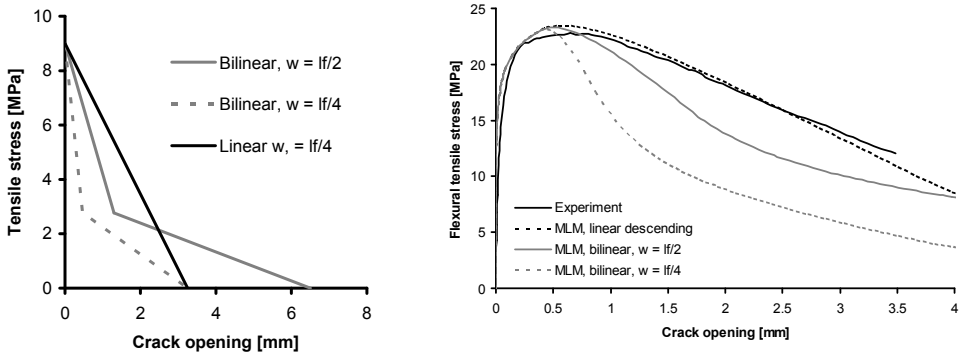

Figure 6.35: Bilinear vs. linear stress-crack width input relation for the HSFRC

The final parameters that were studied in this parameter study are the influence of the linear elastic tensile strength, the hardening strength, and the corresponding strains. Figure 6.36 shows results of simulations for different values of the linear elastic strength (left), from 7 MPa up to 9 MPa while the hardening strength is kept at 9 MPa, and for different values of the hardening strength (right) from 8.5 MPa up to 10 MPa, while the linear elastic strength is kept at 8.5 MPa. It should be noted that when the linear elastic strength was set to 9 MPa, that equals the value of the hardening strength. Therefore, a 'plateau', and not a hardening is implemented; the same holds when the hardening strength is lowered to the value of 8.5 MPa. In case the linear elastic strength was altered, then the corresponding linear elastic strain limit was altered accordingly so that the same E-Modulus of 40 GPa was kept in all simulations. In case the hardening strength was altered, the corresponding hardening strain limit was kept constant at 8‰.

Finally, the hardening strain was varied, as shown in Figure 6.37. The lowest value, 0.2‰, is the linear elastic strain value for the same elastic modulus of 40 GPa to a (hardening) strength of 9 MPa; this means that a linear elastic input relation, with no hardening part, up to the hardening strength, was implemented in that case. Allowing a larger hardening strain, while keeping the hardening strength value constant, results into a slight flexural strength increase, since the compressive strength in the compressive zone is not reached yet at that point.

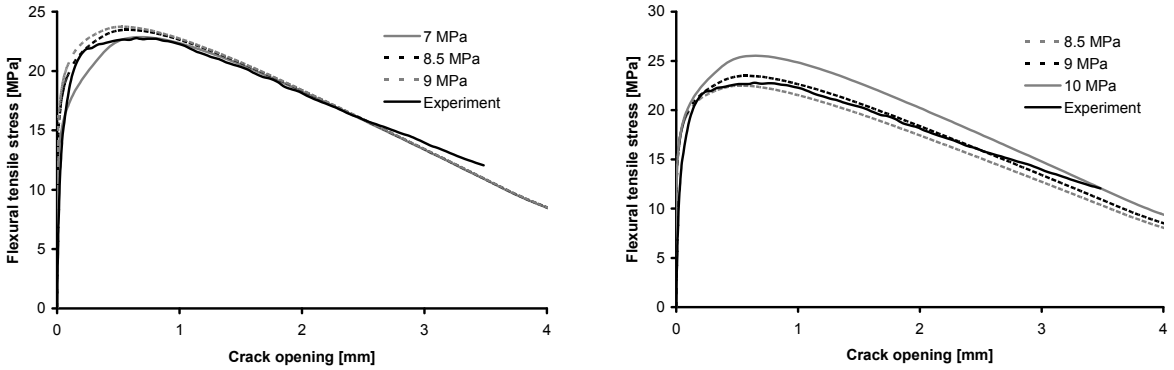

Figure 6.36: Effect of the linear elastic tensile strength (left) and the hardening strength (right) on the model predictions.

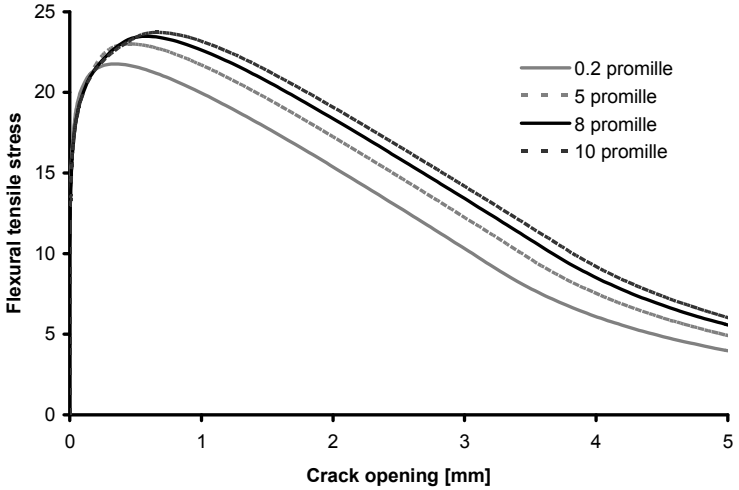

Figure 6.37: Effect of the tensile hardening strain

Concluding, this brief parameter study provides an overview of the effect of all main parameters of the compressive and tensile input relation, as well as the effect of the influence length, which is an important parameter of the model. The parameter study was performed for the HSFRC mixture, which is the main mixture in this study, but the effects can be extended to the other two mixtures as well. Further, the parameter study justifies the chosen input parameters of this study.

6.7 Modelled and measured strain distributions

The strain distributions as measured during the tests and modelled with the multi-layer model will be briefly discussed in the following. This will only be done for the HSFRC mixture, and only for the four point bending tests on notched beams,

because these were the only tests were deformations not only in the tensile zone (crack openings) but also in the compressive zone were measured. Regarding the experiments, the deformations were measured with a measuring length of 100 mm. Therefore, the equivalent strains shown here, were the measured deformations divided by this measuring length. In this case, the deformations measured at the notch tip and at the top fibre of the beam are compared to the modelled strains at the top and bottom layer of the beam; the ones of the bottom layer correspond to the notch tip since in the model, the beam is divided into layers along its ligament height above the notch. Therefore, the last layer corresponds to the notch tip and not the notch mouth.

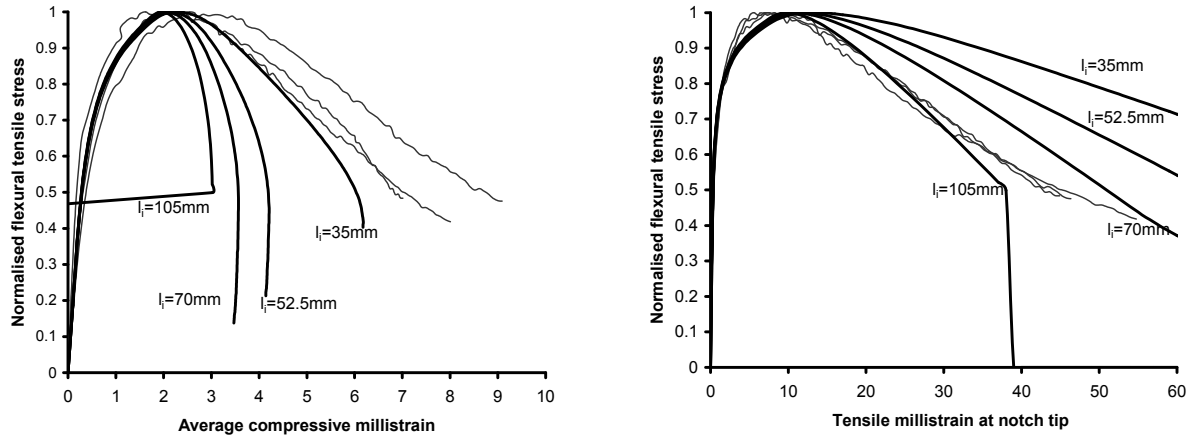

Figure 6.38: Comparison modelled/measured strain distributions for notched four point bending tests with HSFRC.

Figure 6.38 shows the measured and modelled strains for the notched four point bending tests of the HSFRC. On the left, the measured and modelled compressive strains at the top of the beam are plotted with regard to the normalised flexural stresses, that are the stresses of each beam test or the simulation, divided by the corresponding peak flexural stress. On the right, the same plot is shown but for the tensile strains at the notch tip. The modelled strains are shown for different values of the influence length. As can be seen, both in the compressive and in the tensile zone, good agreement between the modelled and measured strains is found up to the peak load, for all values of the influence length. At postpeak, for the standard influence length of the model of 52.5 mm, the modelled compressive strains are less than the measured ones, while the opposite is the case for the tensile strains. However, the experimentally obtained values of the strain distribution cannot be obtained with a different choice of the influence length, since a counteracting effect is obtained for tension and compression. In compression, a smaller value of the influence length would be needed for better agreement with the experimental results, in this case 35 mm give a rather good approximation. In tension, a larger value is needed: here, 105 mm leads to results closer to the experimental results.

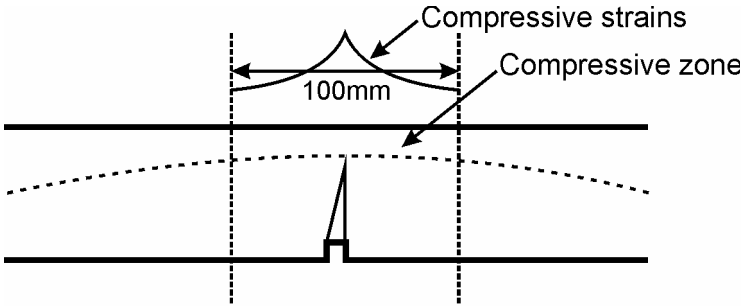

Figure 6.39: Schematic representation of the crack localisation above the crack and the measured average compressive strain.

The discrepancy between the measured and modelled values in the postpeak part does not necessarily mean that the modelled strains are not realistic. What cannot be ruled out are difficulties in a correct strain determination with the used setup and LVDT positions. What can definitely be concluded from the strain distribution is that after passing the peak load, the strains localise, and for the cracked area this means that the compressive zone is being limited to a very restricted height at the top of the beam, as is schematically shown in Figure 6.39. Since deformations are measured over a length of 100 mm, only the average compressive strains can be determined, and the real strains could be even larger. However, a smaller measuring length would not necessarily result into more realistic values, since the crack did not always propagate straight above the notch, therefore it is difficult to capture the exact point of crack localisation. The measured strains in the tensile zone are more realistic since, due to the notch, they can be measured with more accuracy. The strain localisation at postpeak is evident if the strain distribution for these values is plotted along the beam height, with the measured or modelled values at the edges and assuming a linear distribution between them (Figure 6.40). Also, the registered and modelled compressive strains at the top fibre show that at peak load, a compressive strain of 3‰ was registered, which is the assumed linear elastic strain limit in compression. This shows, that at least in the model, the compressive strength is reached, and compressive softening starts at the top fibre. It is very likely that the compressive strength is indeed reached in that part of the beam experimentally; in fact, the assumption of a linear strain distribution is not valid for this fractured part of the beam at these postpeak values. In the tensile region at postpeak, the major crack, in this case predefined by the notch, gradually opens and the rest of the beam is un-loading; therefore, just as was the case in the tensile tests, it is likely that a smaller measuring length was needed than the 100 mm used in order to measure this localisation, and this would imply that larger strains would be valid in the postpeak part than the ones measured with the equipment used. In that case, the measured and modelled tensile strains would be in better agreement.

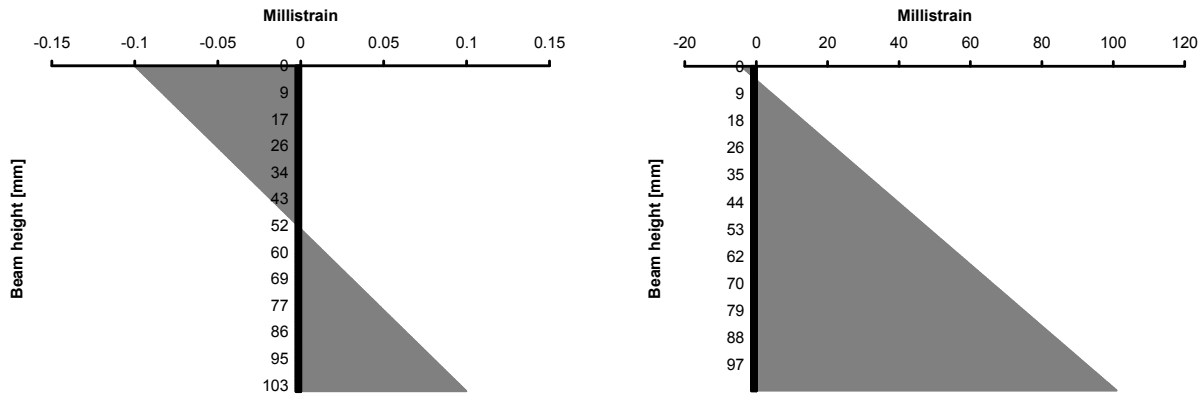

Figure 6.40: Modelled strain distribution along the effective beam height at begin of the simulation (left) and close to failure (right).

Concluding, it can be seen that up to the peak load, the model can predict the strain distribution of the beam. Both the model and experimental results clearly show the localisation and concentration of the compressive zone into a small zone at the top part of the beam. Both the model and the experimental setup can show the strains in the tensile zone with more accuracy than in the compressive zone, especially after the peak load has been reached. Even if compressive failure was not observed during the tests, the modelled and measured compressive strains show that in the localised compressive zone, the acting stresses are close or can even have reached the compressive strength of the mixture.

6.8 Additional modifications of the model

In this section, a variation of the model is proposed, as an alternative solution to model the deflection hardening in the case of un-notched beams without the need of assuming a fixed rotation depth H, which was a semi-empirical approach. It will be shown that with suitable assumptions in the material input relation, that account for the effect of multiple cracking followed by crack localisation into a single crack, the experimental results can be predicted in good agreement. This will be shown only for the un-notched beams of the HSFRC mixture. The assumptions are, however, also valid for the other two mixtures of this study, and in general for deflection hardening materials.

In the case of an ideal single crack material, then the tensile material input relation would be a linear elastic part up to the peak stress and a postpeak softening relation. It has already been discussed that a linear stress-crack width relation is a suitable postpeak relation for fibre concretes reinforced with short fibres, as in case of the HSFRC, where a linear stress-crack width relation up to a limit crack width of one fourth of the fibre length gave a good approximation of the experimental results.

Therefore, for an ideal single crack HSFRC, a linear elastic stress-strain relation up to a peak stress of 9 MPa and a linear stress crack width relation up to a limit crack width of one fourth of the fibre length, 3.25 mm, is assumed.

In case of an ideal multiple cracking material, where an unlimited number of cracks can be formed, without any crack localisation, then the input material relation would be an elastic-ideal plastic relation, meaning a linear elastic part up to the peak stress and an ideal plastic postpeak relation at this peak stress.

For a multiple cracking material, without crack localisation, but with the formation of a finite number of n cracks, the material input relation would be in-between of the two previously described extreme cases. This implies a linear elastic part up to the peak load, and a linear postpeak relation which is more ductile than that of the ideal single crack. It is assumed that for the formation of n=2 cracks, the total crack width would be twice as large as in the case of an ideal single crack material. For n=8, the total crack width would be eight times as large than the crack width of an ideal single crack material. A basic assumption for the definition of a multiple cracking material is that each crack opens independently and all cracks open simultaneously.

This assumed ideal material input relations are shown as an input stress-strain relation in Figure 6.41, on the left. The total crack widths were divided with the influence length in order to obtain the strains. On the right part of the same figure, the outcome of the calculations of the multi-layer model with this input is shown, in form of a flexural tensile stress-deflection relation, and compared to the average experimental curve, which is the dashed line. As can be seen, the peak stress can be predicted in good agreement with the linear elastic material input relation. In case of an assumed number of cracks of 4 and more, then even a stabilization, a small deflection hardening, can occur, but since no localisation is assumed, the descending branch of the experiments cannot be modelled. The deflections are determined from the elastic and inelastic deflections as defined by equations (6.1) and (6.3).

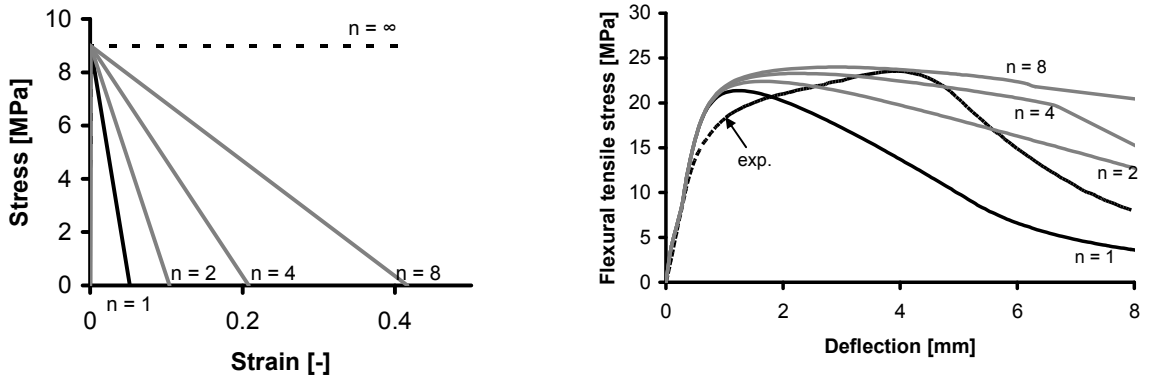

Figure 6.41: Material input for an ideal single crack material or an ideal multiple cracking material with the formation of n cracks (left) and calculated flexural tensile stress-deflection relation (right).

After the previous observations and assumptions, the following step is to combine the material input relations of an multiple cracking material and the ideal single crack material, in order to provide a suitable material input relation for the HSFRC, where the experiments already confirmed that up to the point of crack localisation into one single crack, multiple cracks were formed. It was experimentally confirmed that in a region of the same length as the influence length (62.5 mm), 3 to 4 visible cracks appear among a lot of barely visible hair cracks. The material input relation is shown on the left part of Figure 6.42; as can be seen, the stress strain relation for n=4 cracks is followed up to a certain strain value, after which the relation of a single crack is followed. The strain value corresponding to the transition of multiple to one single crack has to be set in accordance with the experimental results. Here, a strain corresponding to a deflection of 4 mm was chosen, which is a value where the crack localisation and softening part begun in most experimental results. On the right part of Figure 6.42, the predicted stress-deflection relation is shown together with the average curve of the tested beams. As can be seen, in this case a 'deflection hardening' can be modelled without the use of a hardening part in the material input relation or without the implementation of a fixed rotation depth H. However, the experimental curve deviates from linearity prior to the calculated one. The calculated one has a larger value of the first cracking strength, due to the fact that the linear elastic material input relation was set up to a value of 9 MPa. The results of the uniaxial tensile tests (Chapter 4), show that the first cracking load in the experiments performed was between 8 and 8.5 MPa, however, a load increase above that value was still possible.

Therefore, an additional and final adaptation of the material input is a linear elastic stress-strain relation up to 8 MPa, then a load increase up to the value given by the end of the softening part for n=4, with a final drop to the single crack softening relation. In this way, a 'hardening' is implemented. This phenomenon is explained by possible crack formation. In fact, consecutive cracks are formed, each new one at a slightly higher tensile stress. This modified input relation and the calculated stress-deflection relation with this input is shown in Figure 6.43.

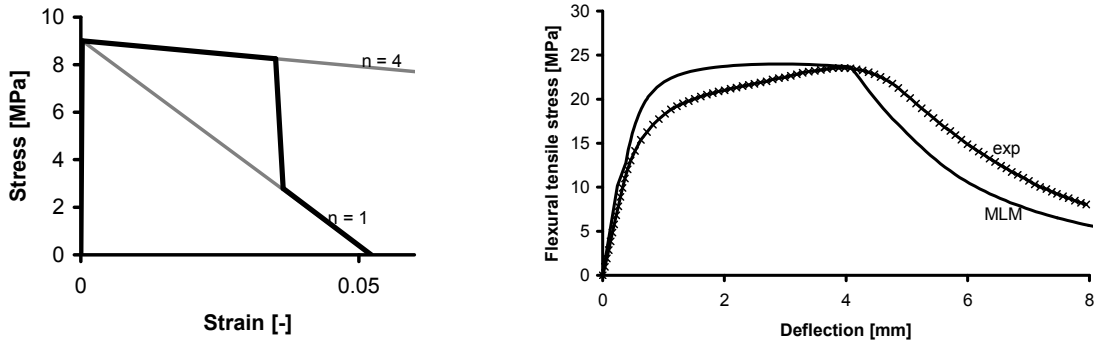

Figure 6.42: Material input (left) and calculated stress-deflection response for the occurrence of multiple cracks followed by crack localisation into a single crack (right).

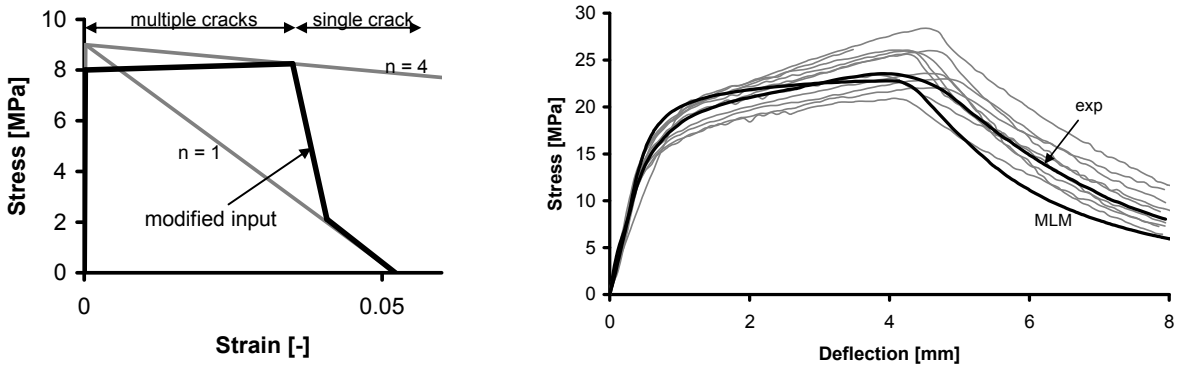

Figure 6.43: Modified material input with a lower linear elastic tensile strength of 8 MPa (left) and calculated and experimental stress-deflection curves (right).

6.9 Concluding remarks

In this chapter, the experimental bending tests were modelled with the multi-layer model, an analytical equilibrium based model. The tensile input was derived from uniaxial tensile test results, either performed in this study or available results from other researchers for the same mixture. The main conclusions that can be drawn are:

- The model is more suitable for notched beams, since the model only accounts for the formation of one crack at midspan. However, its use for un-notched beams in this study is justified by the fact that at postpeak, crack localisation always appeared in a single crack up to failure.
- The model and its input parameters could be studied best on the HSFRC mixture, since experimental data on three point bending tests on notched beams, and four point bending tests on notched and un-notched beams were available. For this mixture, good agreement was found when the results from the uniaxial tensile tests were used as input, but with the deformations transferred into strain with a 35 mm measuring length, which confirmed the assumptions on crack localisaton at post peak.
- The model predicts crack openings from the modelled tensile strain at the bottom fibre. Deflections were modelled from a linear elastic part, derived from equations of a simply supported beam, and an inelastic part, that was derived from rigid body kinematics that depend on a variable rotation depth that is proportional to the crack length.
- The best agreement between the modelled and experimental results with tensile input derived from uniaxial tensile tests was obtained for the HSFRC mixture, and this was the mixture were both the bending tests and the tensile tests were performed in this study, thus the only mixture where the same

casting method (flow method) was used for both types of testing. This shows that the production method is an important parameter that influences the fibre distribution and therefore the structural performance of self-compacting mixtures. Moreover, for the other two mixtures, where the model and experiments were not in that good agreement, this study shows the range of scatter that is possible within the same material.

- The fibre orientation was not implemented as a separate input parameter into the model, since within the testing series all beams were always cast with the same casting method and, as was realised in Chapter 4 after the fibre count by image analysis, similar fibre concentrations and especially fibre orientation factors were obtained. There was a preferential fibre alignment, in favour of the acting loads of the bending tests. Therefore, the tensile input parameters shown here are for a case of favourable fibre alignment and high fibre orientation factors; for the design of actual structural elements, these input values might need to be reduced when a less favourable fibre alignment is expected.
- The modelled and measured strain distributions are in good agreement until the peak load. The compressive strains localise into a very limited zone when the major crack advances, and even though compressive failure was never reached during the tests, the model and also the measured strains indicate that stresses very close to the compressive strength of the mixture are active in the compressive zone prior to the flexural tensile failure.
- In case of un-notched beams, the deflection could be modelled by assuming a constant rotation depth H during the deflection hardening and implementing this into the model. This assumption was verified by the experimental results. It was shown however that the deflection hardening can also be modelled by a combination of material input relations for single crack and multiple crack materials. Initially, a ductile material softening relation of a multiple cracking material is followed in the multiple cracking stage that corresponds to the deflection hardening. This is followed by a steeper softening relation, which transforms the material into a single crack material.

References

AFGC-SETRA (2002) Béton fibrés a ultra-hautes performences, recommandations provisoires.

BARR, B. I. G. & LEE, M. K. (2003) Round Robin Analysis of the RILEM 162-TDF Beam-Bending-Test: Part 2 - Approximation of δ from the CMOD response. *Materials and Structures,* 36**,** 621-630.

BAŽANT, Z. P. & OH, B. H. (1983) Crack band theory for fracture of concrete. *Materials and Structures,* 16**,** 155-177.

DAFSTB (2005) Sachstandbericht Ultrahochfester Beton, Betontechnik und Bemessung. Deutscher Ausschuss für Stahlbeton. Stand: 2005-03-12 (draft version). Beuth Verlag GmbH.

DICK-NIELSEN, L. (2006) Modeling of ECC materials using numerical formulations based on plasticity. IN VOGEL, T., MOJSILOVIC, N. & MARTI, P. (Eds.) *6th International PhD Symposium in Civil Engineering.* Zurich, Switzerland, Institute of Structural Engineering (IBK), ETH Zurich.

GRÜNEWALD, S. (2004) Performance-based design of self-compacting fibre reinforced concrete. *PhD Thesis.* Delft University of Technology.

HILLERBORG, A., MODEER, M. & PETERSSON, P. E. (1976) Analysis of crack formation and crack growth in concrete by means of fracture mechanics and finite elements. *Cement and Concrete Research,* 6**,** 773-782.

HORDIJK, D. A. (1991) Local approach to fatigue of concrete. *PhD Thesis.* Delft University of Technology.

JSCE (2005) Tentative Guideline for Design and Construction of Engineering Cementitious Composites -ECC (Draft version), originally published by JSCE TC 334.

JUNGWIRTH, J. (2006) Zum Tragverhalten von Zugbeanspruchten Bauteilen aus Ultra-Hochleistungs-Faserbeton. *Ecole Polytechnic Federale de Lausanne.* PhD Thesis Nr 3429 (2006).

KABELE, P. (2007) Multiscale framework for modeling of fracture in high performance fiber reinforced cementitious composites. *Fracture of Concrete Materials and Structures,* 74**,** 194.

KOOIMAN, A. G. (2000) Modelling steel fibre reinforced concrete for structural design. *PhD Thesis.* Delft University of Technology.

LI, V. C., STANG, H. & KRENCHEL, H. (1993) Micromechanics of crack bridging in fibre-reinforced concrete. *Materials and Structures,* V26**,** 486-494.

MARKOVIC, I. (2006) High-Performance hybrid-fibre concrete - Development and utilisation. *PhD Thesis.* Delft University of Technology.

ØSTERGAARD, L. (2003) Early age fracture mechanics and cracking of concrete. Experiments and modelling. *PhD Thesis.* Technical University of Denmark (BYG-DTU).

PEDERSON, C. (1996) New production processes, materials and calculation techniques for fibre reinforced pipes. *PhD Thesis.* Technical University of Denmark (BYG-DTU).

PREN1992 (2001) Eurocode 2, Design of Concrete Structures. Final draft ed.

ROELFSTRA, P. E. & WITTMANN, F. H. (1986) Numerical method to link strain softening with failure of concrete. IN WITTMANN, F. H. (Ed.) *Fracture Toughness and Fracture Energy.* London, Elsevier.

XIAO, J., SCHNEIDER, H., DÖNNECKE, C. & KONIG, G. (2004) Wedge splitting test on fracture behaviour of ultra high strength concrete. *Construction and Building Materials,* 18**,** 359-365.

YANG, J. & FISCHER, G. (2005) Investigation of the fiber bridging stress-crack opening relationship of fiber reinforced cementitious composites. IN FISCHER, G. & LI, V. (Eds.) *International RILEM workshop on high performance fiber reinforced cementitious composites (HSFRCC) in structural applications.* Honolulu, Hawaii, USA, RILEM Publications S.A.R.L.

YANG, J. & FISCHER, G. (2006) Simulation of the tensile stress-strain behavior of strain hardening cementitious composites. IN KONSTA-GDOUTOS, M. S. (Ed.) *Measuring, Monitoring and Modeling Concrete Properties. International symposium dedicated to professor Surendra P. Shah.* Alexandroupolis, Greece, Springer.

7.

Modelling the fatigue bending behaviour

This chapter focuses on the implementation of a suitable degradation law for the material input, that accounts for the effect of repeated loading, and can describe phenomena such as the deformation evolution as observed in the fatigue bending tests. The multi layer model, as described in Chapter 6, is used in order to model the fatigue behaviour. The simulation quantifies the effect of fatigue loading on the strengths, stiffness and strains. Only the HSFRC mixture will be regarded in this chapter, but the principal findings can be related to the other two mixtures. The results of the simulation are compared to the experimental findings, with regard to the fatigue lives, crack openings and strains. The proposed model can be easily implemented into, for example, finite element codes, and be used for fatigue calculations of various structural elements.

7.1 Implementation of fatigue into the multi layer model

7.1.1 Basic principles of the model

The model used for evaluating the influences of the fatigue loading on the behaviour of the beams is the multi-layer model, as described in Chapter 6. Only the HSFRC mixture, the main mixture of this study, will be discussed, but the findings can be related to the other two mixtures since the mechanisms and principles of the model remain valid in that case. The HSFRC is the only mixture for which not only fatigue bending tests on un-notched beams, but also a limited series of bending tests on notched beams was performed. In this series, also deformations in the compressive zone were measured, which was not the case in the un-notched tests; therefore, only for the notched specimens, strain distributions, as predicted in the model and as obtained experimentally, can be compared. The basis for all calculations as shown here are the model input parameters as given in Table 6.1 in Chapter 6: that is the HSFRC mixture, with a bi-linear compressive input relation with a strength of 120 MPa at a strain of 3‰ and an ultimate strain of 8‰, a linear elastic strength of

8.5 MPa up to a strain of 0.2‰, a hardening strength of 9 MPa at a strain of 8‰ and a linear stress-crack opening relation up to a maximum crack width of 3.25 mm, one fourth of the fibre length. The number of layers is kept at 500 over the effective beam height, and the influence length is always one half of the effective beam height, 52.5 mm in case of notched tests and 62.5 mm in case of un-notched tests. Since only fatigue four point bending tests, and not three point bending tests, were performed, only four point bending tests will be modelled.

As already mentioned, the same multi-layer model was used for the fatigue tests as was used in the static tests. However, a different iteration procedure had to be applied for the fatigue tests. In the static tests, the peak strain in the tensile zone was gradually increased and the corresponding compressive strain was sought under the condition of a zero normal force. At fatigue loading, a fixed upper load value was applied to the beam. Therefore, the inner moment is set to a constant value, that corresponds to the upper load value. It can be determined by simple force equilibrium conditions for the simply supported beam. The corresponding tensile and compressive strains can then be determined by iteratively solving the conditions of the fixed value of the bending moment and of a zero inner normal force.

In the static case, the model algorithm consisted of a gradual increase of the tensile strain; instead, in the fatigue model, the number of load cycles N is gradually increased, and the material input conditions are modified in accordance with N. Therefore, a cycle dependent material input is implemented, which simulates the damage due to fatigue loading. In that way, the fatigue model is not showing the effects of every single load cycle onto the beam, which would use a considerable computational time, but is showing the gradual effect of the fatigue loading on the deformations, and the total fatigue life of a beam. The principle of the fatigue calculations with the multi-layer model is shown in Figure 7.1.

7.1.2 Implementation of a gradual tensile strength loss due to fatigue

As a first approach, a strength degradation law was implemented into the model, in order to evaluate its possible use for fatigue modelling. Simulations were performed to show the response of both notched and un-notched beams, at upper load levels similar to the experimentally tested load levels. The un-notched HSFRC beams were tested at load levels ranging from 90% to 70% of the average static peak load. The results can be seen in Table 5.2 in Chapter 5. Tests on notched specimens were performed at load levels ranging from 80% to 60%; the results are listed in Table 5.4 in Chapter 5. Therefore, load levels ranging from 60% up to 90% were applied in the multi-layer calculations. It should be noted that a simulated load level of a certain value, for example 80%, does not correspond entirely to the applied upper load of an experiment, but to 80% of the simulated peak load in the static simulation. However, the simulated and experimental average peak load values are quite close, as was shown in Chapter 6.

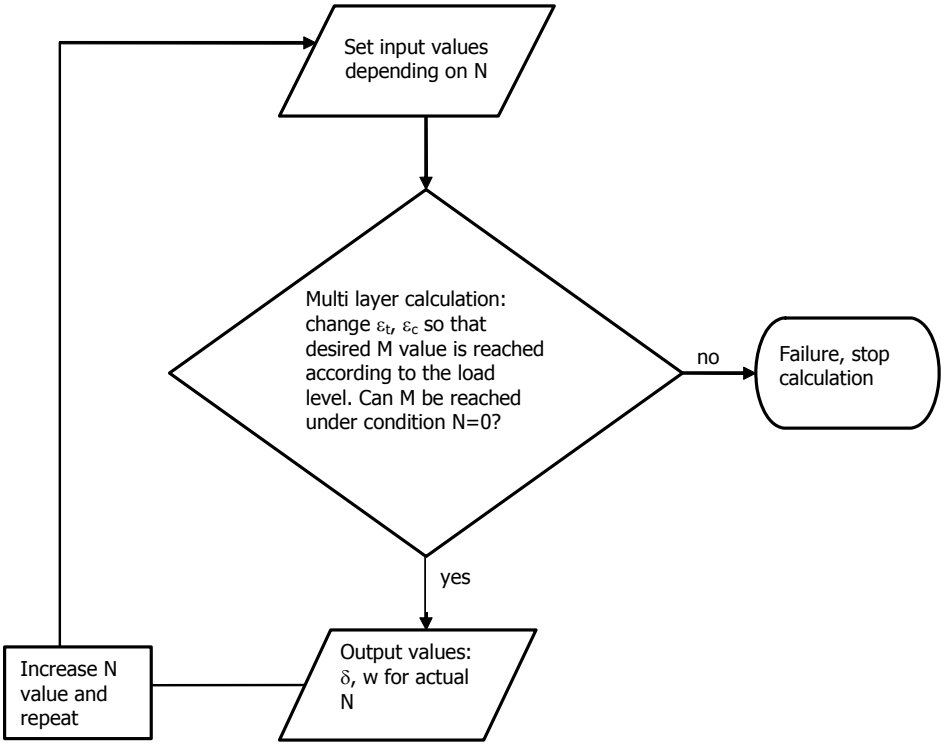

Figure 7.1: Principle of the fatigue calculations with the multi-layer model

As a first approach, a suitable strength degradation relation was sought from the existing literature. Since only load controlled, and not deformation controlled, fatigue tests were performed in this study, it is not possible to derive strength decrease relations from the own experiments. Kessler-Kramer (2002) performed, among others, deformation controlled fatigue tests and found the following linear or bilinear relations between the tensile strength and the logarithms of the applied number of load cycles:

$$f_{ct,N} = f_{ct,0} - 0.2 \cdot \log N \qquad (7.1)$$

or

$$f_{ct,N} = f_{ct,0} \qquad \text{if } \log N \leq 1$$

$$f_{ct,N} = f_{ct,0} - 0.27 \cdot \log N \qquad \text{if } \log N > 1 \qquad (7.2)$$

where $f_{ct,N}$ is the cycle dependent value of the peak tensile strength, $f_{ct,0}$ the initial value at N=0 (static tensile strength) and N the number of load cycles. These equations were found applicable to both normal and high strength concrete without steel fibres.

These two equations were implemented into the multi-layer model. Figure 7.2 shows the relation in case of the linear strength degradation as given in equation (7.1). Shown are the relation for N=0 (same input relation as in the static

input relation for the HSFRC) and for $N=10^7$, when the hardening strength has dropped from 9 MPa to 7.6 MPa and the linear elastic tensile strength from 8.5 MPa to 7.1 MPa. In case of a bilinear strength degradation relation, lower strengths would apply for 10 million load cycles, namely 7.1 MPa for the hardening strength and 6.6 MPa for the linear elastic strength. Only the tensile strength values are decreased in the model, while the corresponding strains, the linear elastic strain and the hardening strain, were left unaltered. Also the compressive input relation was kept constant and independent of N. In that way, the linear elastic stiffness in tension slightly decreases with increasing N, and for large N values, the beam has a different stiffness in tension and compression. Also, since the limit crack width value is kept constant, the slope of the linear softening relation is decreasing with increasing number of cycles to failure.

Figure 7.3 shows the results of calculations with the cyclic material input as described above, for notched beams under four point bending. Plotted are the crack openings with respect to the number of load cycles N. On the left, the results of the simulation in case of a linear strength decrease with respect to log N is implemented, equation (7.1), while on the right the results are shown for a bilinear load decrease as given in equation (7.2). As can be seen, in case of the notched beams only for the 80% load level and a bilinear strength degradation failure was reached before 10 million load cycles, at approximately 9 million load cycles; in all other cases no failure was reached up to 10 million load cycles. Also, the upper load level influences the deformations: larger crack openings are obtained for higher load levels, a fact that is confirmed by the experimental results. In case the failure was reached before 10 million load cycles, the calculated evolution of the crack openings or deflections is showing all three stages of the typical deformation evolution in a fatigue test (cyclic creep curve).

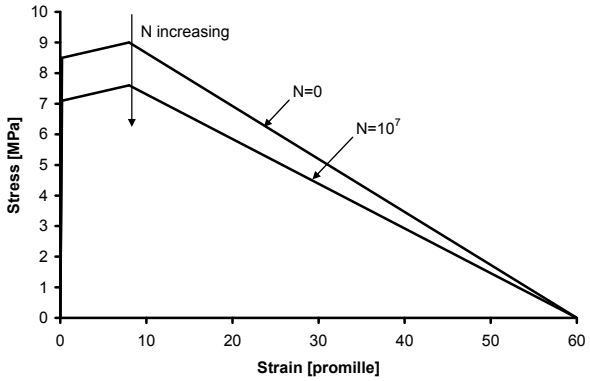

Figure 7.2 Cycle dependent tensile input relation in accordance with the linear strength decrease after Kessler-Kramer (2002), as shown in equation (7.1).

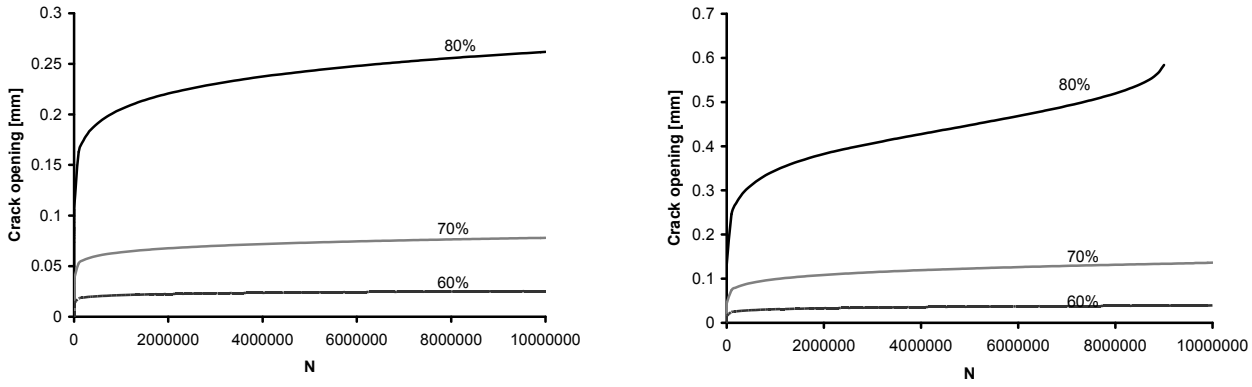

Figure 7.3: Results of the MLM simulation with a strength decrease implementation. Left: linear degradation, eq. (7.1). Right: bilinear degradation, eq. (7.2)

Table 7.1: Results of the experimental and modelled fatigue life after implementation of a gradual fatigue strength loss in the multi layer model.

Load level		**90%**	**80%**	**70%**	**60%**
Experiments notched	N	-	1583780	4806455	7684815
	logN		6.20	6.68	6.89
Experiments un-notched	N	11464	2577654	*10000000*	-
	logN	4.06	6.41	*7.00*	
Model linear decrease	N	52000	*10000000*	*10000000*	*10000000*
	logN	4.72	*7.00*	*7.00*	*7.00*
Model bi-linear decrease	N	4000	9000000	*10000000*	*10000000*
	logN	3.60	6.95	*7.00*	*7.00*

Table 7.1 shows the number of cycles to failure, N, and their logarithmic value, for different load levels, as obtained from the experimental results on notched and un-notched beams for the HSFRC mixture, and as predicted by the multi layer model after the implementation of a linear and a bilinear strength degradation as defined by equations (7.1) and (7.2). Italic values imply that no failure was reached up to 10 million load cycles, when the experiment or calculations were stopped. It should be noted that the results of the model are valid for both notched and un-notched beams. This is due to the fact that in the fatigue model, the applied load level was set in accordance with the peak load of the same model in static calculations. Then, the same number of load cycles to failure are predicted in both cases, at least as long as the input crack widths are not defined to depend on the value of N, since the only difference in the material input is the influence length, which is set in accordance to the effective beam height and is therefore 10 mm larger for un-notched beams.

By comparing the experimental and modelled results as given in Table 7.1, it can be concluded that the bilinear strength degradation, as defined by equation (7.2), is more suitable in order to predict similar number of cycles to failure as obtained by

the experimental results. Due to the high scatter in fatigue results, it is more appropriate to compare the logarithmic values of the number of cycles to failure. The model with the bilinear strength degradation is in better accordance with the results of the un-notched beams, where no failure is predicted, at least not until 10 million load cycles, for upper load levels of 70% and lower.

Figure 7.4 compares the experimentally obtained crack openings and the calculated ones for the notched beams at an upper load level of 70%. In the figure, the maximum, and not the average values, of the crack openings measured on the tests specimens are shown, as obtained from the registered average values and their amplitude during each test. These values correspond to the values in the model, which are only related to the upper load level since the influence of the lower load level is not regarded within this study. As can be seen, the model underestimates the values of the crack openings, in case only a gradual strength decrease is implemented. In the following sections, the model will be modified in order to find a better agreement between measured and calculated displacement values.

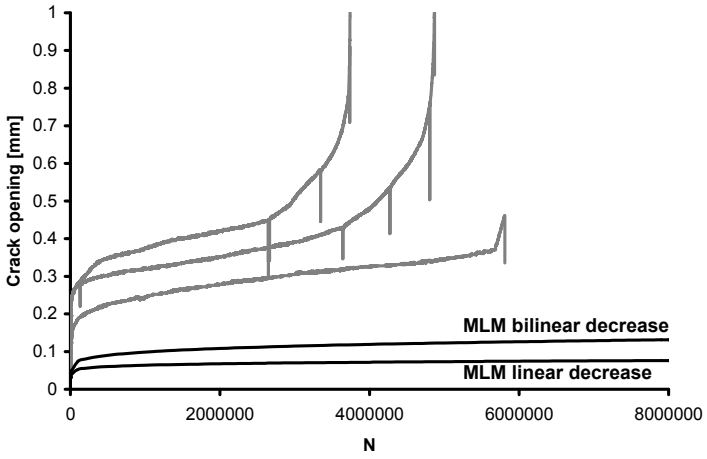

Figure 7.4 Comparison of the calculated and experimentally obtained crack openings for notched beams at an upper load level of 70%.

7.1.3 Implementation of a gradual stiffness decrease

As was shown in the previous section, the implementation of a gradual strength degradation shows tendencies which confirm the experimentally obtained fatigue results. In the following, additional modifications to the cyclic material input relations will be presented. These modifications are implemented for two main reasons. First, in order to have a better model prediction with regard to the experimentally obtained values. However, due to the high scatter in the experimentally obtained results it is almost impossible to find a perfectly fitting model. Second, these modifications are performed in the scope of a parameter study, in order to evaluate the influence and impact of different input relations on the predicted fatigue performance.

In the first approach, fatigue loading was supposed to cause only a gradual degradation of the tensile strength, while the input relation for concrete in compression was kept constant. In that way, as was already mentioned, a different stiffness was assumed in tension than in compression with increasing number of N. However, fatigue tests on concrete in compression have shown the compressive strength and the stiffness in compression decrease with increasing number of load repetitions. The stiffness decrease of a beam subjected to repeated loading in a fatigue tests between two load levels, has been monitored experimentally, for example in Subramaniam et al. (2000). In this study, the stiffness decrease was not registered within the experimental setup but was monitored indirectly, through the deflections. Deflections are inversely proportional to the stiffness, at least in the initial linear elastic stage. In fact, the stiffness during a fatigue experiment has the typical cyclic form already known from the deflection evolution, but continuously decreasing instead of continuously increasing as was the case for the deflections.

In this study, since the stiffness evolution was not monitored directly, only through the deflection, no direct stiffness degradation law, that can be used as input for fatigue calculations, can be obtained. However, indications of the stiffness loss on the experiments performed can be obtained by the run-out specimens, that did not fail before 10 million load cycles, at which the experiments were stopped. These were eventually tested statically up to failure. These specimens showed a higher flexural tensile strength than the average of the specimens tested under static loading only. This could indicate that these run-out specimens might have a high flexural tensile strength, if tested under static loading instead of fatigue, within the natural scatter of the static strength values. More important, these specimens showed a lower stiffness than the stiffness of specimens tested under static loading only. The lower stiffness is related to the damage accumulation in the specimen due to the fatigue loading. From the observed stiffness loss of these run-out specimens compared to the stiffness of the specimens tested under static loading only, a relation for the stiffness decrease can be derived, by assuming that the decreased stiffness corresponds to a stiffness at 10 million load cycles. Only run-out specimens of the HSFRC and hybrid HSFRC mixture were tested statically up to failure; on average, the stiffness decrease of the HSFRC was 38% and of the hybrid HSFRC 31%. Figure 7.5 shows the two average curves for the HSFRC mixture, the one of the specimens tested under static loading only, and the other of the run-out specimens that were tested statically after first having survived ten million load cycles under fatigue loading.

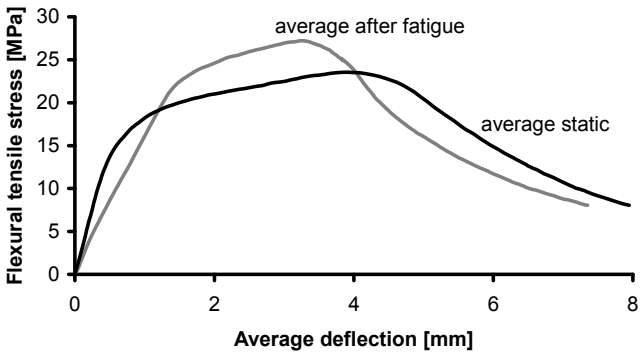

Figure 7.5: Average curves of the HSFRC of the beams tested only statically and the run-out specimens, that survived ten million fatigue load cycles before being tested statically.

A linear decrease of the modulus of elasticity with respect to the logarithm of the number of load cycles was chosen, in a similar form as the linear tensile strength decrease of Kessler-Kramer (2002) given in equation (7.1):

$$E_N = E_0 - a \cdot \log N \qquad (7.3)$$

In this equation, E_N is the E-modulus at a certain number of load cycles, N. E_0 is the initial (static) value of the stiffness for N=0. In case of the HSFRC this is 40 GPa. The constant 'a' is a stiffness degradation factor. In the following, results of calculations with a chosen value a=2 GPa will be shown, which lead to a stiffness of 65% the original value (from 40 GPa down to 26 GPa) at N=10 million, a stiffness decrease of 35%, which is a value close to the experimentally observed values for the run-out specimens. As a first approach, to study the influence of the implementation of a stiffness decrease in the model, two variations were implemented, that serve the purpose of a parameter study rather than to actually compare the results with the experimental tests.

Gradual stiffness decrease – first variant

At first, this stiffness degradation was implemented into the model, while all compressive and tensile strength input values were kept unaltered. The linear elastic compressive and tensile strain limits were altered in accordance with the compressive strength value and the linear elastic tensile strength value so that the stiffness value at a certain N was kept, which means that in the simulation, the linear elastic strain limits were increasing with increasing N. Therefore, in tension, the hardening length slightly decreased with increasing N, since the hardening strain was kept constant at 8‰. Furthermore, the ultimate compressive strain as well as the ultimate crack width were kept constant and independent of N at 8‰ and 3.25 mm. Figure 7.6 shows the tensile and compressive input relations for N=0 (initial case) and $N=10^7$.

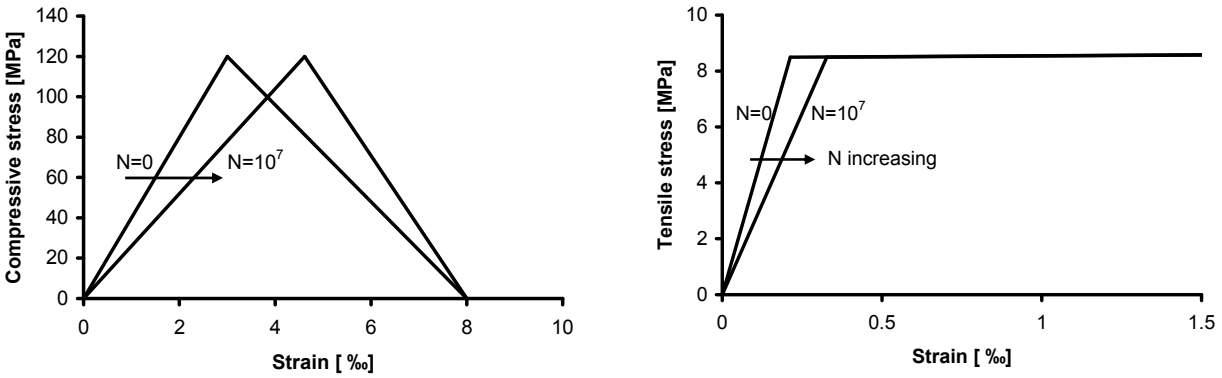

Figure 7.6: Compressive (left) and tensile (right) cyclic input relation with gradual stiffness degradation but the same strength values, first variant.

Figure 7.7 shows the results of the multi-layer model for the HSFRC after the implementation of a gradual stiffness decrease but with no decrease of the input compressive and tensile strength values. The evolution of the crack openings for modelled stress levels of 60%, 70%, 80% and 90% are shown. In all cases, a dependence of the upper load level on the crack openings was observed, as also found from the experimental results. A gradual decrease of stiffness causes an initial phase of rapid increase of deformations, as also observed in the experiments, followed by a phase of constant increase. Since the strengths were not increased, but the linear elastic strains increased in order to result in the desired stiffness for a certain load level, the ductility and deformation ability of the beam is gradually increasing with increasing N, which is the reason no failure could be reached in the simulations, even for load levels of 90% of the peak load, as predicted by the model in the static calculations with the chosen input parameters.

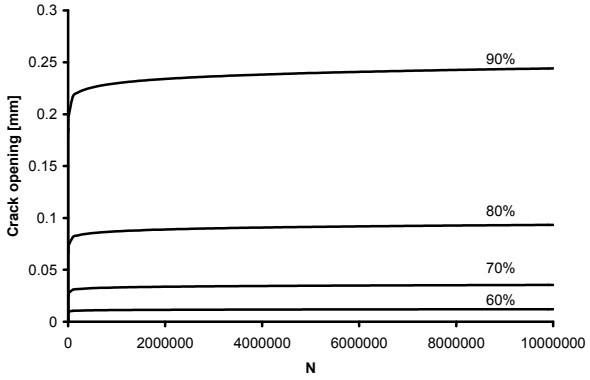

Figure 7.7: Results of MLM modelling with gradual stiffness decrease but no strength decrease for the HSFRC.

Gradual stiffness decrease – second variant

The gradual decrease of stiffness, in accordance with equation (7.3), was also implemented in a second variant. Here, the stiffness decreased while the linear elastic compressive and tensile strain limits were kept constant. This implies that the corresponding compressive and tensile strengths are decreasing with increasing N, in correspondence to the actual stiffness values. Figure 7.8 shows this cyclic material input relation for the initial case, at N=0, and for $N=10^7$. Since the stiffness and strengths are proportional, a linear stiffness degradation with regards to log N, as implemented here, results into a linear strength degradation with regard to log N. Therefore, the strength decreases in a way as observed by (Kessler-Kramer, 2002) in his deformation controlled fatigue uniaxial tensile tests. A chosen degradation coefficient for the stiffness of a=2 GPa leads to a reduction of the compressive strength of 6 MPa * logN and 0.425 MPa * logN for the tensile strength. Therefore, in tension, this corresponds to a more severe degradation than the observed relation of Kessler-Kramer (2002) of 0.2 * logN in his linear relation or 0.27 * logN in the bilinear case. The modelled number of cycles for each load level, as well as the average number of cycles to failure as obtained from the experiments with the HSFRC mixture, are given in Table 7.2.

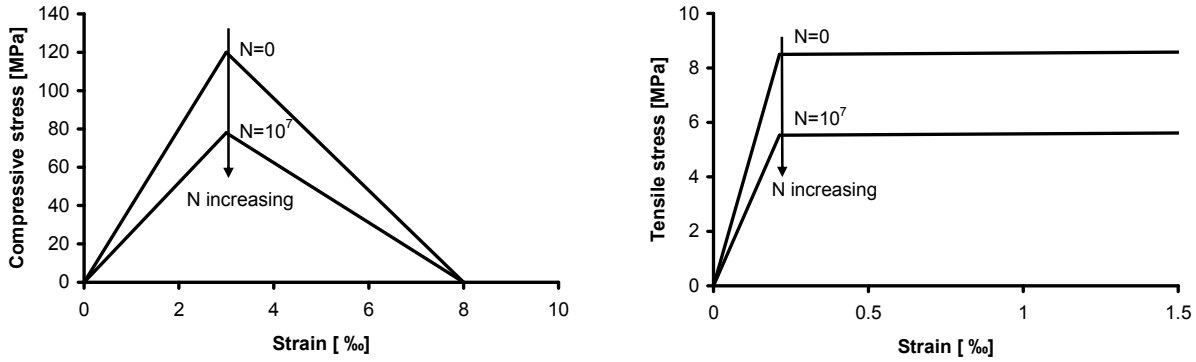

Figure 7.8: Compressive (left) and tensile (right) cyclic input relation with gradual stiffness degradation and decrease of corresponding strength values, second variant.

Table 7.2: Results of the experimental and modelled fatigue life after implementation of a gradual stiffness decrease in the multi layer model.

Load level		90%	80%	70%	60%
Experiments notched	N	-	1583780	4806455	7684815
	logN		6.20	6.68	6.89
Experiments un-notched	N	11464	2577654	*10000000*	-
	logN	4.06	6.41	*7.00*	
Model stiffness decrease first variant	N	*10000000*	*10000000*	*10000000*	*10000000*
	logN	*7.00*	*7.00*	*7.00*	*7.00*
Model stiffness decrease second variant	N	130	16000	1900000	*10000000*
	logN	2.11	4.20	6.28	*7.00*

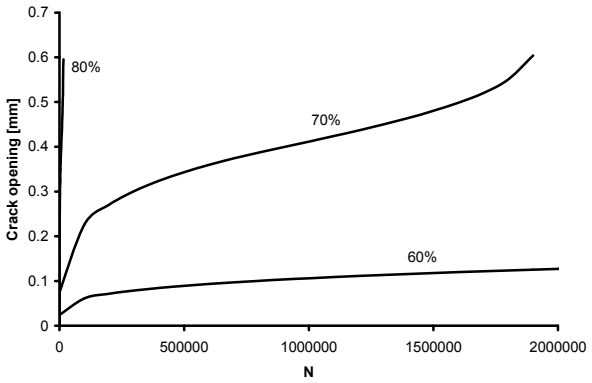

Figure 7.9: Results of the MLM calculations with a gradual stiffness decrease and corresponding strength decrease for notched HSFRC beams.

Figure 7.9 shows the crack widths related to the number of load cycles N for the 60%, 70% and 80% load levels. Again, larger crack widths for higher load levels are predicted, and if failure is reached, then all three characteristic phases of the deformation evolution curve follow from the model. Smaller fatigue lives are predicted compared to the previous calculation with a gradual tensile strength decrease in accordance with the findings of Kessler-Kramer (2002), but this is not surprising, since as already mentioned, the implemented stiffness degradation results in a more severe tensile strength degradation of 0.425 MPa * logN. Here, only the calculations for notched specimens are shown, but calculations for un-notched specimens were also performed and identical fatigue lives are predicted for the same load levels, due to the fact that the applied load levels correspond to a percentage of the modelled peak load.

In the case of an implemented stiffness and corresponding strength decrease, larger crack widths are predicted. Figure 7.10 compares the experimental and modelled crack widths for stress levels of 60%, on the left, and 70%, on the right. The shown experimental curves correspond to the maximum crack widths, that are obtained from the average values and their amplitude that were registered during the experiment. As can be seen, for the 60% load level, the predicted crack widths are smaller than the experimental ones. For the load level of 70%, there is better agreement between the initial and experimental values, but the modelled crack widths are overestimated after this initial phase.

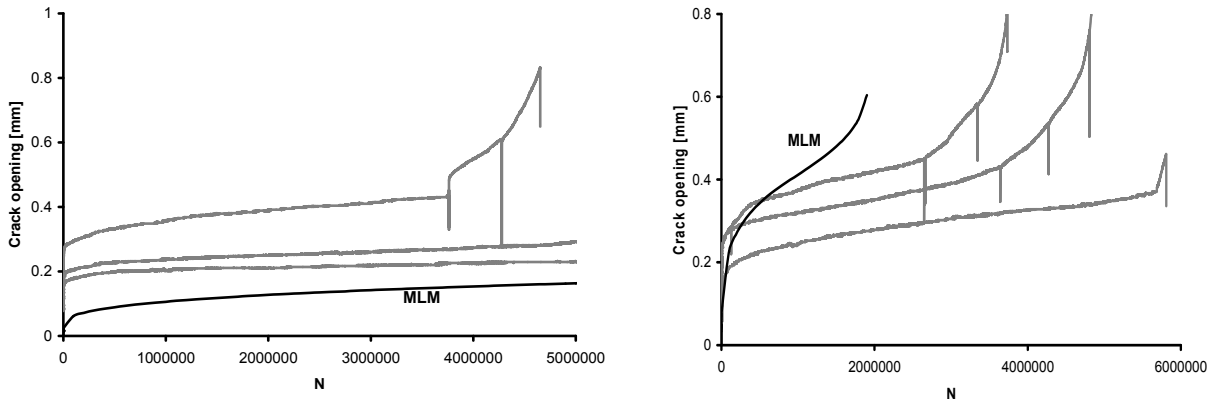

Figure 7.10: Comparison of experimental and calculated crack widths for stress levels of 60% (left) and 70% (right) for notched HSFRC beams.

Since failure was predicted for most calculated load levels with the implementation of gradual stiffness and strength decrease, also modelled 'S-N lines' can be shown, Figure 7.11. These theoretical S-N lines are, with these input parameters, valid for both notched and un-notched beams. In order to put this calculated line into perspective, it is compared to the S-N lines obtained experimentally, for the un-notched beams and for the notched beams, which are also included in Figure 7.11. In this case, the calculated S-N line is closer to the S-N line experimentally obtained for the un-notched HSFRC beams. The latter is also the experimentally obtained line that is statistically more valuable since only a rather limited number of test specimens were tested in case of the notched beams.

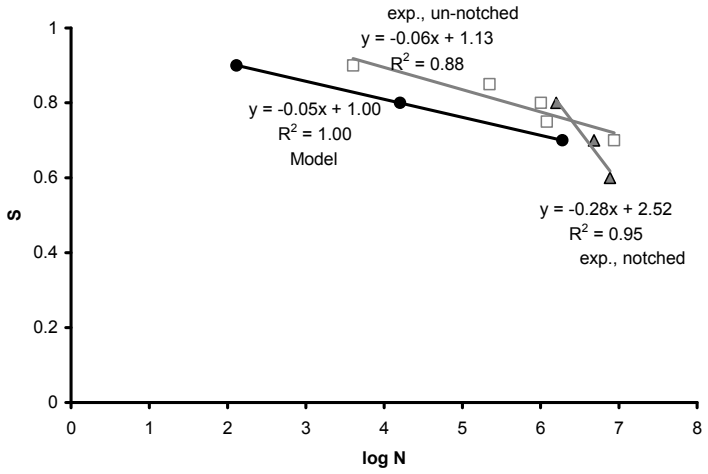

Figure 7.11: Calculated S-N lines for the HSFRC mixture

Further modifications

In the previous calculations, the limit crack width was kept constant; therefore the slope of the softening curve decreased with increasing number of N. This does not

seem very realistic; both cyclic tensile tests, as performed for example by Hordijk (1991), and deformation controlled fatigue tests as performed by Kessler-Kramer (2002), showed that the static envelope curve was followed in case of cyclic tests, and that the limit crack width decreased with increasing number of cycles. Therefore, it seems appropriate to keep the original slope of the stress-crack width relation, and let therefore the limit crack width decrease with increasing number of N, in the fatigue calculations. In the following, calculations were performed with this model, with a gradual stiffness and corresponding strength decrease, and by changing the limit crack width so that the slope remains constant. The tensile input is shown in Figure 7.12, for the initial, static case at N=0 and for $N=10^7$. The compressive input is identical to previous calculations with the shown second variant of the implementation of a stiffness decrease, as shown on the left part of Figure 7.8.

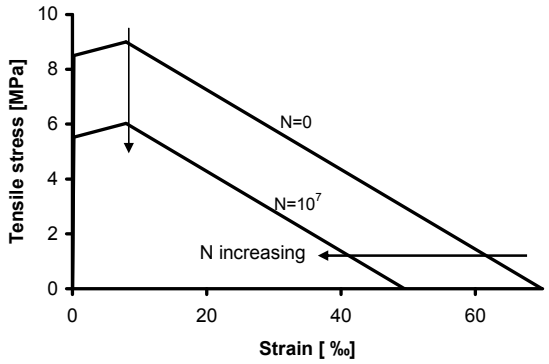

Figure 7.12: Tensile input relation with the limit crack width related to N.

The results of these calculations are shown in Figure 7.13. The calculated fatigue life reduced, but not significantly, compared to the results of the calculations of stiffness decrease with related strength decrease but constant limit crack width. To be precise, 130 load cycles were predicted for an upper stress level of 90%, 14000 at 80%, 1600000 at 70% and no failure up to 10 million load cycles at 60% for both notched and un-notched specimens. These values, when compared to the experimental results, underestimate the average fatigue life of specimens. Since the difference between the implementation of a decreasing ultimate crack width with increasing N did not change the calculated fatigue response significantly, it was chosen not to follow this approach in the final, proposed model for the fatigue bending behaviour of the beams in this study.

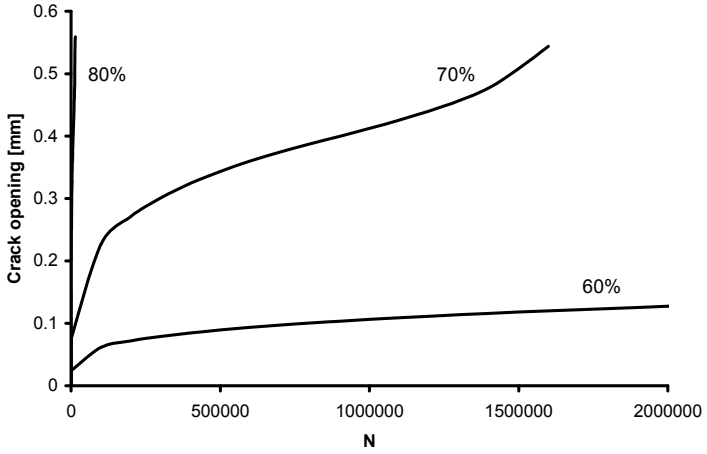

Figure 7.13 Results of calculation with decreasing limit crack width at increasing N

7.2 Proposed fatigue model

In the following, a model will be proposed in order to predict the fatigue life and fatigue deformations, based on the observations of implementation of a gradual tensile strength decrease, as shown in section 7.1.2, and a stiffness decrease, as shown in section 7.1.3. As was shown in the previous section, by implementation of a stiffness degradation, but without decreasing the strengths, as was done in the first variant, the fatigue load bearing capacity was overestimated in the model compared to the experiments. With the second variant, a stiffness degradation with a strength decrease corresponding to the initial strain input values, the opposite was the case, and the fatigue damage accumulation is greater in the model than in the experiments. The scatter in the experimental results hinders the exact reproduction of tests results by the model, but as was shown in section 7.1.2, a gradual tensile strength degradation as observed by Kessler-Kramer (2002) seems more suitable with respect to the predicted fatigue lives, especially with regard to his bi-linear relation with a degradation factor of 0.27*logN. Further, since it was shown that a gradual reduction of the limit crack width has no significant influence on the model, in the proposed model this value was left unaltered at one fourth of the fibre length, at 3.25 mm.

These considerations led to the development of a model that combines the two variants of the implemented stiffness decrease, and leads to a tensile strength decrease as observed by Kessler-Kramer (2002). Basically, the stiffness decrease is kept as described in equation (7.3). The tensile strength is decreased, but this time not to a value that corresponds to the initial linear elastic tensile strain: the tensile strength is chosen to decrease with 0.27*logN, and the linear elastic tensile strain is

gradually increased to match the actual stiffness and strength value for the actual N values. For $N=10^7$, this means that a stiffness of 26 GPa, a linear elastic tensile strength of 6.6 MPa (reduction by 22% of the original value), a hardening strength of 7.1 MPa, and a linear elastic tensile strain of 0.25‰ are reached. The values of the strain where the hardening strength is reached, and the limit crack width are left unaltered. In compression, the compressive strength was decreased, so that at $N=10^7$ the same reduction by 22% was reached as was the case in tension, which results in a decrease of 3.8*logN. The linear elastic strain was increased so that it corresponds to the stiffness and strength values for the actual values of N. At $N=10^7$, the compressive strength has been reduced to 93 MPa, and the linear elastic strain has increased to 3.6‰. The material input relation of the proposed model is shown in Figure 7.14.

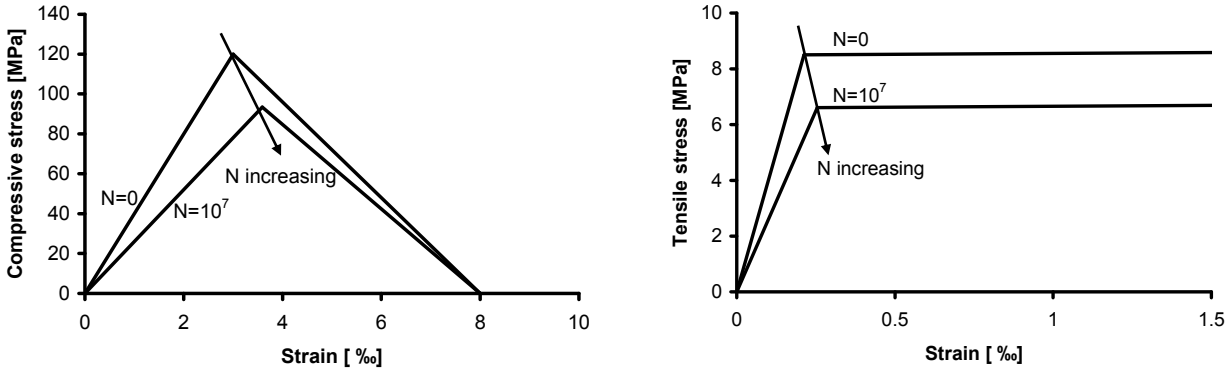

Figure 7.14: Proposed fatigue model: Compressive (left) and tensile (right) material input relation for N=0 and N=10^7.

With the proposed model, fatigue lives of 1500, 2100000, 10^7 and 10^7 (no failure) are predicted for stress levels of 90%, 80%, 70% and 60% respectively, for both notched and un-notched specimens. The predicted fatigue lives are comparable to the results of simulation after implementation of the bi-linear relation of Kessler-Kramer (2002) shown in section 7.1.2, which had the same tensile strength degradation. However, with the proposed model, the deformation values are higher due to the implemented stiffness decrease, and are therefore in better agreement with the experimentally obtained results. Table 7.3 shows, for each upper load level, the predicted number of cycles to failure N, the value of the crack opening w and the deflection δ at failure, together with the average number of cycles to failure from the experimental results. The predicted number of cycles to failure with the proposed model are valid for both notched and un-notched beams. The values for the crack opening and deflection are valid only for notched beams.

Table 7.3: Predicted fatigue lives, crack openings and deflections with the proposed model. Italic values imply that no failure was found.

Load level		90%	80%	70%	60%
Experiments notched	N	-	1583780	4806455	7684815
	logN		6.20	6.68	6.89
Experiments un-notched	N	11464	2577654	*10000000*	-
	logN	4.06	6.41	*7.00*	
Proposed model	N	1500	2100000	*10000000*	*10000000*
	logN	3.18	6.32	*7.00*	*7.00*
	w [mm]	0.595	0.605	*0.190*	*0.055*
	δ [mm]	1.922	2.016	*1.156*	*0.766*

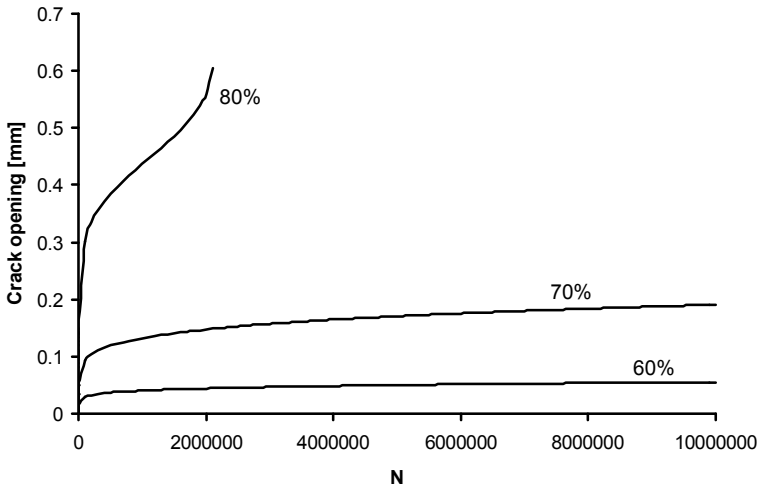

Figure 7.15: Predicted crack width evolution for upper load levels of 80%, 70% and 60% of notched HSFRC beams.

The crack width evolution is shown for the stress levels of 80%, 70% and 60% in Figure 7.15. Figure 7.16 shows the crack openings of the notched beams tested at an upper load level of 80% and the crack widths predicted by the model. The figure shows the maximum experimental crack widths, as derived from the registered mean values and their amplitude during the experiment. Only two experimental results are shown, since the third beam tested at that load level failed rapidly and not enough data points were collected in order to show the complete crack opening evolution. For that upper load level, good agreement between the calculated values and the measured values of one beam was obtained. For load levels of 70% and 60%, the calculated crack widths are smaller than the measured ones. These curves are not shown here, since more emphasis is placed in the measured and calculated strain distributions rather than the displacements, which will be discussed in the following subsection 7.2.1.

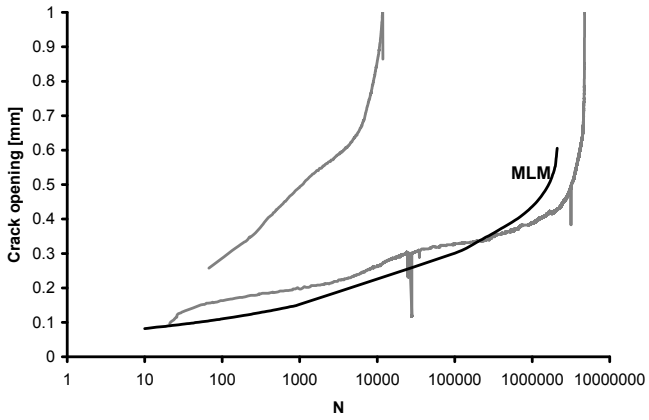

Figure 7.16: Crack opening evolution of the notched HSFRC beams at a load level of 70% and as predicted by the proposed model.

7.2.1 Modelled and measured fatigue strain distributions

So far, the modelled fatigue results have been discussed with regard to the expected number of cycles to failure at a certain load level and the crack openings. In this part, the strain distributions, as modelled with the proposed fatigue model and as measured in the fatigue experiments, will be discussed. Only results of notched specimens will be regarded, since only in that case deformations were measured in the compressive zone of the beam.

The following figures, Figure 7.17, Figure 7.18 and Figure 7.19, show the measured and modelled compressive and tensile strain distributions. In grey, the experimentally measured strains are shown, as registered with LVDTS over a length of 100 mm at the top of the beam (compression) and at notch tip (tension). The 'strains' shown are the measured deformations divided by the measuring length, which implies that the measured strains are the average strains over the measuring lengths, and peaks due to localisation of the compressive zone above the crack, that can be very localised, cannot be registered. However, such localisation effects occur close to failure, therefore for the major part of the fatigue experiment, for most of the specimen's fatigue life, the strain registration is accurate. For the stress level of 80% only two experimental results are shown, since the third one experienced rapid failure and not enough data points were collected in order to show the complete strain evolution. In black, the strain distribution of the multi-layer model calculations are shown. As can be seen, the predicted strains are in fairly good agreement with the experimentally measured values for the stress levels of 80% and 70%, and are slightly under the measured values for the stress level of 60%. Concluding, it can be said that the proposed model is able to describe the strain evolution during a fatigue experiment, in reasonable agreement compared to the experimentally obtained strains.

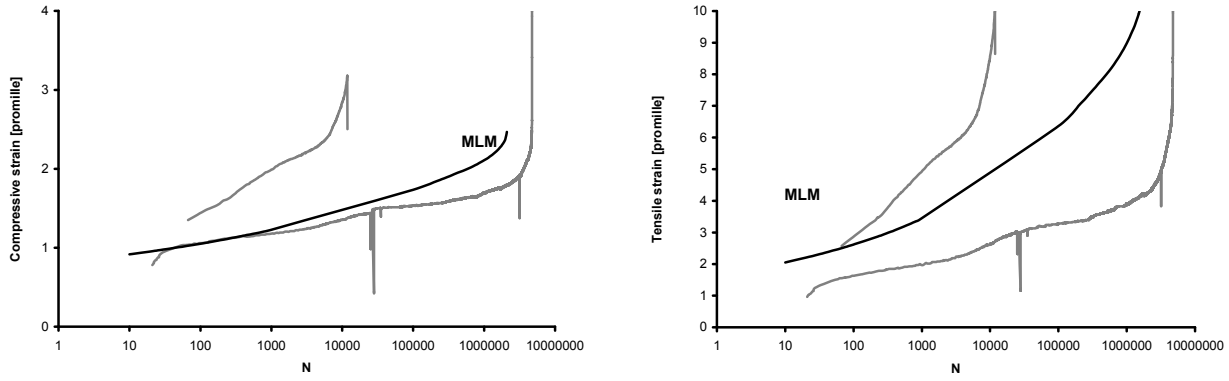

Figure 7.17: Measured and modelled compressive, on the left, and tensile, on the right, strain evolution for an upper stress level of 80%.

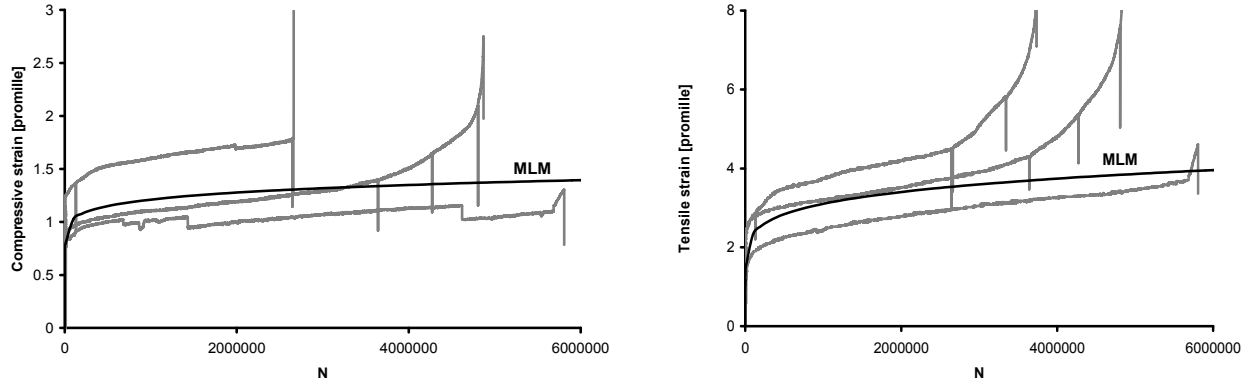

Figure 7.18: Measured and modelled compressive, on the left, and tensile, on the right, strain evolution for an upper stress level of 70%.

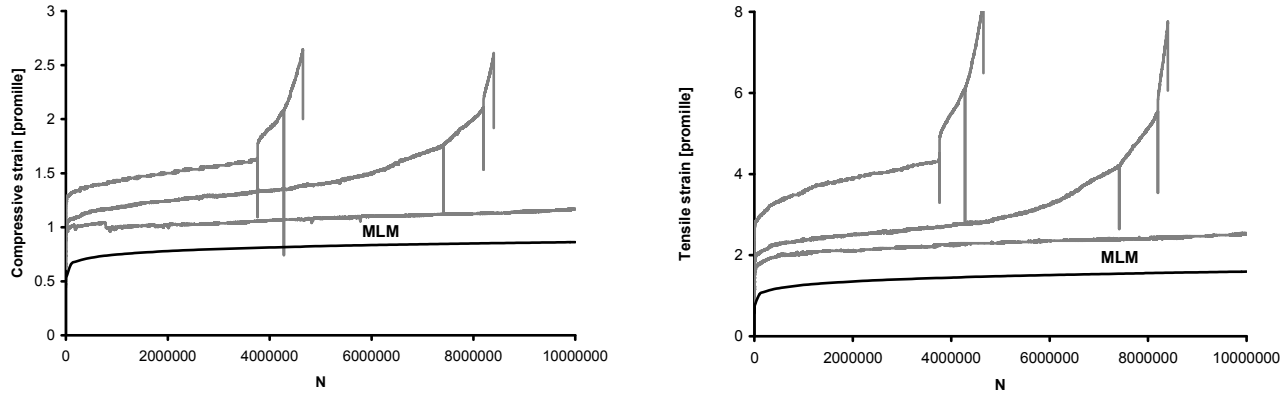

Figure 7.19: Measured and modelled compressive, on the left, and tensile, on the right, strain evolution for an upper stress level of 60%.

7.3 Discussion

The chosen fatigue modelling approach is more a quantitative than a qualitative approach, and is kept simple. This approach is, although simple, capable of showing the effects of fatigue loading, as observed in the experimental part of this study. The same multi layer model, that was used to model the static bending tests, was used for fatigue modelling with appropriate modifications. A cycle-dependent input has to be implemented to take account of the effects of fatigue loading, that was initially set to a cycle dependent decrease of the tensile strength, which has been confirmed by other researchers who performed deformation controlled uniaxial tensile fatigue tests. This approach was eventually modified into a gradual stiffness decrease together with a strength decrease, and resulted into a proposed model that is capable to reproduce the measured strains during a fatigue experiment.

Of course, this is a simplified approach and certain parameters, that have an effect on fatigue loading (see Chapter 5), are not taken into account. These parameters are mainly the loading frequency and the lower load level; however, these parameters were also kept constant in the experiments, therefore their influence is not regarded in the scope of this study. Furthermore, the model uses only a simplified history of damage on the system; for every value of N, the input parameters were adapted in accordance, and calculations were performed as if a new beam with these material input characteristics was loaded statically at the assumed load value. Therefore, it is not surprising that the model might overestimate, rather than underestimate, the fatigue performance of a beam. Time related effects, such as creep during an experiment, are included globally in the model in the chosen stiffness decrease relation, and not from a micromechanical point of view. Nevertheless, even with such a global approach, basic failure mechanisms can be shown, and this approach can also be transposed to other structural elements and into other models, such as finite element codes. For larger elements, such a model can serve in order to show sections or part of structures that are most prone to fatigue.

It should be noted that the simulations were stopped at 10 million load cycles since this was the maximum value of load cycles of the experiments, and also in order to save computational time. Also, 'failure' in the model means that the applied value of the inner moment, corresponding to the upper load level, cannot be reached with the input parameters valid for a certain number of cycles. In all calculations, failure, meaning that the applied moment was not reached, was due to insufficient load bearing capacity in tension; also this is in agreement with the experiments, where always a flexural tensile failure, and never a compressive failure, was observed in the fatigue bending tests.

Not many fatigue models for concrete exist up to now. In most design regulations, design verifications are included in the form of stress limitations with the help of suitable S-N lines. The Model Code 90 (MC90, 1993) includes such

verification for concrete in both compression and tension. Apart from that, the fatigue behaviour can be approached by cyclic stress-strain relations, as defined by Gylltoft (1983), Yankelevsky and Reinhardt (1987) and Hordijk (1991), or similar relations based on rheological material models as proposed by Duda (1991) or Kessler-Kramer (2002) for plain concrete. For fibre reinforced concrete, Matsumoto and Li (1999) developed a fracture mechanics based model for fatigue of fibre reinforced concrete. Cachim (1999) used a viscoplasticity model, based on the envelope curve concept, implemented into a finite element code, to model the fatigue behaviour of fibre reinforced concrete. Zhang et al. (2001) developed a fatigue crack bridging model in tension for plain concrete, with a similar stress degradation function as observed by Kessler-Kramer and given in equation (7.1). The difference of their degradation law is that it is not only given in dependence of the number of cycles to failure, but also of the maximum crack width. The factors in the model are directly related to results of deformation-controlled fatigue tests. This relation was further adapted for ECC materials by Matsumoto et al. (2004) and Suthiwarapirak (2003) in accordance with their experimental results. Suthiwarapirak (2003) included the derived strength decrease relation for ECC materials into a finite element code in order to predict the fatigue life of overlay systems, therefore used a similar approach for the prediction of the fatigue behaviour of a structure as is proposed in this chapter, only without including a stiffness degradation. However, experiments have shown that fatigue loading causes a stiffness degradation, which promotes the use of a model as proposed in this thesis. A subject for further research would be to further refine the input parameters of the model, and possibly extend them into a microscale mechanical model. For this, deformation controlled fatigue tests would be necessary in order to obtain suitable input parameters.

7.4 Conclusions

Concluding, after these calculations and considerations, the proposed model seems suitable to show the failure mechanisms and deformation evolutions of a fatigue loading process. The proposed model consists of a gradual stiffness decrease, with its value at ten million load cycles in accordance with the decreased stiffness as obtained from run-out specimens. An in-between case of the two variants of a stiffness decrease implementation, as documented in section 7.1.3, was chosen, with the decrease in tension chosen to a value of 0.27*logN, a value that seemed most suitable for reproducing the experimental results. The main conclusions, that can be drawn, are:

- All three phases during the deformation evolution in a fatigue experiment can be modelled. Therefore, the model is capable of showing the typical deformation evolution curve, or cyclic creep curve, of fatigue experiments.

- The deformation values depend on the upper load level, a fact hat has been confirmed by the fatigue loading as well. This also further rules out the function of the static load-deformation curve as an envelope curve for the fatigue experiments, since in that case, the deformations at a lower value of the upper load level have to be larger than at a higher value.
- The fatigue lives, as compared to the experimental results, are in better agreement with the results of the tests on un-notched specimens than of the notched ones, and no failure is predicted up to ten million load cycles at an upper stress ratio of 0.7. Also, the modelled and calculated deformations and strains are within the scatter, or at least close to registered values, of the experimental results.
- In the model, failure was always the case due to insufficient tensile load bearing capacity, which is also in accordance with the failure as observed in the fatigue bending tests.
- The model uses as an upper load level a percentage of the peak load, as determined with the same model in the static case (Chapter 6). Therefore, it does not correspond to the exact upper load value for the experimental testing, however the value is not far from it. An additional reason for the obtained differences between the modelled and experimental results can also lie in the fact that in the experiments, since the exact value of the flexural tensile strength is not known, the applied fatigue loading might correspond to a different percentage of the static load than assumed.
- The proposed modelling approach can easily be implemented into other material models, such as finite element codes, and serve for a fatigue evaluation for larger structural elements.
- Even though only results for the HSFRC mixture were shown, the results are valid and can be applied to the other two mixtures of this study as well. This is mainly due to the fact that in the model, the upper load level was set to correspond to a percentage of the calculated peak load by the static model, and not to the load value set as an upper load level in the experiments.

References

CACHIM, P. B. (1999) Experimental and numerical analysis of the behaviour of structural concrete under fatigue loading with applications to concrete pavements. *PhD Thesis.* Faculty of Engineering of the University of Porto.

DUDA, H. (1991) Bruchmechanisches Verhalten von Beton unter monotoner und zyklischer Zugbeanspruchung. *PhD Thesis. Heft 419, Deutscher Ausschuss für Stahlbeton. Beuth Verlag GmbH.*

GYLLTOFT, K. (1983) Fracture mechanics models for fatigue in concrete structures. *PhD Thesis.* Lulea University of Technology.

HORDIJK, D. A. (1991) Local approach to fatigue of concrete. *PhD Thesis.* Delft University of Technology.

KESSLER-KRAMER, C. (2002) Zugtragverhalten von Beton unter Ermüdungsbeanspruchung. *PhD Thesis.* Universität Karlsruhe (TH).

MATSUMOTO, T., CHUN, P. & SUTHIWARAPIRAK, P. (2004) Effect of fiber fatigue rupture on bridging stress degradation in fiber reinforced cementitious composites. *Fracture mechanics of concrete structures, FraMCos 5.* Vail, Colorado, USA.

MATSUMOTO, T. & LI, V. C. (1999) Fatigue life analysis of fiber reinforced concrete with a fracture mechanics based model. *Cement and Concrete Composites,* 21**,** 249-261.

MC90 (1993) Model Code 1990. CEB Bulletin d'Information No 203 ed., Comite Euro-International du Beton CEB-FIP.

SUBRAMANIAM, V. K., O'NEIL, E. F., POPOVICS, J. S. & SHAH, S. P. (2000) Crack Propagation in Flexural Fatigue of Concrete. *Journal of Engineering Mechanics,* 126**,** 891-898.

SUTHIWARAPIRAK, P. (2003) Fracture mechanics based fatigue life analysis of RC bridge slabs repair by fiber cementitious materials. *PhD Thesis.* The University of Tokyo.

YANKELEVSKY, D. Z. & REINHARDT, H. W. (1987) Response of plain concrete to cyclic tension. *ACI Materials Journal,* 84**,** 365-373.

ZHANG, J., LI, V. C. & STANG, H. (2001) Size Effect on Fatigue in Bending of Concrete. *Journal of Materials in Civil Engineering,* 13**,** 446-453.

8.

Conclusions and recommendations for further research

The recently developed high and ultra high strength fibre reinforced concretes are promising new materials that are expected to find more applications in the near future. These could be thin, slender structures, with daring new shapes, elements with reduced total amount of reinforcement, or heavily loaded structures and offshore structures, which can be prone to fatigue. This thesis contributes in further promoting the use of these materials by evaluating and showing, experimentally and through appropriate material models, the bending behaviour under static and fatigue loads, for three exemplary mixture compositions.

In this chapter, the main conclusions are highlighted and recommendations for further research are given. This thesis deals with the static and fatigue behaviour in equal parts; and conclusions on both parts will be given. However, these parts cannot be considered completely independent: in order to correctly evaluate the fatigue behaviour, the static behaviour has to be known. Therefore, the fatigue experiments and modelling are directly based on the prior static experiments and calculations and cannot be regarded separately.

In this thesis, the results were presented in the following way. First, a general introduction was given (Chapters 1-3), which included an introduction to the objectives of the research (Chapter 1), the mixtures used (Chapter 2) and the experimental programme (Chapter 3). Then, in the experimental part, Chapters 4 and 5, the results of the static tests (Chapter 4) and fatigue tests (Chapter 5) are presented. Last, in the modelling part in Chapters 6 and 7, an analytical equilibrium based model (the multi-layer model) has been used to model the experimental results. Chapter 6 shows the input parameters for the model in the static case, for the three mixtures of this study, and compares the calculated beam response to the experimentally obtained one. Chapter 7 shows, exemplary on the HSFRC mixture only, how the model can be adapted to account for fatigue loading. A new model is proposed, that is capable of showing all three stages of the fatigue deformation evolutions, including a prediction of failure. With the proposed model, the calculated

and measured strains and deformations are in reasonable agreement. The main conclusions that can be drawn are therefore taken from Chapters 4-7, the part of this thesis that contains results. More detailed conclusions can be found at the end of these four chapters. Here, only the main aspects will be summarised.

In the following, a brief summary of the experimental programme and the modelling approach will be given, as a reminder, before proceeding to the main conclusions of this study. Two high strength concretes, named HSFRC and hybrid HSFRC, and one ultra high strength concrete, named BSI/CERACEM, were tested in this study. For a joint durability-fatigue research, a collaboration with the university of Karlsruhe, also a second ultra high strength concrete, in this thesis named UHPC, was tested. The main testing method was the four point bending test on un-notched beams of dimensions 125/125/1000 mm, which were tested at a span of 750 mm, loaded in their third points. This method was used for both static and fatigue tests for all four mixtures. The fatigue tests were performed with a constant upper-to-lower load ratio of 0.2 and at a frequency of 10 Hz. The upper load was set to a percentage of the previously determined static load, ranging from 50% up to 90%. For the main mixture of this study, the HSFRC, also static three point bending tests on notched beams, static and fatigue four point bending tests on notched beams, and uniaxial tensile tests were performed. The experimental results were evaluated with an analytical model, the multi-layer model. It was shown that the model is suitable for all three mixtures, and suitable tensile material input relations was obtained by results of uniaxial tensile tests. The model can be used to predict crack openings but also deflections, of both notched and un-notched bending tests. The model was adapted into a proposed model for fatigue, that contains a gradual stiffness decrease and a gradual strength decrease with increasing number of load repetitions. With these adaptations, the model was found suitable to show the deformation evolution and failure mechanism at fatigue loading.

8.1 Conclusions

8.1.1 Static bending behaviour

The static tests show that the BSI/CERACEM, the HSFRC and the hybrid HSFRC were all able to allow an additional load increase after the linear elastic stage; they are all deflection-hardening materials but also strain hardening materials in uniaxial tension. Only the UHPC developed and cast at Karlsruhe University within the scope of the joint experiments did not show this characteristic, due to the shorter fibres and the different fibre orientation. This different fibre orientation came as a consequence of the vibration needed for compaction of the fresh concrete. The UHPC was the only mixture in this study that was not (entirely) self-compacting.

In general, for the materials that provide a strain or deflection hardening, this is better visible in case of material tests on un-notched specimens. However, tests on notched specimens can give a good description of the descending branch and the crack opening of the major crack. For a good evaluation of the material behaviour for such strain hardening materials, it is advisable to perform tests with both notched and un-notched specimens, if possible.

Further, it was found that the flexural tensile strength depends on the applied fibre volume fraction in the mixture (when the mixtures are compared globally among each other) and on the amount of fibres present in the critical beam cross section (when individual beam results of one mixture are compared). The effect of the fibre concentration in a cross-section on the strength is more pronounced than that of the fibre orientation. Factors that influenced the fibre orientation in the three self-compacting mixtures, were the flow direction (both primary and secondary), the flow along formwork boundaries (wall-effect), gravity effects (segregation), as well as the falling height of the concrete poured into the moulds.

The static tests were modelled with the use of an analytical equilibrium based multi layer model. The model was used on the HSFRC, the hybrid HSFRC and the BSI/CERACEM and was able to reproduce the experimental results in good agreement with respect to the crack openings and the deflection. The tensile input parameters were modelled in accordance with uniaxial tensile tests. Only in the case of the HSFRC these uniaxial tests were performed in this study. For the other two mixtures, available results from other researchers were taken. This is the main reason why the model was better suitable for the HSFRC, even though also for the other two mixtures the model showed reasonable agreement with the experimental results. The model, in general, is better suitable for the behaviour notched beams, since the model only accounts for the formation of one crack at midspan. However, its use for un-notched beams in this study is justified by the fact that at the postpeak stage, crack localisation always occurred in a single crack. The model predicts the crack opening from the modelled tensile strain at the bottom part of the beam. The deflection was modelled from a linear elastic part, derived from equations of a simply supported beam, and an inelastic part, that was derived from rigid body kinematics that depend on a variable rotation depth that is proportional to the crack length. In case of un-notched beams, the inelastic deflections during the deflection hardening phase could only be modelled if the rotation depth was kept at a constant value. The experiments confirmed a constant value for the rotation depth in that phase. However, it was also shown that the deflection hardening of the un-notched beams can be modelled with an alternative approach, derived from a combination of material input relations of multiple cracking and single cracking materials.

8.1.2 Fatigue bending behaviour

Even though it is common that fatigue experiments are accompanied by a large scatter, as was also the case in this study, which makes the drawing of definite

conclusions difficult, still a number of conclusions can be drawn from the experimental results in this study. First of all, it was found that a better workability in the fresh state leads to a smaller scatter in the materials' mechanical properties and therefore also reduces the scatter in the fatigue results. The HSFRC mixture had the best workability and flowability in the fresh state, and this was also the mixture that demonstrated the most favourable fatigue performance in terms of the applied load ratio (upper load level divided by the static peak load) and the sustained number of load cycles to failure. Compared to the fatigue performance of normal strength unreinforced concrete, only the HSFRC showed an improved fatigue performance with regard to plain concrete, showing no failure for upper load levels lower than 70%. The study further showed that it is not by definition the material with the highest static strength, which in this study was the BSI/CERACEM, that will have the best fatigue performance. In this case the BSI/CERACEM had a poorer fatigue performance than the HSFRC, mainly due to the fact that this mixture had the highest scatter in the static strength, which was, among others, also related to the poorer workability of this mixture compared to the two HSFRC mixtures. In fatigue, the fibre orientation and concentration seems to be of less importance, at least compared to the role of these parameters in the static performance. The microscopical observations provided valuable insight in the quality of the three mixtures, the observed bond between fibre and matrix, and on local inhomogeneities of the w/c ratio and air content.

Two aspects of fatigue loading that were discussed with the results of the fatigue tests were the possible presence of a fatigue limit, which is a certain load threshold below which specimens will not fail, and the function of the static load-deformation curve as an envelope curve to predict when a fatigue specimen will fail. Regarding the presence of a fatigue limit, this was observed for the two HSFRC mixtures but not for the BSI/CERACEM. Also, the static load deformation curve does not function as an envelope curve for the fatigue experiments, at least not in terms of deflection, crack opening and compressive strains, which were regarded in this study. The only definite relation that was observed between deformations and failure was a unique relation between the slope of the deflection at the second stage of the experiments and the number of cycles to failure, which is valid for all three mixtures.

A joint durability-fatigue testing programme was performed in collaboration with the university of Karlsruhe. These tests were still under completion at the time this thesis was written. However, from the preliminary results, it can already be concluded that the mixtures have an excellent durability and can resist 200 freeze thaw cycles without showing any visible signs of deterioration or spalling of the surface and no significant decrease in their load bearing capacity.

A model, based on the multi-layer model with implementation of a cycle dependent material input, consisting of a gradual stiffness and strength decrease, is proposed. The model can show all three phases during the deformation evolution in a fatigue experiment, and can predict failure when no equilibrium is possible after a

certain reduction of the input properties. The model shows that the deformation values depend on the upper load level, a fact hat has been confirmed by the experiments. This also, just as observed in the experiments, rules out the function of the static load-deformation curve as an envelope curve for the fatigue experiments. In the model, failure always occurred due to insufficient tensile load bearing capacity, which is also in accordance with the failure as observed in the fatigue bending tests. The model predicts the fatigue strain evolution in good agreement with the experimentally measured strain evolution of notched beams.

8.2 Recommendations for further research

Research is a long lasting process, and even at the end of a project the results often show the need for additional studies and experiments. It is not surprising that also this study, even though it provides answers and a modelling solution for the static and fatigue bending behaviour of high and ultra high strength fibre concrete, also yields a number of new research questions. The main goal when utilising these materials, however, is to promote them into new applications, and establish them in the building industry. In that aspect, the most important continuation of this study is for it to result in design guidelines and recommendations. At the time this thesis was written, it seems that this goal is in the process of being reached: already, first interim regulations exist on ultra high performance materials (AFGC-SETRA, 2002) or ECC materials (JSCE, 2005), or are in the process of being established (DAfSTB, 2005). Also, international committees and task groups have been formed, such as the task group on ultra high strength concrete of the *fib* (federation international du beton), that are intending to publish international design guidelines for ultra high strength concretes in the near future.

A joint fatigue durability experimental programme was started within this study, which will be completed in the work of Dipl.-Ing. Jennifer Scheydt. This thesis has to mention her work, which is expected to be completed in 2009, as a continuation of this study with regard to the durability of such ultra high strength mixtures. The present study showed the mechanical durability in terms of fatigue, while hers will show the environmental durability in terms of freeze-thaw resistance and chloride attack. This environmental durability, from the results obtained so far, already seems exceptional for these mixtures, and by far superior to normal strength concrete.

The microscopical study showed that all three mixtures cast in Delft can be further improved in order to achieve a more homogeneous binder and a better bond between the fibres and the matrix. In that aspect, a more extensive microscopical study, not only limited to three specimens, will be useful to further support these findings. Combined with a mixture optimisation study it will further improve the mixtures, and by improving the bond between the fibres and matrix the structural behaviour will be better, not only for static loading but also in fatigue. In that aspect,

also static and cyclic single fibre pull-out tests will provide further insight in fibre crack bridging and stress transfer.

In this study, only experiments on beams without rebar reinforcement were performed. However, in real structural full-scale applications it is more likely that these materials will be used with a combination of steel fibres and rebars, where the steel fibres might even replace the transverse and shear reinforcement. This is another point of further research, which would also imply experiments on larger scale structural elements.

Regarding fatigue and fatigue failure mechanisms of concrete and similar cementitious materials, there is still a need for fundamental research on plain concrete (without fibre reinforcement) in order to fully understand the damage mechanisms. Influences of the frequency and the moisture content are parameters that were not regarded in this study but should be included in future studies. Coupling of moisture, corrosion and fatigue is an interesting fundamental research field for structures exposed to natural environmental conditions. Also, in order to further evaluate the fatigue performance of these high strength fibre concretes and establish a more detailed, micromechanical or rheological model, results of a deformation controlled fatigue testing series would be an additional aid.

This thesis contained a significant experimental part, and a modelling part with input parameters on a macro-scale. In the future, this model has to be expanded into a more detailed meso- and micro scale model for a complete understanding of the material.

Further, one should not forget that these high strength fibre materials, are considerably more expensive compared to conventional concrete, and this is an additional reason these materials have not found many large scale applications so far. The higher costs lie in the steel fibres, the high cement content, and the use of expensive fillers and additives. Moreover, the high cement content does not classify these mixtures as environmentally friendly, since high CO_2 emissions are released during the cement production. These considerations result into two additional points for research. First, further optimisation of the mixtures, finding mixtures with the least fibre and cement content but still meeting the demands on material strengths and durability. Second, by developing a design approach that includes the expected service life and maintenance costs: These mixtures are very durable, and a longer service life and less maintenance costs can be expected. If these considerations are included in the design process, then these mixtures would not be as expensive as they appear to be when only the material and production costs are regarded and compared to normal strength concrete.

References

AFGC-SETRA (2002) Béton fibrés a ultra-hautes performences, recommandations provisoires.

DAFSTB (2005) Sachstandbericht Ultrahochfester Beton, Betontechnik und Bemessung. Deutscher Ausschuss für Stahlbeton. Stand: 2005-03-12 (draft version). Beuth Verlag GmbH.

JSCE (2005) Tentative Guideline for Design and Construction of Engineering Cementitious Composites ECC (Draft). Japanese Society of Civil Engineers (JSCE). JSCE TC 334.

Symbols and Abbreviations

Latin Capital Characters

$A^{*}_{debonding}$	Surface area under the fibre pullout diagram
A_f	Cross-sectional area of fibres
A^{f}_{fr}	Surface area of fibre exposed to action of frictional stress
E	Young's modulus
E_0	Initial value of Young's modulus at N=0
$E_{1\text{-}2}$	Energy needed to form the first through crack
$E_2 = E_3 = E_n$	Energy required to create a new through crack
E_c	Young's modulus in tension
E_f	Modulus of elasticity of fibres
E_N	Load cycle dependent value of Young's modulus
F_{max}	Upper load value in a fatigue test
F_{min}	Lower load value in a fatigue test
F_{static}	Peak load in a static test
G	Fracture energy
G_F	Fracture energy
G_{II}	Fracture energy during debonding process
G_m	Matrix fracture energy
H	Rotation height
I	Second moment of inertia
L_f	Fibre length
M	Bending moment
N	In Chapter 4: Counted number of fibres in cross section
N	In Chapters 5&7: Number of load repetitions in a fatigue test, fatigue life
N	In multi-layer model: resulting inner normal force
N_f	Theoretical number of fibres in cross section according to the fibre volume content of the mixture
N_u	Number of load repetitions up to failure

P	Force, Load
P_d	Frictional pullout force
R	Lower to upper load ratio
S	Stress or load ratio, ratio between the upper load (stress) level and the static peak load (strength)
U_{db}	Debonding Energy
ΔU_{fm}	Decrease in matrix strain energy
$\Delta U_{f\text{-}mc}$	Increase of fibre strain energy
$\Delta U_{f\text{-}mu}$	Increase in fibre strain energy multiple cracking
ΔU_{fr}	Frictional energy between fibres and matrix
V	Coefficient of variation
V_{ef}	Effective volume quantity of fibres
V_f	Applied fibre volume quantity
V_m	Matrix volume fraction

Latin Small Characters

a	In Chapter 4: Major axis of ellipse (ellipse = visible fibre in cross section)
a	In Chapter 6: notch depth
a	In Jungwirth's parabolic softening relation for BSI/CERACEM: experimentally obtained parameter
a	In Chapter 7: stiffness degradation factor
b	In Chapter 4: Minor axis of ellipse (ellipse = visible fibre in cross section)
b	Beam height
b	In Jungwirth's parabolic softening relation for BSI/CERACEM: experimentally obtained parameter
c	In Jungwirth's parabolic softening relation for BSI/CERACEM: experimentally obtained parameter
d_0	density of concrete at demoulding
da/dN	Slope of crack width increase in second stage of fatigue crack width evolution curve
Δd	Fibre-matrix slip
d_{max}	Maximum aggregate size (diameter)
ds	solid density of granular mixture
f	Testing frequency of a fatigue test
f_{ccd}	Design value of compressive strength (EC2)
$f_{ct,0}$	Initial value of the tensile strength at N=0
$f_{ct,ax}$	Uniaxial tensile strength

$f_{ct,hard}$	Hardening strength
$f_{ct,N}$	Load cycle dependent tensile strength
h_i	height of an individual layer
h_{lig} or h	Effective beam height (ligament height)
l	Span length
l_i	Influence length used in multi-layer model
l_m	Measuring length
n	Number of layers used in the multi layer model
n	In Chapter 6: number of cracks
r	Fibre radius
w	crack opening
w/b	water to binder ratio
w_0	Critical crack width in Hilleborg's fictitious crack model
w_0	In bi-linear softening relation: ultimate crack width
w_c	In bi-linear softening relation: crack width at intersection point
x	Average of test values

Greek Characters

α	Ratio between matrix and fibre E modulus multiplied by corresponding volume fraction
β	Material constant (empirical) of the Aas-Jacobsen fatigue relation
δ	According to context, deflection or displacement
δ_{el}	Elastic deflection
δ_{mu}	Measured displacement at first through crack
dδ/dN	Slope of deflection increase at second stage of fatigue deflection evolution curve
ε_{cc}	Compressive strain (definition in accordance with EC2)
ε_{cc1}	Elastic limit strain in EC2 parabolic relation
ε_{cc1u}	Ultimate limit strain in EC2 parabolic relation
ε_{cc2}	Elastic limit strain in EC2 linear relation
ε_{cc2u}	Ultimate limit strain in EC2 linear relation
ε_{ct}	Tensile strain
ε_i	initial strain
ε_{mu}	Strain at which first through crack is formed
η	Dimensionless fibre orientation factor
θ	out-of-plane angle of a single fibre in regarded cross-section
θ_i	out-of-plane angle of an individual fibre i

σ	Standard deviation
σ_{cc}	Compressive stress (definition in accordance with EC2)
σ_{ct}	Tensile stress
σ_{max}	Upper stress level in a fatigue test
σ_{min}	Lower stress level in a fatigue test
τ_f	Average frictional stress at fibre matrix interface
φ	in-plane angle of a single fibre in regarded cross-section
ϕ	Rotation angle

Abbreviations

AC	Alternating Current
BSI	Beton Special Industriel (Special Industrial Concrete)
BSI/CERACEM	One industrial ultra high performance concrete, and one of the four mixtures used in this study
CARDIFRC	One ultra high strength concrete developed at Cardiff University, not used in this study
$CEMTEC_{multiscale}$	One ultra high strength concrete developed at the LCPC, not used in this study
CMOD	Crack Mouth Opening Displacement
CT	Computerised Tomography
DUCTAL	One industrial ultra high performance concrete, not used in this study
ECC	Engineered Cementitious Composites, very ductile group of concretes
HFRC	High Strength Fibre Reinforced Concrete, used name for one of the four mixtures in this study
HPFRCC	High Performance Fibre Reinforced Cementitious Composites, term defined for strain hardening fibre concretes
hybrid	The term hybrid in this study is used to refer to mixtures with utilisation of different fibre lengths
hybrid HSFRC	Hybrid High Strength Fibre Reinforced Concrete, used name for one of the four mixtures in this study
LVDT	Linair Variable Displacement Transducer
MLM	Multi-layer model
RH	Relative Humidity
RPC	Reactive Powder Concrete
UHPC	Ultra High Performance Concrete, and used name for one of the four mixtures of this study

CURRICULUM VITAE

Eleni Sofia (Lena) Lappa was born in Darmstadt, Germany, on the 23rd of July 1976. She followed her parents to Athens, Greece in 1980 where she eventually graduated from the German School of Athens in 1994. In October of the same year she returned to her birthplace and started her studies of Civil Engineering at Darmstadt University of Technology, where she eventually received her Diploma in 2001, specialising in Structural Mechanics. During her studies, she was able to spend a few months at Delft University of Technology, which set the stage for her Ph.D. research at the concrete structures group conducted from November 2001 – February 2007, under the tutelage of Prof.dr.ir. J.C. Walraven and dr.ir. C. van der Veen. The research resulted in this thesis, her first book. In April 2007, she joined Shell Exploration & Production Europe, located in Assen, the Netherlands, as a structural engineer for offshore structures.

ACKNOWLEDGEMENTS

This thesis was the result of a long struggle, a struggle with mainly me but also other external factors. That you can read this now means that the struggle finally reached its end. It was a long journey, but as the great poet C.P. Cavafy states in his work 'Ithaka', it is the journey that makes it worthwhile, not the destination itself. The journey would not have been possible without the contribution of a great number of people:

First of all I have to thank my promotor, Joost Walraven, for giving me the opportunity to join his group and giving me this challenging research project. He was always able to lift my spirits while I was in despair with my data, and I am very grateful for that. I also acknowledge the opportunity to work in the fib task group on ultra high strength concrete and want to express my gratitude to all committee members for the interesting discussions and communications we had during the meetings. Without the supervision of Cor van der Veen I doubt I would have been able to finalise this thesis. The experiments of this study could not have been performed without the help and technical expertise of the laboratory personnel, as of Ron Mulder, Rene van der Baars and Ton Blom for the casting of the specimens and Albert Bosman, Ger Nagtegaal, Arjen van Rhijn, Fred Schilperoort, Michel van Aggelen, Kees van Beek and Edwin Schaars for conducting the experiments.

This research could not have been completed without the financial support of the Technology foundation STW, and in that aspect I would like to thank Magriet Janszs and the members of the user's committee for the fruitful meetings. The materials needed for one of the mixtures were provided by Sika, and I would like to thank Isabelle Lallemant, Sandrine Chanut and Thierry Thibaut for their time.

I am happy that this research contains collaboration with Karlsruhe University, and I hope this will be the beginning of an ongoing collaboration. Thanks to Jennifer Scheydt, dr. Gunter Herold and professor Harald Müller for their contribution.

I would like to express my gratitude to the thesis committee members for their interest and valuable comments on my work. Especially professor Jan Woerner, who reserved time for my defence despite being one of the busiest persons I know.

All my colleagues I met at the concrete structures group, and especially the PhD researchers, for technical (and not only) discussions, coffee breaks and drinks. Thanks Maya, Cees, Ye, Steffen, Petra, Eddie, Herbert (to you a special thanks for the help with the Dutch translations in this thesis), Sonja, Eelke, Roy, Ivan.

If I learned something during my time at university is that help is not something one can take for granted. Help was not always found where it was expected, and I am more than grateful for everybody who supported me, professionally and personally. In this aspect I would like to mention Rob Polder, Timo Nijland, Thomas Voigt, Surendra Shah, Nilufer Ozyurt, Marko Orgass. I was fortunate to participate in a number of technical conferences and courses, and meet other researchers with whom we extended concrete discussions into the small hours. Thanks to Yvette Klug, Holger Schneider, Kai Bunje, Essayas Gebreyouhannes, Miguel Azenha, Alberto Meda, Zila Rinaldi, Juergen Huber, Dirk Lowke, Petra Rucker, Alex Karakas, Joerg Jungwirth, to name a few.

Delft and the Netherlands can be a very depressing place, especially in cold and grey winter months, if not for the sake of friends that I had the honour to meet: Nikolai, Åse, Sandra, Thorsten, Konca, Julia, Astrid, Alex, Luuk, Nico, Stephan, Ali, Mike, Helen, Alexis, Giampietro, Tamara, Lara, Simon, Dan, Silvia, Loic, Agnes, Betrand, Greg, Alet, Colossus, Emile, Eleonora, Jorge, Bea – there were too many to mention in this list, thank you all. A special acknowledgement to Aletta who, in my opinion, wrote the perfect thesis in a standard I can never reach.

Special thanks go to Nicolas, for his continuous support in the past years, and for enduring my moodswings. Thanks for all the patience especially during the final phase of my PhD, where I could not always be a social, cheerful person.

My final thanks go to my family, especially my grandparents, my brother Paris, my uncle Bertold, my cousin Elly and most of all my parents who believed in me, where always there when I needed them, inspired me by making me follow their profession as engineers, and financed my civil engineering studies in Germany.

Λένα Λάππα

And if you find her poor, Ithaca won't have fooled you.
Wise as you will have become, so full of experience,
you will have understood by then what these Ithacas mean.
Ithaka, C.P. Cavafy, 1911.

Κι αν πτωχική την βρεις, η Ιθάκη δεν σε γέλασε.
Ετσι σοφός που έγινες, με τόση πείρα,
ήδη θα το κατάλαβες η Ιθάκες τι σημαίνουν.
Ιθάκη, Κ.Π. Καβάφης, 1911.